



REHVA Community of Young Professionals

BOOK OF PAPERS

2020

Online

HVAC World
Student Competition 2020

REHVA
Student Competition 2020

Our Sponsors



BOOK OF PAPERS

2020

Online

Table of content

INTRODUCTION	4
RESULTS	7
1ST PLACE HVAC WORLD STUDENT COMPETITION	8
1ST PLACE REHVA STUDENT COMPETITION	8
2ND PLACE HVAC WORLD STUDENT COMPETITION.....	15
2ND PLACE REHVA STUDENT COMPETITION	20
3RD PLACE HVAC WORLD STUDENT COMPETITION.....	27
3RD PLACE REHVA STUDENT COMPETITION	32
HVAC WORLD STUDENT COMPETITION OTHER PARTICIPANTS' CONTRIBUTION	38
REHVA STUDENT COMPETITION OTHER PARTICIPANTS' CONTRIBUTION	51
EVENT PICTURES	109

Introduction

Arash Rasooli

The Book of papers is presented by RCYP (REHVA Community of Young Professionals). The RCYP aims to facilitate professional activities and knowledge exchange between young professionals (below 35 years) in the fields of indoor climate, HVAC, building physics, and building services. In the current book, the papers written by the participants of the REHVA Student Competition and the ones from the HVAC World Student Competition are presented. The winners of each competition are also shown at the beginning. At the end of the book, the photos of the events can be found.

REHVA Student Competition

Ever since 2005, REHVA has been organizing a yearly international competition to award the best HVAC students in Europe. REHVA member associations nominate one entry per country to the competition after having organized their national level competitions. The submitted works are based on a Master or Bachelor work and can cover any topic in the fields related to REHVA. The Student competitions are organized during the REHVA Annual Meetings and the Students receive a trophy with their names engraved in it, which is then handed over next year to the next winner. The trophy has been traveling long in the past decade, carrying the names of all the proud winners since 2005.

HVAC World Student Competition

In 2013, REHVA founded a World Student competition with several its international partner associations. Ever since 2016, the HVAC World Student Competition has been taking place between students nominated by REHVA (EU), ASHRAE (United States), CAHVAC (China), FAIAR (South America), ISHRAE (India), SAREK (South Korea) and SHASE (Japan). Each association may send one candidate from their region or continent. REHVA's candidate in the HVAC World Student Competition is the winner from REHVA Student Competition. The other MoU partners organise the HVAC World Student Competition according to the same rules around the world with the participation of REHVA in the jury. The first competition was held in 2016 by REHVA in Denmark. REHVA co-finances the participation of the European candidate in these global competitions.

REHVA and HVAC World Student Competitions 2020

REHVA Student Competition 2020 was held online due to the COVID-19 pandemic conditions, on the 11th of January 2021. Sixteen representatives from 14 different countries took a part in the competition. The 1st place and the trophy were awarded to Maaïke Leichsenring, from Delft University of Technology, the Netherlands, for her work on “Flow Visualization of Ammonia inside a Corrugated Plate Heat Exchanger Condenser”. The second prize was awarded to David Stanek from Czech Republic and the third prize was awarded to Asur Pablo Menéndez Inchusta from Spain.

The Jury was composed by, Jorma Säteri, Murat Çakan, Francis Allard, Ivan Chmúrny, Karel Kabele, Robert Gavriľiuc and Ivo Martinac and chaired by Manuel Gameiro da Silva.

The HVAC World Student Competition 2020 took place online on May 27th, 2021, in collaboration with ISHRAE. The competition was held between the competitors representing ASHRAE (United States), ISHRAE (India), CAHVAC (China), SAREK (South Korea), and REHVA (Europe). The first prize was awarded to Maaïke Leichsenring (REHVA, the Netherlands, Europe) with her work on the topic “Flow Visualization of Ammonia inside a Corrugated Plate Heat Exchanger Condenser”. The next two prizes were awarded to Jianyun Wu (CACHVAC, China) and Yong Woo Song (SAREK, South Korea), respectively.

The jury team members included, Jun Choi, Joe Firrantell, Narayanan Srikantan Chandrasekar, and Angui Li and chaired by Manuel Gameiro da Silva.

The HVAC World Student Competition 2020 was the 2nd time that REHVA’s representative won the 1st prize. REHVA’s first 1st prize in the HVAC World Student Competition was won in 2016 by Arash Rasooli, also from the same faculty and university, at CLIMA 2016, Aalborg, Denmark.

Both competitions are sponsored by Eurovent Certita Certification.

About RCYP (REHVA Community of Young Professionals)

The RCYP was founded in 2020 by REHVA and coordinated by Arash Rasooli, the first winner of REHVA and HVAC World Student Competition (2016). REHVA seeks the objective of advancing its programs and services for young engineers, helping them build their professional foundations and career. REHVA organises courses for students and young professionals and promotes their participation in the REHVA network event by discounts. REHVA will support the joint activities defined together with the RCYP members and offer advantages relying on the existing REHVA knowledge sources and services, such as free or discounted access to REHVA guidebooks, events and trainings, publication possibility in the REHVA Journal, specific sessions at REHVA events for the community.

The CLIMA World Congresses are inviting young researchers to submit abstracts. If students team-up and purchase REHVA guidebooks they receive a discount. RCYP is building an online community and information hub tailored to the interest of community members.

For any inquiries, feel free to contact us at rcyp@rehva.eu.

Results

HVAC World Student Competition 2020



FINAL RESULTS



JIANYUN
WU



2



MAAIKE
LEICHSENRING



1



YONG WOO
SONG

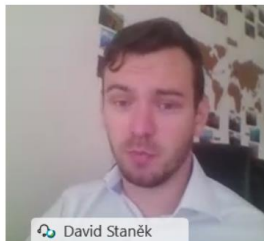


3

REHVA Student Competition 2020



FINAL RESULTS



David Staněk



DAVID STANEK

2



Maaïke Leichsenring



MAAIKE
LEICHSENRING

1



Asur Menendez Inchusta



ASUR PABLO
MENÉNDEZ INCHUSTA

3

1st Place
HVAC World
Student Competition

Maaike
Leichsenring
The Netherlands

1st Place
REHVA
Student Competition

Flow Visualization of Ammonia inside a Corrugated Plate Heat Exchanger Condenser

Maaïke Marie-Louise Leichsenring

Abstract— As ammonia is environmentally benign, a growing global interest takes place in the continuous use of ammonia for commercial applications in heating, ventilation, air-conditioning and refrigeration (HVAC &R) systems. Think about heat pump systems, indirect space conditioning in buildings and large air-conditioning plants at airports. However, despite the fact that ammonia is amongst the oldest of all the refrigerants, a scientific knowledge gap exists on condensing ammonia which results in faulty heat exchanger designs. This study shows the first flow visualization results of vertical downward condensing ammonia in a corrugated plate heat exchanger. A 25 mm thick corrugated transparent polymer plate has been machined to enable flow visualization. The study distinguishes between partial film and film flow and the influence of mass flux and vapor quality is observed. The heat transfer coefficients of the varying flow patterns are compared and show different characteristics. The experimental operational conditions are compared to a conventional flow pattern map of air/water two-phase flow in plate heat exchangers and showed contradicting results. Therefore, a separate flow pattern map for downward condensing ammonia is proposed and should be relied on when the flow pattern of downward condensing ammonia is to be predicted. The results show that more visualization studies are required to extend the applicability of the flow pattern maps for different condensing fluids.

Index Terms— Flow patterns, plate heat exchangers, flow visualization, condensing ammonia

I. INTRODUCTION

Plate heat exchangers (PHEs) have a wide range of applications due to their superior performance in relation to favourable heat transfer coefficients (HTCs), compactness, design flexibility and thermal effectiveness [1]. However, the two-phase behaviour inside the PHEs is not yet fully understood, resulting in over or under-estimating by several published heat transfer and pressure drop correlations, which are limited by the range of conditions they cover [2]. Reference [3] concludes that better predictions of flow patterns in plate heat exchangers will improve the calculation of heat transfer and pressure drop. Flow patterns are determined visually by an experimental setup where the flow is observed through a transparent plate. Flow patterns are defined by the geometric configurations of vapor and liquid and are classified into four main flow patterns: bubbly, slug, churn and film flow. The sequence of occurrence is based on the increase of the vapor mass flux. References [4], [5] and [6] conclude that the average vapor quality also plays a significant role, as it is observed that a low vapor quality corresponds to bubbly flow and a high vapor quality to film flow. It is expected that the various flow patterns relate to different forms of heat transfer. Reference [7] concludes that film flow shows particularly favourable heat transfer enhancement as

compared to the other flow regimes. A flow pattern map (FPM) helps distinguish the various regimes in a graphical way. Reference [3] created an FPM for two-phase vertical downward flow in plate heat exchangers including the fluid property modifying group Λ [-], see (1), that enables the inclusion of fluid properties into the FPM. The parameter is defined as a function of the liquid properties relative to those of water under the same conditions:

$$\Lambda = \mu_L \mu_w^{-1} \rho_L^{-1/4} \rho_w^{1/4} \sigma_L^{-3/4} \sigma_w^{3/4}, \quad (1)$$

where the fluid properties μ , ρ and σ represent the dynamic viscosity, density and surface tension. The subscript L represents the liquid of the fluid and w represents water at the same operational conditions. The axes of the FPM make use of dimensionless groups: the liquid Reynolds number Re_L [-] and the two-phase Froude number Fr_{TP} [-]. The liquid Reynolds number is defined by (2):

$$Re_L = G(1-x)d_h \mu_L^{-1} \quad (2)$$

Where G [$\text{kgm}^{-2}\text{s}^{-1}$] is the total mass flux, x [-] the vapor quality and d_h [m] the hydraulic diameter. The two-phase Froude number is defined by (3):

$$Fr_{TP} = xG(gd_h \rho_G (\rho_L - \rho_G))^{-0.5} \quad (3)$$

Where g [kgm^{-2}] represents the gravitational constant. Flow visualization of pure ammonia condensing flow inside a corrugated vertical plate heat exchanger has not been investigated previously. This study compares the results of pure ammonia flow visualization in a vertical downward PHE to the FPM constructed by [3]. Section II explains the experimental setup and the performed research to enable the construction of a durable transparent test plate. Section III explains the test procedure and section IV discusses the results of the visualization experiments.

II. EXPERIMENTAL SETUP

A. Experimental Apparatus and Procedure

In cooperation with the Delft University of Technology, Bluerise B.V. constructed a small scale test plant to test the performance of a cycle for Ocean Thermal Energy Conversion (OTEC) purposes, which contains similar components to that of a refrigeration cycle. The 100 W OTEC-demo consists of an Organic Rankine cycle using pure ammonia as the working fluid. Fig. 1 shows a schematic representation of the experimental setup. Pure ammonia is vaporized while flowing through the evaporator due to the counter current hot water flow. The separator splits the remaining liquid ammonia from the

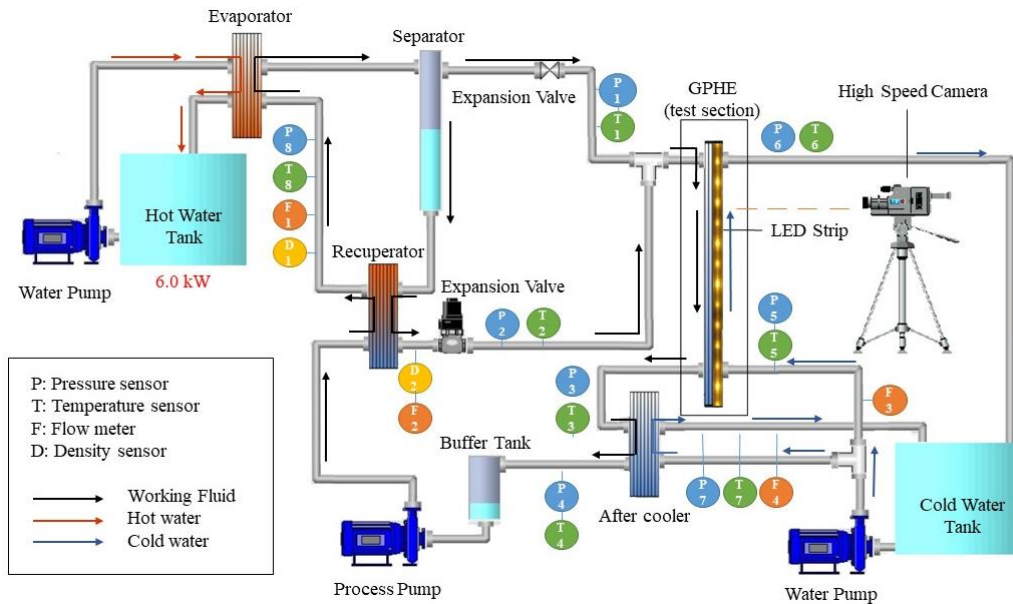


Figure 1: Experimental setup diagram of OTEC demo cycle

vapor and sends it to the recuperator, which acts as a preheater for the ammonia that is to be heated. The pure ammonia vapor flows through a turbine and is reunited right before the test section. The two-phase working fluid is condensed in the Gasketed Plate Heat Exchanger (GPHE) by a cold-water stream from the cold-water tank. A sub-cooler and buffer tank are placed to guarantee that all vapor in the working fluid flow is fully condensed by the time it reaches the process pump. The hot water tank is heated by a heating coil and the cold-water tank is connected to a refrigeration system.

B. Test section for Visualization

The test section is a GPHE, containing a cold-water channel and a working fluid channel. Table 1. gives the detailed geometric parameters of the stainless-steel plate used for heat transfer. Figure 2 shows its schematic diagram. The PHE includes a 95 cm x 12.5 cm transparent corrugated polymer plate that enables visualization of the condensing ammonia on the working fluid side. This visualization plate has the same geometric specifications as the heat transfer plate except for the plate thickness, which is 25 mm.

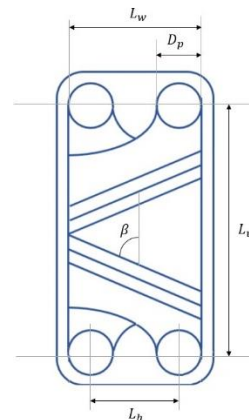


Figure 2: Schematic representation of the heat transfer plate

The plate is illuminated by a 500 cm LED strip including 300 LED's that encircles the plate from its sides twice. A 3000 fps high speed camera is placed in front of the visualization plate to capture the flow patterns under varying operating conditions. Fig. 3 shows the transparent polymer plate, the visualization section including pressure plate and illumination and the placement of the camera.

Table 1. Geometric parameters of the heat transfer plates

Channel gap d_g	1.72 [mm]	Plate length L_p	0.668 [m]
Chevron angle β	63 [°]	Plate pitch p_{cp}	2.3 [mm]
Corrugation pitch p	7.5 [mm]	Plate thickness d_p	0.58 [mm]
Corrugation Wavelength λ_{wave}	6.67 [mm]	Plate width L_h	0.06 [m]
Effective heat transfer area A_e	0.537 [m ²]	Port diameter D_p	0.035 [m]
Effective width heat transfer L_w	0.095 [m]	Thermal conductivity κ	16.3 [Wm ⁻¹ K ⁻¹]



Figure 3: Left) Visualization section. Right) Visualization section and position high speed camera.

C. Material Selection of Visualization Plate

The challenge is finding a material that meets the following criteria: Chemically compatible to ammonia, transparency, high strength (able to withstand an operational pressure up to 12 bar) and easy to machine into the corrugation patterns. References [6] and [8] use glass in front of a flat plate. However, machining a brittle material such as glass into a corrugation pattern contains large risks on mechanical performance due its brittle structure [9]. The latter stresses the importance of finding a polymer (as is used by [4], [10], [11] and [7]) that meets the requirements. According to reference [12], Polystyrene (PS) is a polymer that meets the optical, mechanical and machinability criteria. Generally, it is stated that this material is chemically compatible to ammonia [12] but it is not mentioned for which experimental conditions this applies such as phase, temperature, pressure and the ammonia being a pure fluid or a diluted mixture. Therefore, several samples are placed in a pressure vessel filled with pure, liquid ammonia at a pressure of 8 bar absolute and ambient temperature for four days. The samples are machined into the desired corrugated pattern, compressed onto each other by two stainless steel clamps. Fig. 4 shows the clamped corrugated samples before and after the test. The material shows a slight bend and tiny damages on the locations of contact between the samples, but it did not reduce the transparency significantly. A sheet of PS has a maximum thickness of 4.75 mm, onto which the corrugated pattern is machined by a CNC-machine. The corrugated PS sheet is glued with a UV light curing adhesive onto a Polymethylacrylate (PMMA) plate of 20 mm thickness to benefit from the superior mechanical properties that PMMA has relative to PS.

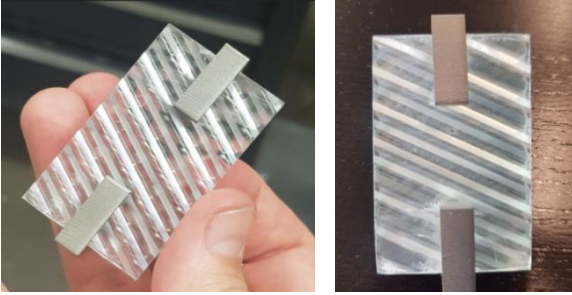


Figure 4: Left) PS Samples before test. Right) PS Samples after test.

III. TEST PROCEDURE

The ammonia mass flux G_a [kgm^{-2}s] is determined by (4). The ammonia mass flow \dot{m}_a [kgs^{-1}] is measured by flow meter F1, see Fig. 1. The flow passage area A_f [m^2] is calculated by multiplying the effective heat transfer width L_w [m] with the channel gap d_g [m].

$$G_a = \dot{m}_a A_f^{-1} \quad (4)$$

The single-phase condition at the outlet of the after cooler is used to determine the enthalpy of the liquid ammonia. The average vapor quality \bar{x} [-] inside the GPHE is determined by (5), where x_{in} [-] and x_{out} [-] represent the vapor qualities at the in- and outlet of the condenser. An energy balance is used to determine the two-phase

enthalpy at the inlet of the after cooler, which is assumed to be the same as the enthalpy at the outlet of the GPHE. A second energy balance determines the enthalpy of the ammonia at the inlet of the GPHE h_{in} [kgkJ^{-1}] which is determined by (6). $h_{L,sat}$ [kgkJ^{-1}] and $h_{V,sat}$ [kgkJ^{-1}] represent the saturated liquid and vapour phase enthalpy of the ammonia at the inlet conditions of the condenser.

$$\bar{x} = 0.5(x_{in} + x_{out}) \quad (5)$$

$$x_{in} = (h_{in} - h_{L,sat})(h_{V,sat} - h_{L,sat})^{-1} \quad (6)$$

Experiments are performed where the mass flux G_a is kept constant and the vapor quality x_{in} is increased. Both the influence of the mass flux and inlet quality on the flow configurations are recorded for the top, middle and bottom windows.

IV. EXPERIMENTAL RESULTS

For all recorded conditions, a framerate of 3000 fps with a resolution of 1024 x 1024 pixels is used. The transparent plate remained intact for 7 days, but on the 8th day of performing experiments degradation in the material was visible in the form of small cracks in the PS surface and crystal shaped spots between the PS and PMMA layer that grew in size over time. It is concluded that PS has a limited durability when in contact with pure ammonia.

A. Flow Pattern and Flow Path

For all performed experiments, no bubbles, slugs or churns were detected, and only film flow and partial film flow are observed. The path of the flow remained similar under the various circumstances. Fig. 5 shows the path of the flow over the different windows. Due to the shapes of the distribution zone at the inlet, the liquid flow is pushed to the left which causes most of the liquid flow to disperse over the left upper diagonal of the window. It is expected that in that zone also vapor is present, but less than in the lower diagonal. The area of the upper diagonal covered by mainly a rough liquid film decreases for smaller mass fluxes. This area is indicated by the zones that reflect light in various directions.

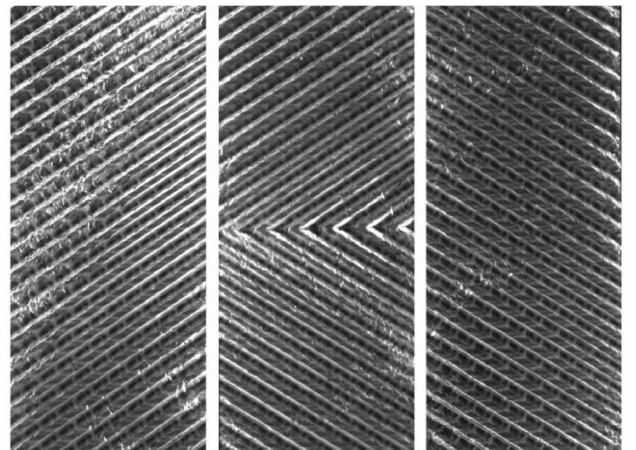


Figure 5: $G = 91$ [$\text{kgm}^{-2}\text{s}^{-1}$], $\bar{x} = 0.27$ [-]. Left) Top window. Middle) Middle window. Right) Bottom window.

Most of the vapor flows at the lower diagonal of the top window, indicated by a still image. In the middle window the corrugation direction switches and this sudden change in flow direction causes the liquid to evenly distribute over the corrugations in the lower part of the middle window. Less vapor is detected. The bottom window is mostly covered in a smooth liquid film.

B. Influence of Mass flux and Vapor Quality on flow configuration

A distinction can be made between film flow and partial film flow. Film flow includes a liquid layer on both plates while partial film flow leaves dry zones when the amount of liquid film is limited and unable to cover the entire plate. If partial film flow occurs in the GPHE and dry zones are present on the transparent plate, an opaque surface will be visible. The dry zones are indicated by a black circumference, see Fig. 6 and 7. Only the top window is represented in the figure since this window shows the varying configurations most clearly.

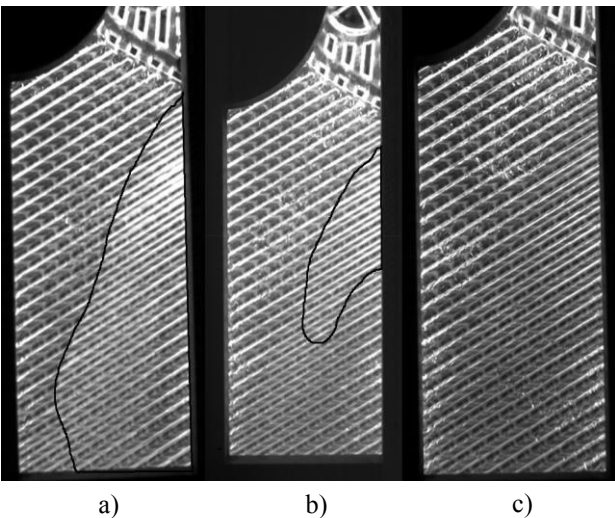


Figure 6. $\bar{x} = 0.31 [-]$. a) $G = 43 [kgm^{-2}s^{-1}]$ b) $G = 64 [kgm^{-2}s^{-1}]$ c) $G = 81 [kgm^{-2}s^{-1}]$.

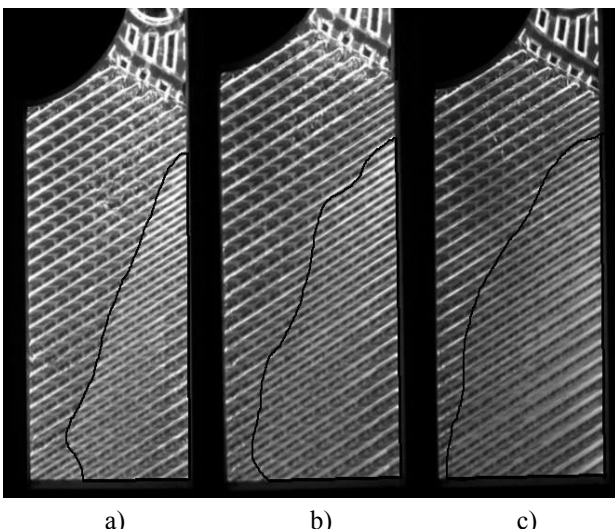


Figure 7. $G = 43 [kgm^{-2}s^{-1}]$. a) $\bar{x} = 0.22 [-]$ b) $\bar{x} = 0.48 [-]$ c) $\bar{x} = 0.62 [-]$

Fig. 6 shows that for a constant vapor quality but increasing mass flux the dry zone decreases. Fig. 6 a, b indicate partial film flow by the occurrence of the dry zone. Fig. 6 c shows that for an increased mass flux of $81 kgm^{-2}s^{-1}$, the dry zone disappears, i.e. indicating film flow. This indicates that the mass flux G has a strong influence on the flow pattern transition from partial film flow to film flow. A low mass flux shows smooth liquid film characteristics, indicated in the upper left diagonal of Fig. 6 a by a clear image. For increasing mass flux, the film transitions to rough film characteristics, see Fig. 6 c, indicated by the strong light reflectance of the left upper diagonal. Fig. 7 shows that for a constant mass flux and an increasing vapor quality the area of the dry zone increases. This only occurs for lower mass fluxes and within partial film flow only.

C. Data reduction of experiments

The experimental results indicate that the occurrence of the dry zone is the main visual phenomenon that distinguishes partial film flow from film flow. Therefore, quantification of the dry zone fraction $\epsilon_A [-]$ leads to a parameter which can provide insight on its relation to mass flux, vapour quality and heat transfer characteristics. The dry zone fraction is defined by (7):

$$\epsilon_A = A_{dry}A_e^{-1}, \quad (7)$$

where $A_{dry} [m^2]$ is the area of the dry zone on the plate and $A_e [m^2]$ the effective heat transfer area of the plate. Image processing by Matlab is used to quantify the dry zone fraction ϵ_A , by assuming that moving liquid is represented by pixel values that change over time, whereas the vapor is represented by pixel values that remained constant over time. This is done for all performed experiments. Fig. 8. presents the results of image processing by Matlab of two experiments which correspond to the observed results of Fig. 6a and Fig 7c. Fig. 8a. shows a large dry zone in the bottom left diagonal indicated by the light blue area on the plate, which is in line with the visual observations. The dry zone indicated in Fig. 8b shows similar results to Fig. 7 but a larger area than the visual observations indicate. For all experiments, the results of Matlab processing were in line with the described physical phenomena in section B.

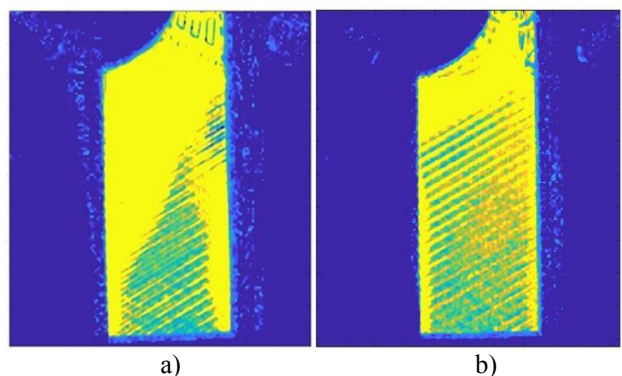


Figure 8. Processed images by Matlab where blue pixels indicate a static image and yellow /orange represents liquid movement.. a) $G = 43 [kgm^{-2}s^{-1}]$, $\bar{x} = 0.31 [-]$, b) $G = 43 [kgm^{-2}s^{-1}]$, $\bar{x} = 0.62 [-]$.

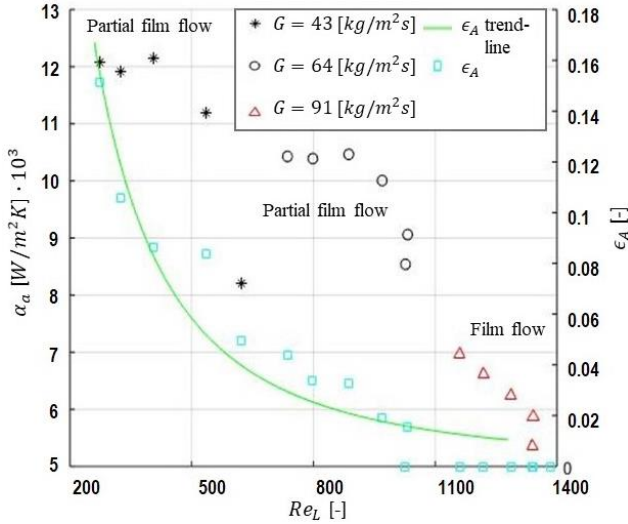


Figure 9. HTC's of condensing ammonia, dry zone fraction and liquid Reynolds number for various mass fluxes obtained from the visualization experiments.

Therefore, quantification of the dry zone fraction ϵ_A was concluded to be successful. The HTC's of condensing ammonia α_a [$\text{Wm}^{-2}\text{K}^{-1}$] were determined by (8):

$$U = 1 / \left(\frac{1}{\alpha_a} + \frac{1}{\alpha_w} + \frac{d_p}{\kappa} \right) \quad (8)$$

Where U [$\text{Wm}^{-2}\text{K}^{-1}$] is the overall heat transfer coefficient determined by heat balance and α_w [$\text{Wm}^{-2}\text{K}^{-1}$] is the heat transfer coefficient of the cooling water determined by previously obtained single phase heat transfer correlations by [3]. Fig. 9 presents the HTC's of condensing ammonia α_a , the liquid Reynolds number Re_L and the dry zone fraction ϵ_A and trend line for various mass fluxes. It can be observed that the HTC's for film flow show more linear characteristics than partial film flow, and that for increasing dry zone fraction the non-linear characteristics for partial film flow increases. Partial film flow shows favourable HTC's over film flow, and is concluded to be the preferred flow pattern with respect to heat transfer.

D. Comparison of Results to Flow Pattern Map by [3].

The operating conditions of the experiments are represented in Fig. 10. Figure 10 shows an FPM generated by [3] for plate heat exchangers that makes use of the dimensionless quantities Re_L and $Fr_{TP}\Lambda$ which account for gravity, viscous forces and inertia. This construction is based on results from previous visualization experiments for two-phase vertical downward flow of mainly air-water mixtures in plate heat exchangers. The dimensionless fluid property modifying parameter Λ is included on the Y-axis to correct for fluid property deviations of other fluids. This parameter is included to widen the applicability of the map from air-water to multiple fluids, such as refrigerants. The viscosity, surface tension and vapour-liquid density ratio of ammonia locate its operating conditions at high values of the y-axis. For the experimental conditions of the flow

visualization experiments in this research, the map predicts churn flow. The results of the flow visualization experiments show film and partial film flow, which indicates that this map is not yet applicable for ammonia flow pattern prediction.

E. Proposed Flow Pattern Map

An FPM for the downward condensing ammonia in the GPHE is constructed based on the parameters proposed by [3]. Fig. 11 presents the proposed FPM for downward condensing ammonia inside a GPHE with a corrugation angle of $\beta = 60^\circ\text{C}$. This map can be used to predict the occurring flow pattern of downward condensing ammonia in a PHE operational conditions within the indicated limits. The map includes the experimental conditions of the visualization experiments and the dashed line describes the transition from partial film flow to film flow. An indication for rough film flow and smooth film flow is included that describe the transition from a smooth liquid film to a rough liquid film. The proposed transition line differs from the transition line proposed by [3] as it is in opposite direction and slightly curved. The deviation can be explained by the fact that constructed transition lines proposed in the FPM by [3] are based on observed flow patterns in previous studies. The transition lines for the upper half of the FPM, i.e. $Fr_{TP}\Lambda^{-0.5} > 1.8$, are based on few experiments. The experimental conditions of the visualization experiments are between $1.8 < Fr_{TP}\Lambda^{-0.5} < 5.0$ and the results of this visualization study can be used to improve the accuracy of the FPM constructed by [3]. More visualization studies with a wider range of experimental conditions on condensing flow of pure ammonia in vertical PHEs are required to accurately describe the flow pattern behaviour of pure ammonia in this type of heat exchangers and to extend the applicability of FPMs for different fluids.

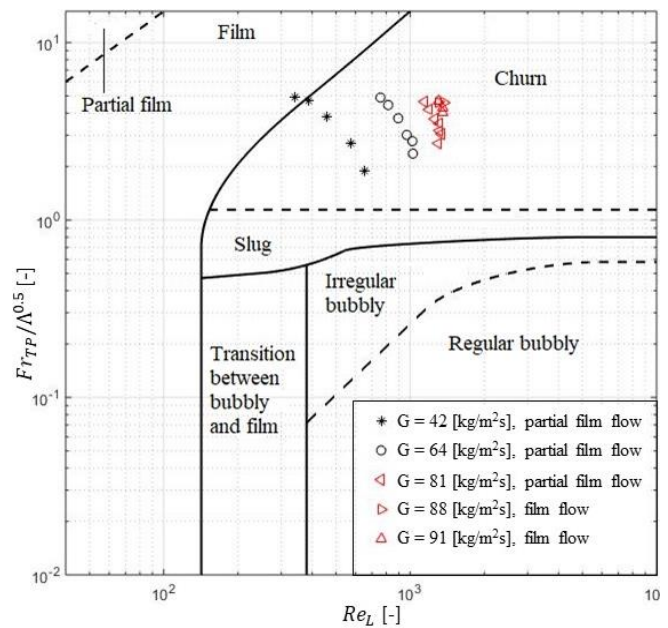


Figure 10. Experimental operating conditions shown in simplified flow pattern map of two-phase flow in PHEs by [3].

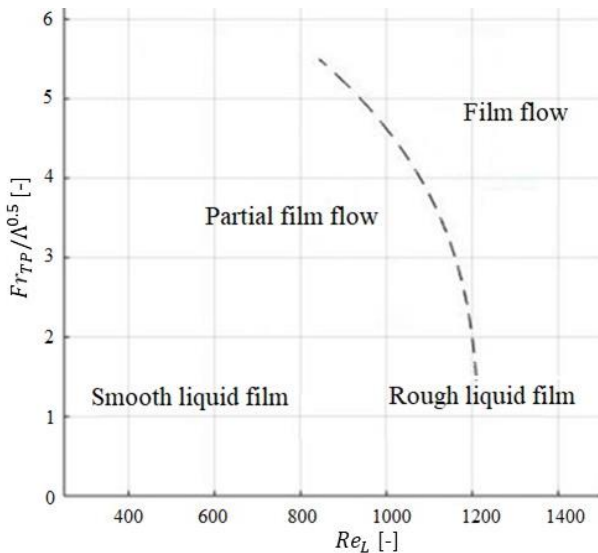


Figure 11. The proposed flow pattern map as a function of Fr_{TP}, Λ and Re_L for condensing ammonia inside a corrugated GPHE describing the transition from partial film flow to film flow.

V. DISCUSSION OF RESULTS

PS is compatible for flow visualization of ammonia for seven days. For future visualization studies, it is advised to test the chemical compatibility of Polypropylene (PP) as PP is expected to have an improved chemical compatibility to pure ammonia. During the flow visualization experiments, the cold water flow varied significantly due to limits of the OTEC setup which influenced the HTC's of ammonia. Flow patterns are defined visually, therefore flow pattern classification remains subjective to this day. The approach of performing the experiments and the experimental conditions influence the judgement of the observer on how flow patterns are related to transition lines in the FPM. The proposed FPM shows a curve based on the experimental conditions. However, if another approach was executed the experimental conditions might have formed another structure on the FPM. This note should be taken into account when forming FPMs or making assumptions on the flow pattern behaviour based on FPMs constructed from a limited amount of experiments.

VI. CONCLUSIONS

The flow morphology of pure ammonia in a vertical downward GPHE has been captured. A corrugated visualization plate is produced from transparent PS by a CNC-machine and has proven to be chemically compatible to pure ammonia for several days and mechanically resistant to a condensation pressure up to 7 bar absolute. For all conditions introduced, film flow and partial film flow are observed. The flow patterns were most visible on the top window, where most of the liquid phase covers the left upper diagonal and most of the vapor the lower diagonal of the window. An increased vapor quality increases the area of the indicated dry-zone (partial film flow) on the visualization plate. The mass flux determines the transition from partial film flow to film flow. Increasing the mass flux enhances the rough film flow, creating more liquid entrainment in the lower diagonal resulting in film flow. Partial film flow shows favourable

HTCs over film flow and increases with the dry zone fraction. The operating conditions during the performed ammonia condensation experiments (liquid Reynolds number and two-phase Froude number) have been indicated in the FPM constructed by [3]. The results indicate that the film flow and partial film flow transition line needs to be moved to higher values of the Re_L than indicated in the FPM which is mainly based on air-water experiments. For this reason, an FPM is proposed for condensing ammonia inside a corrugated GPHE describing the transition from partial film flow to film flow. The results of this study can be used to improve performance calculations of condensing ammonia in plate heat exchangers. More extensive visualization studies are required to:

- Extend the applicability of the FPM for different condensing fluids inside GPHE's
- Improve two-phase correlations for ammonia on a large scale and therefore optimize heat exchanger designs used in HVAC &R systems.

ACKNOWLEDGEMENTS

I would like to acknowledge the financial support from the China Scholarship Council and Koudegroep Delft-Wageningen.

REFERENCES

- [1] K. Thulukkannam. 2013, *Heat Exchanger Design Handbook*, Taylor & Francis Inc., Boca Raton.
- [2] R. Amalfi, F. Vakili-Farahani and J. Thome. "Flow boiling and frictional pressure gradients in plate heat exchangers," *International Journal of Refrigeration*, vol 61, pp. 166-184, 2016.
- [3] X. Tao, M. Nuijten & C. Infante Ferreira, "Two-phase vertical downward flow in plate heat exchangers: Flow patterns and condensation mechanisms," *International Journal of Refrigeration*, vol 85, pp. 489-510, 2018.
- [4] Al-Zaidi, M. Mahmoud and T. Karayiannis, "Condensation flow patterns and heat transfer in horizontal microchannels," *Experimental Thermal and Fluid Science*, vol 90, pp. 153-173, 2017.
- [5] H. Arima, J. Kim, A. Okamoto and Y. Ikegami, "Local boiling heat transfer characteristics of ammonia in a vertical plate evaporator," *International Journal of Refrigeration*, vol 33, pp. 359-370, 2008.
- [6] H. Arima, A. Okamoto & Y. Ikegami, "Local boiling heat transfer characteristics of ammonia/water binary mixture in a vertical plate evaporator," *International Journal of Refrigeration*, vol 34, pp. 648-657, 2011.
- [7] P. Vlasogiannis, G. Karagiannis, P. Argyropoulos, and B. Bontozoglou, "Air-water two-phase flow and heat transfer in plate heat exchanger," *International Journal of Multiphase Flow*, vol 28, pp. 757-772. 2001.
- [8] Z. Xue, W. Qu and M. Xie, Full visualization and startup performance of an ammonia pulsating heat pipe. *Propulsion and power research* 2(4), pp. 263-268, 2013.
- [9] J. Lutgendorf, "Structural design of glass geometries," Delft: Delft University of Technology, 2014.
- [10] V. Grabenstein, A. Plzin and S. Kabelac, "Experimental investigation of the flow pattern, pressure drop and void fraction of two-phase flow in the corrugated gap of a plate heat exchanger," *International Journal of Multiphase Flow*, vol 91, pp. 155-169, 2016.
- [11] E. Jassim, T. Newell, and J. Chato, "Two-phase flow visualization in chevron and bumpy style flat plate heat exchangers," *Heat transfer Engineering*, vol 27, 2006.
- [12] CES Edupack 2018, Granta Design Limited.

2nd Place
HVAC World
Student Competition

Jianyun Wu
China

Experimental Investigation on Humidity-sensitive Properties of Polyimide Film for Humidity Sensors

Jianyun Wu, Wenhe Zhou (✉), Xiaowei Wang, Shicheng Li
 School of Environmental and Municipal Engineering, Lanzhou Jiaotong University, Lanzhou, China 730070
zwh6888@mail.lzjtu.cn

Abstract—Due to excellent properties, polyimide (PI) films are widely used in capacitive humidity sensors as the humidity-sensitive medium. However, some key properties of this film are uninvestigated and need further research, especially those related to sensor characteristics. So, samples of PI films were self-synthesized in a lab. In order to test their effective diffusion coefficients using the self-build test system, films were created from different chemical combinations (PMDA-ODA, BPDA-ODA, BPDA-BAPP, PMDA-BAPP) with four separate concentrations (23%, 20%, 17%, 15%). They were tested in three disparate temperatures (20°C, 35°C, 50°C), respectively. The effective diffusion coefficients of water molecules in these four films were $6.11 \times 10^{-13} \text{m}^2/\text{s}$ for PMDA-ODA, $6.38 \times 10^{-13} \text{m}^2/\text{s}$ for BPDA-ODA, $6.14 \times 10^{-13} \text{m}^2/\text{s}$ for BPDA-BAPP, and $5.86 \times 10^{-13} \text{m}^2/\text{s}$ for PMDA-BAPP. The effective diffusion coefficients of water molecules in these PI films were $6.08 \times 10^{-13} \text{m}^2/\text{s}$, $5.86 \times 10^{-13} \text{m}^2/\text{s}$, $4.25 \times 10^{-13} \text{m}^2/\text{s}$ and $3.76 \times 10^{-13} \text{m}^2/\text{s}$ ordered by decreasing concentration of PI film. When the environment temperature rises from 20°C to 50°C, the effective diffusion coefficient rises from $6.38 \times 10^{-13} \text{m}^2/\text{s}$ to $1.67 \times 10^{-12} \text{m}^2/\text{s}$. The results should greatly enhance the properties improvement of the capacitive humidity sensor.

Index Terms—Effective diffusion coefficient, humidity-sensitive properties, polyimide Film.

Introduction

Capacitive humidity sensors are widely used in many fields, whose characteristics are mainly dependent on the sensing film[1-2]. Polyimide (PI) film is commonly used as humidity sensitive material due to its stability and absorbency properties[3]. The research for improving humidity sensors has been ongoing and numerous, but most of that research is focused on the sensor itself. Therefore, there is a glaring vacancy of research on PI films, an essential component of this system; especially properties of the PI film related to sensing characteristics. This is a barrier to improve sensors as a whole. This paper will fill that research void.

II. PREPARATION OF POLYIMIDE FILMS

In this paper, two kinds of binary anhydrides and diamines were chosen to form four types of films. Fig. 1 shows the fabrication progress of PI films. The chemicals used to prepare PI films are listed in Table I.

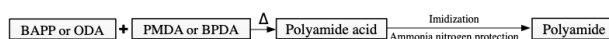


Figure 1. The flow chart of PI preparation

TABLE I.
 THE EQUIPMENT AND THE MODEL AND PRECISION

Reagent	Specification	Manufacture
BAPP	98%	Shanghai Aladdin biochemical technology co. LTD
PMDA	98%	Shanghai Aladdin biochemical technology co. LTD
ODA	98%	Shanghai Aladdin biochemical technology co. LTD
BPDA	97%	Shanghai Aladdin biochemical technology co. LTD
DMAC	Analytically pure	Shanghai zhongqin chemical reagent co. LTD

Firstly, the binary anhydride and diamine with same molar mass were put into DMAC. They were stirred and heated to obtain PI acid. The acid with different concentrations can be obtained by changing the mass of binary anhydride and diamine. Then, PI acid was dropped on the glass sheet gripped in the spin coater. By controlling the quantity of PI acid and rotation speed of spin coater, the thickness of PI films can be changed. Finally, put the glass sheets into the electric furnace controlled and heated. After the process of dehydration cyclization, the PMDA-ODA, BPDA-ODA, BPDA-BAPP and PMDA-BAPP PI films were created. They were in varying concentrations (23%, 20%, 17% and 15%).

III. TEST FACILITY FOR EFFECTIVE DIFFUSION COEFFICIENT

The test system is shown in Fig. 2. The main devices of this test system are shown in Tab. II. Before the test, plenty of moist and dry air must be produced from generators and stored in gasholders separately. The PI film was then hung on the hook of the electronic scales in the test chamber in order to test its original mass. Refer to Fig. 2, the valve 14 was opened to let the film absorb the moisture from the moist air. When the mass of film reached stabilization, the time of whole process and the film mass were recorded after absorption. In addition, the chamber humidity was recorded before and after the test. Then the chamber humidity reduced by inletting the dry air. The process was repeated three times to gain more data. Finally, the effective diffusion coefficient of the water molecule in disparate films can be calculated.

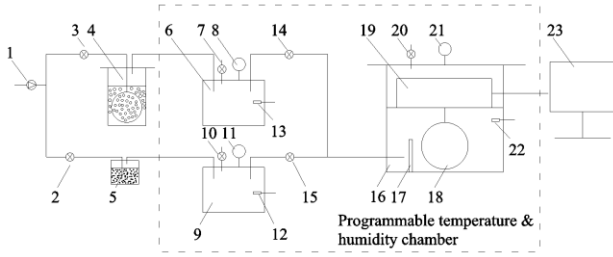


Figure 2. The schematic diagram of test system on diffusion coefficient

1-air pump; 2,3,7,10,14,15,20-valve; 4-humidity generator; 5-dryer; 6-gasholder of moist gas; 8,11,21-pressure gage; 9-gasholder of low humidity gas; 12,13,22-temperature and humidity sensor; 16-adsorption chamber; 17-baffle; 18-PI film; 19-electronic scales; 23-computer

TABLE II.
THE EQUIPMENT AND THE MODEL AND PRECISION

Name	Model	Precision
Electronic scales	HZ-104/55S	1/100000
Oilless air compressor	SQ12	
Temperature and humidity sensor	RS-WS-N01-SMG-7	±2%RH(5%RH~95%RH, 25°C); ±0.4°C(25°C)
Constant temperature humidity chamber	HWHS-225-0	±0.1%RH; ±0.1°C

IV. TEST DATA AND THE PROCESSING

A. The calculation equations of effective diffusion coefficient

Equation (1) relates the mass flow rate and the partial pressure gradient of vapour[4].

$$g_v = -\delta \cdot \nabla p_v \quad (1)$$

Where g_v is the mass flow rate of vapour, kg/s. δ is the effective permeability, kg/(m·s·Pa). p_v is the partial pressure of vapour, Pa.

According to Fick's first law, the one-dimension instability mass flow rate of water molecules can be expressed as follows when the temperature is constant.

$$g_v = -\rho \cdot D \cdot (\partial w / \partial x) \quad (2)$$

Where ρ is the performance density of PI film, kg/m³. D is the effective diffusion coefficient of water molecules, m²/s. w is the moisture mass percentage, kg/kg. x is the distance of water molecules diffusion on one direction, m.

Based on the isothermal adsorption, (2) can be described as follows [5]:

$$g_v = -\rho \cdot D \cdot (\partial w / \partial \varphi) \cdot (\partial \varphi / \partial x) \quad (3)$$

Where φ is the environment relative humidity, %RH.

Both partial pressure of vapour in PI film and relative humidity are linear distribution during steady state diffusion, so g_v can be expressed as follow [6]:

$$g_v = -\rho \cdot D \cdot \left(\frac{\partial w}{\partial \varphi} \right) \cdot \frac{\varphi_2 - \varphi_1}{l} = -\rho \cdot D \cdot \left(\frac{\partial w}{\partial \varphi} \right) \left(\frac{1}{p_{vs}} \right) \cdot \left(\frac{p_{v2} - p_{v1}}{l} \right) \quad (4)$$

where l is the thickness of PI film, m. p_{vs} is the partial pressure of saturated steam in experimental temperature, Pa.

Based on Equation (1) and (4), the following equation can be deduced [6]:

$$D = (\delta \cdot P_{vs} / \rho) \cdot [1 / (\partial w / \partial \varphi)] \quad (5)$$

According to (5), it is obviously that the key to obtain effective diffusion coefficient of water molecule is getting effective permeability coefficient and moisture sorption isotherm of water molecule.

The effective permeability of water molecules can be tested according to Astm Standards[4], the calculations are as follows:

$$\delta = \xi \cdot (1/2) \quad (6)$$

where ξ is the water molecular permeability, it can be described as (7):

$$\xi = g / \Delta p_v = g / [p_{vs} \cdot (RH_1 - RH_2)] \quad (7)$$

where Δp_v is the vapor pressure difference, Pa RH_1 and RH_2 are the ambient relative humidity after and before the moist gas is into the chamber, % g is the wet flow density, which can be described as Equation (8):

$$g = (\Delta m / \Delta t) / A \quad (8)$$

where Δm is the mass change, kg and Δt is the time, s. A is the area of PI film, m².

According to (6), (7) and (8), the equation of effective permeability coefficient of water molecules can be obtained:

$$\delta = \Delta m \cdot l / [2A \cdot \Delta t \cdot p_{vs} \cdot (RH_1 - RH_2)] \quad (9)$$

Firstly, the partial pressure of vapour and temperature in the film are different from those in the environment. When PI film is exposed in the environment for a certain time, the partial pressure of vapour and temperature in the film matches those in environment. At this time, the equilibrium moisture content, w , is the ratio between water mass that can be separated from the film and the mass of dry PI film. The moisture sorption isotherm $w(\varphi)$ is the curve that linked by equilibrium moisture contents under different relative humidity. According to the ISO 12570[7], the moisture percentage can be obtained by the following equation:

$$w = (m - m_0) / m_0 \quad (10)$$

where m is the mass of PI film in a certain environment relative humidity, kg. m_0 is the mass of dry PI film, kg.

The Peleg model can describe the expression of w and φ with these parameters [9]:

$$w(\varphi) = k_1 \varphi^{n_1} + k_2 \varphi^{n_2} \quad (11)$$

where k_1 , k_2 , n_1 , n_2 are constants ($n_1 < 1$ and $n_2 > 1$). When k_1 is proximately to k_2 , and the relative humidity is low, the first item is much bigger than the second one. While the relative humidity is high, the situation is opposite. Because

the relative humidity of tested environment is lower than 50%RH, the Equation (11) can be simplified as follow:

$$w(\varphi) = k\varphi^{n_1} \quad (12)$$

According to (5), (9) and (12), the effective diffusion coefficient, D, can be described as (13):

$$D = \Delta m \cdot l / [2A \cdot \Delta t \cdot (RH_1 - RH_2)] \cdot [1/(\partial w / \partial \varphi)] \quad (13)$$

As long as Δm , l , A , Δt , RH_1 , RH_2 and $w(\varphi)$ are tested, the effective diffusion coefficient can be obtained.

B. The chemical combinations influence on film humidity-sensitive property

Four films were chosen to test in 20°C. They were shown in Table 3. The areas of them were 0.01m² and the thicknesses were 0.025mm. In addition, the concentrations were 20%. The results are listed in Tab. III.

TABLE III.
THE PERMEABILITY COEFFICIENTS AND EFFECTIVE DIFFUSION COEFFICIENT OF FOUR FILMS

Type	$\delta(\text{kg}/(\text{m}\cdot\text{s}\cdot\text{Pa}))$	$w(\varphi)$	$D(\text{m}^2/\text{s})$
PMDA-ODA	5.079×10^{-16}	$0.0312\varphi^{0.17898}$	6.11×10^{-13}
BPDA-ODA	7.425×10^{-16}	$0.02073\varphi^{0.32248}$	6.38×10^{-13}
BPDA-BAPP	4.686×10^{-16}	$0.06077\varphi^{0.1079}$	6.14×10^{-13}
PMDA-BAPP	3.569×10^{-16}	$0.06997\varphi^{0.0863}$	5.86×10^{-13}

According to Tab.III, four PI films ordered by increasing effective permeability coefficient are PMDA-BAPP, BPDA-BAPP, PMDA-ODA, BPDA-ODA. However, the effective diffusion coefficients of different PI films are similar, and there's no evident regularity. Therefore, the chemical combinations have little influence on humidity-sensitive property of PI film. Additionally, The BPDA-ODA PI film has the best humidity-sensitive property, because both its effective permeability coefficient and effective diffusion coefficient are highest among all the films.

C. The concentration influence on film humidity-sensitive property

The concentration influence on humidity-sensitive property was discovered by testing PMDA-BAPP films with varying concentrations. The films areas were 0.01m², and their thicknesses were all 0.0025mm. The test ran in 20°C. And results are shown in Tab. IV.

TABLE IV.
THE CONCENTRATION EFFECTS ON THE COEFFICIENTS

Concentration (%)	$\delta(\text{kg}/(\text{m}\cdot\text{s}\cdot\text{Pa}))$	$w(\varphi)$	$D(\text{m}^2/\text{s})$
23%	4.391×10^{-16}	$0.05236\varphi^{0.11929}$	6.08×10^{-13}
20%	3.569×10^{-16}	$0.06997\varphi^{0.0863}$	5.86×10^{-13}
17%	2.314×10^{-16}	$0.12907\varphi^{0.06001}$	4.25×10^{-13}
15%	1.924×10^{-16}	$0.05734\varphi^{0.10696}$	3.76×10^{-13}

Table IV shows that with the concentration decrement of PI film, both the effective permeability coefficient and diffusion coefficient decrease similarly. Therefore, the higher the concentration, the better the humidity-sensitive property of PI film is, also the better the property of humidity sensor.

D. The temperature influence on film humidity-sensitive property

The BPDA-ODA films with 0.025mm thickness and 20% concentration were tested in 20°C, 35°C and 50°C. The results are shown in Tab. V.

TABLE V.
THE TEMPERATURE EFFECTS ON THE COEFFICIENTS

Temperature	$\delta(\text{kg}/(\text{m}\cdot\text{s}\cdot\text{Pa}))$	$w(\varphi)$	$D(\text{m}^2/\text{s})$
20°C	7.425×10^{-16}	$0.02073\varphi^{0.32248}$	6.38×10^{-13}
35°C	4.749×10^{-16}	$0.01297\varphi^{0.43392}$	1.00×10^{-12}
50°C	2.994×10^{-16}	$0.0046\varphi^{0.68938}$	1.67×10^{-12}

According to Tab. V, with the increase of temperature, the effective permeability coefficient decreases rapidly, since the partial pressure of saturated steam increases dramatically when experimental temperature rises. While effective diffusion coefficient augments contrarily. Clearly, the temperature has an appreciable impact on humidity-sensitive property of PI film. The higher the temperature, the better the humidity-sensitive property of PI film is.

V. CONCLUSIONS

- 1) The tested effective diffusion coefficient of PI film is valuable for researches on porous media. It also provides experimental data for numerical simulations.
- 2) The self-built system and test method for humidity property of PI film and porous film is practical.
- 3) The BPDA-ODA type of PI film with higher concentration should be used as sensing film in humidity sensors to improve its sensitivity.
- 4) The temperature has a significant impact on humidity-sensitive property of PI film, it becomes better when temperature increases.

ACKNOWLEDGEMENT

This project is supported by the National Natural Science Foundation(Number 51466007).

REFERENCES

- [1] Chen Meijuan, 2015. A parallel plate capacitive humidity sensor based on PI film and numerical study on its characteristics, Lanzhou jiaotong University.
- [2] X. He, et al.,2017. Research on Dynamic Characteristics Model of Parallel Plate Capacitive Humidity Sensor, Instrument Technique and Sensor.2017(4):5-26.
- [3] W. Zhou, et al., 2017. Numerical study on response time of a parallel plate capacitive polyimide humidity sensor based on microhole upper electrode. Journal of Micro/Nanolithography, MEMS, and MOEMS, 16(3):034502.
- [4] R. Concepts, 2014. E96-93 Standard test methods for water-vapor transmission of materials. Annual Book of Astm Standards

- [5] F. Collet, et al., 2011. Water vapor properties of two hemp wools manufactured with different treatments. *Construction & Building Materials* 25(2): 1079-85.
- [6] Siyang Yi. 2016. Experimental measurement of the effective water vapor diffusion coefficient of porous building materials by a transient technique toward energy-efficient buildings, Zhejiang University.
- [7] ISO, 2014. ISO 12570: Hygrothermal performance of building materials and products Determination of moisture content by drying at elevated temperature.
- [8] M. Peleg, 1993. Assessment of a Semi-empirical Four Parameter General Fmodel for Sigmoid Moisture Sorption Isotherms. *Journal of Food Process Engineering* 16(1): 21–37.

2nd Place
REHVA
Student Competition

David Stanek
Czech Republic

Reuse of waste heat from IT equipment

David Staněk

Abstract—There is a large potential in energy savings when it comes to reusing waste heat from IT equipment. In the study, a calculation on waste heat recovery from a virtual data center has been evaluated on a specific residential building. The data center has been designed based on knowledge gained on personal in-situ data gathering as well as on authors studying the given issue.

Index Terms—Data centers, heating and domestic hot water, IT equipment, waste heat

Introduction

The worldwide electric energy consumption of data centers (DC) has reached 205 TWh in the year 2018 [1]. For comparison, the total electricity consumption of Portugal as of year 2018 was only 52 TWh, making the data center electricity consumption four times higher [2]. Electronic chips transfer around 99 % of their electrical power into heat. For a normal DC this means a specific heat load of 1-3 kW/m² [3]. DC operators are pursuing a higher efficiency of their DCs because of increasing energy costs as well as a green image. Modern DCs often use a system of free cooling technology, adiabatic cooling and an effective hardware and hardware regulation [4][5]. Even though modern approaches are in use, there is great potential in reusing waste heat from the IT systems, which is not regularly harvested.

I. DATA CENTERS AS A SOURCE OF HEAT

Two DCs in the Czech Republic have been analyzed to gather information about their waste energy reuse. The first was directly owned by a Czech technological company with an installed IT power of 1 000 kW [6]. The second DC rented rack space to end users often mid-sized companies and cloud servers [7]. The installed IT power was 814 kW. Both DCs were air cooled using a cold-hot aisle cooling system. The later DC has granted valuable data, directly from their BMS system. Free cooling technology has been used up to an outside temperature of 14 °C. The analyzed data consists of the whole DC and an exemplar server room (SR).

A. Stability of heat generated in DCs

The analyzed data shows a high stability in IT power consumption which directly converts to stable heat output. The maximum divergence in the SR was 14 % (128 to 147 kW). The whole DC than recorded a divergence of 3 % (368 to 378 kW). At the time of the visit the DC had a max active IT power of 651 kW (total 814 kW).

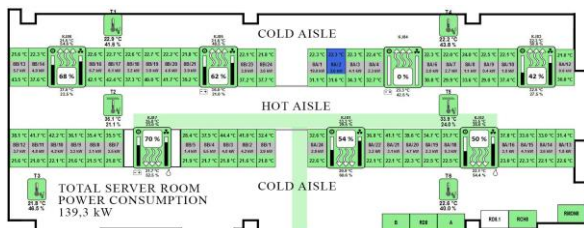


Figure 1: Typical server room of analyzed DC [7]

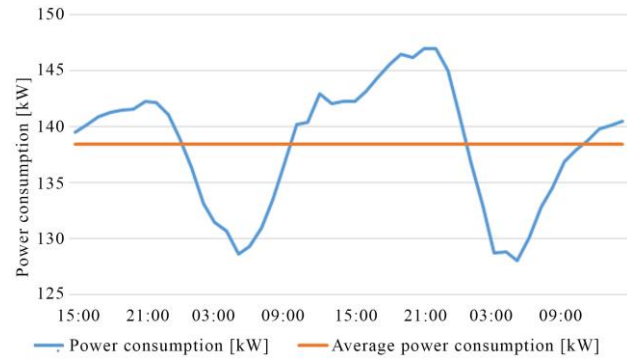


Figure 2: Power consumption of the analyzed typical server room [7]

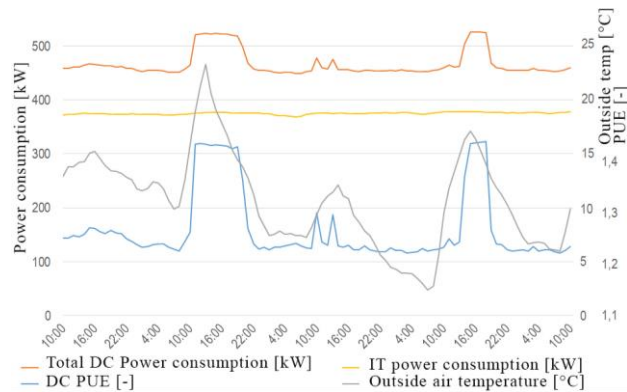


Figure 3: Power consumption of the analyzed DC with reference to PUE and outdoor air temperature [7]

A Finnish study by M. Wahlroos focused on using DC waste heat for district heating comes forward with a similar outcome of high stability of DC waste heat production [8].

B. Regulation of heat generated in DCs

A large issue associated with DCs as a source of heat is the low possibility of regulating the heat generated. The DC is essentially a commercial company and its products are a number one priority for its operation. Based on communication with managers of the visited DCs, there is little to no potential in regulating the heat generated based on the heat demand. This means, that the heat is generated constantly at similar levels throughout the year.

Another research, led by C. Jiang, studied energy consumption and efficiency of modern data centers [5]. An important part of the study was focused on energy proportionality and energy efficiency of studied servers. Energy proportionality shows the effect of lowering computing power of a computer chip on its electricity consumption. Energy efficiency refers to ratio between the server computing power and electrical power consumption. The results were important for this case study as they presented little effect of decreased computing power on the specific electrical power consumption and thus the heat generated in IT equipment.

Based on these data, the waste heat from DC is considered constant, stable but hard to regulate based on heat demand.

II. DATA CENTERS AND ENERGY

Modern technologies and energy-efficient approach help in decreasing specific power consumption of DCs. PUE values are used for a comparison of DC energy efficiency. PUE stands for Power Usage Effectiveness and is calculated as the total energy supplied to a DC divided by electric energy consumed purely by IT equipment [9]. A lower PUE value indicates a higher efficiency. Average up to date DCs have a PUE of around 1.6, however modern, high end DCs can go as low as 1.2 – 1.1 [10].

$$PUE = \frac{E_{DC}}{E_{IT}} \quad (1)$$

E_{DC} = Data center total energy consumption
 E_{IT} = IT equipment electricity consumption

For the topic of waste heat recovery, a different approach is preferred. The alternative method is the Energy Reuse Factor (ERF) which is calculated as a ratio between the reused energy of the DC and total energy supplied to the DC [10]. Normal DC without waste heat reuse have an ERF = 0. ERF of 1 means all energy consumed by the DC is reused.

$$ERF = \frac{E_{REUSE}}{E_{DC}} \quad (2)$$

E_{DC} = Data center total energy consumption
 E_{REUSE} = Reused energy of the DC

The last metric used is the Energy Reuse Effectiveness (ERE). The ERE value indicates how well the DC maintains its energy flows and reuses energy.

$$ERE = \frac{E_{DC} - E_{REUSE}}{E_{IT}} \quad (3)$$

III. THEORETICAL CASE STUDY

A full-scale concept of waste heat recovery from a DC has been prepared. The study evaluated a combination of DC with a selected residential complex of apartment blocks situated in Prague, Czech Republic. The complex consisted of three apartment towers with several commercial areas. This object will be later referred to as Main residential object (MRO). The aim was to verify if a DC can be effectively used as an alternative heat source. Chosen architectural and energy information about the MRO are presented in the table below.

Table 1: Information about Main residential object

Project name	Park Hloubetin
Location	Prague, Czech Republic
Year of construction	2016
No. flats	117
No. residents	334
Winter outside extreme temp.	-12 °C
Winter outside average temp.	4,3 °C
Heating degree days- average	3 237 K.day
Specific heat demand	12 kWh.(m2.a)-1
Total heat loss	167 kW
Heat demand for heating	411 MWh.a-1
Heat demand for domestic hot water preparation	382 MWh.a-1



Figure 4: Layout plan of the Main residential object

The chosen cooling technology of the DC was direct hot water cooling.

A. Direct hot water cooling

Direct hot water cooling is a special technology used in server cooling, where demineralized water is brought directly to high heat producing hardware, such as CPUs, GPUs, and RAMs. Heat is transferred via a conductive aluminum plate. The advantage is a high efficiency of heat transfer, where between 90-95 % heat is transferred and taken away by water [13]. The other advantage is a high cooling stability with a decreased risk of local heat islands as well as a higher rack density of up to 100 kW/rack [11]. The main disadvantages are the requirement to use a specialized hardware, a potential for water leakage and a necessity to cool the remaining low power components by air, which accounts to 10-20 % of heat produced in the server. The temperature of the outgoing hot water may reach 65 – 70 °C without any risk to the cooled hardware. This enables almost all year free cooling in most European regions.

B. Server cooling design

1) Server cooling

An exemplar server has been used to design its cooling system as shown in Fig. 5. The temperature gradient has been set to 45/65 °C, which allows for direct heating and domestic hot water (DHW) preparation. Pipe width has been calculated as 4 mm for optimal liquid velocity. Characteristics of liquid flow for various server power densities are shown in Tab.2. [14]

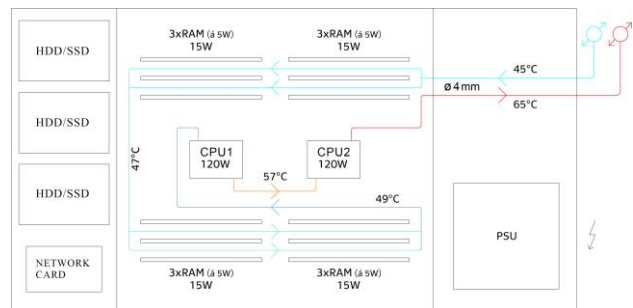


Figure 5: Typical server cooling system

Table 2: Server cooling parameters

Server power density	Server heat cooled by liquid [W]	Liquid mass flow [kg.h ⁻¹]	Liquid velocity [m.s ⁻¹]	Re [-]	Type of liquid flow
High	593	25,4	0,55	3 824	Turbulent
Medium	285	12,2	0,27	1 911	Laminar
Low	142,5	5,0	0,14	956	Laminar

2) IT chip temperature limit

With such high outgoing temperatures (65 °C) the danger of hardware overheating risk had to be analyzed. The highest allowed temperatures for CPU and GPU chips range between 90-105 °C, depending on the manufacturer. Based on [15] the maximal safe operational temperature of CPUs, GPUs and RAMs is 78-85 °C.

The chip with highest risk of overheating is labeled CPU2 in Fig. 5. The temperature gradient on the chip is 57/65 °C. The temperature difference between the cooling liquid and the CPU has been calculated using the overall heat transfer coefficient (4)(5). Heat transfer coefficient between cooling water and the surface layer of the piping (6) has been calculated using Nusselt number. Nusselt number has been determined using Pohlhausens equation for laminar and transitional forced flow over plates (7) [16]. A second value defining Nusselt number was defined from scientific literature for comparison (F. Incropera) [17]. The maximum calculated temperatures on CPU2 do not exceed 80 °C for any CPU power density. The set temperature gradient of 45/65 °C on the server is thus safe. A full list of theoretical maximum temperatures based on CPU power are in Tab.3.

$$\Delta t = \frac{\dot{Q}}{\bar{u} \cdot S} \quad (4)$$

$$\bar{u} = \frac{1}{\frac{1}{h_i} + \sum \frac{l}{\lambda}} \quad (51)$$

$$h_i = \frac{Nu \cdot \lambda_w}{L} \quad (6)$$

$$Nu = 0,664 \cdot \sqrt{Re} \cdot \sqrt[3]{Pr} \quad (7)$$

$$Re = \frac{v \cdot D_h}{\nu} \quad (8)$$

- \dot{Q} = server heating power [W]
- \bar{u} = overall heat transfer coefficient [$W \cdot m^{-2} \cdot K^{-1}$]
- S = CPU chip area [m^2]
- h_i = heat transfer coefficient surface/liquid [$W \cdot m^{-2} \cdot K^{-1}$]
- l = piping wall thickness [$m^2 \cdot K \cdot W^{-1}$]
- λ = thermal conductivity [$W \cdot m^{-1} K^{-1}$]
- λ_w = thermal conductivity of water at 61 °C [$W \cdot m^{-1} \cdot K^{-1}$]
- L = characteristic dimension [m]
- Nu = Nusselt number [-]
- Pr = Prandtl number of water at 61 °C [-]
- v = velocity of water flow [$m \cdot s^{-1}$]
- D_h = hydraulic diameter [m]
- ν = kinematic viscosity of water at 61 °C [$m^2 \cdot s^{-1}$]

Table 3: Maximal CPU chip temperatures

CPU power density	Nusselt number [-]	Temperature difference [°C]	CPU chip temperature [°C]
High [240 W]	Calculated = 25,9	6,1	71,1
	Literature = 8,2	13,3	78,3
Medium [120 W]	Calculated = 18,3	3,8	68,8
	Literature = 8,2	6,7	71,7
Low [60W]	Calculated = 13,0	2,4	67,4
	Literature = 8,2	3,3	68,3

C. Rack cooling design

The rack case (RC) can mount 42 (in some cases more) individual servers. RCs used in direct water cooling technology are different to classical, air cooled models. An exemplar RC has been modeled in the study for illustration and cost estimation. A model is shown in Fig. 6. The cooling circuit inside the RC is separated from the main branch in the DC by an inbuilt heat exchanger. The primary role of the heat exchanger is to separate pressure levels on the two sides as well as improving control of each individual RC cooling power. Each RC further contains an expansion tank, safety valve and a circuit pump. The cooling circuit of the RC is connected via a reverse return system for simple regulation. The heat exchanger between Rack cooling and DC cooling is 65/62 °C. [14]

D. Data center cooling design

A DC consists of dozens of RCs. The main cooling branch connects on the primary side to a heat exchanger, separating demineralized water on the DC side, with heating water on the boiler room side of the MRO. The temperature gradient of this heat exchanger is designed at 62/60 °C. The secondary side of the DC cooling branch connects to heat exchangers that are a part of each RC, discussed above. Liquid flow into the RCs is controlled by a set of motor controlled two-way valves. The DC's cooling circuits temperature gradient are set to 42/62 °C and are designed via a reverse return system for simple regulation. A schematic diagram is presented in Fig. 7.

A very important part of the DC's cooling circuit are dry chillers. These are in use when the object's demand for heat is lower than the heat supplied from the DC. The cooling capacity of the dry chillers must higher than IT heat capacity to ensure safe DC operation. Due to the high temperatures in the cooling systems, free cooling may be used throughout the year. [14]

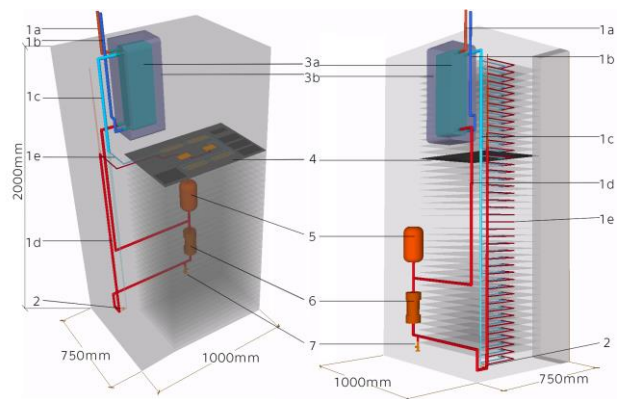


Figure 6: Rack cooling design

- 1a Return Piping Φ 20 mm
- 1b Supply piping Φ 20 mm
- 1c Supply piping inside RC Φ 18 mm
- 1d Return piping inside RC Φ 18 mm
- 1e Server connection piping Φ 4 mm
- 2 Safety bypass
- 3a Heat exchanger SWEP B15Tx57/2P
- 3b Thermal insulation 50 mm
- 4 Server See Fig. 5
- 5 Expansion vessel 2 l
- 6 Pump max 1080 l/h at 73 kPa
- 7 Safety valve 1" x 1 1/2"

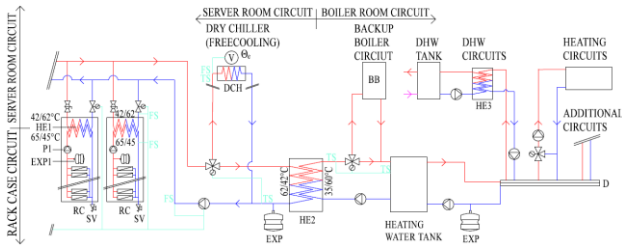


Figure 7: Schematic diagram of DC connection with the Main residential object's heating system

E. Main residential object heating and domestic hot water preparation

The temperature of hot water received from the DC's cooling system is 60 °C. This temperature is optimal for domestic hot water preparation as well as object heating. The MRO includes several hot water tanks for energy storage (5 880 l for DHW and 8 420 l for heating). There is a backup gas boiler situated in the boiler room with a heating power of 160 kW to cover the complete heat loss of the building. [14]

IV. COMPLEX DESIGN

The study's main objective is to estimate the potential for energy and emission savings by reusing waste heat from DCs in an object with a different purpose. It is however important to realize, that an introduction of a new operation will increase the total energy consumed, especially considering a highly energy challenging service such as a DC. The waste heat from DCs is often not effectively reused even in new, high standard DCs. The method for calculation energy and emission savings is based on the fact, that DCs are never constructed primary as a heat source. Taking these facts into account, all energy and emission savings have been calculated from the sum of individual operations (residential and DC). A similar approach has been adopted by the German supercomputer Aquasar [18] or the decentralized system of Cloud and Heat [19].

A software calculation tool has been created for an In-depth analysis of the presented intention of reusing DC waste heat in a residential/administrative building. The tool has been used for the MRO to design the size of the DC and set the saving potentials. Several DC sizes have been evaluated with three interesting outcomes selected for presentation, shown in Tab. 4. And Figs. 8-10. [14]

Table 4: Energy parameters of simulated DC sizes

Var	Heat demand coverage	Installed power of IT equipment [kW]	Usable power of IT equipment [kW]	Expected DC floor size [m2] *	ERF [%]
1	Only DHW	96	44	60	76,0
2	DHW + heating down to 6 °C	256	117	165	52,5
3	DHW + heating	463	211	280	32,6

* Including technical and administrative areas.

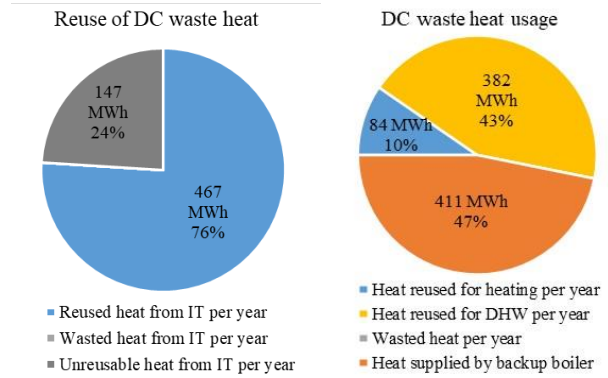


Figure 8: Reuse of DC waste heat for var. 1

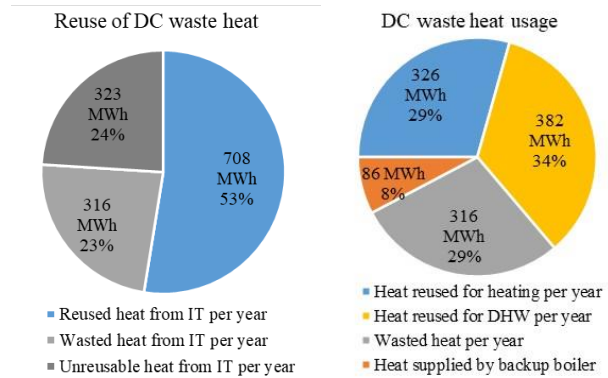


Figure 9: Reuse of DC waste heat for var. 2

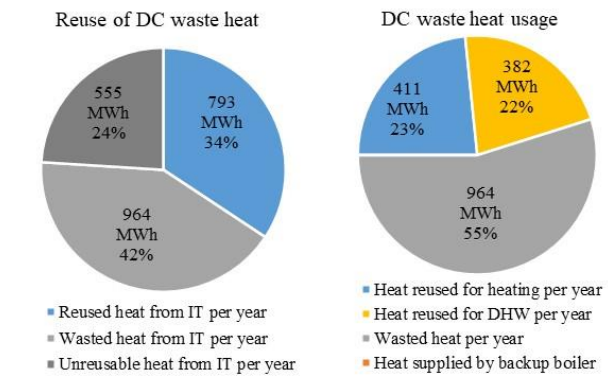


Figure 10: Reuse of DC waste heat for var. 3

The option, that has been evaluated as the most cost-efficient covers complete domestic hot water preparation and heating down to 6 °C of outside temperature. The reason was a combination of factors, most importantly achieving a high waste heat reuse efficiency in a combination with a decent DC size. The smaller DC achieved higher ERF, but the small size would make it harder in a competitive sense. The larger scale DC is oversized.

The medium sized DC of 256 kW installed IT power was used for further purposes and evaluations in this study.

V. OBJECTIVE EVALUATION

A. Environmental evaluation

The environmental criteria have been evaluated for the combined consumption of MRO and DC.

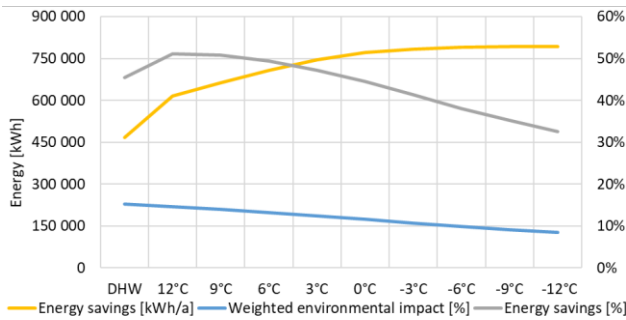


Figure 11: Chart of environmental evaluation

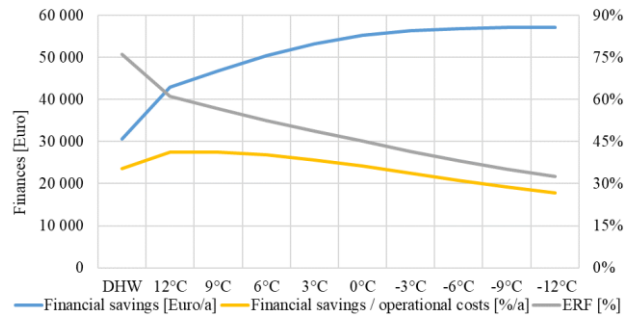


Figure 12: Chart of economical evaluation

In this case study, the total energy savings were calculated to be 708 MWh/year, which accounts to 49,4 % of the total energy consumption.

Weighted ecological saving have been calculated based on the Czech method SBToolCZ [20]. According to this method, the total effect on the environment was lowered by 13,2 %. The method SBToolCZ is a Czech alternative similar to the worldwide counterparts of LEED or BREEAM.

Due to the possibility of an all year free cooling incorporation, the expected PUE of the DC itself is <1.2. A chart of environmental evaluation is present in Fig. 11 presenting several possible DC sizes and their environmental impacts. The selected DC size and its effect are shown in Tab. 5.

Table 5: Environmental evaluation

Energy consumption of the Main residential object	794 MWh
Energy consumption of the Data center	1 348 MWh
Combined Energy consumption of MRO and DC without waste heat reuse	2 142 MWh
Combined Energy consumption of MRO and DC with waste hear reuse	1 433 MWh
Energy savings due to waste heat reuse	709 MWh
Percentage of energy saved	33,1 %
Weighted emission reduction	13,2 %
Energy Reuse Factor (ERF)	52,5 %

B. Economical evaluation

The first step in the economical evaluation was to calculate the extra costs of installing water cooling technology in contrast to the typical, air cooling technology in the DC. Investments, such as special rack cases and servers modified for direct water cooling, piping, dry chillers, heat exchangers and a more complex regulation were included. The final sum was set at 76 000 Euro.

The Main residential object can achieve around 50 000 Euro/year in savings (compared to district heating). Furthermore, the DC can save around 17 200 Euro/year thanks to water cooling technology. The savings on the DC part are mainly on mechanical ventilators and chillers. The total cash savings are calculated as 67 200 Euro/year.

The discounted payback period is only 1.3 years.

A chart of economical evaluation is present in Fig. 12 presenting several possible DC sizes and their economic impacts.

The total price of installed IT is roughly 2.6 million Euro and the expected revenue of the DC around 2 million Euro/year. From the perspective of a DC owner, the scale of money saved is relatively small.

VI. CONCLUSION

Data centers have been evaluated as a stable, but hard to regulate source of low potential heat. The optimal technology for waste heat reuse from IT technology is direct hot water cooling. The main advantage of this technology is high temperature output of the cooling liquid ($\approx 65 \text{ }^\circ\text{C}$), which may be used directly for heating and domestic hot water preparation. Due to the fact, that heat generated in the DC can hardly be regulated during the year, a constant consumption of heat through the year is preferred. An example may be a low-energy residential building, where the heat demand for domestic hot water preparation is significant.

Liquid cooling technology is not frequently used in today’s DCs. The main reasons are a small product market, increased entry costs and an often unfounded fear of a possible accident. This is one of the largest issues to overcome when striving for efficient waste heat reuse from IT.

This offered solution is very efficient from an environmental perspective. By combining the two separate building operations, the total energy consumption is decreased by 33 %. The weighted emissions were lowered by 13 %, based on the Czech authorized LCA method SBToolCZ.

Reusing waste heat from IT equipment is a nonviolent method, that leads to decreasing energy demands of DCs, which use around 2 % of the world’s electricity consumption. The main barriers are liquid cooling technology installation and a connection of two, till today, separate operation branches. If the obstacles are overcome, this method is operational and viable. This example of integrated design is one of the options to achieve European and worldwide environmental targets while achieving economical revenue.

REFERENCES

- [1] E. Masanet, A. Shehabi, N. Lei, S. Smith, J. Koomey, 2020 [online] “Recalibrating global data center energy-use estimates,” Science. <https://science.sciencemag.org/content/367/6481/984>
- [2] International Energy Agency (EIA) [online] *Key energy statistics, Portugal*, 2018. <https://www.iea.org/countries/portugal> (Accessed 2020-07-17)
- [3] N. Rasmussen, [online] “Calculating Space and Power Density Requirements for Data Centers,” Schneider Electric.

<https://www.apc.com/us/en/support/resources-tools/white-papers/calculating-space-and-power-density-requirements-for-data-centers.jsp>

- [4] H. M. Daraghme, Wang Chi, 2016 [online] “*A review of current status of free cooling in datacenters*,” Elsevier. <https://doi.org/10.1016/j.applthermaleng.2016.10.093>
- [5] C. Jiang, Y. Wang, D. Ou, B. Luo, W. Shi, 2016 [online] “*Energy Proportional Servers: Where Are We in 2016?*” Institute of Electrical and Electronics Engineers (IEEE) <https://ieeexplore.ieee.org/document/7980102/> ISBN: 978-1-5386-1792-2
- [6] Interview with the manager and in-situ visit of DC Kokura, Seznam.cz, a.s., Prague, the Czech Republic conducted 01.02.2019.
- [7] Interview with the managers and in-situ visit of DC TTC Teleport a.s., Prague, the Czech Republic conducted 07.03.2019
- [8] M. Wahlroos, M. Parssinen, J. Manner, S. Syri, 2017 [online] “*Utilizing data center waste heat in district heating – Impacts on energy efficiency and prospects for low-temperature district heating networks*,” Elsevier. www.sciencedirect.com/science/article/pii/S0360544217314548
- [9] International Organization for Standardization (ISO) [online] *ISO/IEC 30134-2:2016 Information technology — Data centres — Key performance indicators — Part 2: Power usage effectiveness (PUE)*, <https://www.iso.org/standard/63451.html>
- [10] M. Avgerinou, P. Bertoldi, L. Castellazzi, 2017 [online] “*Trends in Data Centre Energy Consumption under the European Code of Conduct for Data Centre Energy Efficiency*,” MDPI. www.mdpi.com/1996-1073/10/10/1470/pdf
- [11] J. Neudorfer, 2017 [online] “*Liquid cooling in data centers: Time to get over your fears!*” The green grid <https://www.thegreengrid.org/en/get-involved/events/liquid-cooling-data-centers-time-get-over-your-fears>
- [12] International Organization for Standardization (ISO) [online] *ISO/IEC 30134-6 Information technology — Data centres — Key performance indicators — Part 6: Energy Reuse Factor (ERF)*, <https://www.iso.org/standard/71717.html>
- [13] J. Neudorfer, M. J. Ellsworth, D. P. Kulkarni, H. Zien, 2017. [online] “*Liquid cooling technology update*,” The green grid. www.thegreengrid.org/en/resources/library-and-tools/442-WP
- [14] D. Staněk, 2018. “*Využití odpadního tepla z výpočetní techniky*”. Czech Technical University in Prague, Faculty of Civil Engineering <https://dspace.cvut.cz/handle/10467/84268>
- [15] K. Ebrahimi, G. F. Jones, A. S. Fleischer, 2014 [online] “*A review of data center cooling technology, operating conditions and the corresponding low-grade waste heat recovery opportunities*,” Elsevier. www.sciencedirect.com/science/article/pii/S1364032113008216
- [16] M. Barták, 2010. “*Úvod do přenosových jevů pro inteligentní budovy*”. Czech Technical University in Prague, Faculty of Mechanical Engineering
- [17] F. P. Incropera. “*Fundamentals of heat and mass transfer – 3rd ed.*” John Wiley and Sons, INC., 1990. ISBN 9780471304586.
- [18] S. Zimmermann, I. Meijer, M. K. Tiwari, S. Paredes, B. Michel, D. Poulidakos, 2012 [online] “*Aquasar: A hot water cooled data center with direct energy reuse*,” Elsevier. www.sciencedirect.com/science/article/pii/S0360544212003350
- [19] Cloud and Heat [online] <https://www.cloudandheat.com/en> [cit. 02.01.2020]
- [20] M. Vonka et al., 2013. “*SBToolCZ pro bytové domy*,” Czech Technical University in Prague, Faculty of Civil Engineering. ISBN 978-80-01-05125-2

3rd Place
HVAC World
Student Competition

Yong Woo Song
South Korea

Reduction of pollutants applied with photocatalysts in ventilation duct system

Yong Woo Song¹, Jin Chul Park²

¹Doctoral course, Graduate School, Chung-Ang University, Seoul 06794, Korea, yongma0930@cau.ac.kr

²Professor, School of Architecture and Building Science, Chung-Ang University, Seoul 06794, Korea, jincpark@cau.ac.kr

Abstract—This study confirmed the effect of NO_x reduction by applying the TiO₂ photocatalyst, which has a pollutant decomposition effect, to the ventilation duct system, one of the HVAC systems, to reduce nitrogen oxides, one of the representative pollutants. The actual duct system was designed and manufactured, and it was confirmed by comparing the reduction effect based on the lowest concentration arrival time through the nitrogen oxide concentration and UV-A irradiance changes with the ISO 22197-1:2007 experiment method. As a result, the use of a duct system with a TiO₂ photocatalyst showed a sharp increase in the effect in high UV-A irradiance and low NO_x concentration, and it has been confirmed that a certain level of effect can be obtained even if the irradiance is reduced depending on the life of the UV-A lamp. In addition, it has been shown that the reduction effect can be achieved at NO_x concentrations similar to the actual environment. Based on this study, it is expected to be used as basic data for the development of a TiO₂ photocatalyst HVAC system that can be applied to underground parking lots, apartment ventilation units, and shopping centers, which are difficult to apply UV light.

Index Terms—TiO₂ photocatalyst, Particulate matter precursor, Duct system, UV-A irradiance, NO_x concentration.

Introduction

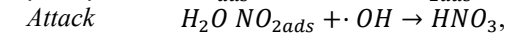
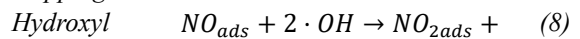
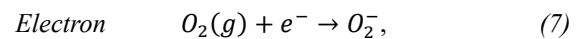
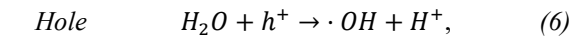
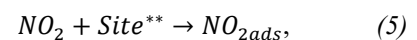
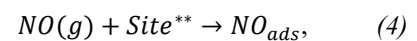
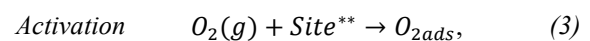
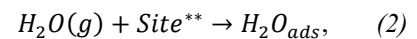
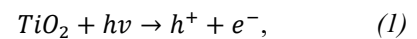
Despite the government's efforts, the concentration of particulate matter in Korea exceeds the WHO level, which is 1.5 to 2 times higher than that of OECD's major cities [1]. Particulate matter components include NO_x, SO_x, carbon and minerals [2], of which nitrogen and sulfur oxides account for about 60%. In particular, nitrogen oxides accounted for 42.3% [3-4] in Korea.

These nitrogen oxides can be called particulate matter precursor, a representative pollutant, and the reduction of the precursor, which is a basic material among the measures to reduce the concentration of particulate matter, is expected to reduce the production of particulate matter, which is a representative pollutant.

There are various ways to reduce nitrogen oxides and sulfur oxides, which are representative precursors of particulate matter, but among them is the TiO₂ photocatalyst, a method that has been actively studied recently. TiO₂ photocatalysts cause ultraviolet and photochemical reactions to produce a radical hydroxide with strong oxidation, and the radical hydroxide is believed to be able to inhibit the production of particulate matter by breaking down nitrogen oxides and sulfur oxides[5].

TiO₂ photocatalyst, such as Equation (1)-(8), has the properties of decomposing pollutants by forming strong oxidation forces ·OH and O₂ radical on the surface through

photochemical reactions with UV-A ultraviolet (350–380 nm) present in the atmosphere [6].



where hv is the energy of the UV radiation, $Site^{**}$ is the surface of TiO₂, and $\cdot OH$ is the hydroxyl radical.

Currently, the utilization of TiO₂ photocatalysts is expanding through application to concrete [7-8] and stone [9-10], and although the effect has been confirmed through standard experiments [11-12], it is difficult to apply it to spaces that are difficult to utilize indoor and ultraviolet rays (indoor, parking lots, underground shopping malls, etc.) due to limitations that maximize the effect when responding to ultraviolet rays.

Therefore, this study applied ultraviolet lamps and TiO₂ photocatalyst inside ventilation ducts that can be used in apartment buildings, parking lots, underground shopping malls, and sales facilities, which are difficult to use indoor and ultraviolet. The flow chart of this study is shown in Figure 1.

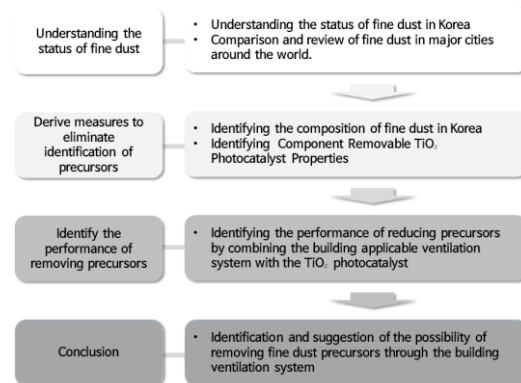




Figure 1. Flow chart of study

Methodology

This study actually manufactured and designed duct system so that they can be combined with TiO₂ photocatalyst coatings and UV lamps, and the experiment was conducted on nitrogen oxides, which are typical pollutants. In the case of measurement equipment used in the experiment, it is shown in Table 1.

TABLE I.
TEST MEASUREMENT EQUIPMENTS

Name	Serinus 40	
Measurement	NO, NO ₂ , NOx	
Range	0 ~ 20 ppm	
Precision	0.4 ppb or 0.5 %	
Sample Flow Rate	0.3 Slpm	
Name	DLC-0.5K 220/240	
Capacity	0.5 KVA (500 VA)	
Input / Output	220 V / 5-240 V	
(electric) Current	2 A	

The experiment was conducted in three main categories, and the conditions of the experiment conducted in this study are as shown in Table 2.

TABLE II.
TiO₂ PHOTOCATALYST APPLIED DUCT SYSTEM TEST CONDITIONS

UV-A irradiance change condition				
NOx Concentration	1.00 ppm			
UV-A irradiance	7.5 W/m ²	10.0 W/m ²	12.5 W/m ²	15.0 W/m ²
Change rate	25% down	Basic	25% up	50% up
NOx concentration change condition				
UV-A irradiance	10.0 W/m ²			
NOx Concentration	0.25 ppm	0.50 ppm	0.75 ppm	1.00 ppm
Change rate	75% down	50% down	25% down	Basic

First, we confirmed the possibility of reduction by setting the NOx concentration (1.00 ppm) presented in ISO 22197-1:2007[13] and the UV-A irradiance (10 W/m²).

Second, the photochemical reaction of TiO₂ photocatalyst is determined by applying 25% reduction, 25% and 50% increase change (7.5, 12.5, 15.0 W/m²) of UV-A irradiance using slidax as an international standard experimental condition.

Third, the trend of the reaction was confirmed by applying the NOx concentration of nitrogen oxides applied to the experiment by 25%, 50%, and 75% (0.75, 0.50, 0.25 ppm) compared to the international standard experimental condition of 1.00 ppm.

The duct system applied to the experiment was manufactured using stainless pipes to prevent chemical reactions, and the wind speed inside the duct was applied at

1m/s. The picture of the duct system used in this experiment is shown in Figure 2.

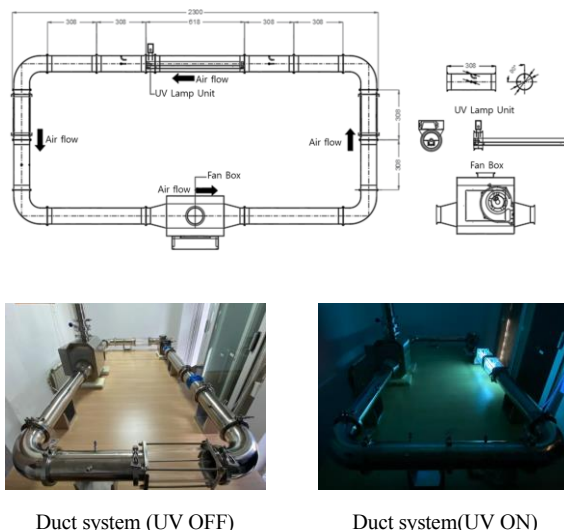


Figure 2. TiO₂ Photocatalyst Applied Duct System

In order to reduce the pressure difference between inside and outside the duct and the error that can occur during the test, it was conducted three times for each condition, and the flow rate of the injected NO gas and the measured NO gas remained constant. The flow rate and experimental system of each section are shown in Figure 3.

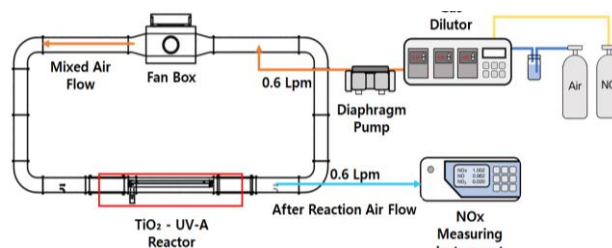


Figure 3. Experimental diagram and applied flow rate

Data presentation and Discussion

UV-A irradiance change test result

To verify the NOx reduction performance of ventilation duct systems with TiO₂ photocatalytic coating agents, the UV-A irradiance applied together in the duct system was changed to confirm the effect change with the lowest concentration reaching time. For UV-A irradiance, 25% reduction and 50% increase in irradiance were applied considering the degradation of UV-A lamps, and the results are shown in Figure 4, Table 3.

TABLE III.
EXPERIMENTAL RESULTS OF CONTAMINANT (NOX) REDUCTION BY UV-A IRRADIANCE CHANGES

UV-A irradiance	15.0 W/m ²	12.5 W/m ²	10.0 W/m ²	7.50 W/m ²
NOx reduction time	25 min	72 min	101 min	113 min

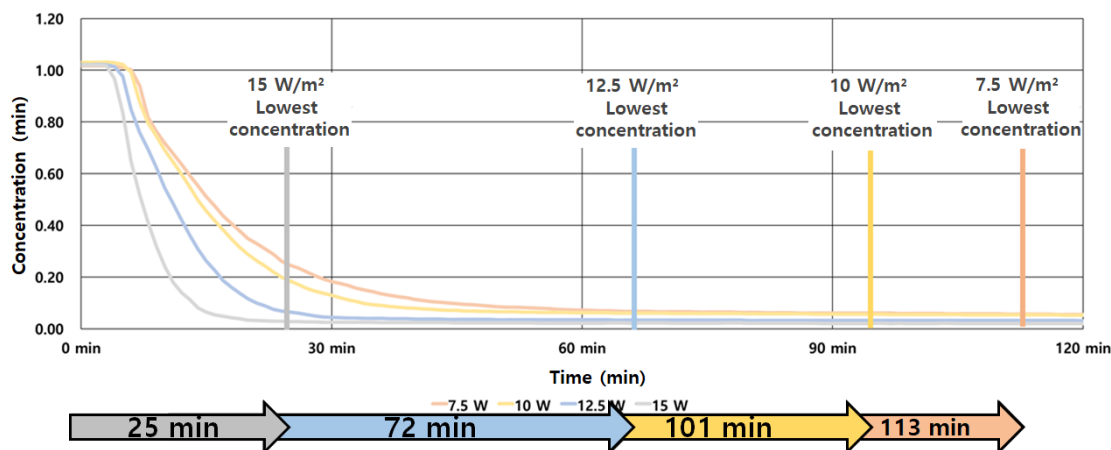


Figure 4. Result of UV-A irradiance Contaminant (NOx) Reduction Time Change

As a result of confirming the minimum concentration arrival time of NOx due to the decrease in UV-A irradiance, it was confirmed that the reduction time was drastically reduced due to the increase in UV-A irradiance. In addition, even if the UV-A irradiance is reduced by 25%, the reduction time is delayed by about 10 minutes, indicating that the NOx reduction of the TiO₂ photocatalyst can be expected over a certain UV-A irradiance.

Experiments show that the reduction time increases rapidly with experimental NOx concentrations. In particular, from the 0.75 ppm condition, which was reduced by 25%, it was found that the time was reduced by more than 50% compared to the standard experimental condition.

Based on this, the concentration of the actual environment is expected to reduce the time of reduction further compared to the experimental results.

NOx Concentration change test result

Previously, the NOx reduction performance was confirmed by changing UV-A irradiance, and the effectiveness of TiO₂ photocatalytic duct systems at NOx concentrations similar to the actual environment was also determined.

For NOx concentrations, 1.00 ppm, an international standard experimental condition, is difficult to realize under real conditions, confirming the reduction time due to reduction compared to standard conditions. The results are shown in Figure 5, Table 4.

Discussion

In order to reduce particulate matter, a representative pollutant, TiO₂ photocatalyst, one of the methods for reducing nitrogen oxides, a particulate matter precursor, was applied to duct equipment. As a result, UV-A irradiance increases, and the lower the concentration, the more the effect of reduction increases.

In particular, in the case of UV-A irradiance, the effect is expected to increase rapidly if the concentration is more than 15W/m², and if the concentration is less than 0.75ppm, so it is judged that the effect can be expected at the concentration of real condition.

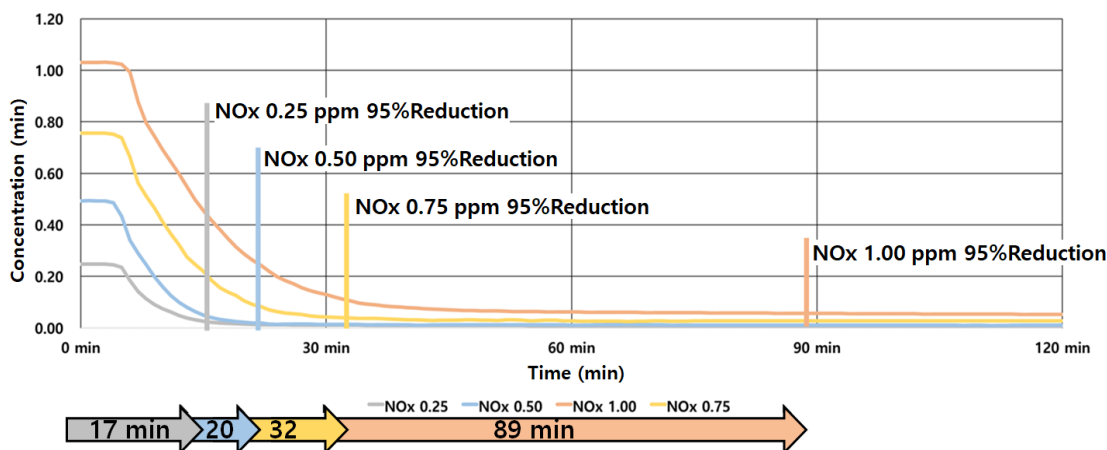


Figure 5. Result of time change of pollutant (NOx) reduction due to NOx concentration change

TABLE IV.
EXPERIMENTAL RESULTS OF REDUCING POLLUTANTS (NOX) DUE TO CHANGES IN NOX CONCENTRATION

NOx concentration	0.25 ppm	0.50 ppm	0.75 ppm	1.00 ppm
NOx reduction time	17 min	20 min	32 min	89 min

Conclusion

This study confirms the effect of the TiO₂ photocatalyst, which has the effect of reducing particulate matter precursor, a representative pollutant, according to various conditions when applied to the HVAC system, and the contents of the study can be summarized as follows.

First, Korea's particulate matter concentration has the worst environment among OECD countries, and nitrogen oxides account for the largest proportion of fine dust. Among the various methods that can reduce this, TiO₂ photocatalyst is expected to be applied to HVAC systems even in spaces where ultraviolet light is difficult to apply.

Second, the duct device was designed and manufactured to combine the TiO₂ photocatalyst and the HVAC system, and the reduction effect due to UV-A irradiance and NO_x concentration change was confirmed by comparing the lowest concentration arrival time. In all conditions, the ISO 22197-1: 2007 standard was applied as a standard experiment, and the effects of each condition were confirmed.

Third, UV-A irradiance change experiments confirmed that a 50% increase in UV-A irradiance reduces the time by 78% compared to standard conditions, allowing the lowest concentration to be reached in approximately 25 minutes. Furthermore, experiments with the NO_x concentration change confirm that applying a 75% reduction in NO_x concentration reduces the minimum concentration reach time by about 81%, which can reach the lowest concentration in about 17 minutes.

Fourth, based on the experiment, if the photocatalyst reaction section is applied to the heat exchanger and the duct of a large space in apartments, it will be able to reduce nitrogen oxides and reduce the generation of fine dust at the same time. In addition, the inflow of UV rays such as underground parking lots, shopping centers, and underground shopping malls is difficult, and if it is installed in a place where indoor air congestion can occur, it will be effective in improving air quality.

REFERENCES

- [1] IQAir, "2019 WORLD AIR QUALITY REPORT (Region&City PM2.5 Ranking)". Available online: <https://www.iqair.com/world-most-polluted-cities/world-air-quality-report-2019-en.pdf>
- [2] Wang, Z.; Liu, J. Spring-time PM_{2.5} elemental analysis and polycyclic aromatic hydrocarbons measurement in High-rise residential buildings in Chongqing and Xian, China. *Energy Build.* 2018, 173, 623–633.
- [3] National Air Pollutants Emission 2010, National Institute of Environmental Research, Ministry of Environment. Available online: <http://www.me.go.kr/mamo/web/index.do?menuId=588> (accessed on 26 May 2020).
- [4] National Institute of Environmental Research, Amount of Emissions by Air Pollutant Sector in 2016. Available online: <http://airemiss.nier.go.kr/mbshome/mbs/airemiss/index.do> (accessed on 26 May 2020).
- [5] Fujishima, A.; Zhang, X.; Tryk, D.A. TiO₂ photocatalysis and related surface phenomena. *Surf. Sci. Rep.* 2008, 63, 515–582, doi:10.1016/j.surfrep.2008.10.001.
- [6] Ballari, M.M.; Hunger, M.; Hüsken, G.; Brouwers, H. J. H. NO_x photocatalytic degradation employing concrete pavement containing titanium dioxide. *Appl. Catal., B* 2010, 95, 245–254, doi:10.1016/j.apcatb.2010.01.002.
- [7] Cassar, L.; Pepe, C.; Tognon, G.; Guerrini, G. L.; Amadelli, R. White cement for architectural concrete, possessing photocatalytic properties. *Proceedings of the 11th Int. Congr. on the Chemistry of Cement*, Durban, South Africa, May 2003
- [8] Shihui Shen, Maria Burton, Bertram Jobson, Liv Haselbach, Pervious concrete with titanium dioxide as a photocatalyst compound for a greener urban road environment. *Construction and Building Materials* 35(2012), pp. 874-883, doi : 10.1016/j.conbuildmat.2012.04.097.
- [9] Wang, H., Jin, K., Dong, X., Zhan, S., & Liu, C. (2018). Preparation technique and properties of nano-TiO₂ photocatalytic coatings for asphalt pavement. *Applied Sciences*, 8(11), 2049, doi : 10.3390/app8112049.
- [10] Wang, D., Leng, Z., Hüben, M., Oeser, M., & Steinauer, B. (2016). Photocatalytic pavements with epoxy-bonded TiO₂-containing spreading material. *Construction and building materials*, 107, 44-51, doi : 10.1016/j.conbuildmat.2015.12.164.
- [11] Yong Woo Song, Min Young Kim, Min Hee Chung, Young Kwon Yang, Jin Chul Park, NO_x-Reduction Performance Test for TiO₂ Paint, *Molecules*, 2020, 45, 4087, doi:10.3390/molecules25184087.
- [12] Yong Woo Song, Seong Eun Kim, Yong Gi Jung, Jae Yun Yoo, Jin Chul Park, Controlling Nitrogen Oxide and Ultraviolet-A irradiance in ventilation duct system using TiO₂ photocatalyst, *Building and Environment*, 2021, 199, 107881 doi.org/10.1016/j.buildenv.2021.107881.
- [13] DIN German Institute for Standardization. *Fine Ceramics (Advanced Ceramics, Advanced Technical Ceramics)—Test Method for Air-Purification Performance of Semiconducting Photocatalytic Materials—Part 1: Removal of Nitric Oxide*; Beuth Verlag GmbH: Berlin Germany, 2007.

3rd Place
REHVA
Student Competition

Asur Pablo
Menendez Inchusta
Spain

Experimental characterization of a transcritical CO₂ vapor compression system with thermoelectric subcooling

A. P. Menéndez (Atecyr).
 P. Aranguren, D. Sánchez

Due to the restrictive environmental regulations in the use of refrigerants, CO₂ is being used as working fluid as it has an ultra-low global warming potential. However, high working ambient temperatures provoke transcritical operating conditions, which drastically reduce the efficiency of these systems. Different designs have been made to improve the working conditions, for large capacity plants, some mechanisms as ejectors, parallel compression or mechanical subcooling are used. However, these solutions would be too expensive for a small system. In order to solve this problem, a thermoelectric subcooler was installed at the exit of the gas-cooler of a vapor compression system with the purpose of increasing the efficiency of the system in transcritical operation. The objective of this project is to study the behavior of the machine when different parameters such as the discharge pressure, the voltage supply to the thermoelectric subcooler or the ambient temperature are modified. Moreover, this study will obtain the optimal working point of the machine.

Key words—CO₂, Subcooling, Thermoelectric Peltier Cooler, Vapor Compression Refrigeration, Transcritical

Nomenclature

L	Annual refrigeration leakages (kg)
n	Number of working years of the installation
m	Refrigerant charge (kg)
α_{re}	Coefficient of fluid recuperation when renewing the charge (from 0 to 1)
E_{an}	Annual power consumption of the system (kWh)
β	Indirect emission factor (kg CO ₂ /kWh)
\dot{Q}_{CS}	Heat flux on the cold side of the module (W)
\dot{Q}_{HS}	Heat flux on the hot side of the module (W)
N	Number of thermocouples in a thermoelectric module
α	Seebeck coefficient (V/K)
I	Electric current (A)
T_C^{TEM}	Temperature of the cold surface of the module (K)
T_H^{TEM}	Temperature of the hot surface of the module (K)
r	Resistivity (Ohm)
k	Conductivity (W/K)

$\dot{W}_{electric}$ Electrical power supplied to the modules (W)

V Voltage applied to the modules (V)

1. Introduction

Throughout the history of refrigeration, a multitude of working fluids have been used. The reason behind so much change has been either the development of more efficient fluids or the discovery of characteristics that are harmful to people or the environment. It is the latter reason that has led to one of the greatest revolutions in the world of refrigerants.

During the last decades, the use of these fluids has been regulated due to the harmful effect they were causing to the environment. with regulations extracted from the Montreal and Kyoto's protocols, among others, among which F-gas stands out [1], figures were created that quantified the effect of these fluids on the environment. The first was the ODP (*Ozone Depletion Potential*), which quantifies the power of destruction of the ozone layer of the refrigerants, and a maximum ODP of 0 was established taking as a reference the refrigerant R-11 whose ODP is 1 [2]. Moving on to the most important built figures, the GWP₁₀₀ (*Global Warming Potential*) should be mentioned first. This quantifies the global warming potential, in 100 years, of these compounds when released into the atmosphere. After the F-gas regulation a maximum value of GWP₁₀₀ of 150 was imposed, taking as reference the CO₂ (R-744) whose GWP₁₀₀ is 1. In Table 1, several of the most common refrigerants are shown with their corresponding ODP and GWP₁₀₀ [3]. Therefore, most commercial refrigerants used to date are prohibited. However, as can be easily deduced, refrigerants do not only pollute when released into the atmosphere. Therefore, the TEWI parameter (*Total Equivalent Warming Impact*) was created, a figure that brings together all the processes in which these fluids are involved and pose a risk to the environment. This figure takes

TABLE I. ENVIRONMENTAL IMPACT COEFFICIENTS OF SOME COMMOND REFRIGERANTS

Refrigerant	Formula	ODP	GWP ₁₀₀
R-11	CCl ₃ F	1	4660
R-32	CH ₂ F ₂	0	677
R-134a	CH ₂ FCF ₃	0	1300
R-152a	CH ₃ FCF ₂	0	138
R-290	C ₃ H ₈	0	3
R-404A	44% VHF ₂ CF ₃	0	3943
	4% CH ₂ FCF ₃		
	55% CH ₃ CF ₃		
R-410A	50% CH ₂ F ₂	0	1924
	50% CHF ₂ CF ₃		
R-600a	C ₄ H ₁₀	0	3
R-1234yf	CF ₃ CF=CH ₂	0	1
R-744	CO ₂	0	1

into account both direct pollution, produced by coolant leaks, and indirect pollution, produced by the renewal of the fluid used and the electrical energy consumed during its life. Equation (1) shows the expression for determining the TEWI.

$$TEWI = (GWP_{100} \cdot L \cdot n) + (GWP_{100} \cdot m \cdot (1 - \alpha)) + (n \cdot E_{an} \cdot \beta) \quad (1)$$

Considering all these aspects described, research in the field of refrigeration is focusing on finding a fluid that can combine good working properties and optimal GWP and TEWI. One of these refrigerants, which had already been used in the first cooling systems, is CO₂ (R-744), as it has really attractive properties for a refrigerant and an exceptionally low global warming potential. The research done by Kim MH, Pettersen J, Bullard CW et al. [4], presents a broad study of CO₂ as a refrigerant among other aspects. Some of the most important information that must be subtracted is the low critical point of the carbon dioxide. When being subjected to high working temperatures, the fluid reaches critical conditions. That is, when working at some point in the system above the critical point, which is from 31.98 °C and 73.77 bar, the properties of the fluid undergo drastic changes which eventually cause the efficiency of the system to be greatly reduced. Conditions that can be easily found in the south of Europe.

As for the refrigeration system is concerned, the study begun by considering the simple cycle, which is composed by 2 heat exchangers: the evaporator (extracts heat from the cold reservoir) and the condenser (transfers heat to the hot reservoir), a volumetric valve and a compressor. With this simple configuration the efficiency obtainable is limited. Therefore, various configurations and technologies have been developed to increase the COP (*Coefficient of Performance*), which is a figure that compares the cooling capacity obtained against the work introduced. Among these, the intermediate heat exchanger (IHX) [5], the Flash Gas Bypass [6], the ejector [7], the mechanical subcooling [8] or the thermoelectric subcooling should be highlighted. All these try to increase the enthalpy jump produced in the evaporator, which is directly related to the amount of heat absorbed in the place to be cooled. These configurations are indisputable. However, all except the last one mentioned, are excessively expensive for medium and low capacity equipment, as well as complicated operation and maintenance.

Thermoelectric cooling is present in many everyday appliances such as small refrigerators or wine cellars, but thermoelectric sub-cooling applied to refrigeration cycles with vapor compression must be studied in depth because theoretical studies confirm that it is a viable solution that could become a revolution in the medium and low capacity refrigeration sector [9]. Furthermore, it is worth adding the low production, operation and maintenance costs required by thermoelectricity, as well as its high reliability, robustness, and ease of use.

Therefore, the hybridization of the refrigeration technology with steam compression and thermoelectricity, especially in installations with CO₂, would produce important improvements in the global operation of the installation and therefore be presented as a very novel solution with great possibilities of implementation in small and medium size equipment.

This project was born from the collaboration between two research groups, the GIT research group of the Universitat Jaume I (UJI), which contributed with its wide knowledge in the field of refrigeration (particularly with the use of CO₂ as a working fluid); and the ITF group of the Universidad Pública de Navarra (UPNA), which has a great background in the branch of

thermoelectricity and its applications. From this fruitful collaboration emerged the main objective of this End of Degree Project: The experimental characterization of a cooling system, working with transcritical CO₂ and with thermoelectric subcooling. For this purpose, the cooling system was previously built and tested without thermoelectric subcooling using these values to validate the computational model that contemplates the cooling cycle with thermoelectric subcooling. Thanks to the validated model, the feasibility of technological hybridization is studied, leading to the incorporation of the thermoelectric sub-cooler in the CO₂ installation to obtain the improvements in experimental COPs.

This study tries to demonstrate the viability of the use of CO₂ in adverse environmental conditions, which can be easily found in Spain, thanks to the TESC (*Thermoelectric Subcooling*) configuration. This combination results in a very novel system that has hardly been studied experimentally and that could lead to a new generation of medium and low power cooling systems.

2. Computational study of the combination of vapor compression and thermoelectric subcooling for transcritical CO₂

2.1. Experimental study of the initial configuration

As previously mentioned, the first step after the construction of the initial installation was to test it under different working conditions. The following ambient conditions were set for testing the installation: evaporation temperature of -10°C, useful superheat of 1.5-2°C, outside temperature of 30°C and relative humidity of 55-60%, class IV climatic conditions.

To obtain the different working points, the discharge pressure was varied by changing the refrigerant charge. The results obtained for the constructed installation can be seen in Figure 1.

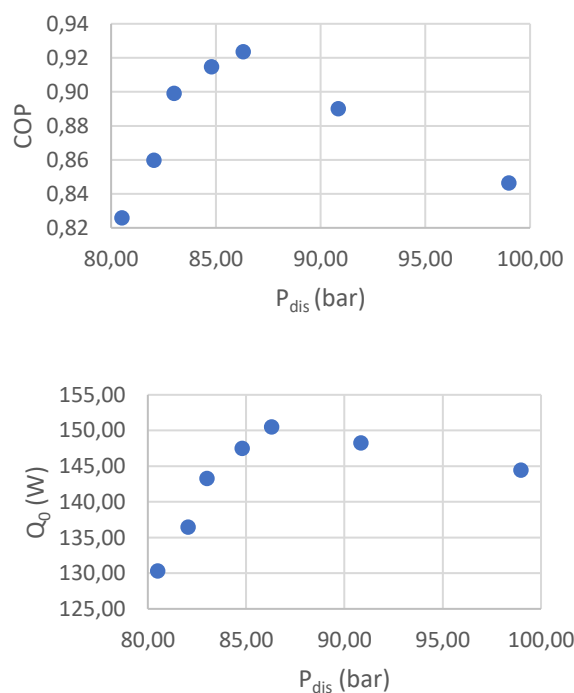


Figure 1. COP and cooling capacity obtained for different discharge pressures with the initial installation.

As can be seen, the trend in the results is clear, as the discharge pressure increased, so did the enthalpy jump, so both the cooling capacity and the COP increased. However, when certain discharge pressure values were reached, the extra work required by the compressor and its consequent drop in efficiency due to the actual operating point, caused both factors under study to worsen.

2.2. Computational model and validation

To validate the results obtained experimentally, a computer model was developed using the program MATLAB. The main objective of this step was to create a tool that could predict the behavior of the installation when working conditions vary. The model included all the characteristics of the installation, compressor, test conditions, as well as the functions required to calculate the thermodynamic processes that occur in it. In this way, a sweep of the discharge pressures obtains the different working points to be validated.

As shown in Figure 2, the model is capable of predicting the operation of the refrigeration system, especially in the area of increasing COP and optimum operation. However, on the right side of the graph, it can be seen that the slope of the experimental values is steeper than the model. This may be due to several uncertainties that were neglected. The conclusion to extract from this study is that the model was able to predict the performance of the system when working with lower discharge pressures, which are the ones obtained at the optimum working points. As the pressure increases, the properties of the fluid get worsened producing a decrease in the global efficiency.

2.3. Computational model with TESC

Once it was demonstrated that the computational model of refrigeration worked correctly, a thermoelectric cooling sub-model was included, which the ITF group of the Public University of Navarra treasures after many years of research. This model includes all the thermoelectric processes (Seebeck, Joule, Peltier, and Thomson effects) and has been validated previously. The sub-model designed will be based on the thermoelectric module DT12-8L from Marlow industries.

The main effect of the thermoelectric subcooling and the TEMs (*Thermoelectric Modules*), is the Peltier effect. Due to this, a module would extract heat from one of its surfaces and dissipate this heat on the other surface, plus the electric consumption.

In order to fully model the TEMs performance, several temperature dependent figures such as the Seebeck coefficient or the thermal resistances of the dissipation system, should be studied. For the first case, several studies were carried out with the subcooling system and the data was treated and approximated, to simplify the model. Then, for the thermal resistances of the dissipation system, in a previous investigation made by P. Aranguren et al. [10], the researchers studied the benefits of combining heat pipes with TEMs to dissipate heat. Representative values of this study were selected.

The TESC system was proposed, heat would be extracted from the refrigeration system with the help of heat pipes ending in TEMs. So, gathering all the thermoelectric effects and applying them to the case of study, the following equations that model the performance of the TESC were obtained. Equations (2) and (3) represent the heat transfer occurring on the cold and hot side, respectively, of the modules; (4) is the general expression of a thermal machine and (5) models the current consumption.

$$\dot{Q}_{CS} = 2N \left(\alpha I T_c^{TEM} - \frac{1}{2} I^2 r - k(T_H^{TEM} - T_c^{TEM}) \right) \quad (2)$$

$$\dot{Q}_{HS} = 2N \left(\alpha I T_H^{TEM} + \frac{1}{2} I^2 r - k(T_H^{TEM} - T_c^{TEM}) \right) \quad (3)$$

$$\dot{Q}_{HS} = \dot{Q}_{CS} + W_{electric} \quad (4)$$

$$I = \frac{V - 2N\alpha(T_H^{TEM} - T_c^{TEM})}{2Nr} \quad (5)$$

Being a TESC system, the TEMs are located at the exit of the condenser/gas-cooler, to obtain the subcooling of the refrigerant. With the purpose of knowing the global operation of the hybrid system, different parameters of the system were modified, such as the voltage of the thermoelectric modules or the discharge pressure, as shown in Figure 3 in which four thermoelectric modules have been simulated.

The most important conclusion to be drawn from these results is the promising potential that thermoelectric subcooling appears to have. The inclusion of thermoelectric cooling in the cycle has meant a theoretical increase of 21.06% in the COP.

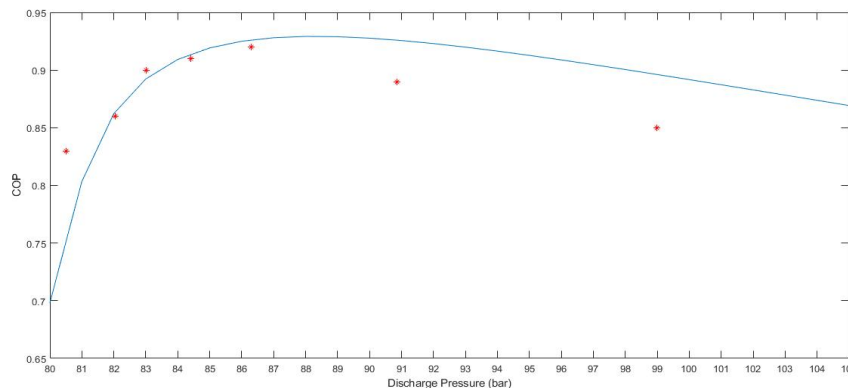


Figure 2. Comparison of the variation of the COP with the discharge pressure between experimental (dots) and computational tests (continuous line).

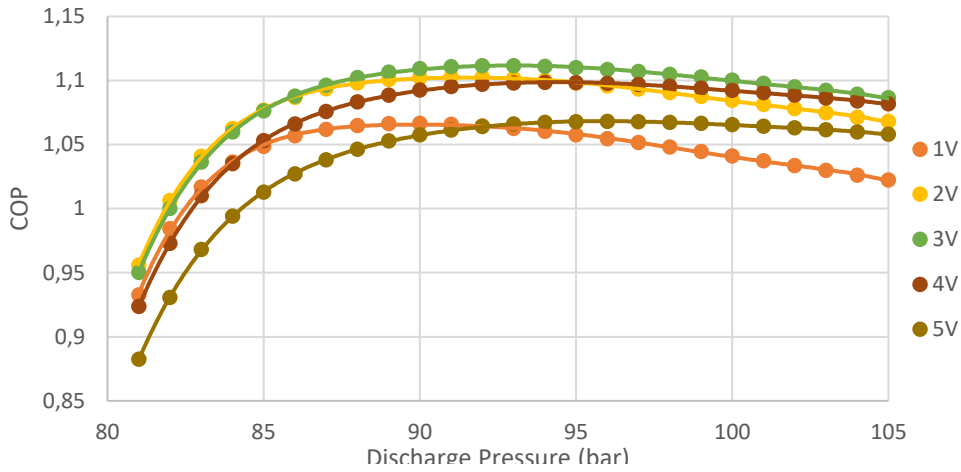


Figure 3. Computational results of the values of COP variation with the discharge pressure for several voltages applied to the TESC.

3. Experimental study of the COP increase of a vapor compression system with trans-critical CO₂ thanks to thermoelectric subcooling

Considering the promising results obtained, the thermoelectric subcooling module, Figure 4 left, was built to be placed in the experimental facility. This device consisted of 4 thermoelectric modules model DT12-8L, which would be placed between the CO₂ flow and the environment. In order to optimize the system, a channel exchanger was placed in the cold side of the modules, while a heat pipe was placed in the hot side. It should be noted that this is a unique installation since it has been developed in its entirety to demonstrate the viability of thermoelectricity as a technology to be implemented in the sector of refrigeration by vapor compression.

After the new configuration of the installation was set, it was expected that the cycle would change from the initial one. In order to evaluate this change, the tests carried out on the initial installation were replicated, modifying the voltage at each of the discharge pressures with which the thermoelectric modules were fed, since it was observed, thanks to the computer model, that this parameter is vital for optimizing the operation of the system.

The main goal of the experimentation was to check the changes that the new configuration produced in the results obtained. So, the same procedure and same initial conditions, as in the initial procedure, explained in section 2.1, were followed. In order to have an overall understanding of the installation performance, four different loads of carbon dioxide were analyzed. The main difference in the procedure between the initial configuration and the one with the TESC system was, that it was needed to find not only the optimum working point for each CO₂ charge, but also to find the optimum voltage applied to the modules. Hence, each

load was tested 5 times, finding the desired stationary state of the installation with voltages of 0, 1, 2, 3 and 4 V.

The results obtained were very promising, as shown in Figure 5. This figure represents the effect of including the thermoelectric subcooling on the cooling capacity and the COP, as a function of the voltage applied to the Peltier modules.

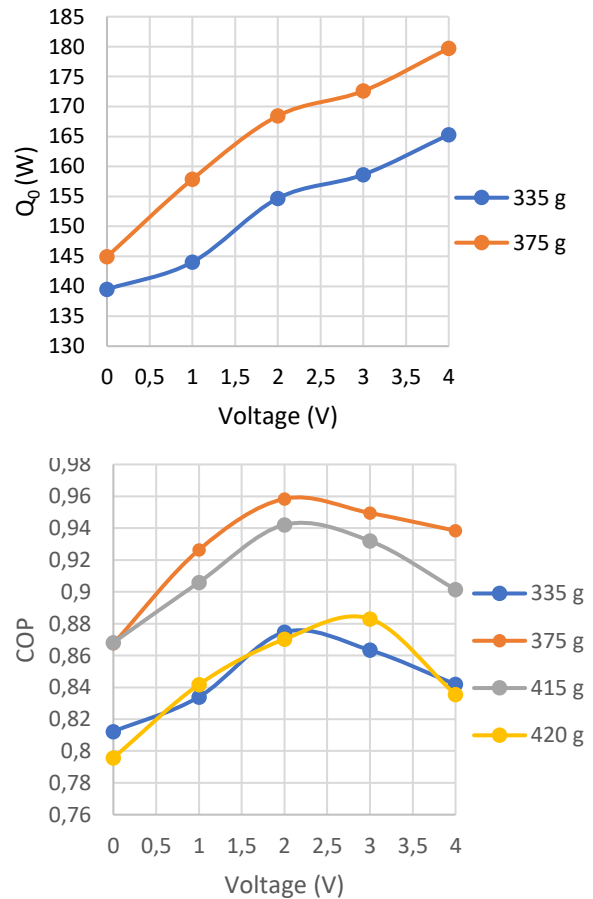


Figure 5. Variation of the cooling capacity and the COP with the voltage applied to the TEMs.



Figure 4. TESC system (left) and final installation (right)

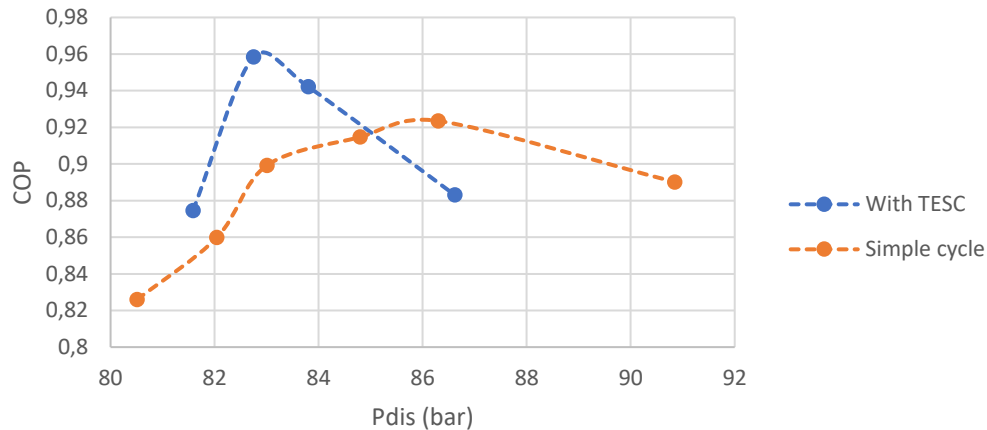


Figure 6. Variation of the COP with the discharge pressure of the tests with the initial installation and the tests using the TESC configuration.

It is easy to see the great impact that the addition of thermoelectric modules has on the system. An increase of 24% in the cooling power is observed when the modules are fed at 4 V while the increase in COP achieved experimentally amounts to 10.5%, a more than considerable value when considering the hybridization of vapor compression cycles with thermoelectric technology.

To these promising results should be added the fact of the optimum pressure reduction, a fact to be considered, since it leads to the installation working in more favorable conditions, as shown in Figure 6. This figure shows the optimum POPs for each discharge pressure for the case of the initial cooling installation and the case that includes thermoelectric subcooling.

4. Conclusions

Nowadays society is facing one of its greatest challenges, global warming. In particular, the historically highly changing refrigeration sector is facing the challenge of complying with extremely strict regulations while meeting the demands of users. So far, there are two lines of research, the development of new refrigerants that comply with regulations; and the improvement in current technologies to be able to use disused refrigerants. This is where the project started, as it tried to make it possible to use a refrigerant with a small polluting power in any location or area.

This project focused on combining thermoelectric refrigeration with vapor compression technology with a CO₂ cycle. It is a project that has deepened in an area that until now was almost unexplored. Previously, computer models had been made with this configuration. However, it is extremely difficult to find prototypes that combine both technologies. For this reason, the results obtained are very novel and shed light on a future for the technology that was uncertain, since with this prototype both the cooling power and the efficiency of the system have been significantly increased, among other factors.

Ultimately, with this project a wall has been broken. It has been proven that the use of CO₂ in a refrigeration system with harsh conditions, may be feasible when improving the installation, as this was a prototype made in a laboratory. By the selection of the optimum components for this type of installation and the industrialization of the building process, a more efficient

installation would be obtained. Moreover, the thermoelectric subcooling system has demonstrated to be a really good alternative to the common subcooling configurations, in low to medium capacity refrigeration systems. Opening a field of study that has not been broadly investigated, which could end up having great industrial repercussion.

5. References

- [1] M. Schulz and D. Kourkoulas, "Regulation (EU) No 517/2014 of the European Parliament and of the Council of 16 April 2014 on fluorinated greenhouse gases and repealing Regulation (EC) No 842/2006," Off. J. Eur. Union, vol. 2014, no. 517, p. L150/195-230, 2014.
- [2] The European Parliament and the Council of the European Union, "REGULATION (EC) No. 1005/2009," Off. J. Eur. Union, vol. L 286, 52, 2009.
- [3] T. F. Stocker, Climate change 2013. 2014.
- [4] Kim MH, Pettersen J, Bullard CW. Fundamental process and system design issues in CO₂ vapor compression systems. vol. 30. 2004. doi:10.1016/j.peccs.2003.09.00.
- [5] D. Sánchez, J. Patiño, R. Llopis, R. Cabello, E. Torrella, and F. V. Fuentes, "New positions for an internal heat exchanger in a CO₂supercritical refrigeration plant. Experimental analysis and energetic evaluation," Appl. Therm. Eng., vol. 63, no. 1, pp. 129–139, 2014.
- [6] R. Cabello, D. Sánchez, J. Patiño, R. Llopis, and E. Torrella, "Experimental analysis of energy performance of modified single-stage CO₂transcritical vapour compression cycles based on vapour injection in the suction line," Appl. Therm. Eng., vol. 47, pp. 86–94, 2012.
- [7] C. Lucas and J. Koehler, "Experimental investigation of the COP improvement of a refrigeration cycle by use of an ejector," Int. J. Refrig., vol. 35, no. 6, pp. 1595–1603, 2012.
- [8] R. Llopis, R. Cabello, D. Sánchez, and E. Torrella, "Energy improvements of CO₂ transcritical refrigeration cycles using dedicated mechanical subcooling," Int. J. Refrig., vol. 55, pp. 129–141, 2015.
- [9] Astrain, D.; Merino, A.; Catalán, L.; Aranguren, P.; Araiz, M.; Sánchez, D.; Cabello, R.; Llopis, R. Improvements in the cooling capacity and the COP of a transcritical CO₂ refrigeration plant operating with a thermoelectric subcooling system, Applied Thermal Engineering, 155, 110-122, 2019.
- [10] P. Aranguren, S. DiazDeGarayo, A. Martínez, M. Araiz, D. Astrain, "Heat pipes thermal performance for a reversible thermoelectric cooler-heat pump for a nZEB", Energy and Buildings, Volume 187, 2019, Pages 163-172

HVAC World
Student Competition
Other Participants' Contribution

Joshua Vasudevan	USA
Khyati Paghdar & Raj Gupta	India

Predicting Thermal Comfort Using Thermal Imaging Technology

Joshua Vasudevan¹, Mahroo Eftekhari¹, Xiaoyan Luo¹, Faisal Durrani¹

¹School of Architecture, Building and Civil Engineering, Loughborough University, Leicestershire, United Kingdom. LE11 3TU

j.vasudevan@lboro.ac.uk, m.m.eftekhari@lboro.ac.uk

Abstract - Previous field studies in thermal comfort were aimed at understanding the relationship between indoor environmental conditions and occupants thermal comfort sensation. In many experiments, the physiological parameters were used to predict thermal comfort. This study however focuses on predicting the occupant's indoor thermal comfort using non-intrusive physiological measurement. The relationship between thermal images of occupants, skin temperatures and their thermal comfort together with the practical applicability of this method for predicting thermal comfort was investigated. Experimental studies were conducted in an environmental chamber as well as field studies for validation of the comfort study results from a large open plan mixed mode ventilated office during July 2019. Thermal sensations of the participants were compiled using questionnaires, together with measured physical and physiological factors. Thermal images of the face were captured during the experiments. Based on the experimental data, a model for predicting an individual thermal comfort using thermal imaging and skin temperature was developed. The proposed evaluation method based on thermal imaging and Fanger's PMV scale provides a non-intrusive and simple method to evaluate an individual's indoor thermal comfort.

Index terms- Thermal comfort, Indoor Environmental Quality, Thermal imaging, Occupant comfort.

Introduction

Nowadays Infrared imaging technology is used in many mobile devices. In the field of medicine, thermography is used for breast screening to detect cancer at its earlier stage [1]. During pandemic in 2003, government and airport personnel used thermography to detect suspected flu cases [2]. Technological innovation is increasing and the whole world is moving towards technology. Recently, research has been conducted in vehicles to regulate the cabin temperature using thermography to predict the driver's thermal comfort and automate cabin environment settings [3]. Building energy management systems (BEMS) have been used to maintain the indoor thermal comfort in buildings through which the set point temperature can be specified and maintained through the thermostat. The thermostat temperature settings in an office building with 240 rooms has been investigated in Beijing during a summer week from August 16th to 23rd 2012 [4]. The statistics show that in summer only 50% of the thermostat temperature

settings fall in the comfortable temperature range of 23 – 26 °C recommended by ASHRAE [5]. Moreover, 22% of thermostats temperature settings were lower than 16 °C. Room occupants don't desire to have these extremely high or low temperature. All they want is to quickly cool down or heat up the room. After returning to work they tend to forget to change the temperature setting back to the comfortable range until the environment gets over cooled or overheated which reduces their productivity. This results in more energy demand for heating and cooling and an uncomfortable thermal environment. This inappropriate indoor thermal comfort leads to higher possibility of personal errors, lower productivity and higher energy consumption in the buildings [6]. Therefore, indoor thermal comfort should be maintained properly and automated in buildings.

II. LITERATURE REVIEW

People spend most of their time indoors therefore the indoor thermal environment should be comfortable enough to make the occupants feel comfortable so that it will increase their health and productivity [7]. Thermal comfort express the satisfaction of the thermal environment in the mind of people [5]. Thermal comfort assessment not only improves the wellbeing of the occupants but also helps to increase the energy efficient performance of the systems in building. Thermal comfort can be assessed by many models which were developed by researchers but the first steady state model was developed by Fanger and he used the thermal sensation scale of +3(hot) to -3(cold) [8] which is still the standard comfort tool for thermal comfort assessment. This was followed by the development of the adaptive model since occupants tend to adapt to their thermal environment by making certain changes [9]. Various physiological and physical aspects were used by the researchers to access the thermal perception of occupants in indoor. One of the physical aspect which has been used [10] [11] is the skin which is then related to the thermal sensation of occupants and their physical responses in the thermal comfort study. Previous studies looked at the occupant's comfort level for thermally conditioned buildings using the Fanger's model. Skin is one of the sensory organs adopted by many researchers in the process of determining thermal comfort of the occupants since it has a physiological interface with the thermal environment.

When the physiological regulations are minimized then thermal comfort occurs [5] [12]. The human body's core temperature is maintained within a small range between 36°C and 38°C and the two most important sensors controlling the body temperature are located in the skin and hypothalamus [13]. The skin has thermoreceptors in the body [14] and the thermoreception process allows humans to regulate behavioural and autonomic thermoregulatory responses [15]. Detecting these human physiological responses provides a way for researchers to understand human thermal comfort levels under different conditions and this idea was implemented by measuring the human bio signal variations such as skin temperature, heart rate and respiration rate [16]. Liu [17] observed the time gradient of the skin temperature that can predict the thermal sensation in cold environments and its correlation with the heat loss from the skin. The mean skin temperature has been used to evaluate the personal thermal sensations in various studies [18] [19] [20]. A new model was developed by Weiwei [10] in order to evaluate the individual thermal comfort using the mean skin temperature. The study had 22 subjects whose local skin temperatures were recorded at the air temperature of 21°C, 24°C, 26°C and 29°C. The results below show the mean skin temperature obtained by the study and their thermal comfort based on the experimental data obtained.

Cool discomfort, if $T_{sk} < 32.6$ °C; Comfort, if 32.6 °C $\leq T_{sk} \leq 33.7$ °C and Warm discomfort, if $T_{sk} > 33.7$ °C Korukcu [3] found that the forehead skin has an almost uniform distribution of temperature and it is usually exposed to the environment. The hand has more thermoreceptors than other parts of the body therefore previous researches used the hands skin temperature to evaluate human thermal sensation. Ruth [21] suggests that measurement must be made on the human body surface which are homogeneous with respect to temperature and reflect reasonable changes in true mean skin temperature. The mostly exposed part of the human body is the facial skin because hands can be covered in clothes or under the table in offices, but a face will be exposed to the thermal environment all the time. Facial temperature is of great interest for the evaluation of the cerebral thermoregulation and it is the index of the autonomous nervous system activity [22]. The thermal analysis by thermography stands as an interest because any body, at certain temperature, emits energy in the form of infrared radiation. In all living organisms, thermography manifestation of the blood irrigation can be controlled by the activity of the sympathetic nervous system [23]. A study was conducted in FIAT Albea 2005 car parked outside in which they measured the ordinary transient temperature difference between drivers' cabin and the drivers face and they used thermal camera to capture thermography to predict thermal comfort in vehicles [24]. A gap remains with the integration of novel approach with thermal imaging technology to calculate the skin temperature and mapping the thermal comfort of the occupants. These images and heuristic algorithms can be linked with BEMS to automatically adjust the

environmental condition to improve human thermal comfort and energy in buildings.

In order to overcome the research gaps, which showed that it is critical to explore non-intrusive methods and complicated analysis of thermal images to predict thermal sensation of people, this study investigates the practical method of analysing infrared thermal images and using mean skin temperature of the human face to map the range of skin temperature for each of 7 scales of Fanger's PMV.

III. METHODOLOGY

A. Experimental setup

The experimental survey took place in two places one in the controlled environmental chamber. The second survey took place in a real scenario in an open plan building which is a mixed mode ventilated. The experiment was carried out during the period from 01st July to 19th July, which was a typical summertime in the UK. All the experiments were conducted during the afternoon from 13:00 to 16:30. The experiments were conducted inside an environmental chamber which had the capacity to create an indoor environment condition of 50°C to -10°C. The length and breadth of the chamber is 4 m. The room had normal office lighting and the temperatures were pre-set for each timing in the computer program. The participants were instructed to sit in a normal office chair just opposite to the air conditioning vents with equal spacing between them (Fig. 1). Air temperature and relative humidity of the ambient indoor environment were monitored and recorded for every minute interval by Testo 925 thermo sensor which was placed near the participants at a height of 1.1m near their face. The thermal camera was FLIR T640bx camera. The camera has a high quality 30,200-pixel (640 x 480) image quality. It has an accuracy of ± 2 °C [25]. The camera has features that can blend together a thermal image with a normal image or alternatively superimpose IR over a digital image inside a fully adjustable window [25]. The technical specification of the FLIR T640bx is given in Table. 1. In order to validate the accuracy of the thermal camera i-buttons were used on two participants.



Figure 1. Experimental chamber

B. Experiment protocol

Each participant participated only once during the field studies. In total the 20 participants comprised of 11 females and 9 males whose images and questionnaires were collected. They were all students and were not taking any medication. The age range of the participants was 20 to 30 years old with an average age of 24. The subjects were divided into groups of 3 people each day with different combination of transient temperatures. The chamber's relative humidity was in the range of 40 – 60%. The subjects stayed in a buffer room for 10 minutes to get adapted to the indoor temperature and feel comfortable before entering the chamber.

They were asked to sit in the chamber and the temperature was set in the range of (14-32)° C and their thermal comfort was recorded every 15 minutes through the questionnaire and their thermal image was taken every 5 minutes through the FLIR camera. Then the temperature was increased by 3°C and maintained for 15 minutes and the thermal comfort sensation and the thermal image was recorded for every 5 minutes.

TABLE I.
THERMAL CAMERA SPECIFICATION (Source: Tester, 2019)

Features	Description
Thermal sensitivity	<0.035°C at 30°C
Zoom	8X continuous
Temperature range	-40°C to 650°C
Image resolution	640 x 480 pixels
Spectral range	7.5 to 14µm
Image modes	Thermal/Visual/Fusion/P-i-P
Measurement modes	10 spot meters, 5 box areas, isotherm, Delta-T, auto hot/cold

For the first three days the subjects were introduced into the environment where the temperature changes from cold to hot after that for the next three days the temperature was changed from hot to cold. During the experimental period the occupants could change their clothes. This is because to monitor the skin temperature irrespective of the clothing however the clo values were observed and were used to calculate the PMV.

The research building chosen for validating the chamber values in real scenario is located at Loughborough University. This is a deep open plan office and survey was carried out between 12th - 15th July between 13:45 to 14:45 p.m. The occupants recorded their thermal sensation every 15 minutes, and their thermal image was captured using the FLIR 640bx. The occupants were from a range of different nationalities and culture. A total of 24 occupants took part in the survey (9 females and 15 males). Since it was summertime the ventilation systems were working, and the heating system was off. In order to measure the indoor environmental conditions such as the air temperature, humidity and CO₂ levels, the HOBO MX was used, and the mean radiant temperature was measured using a global thermometer.

IV. RESULT ANALYSIS

The thermal images were analysed using MATLAB. A program code for extracting the mean skin temperature from the thermal image was created. When the code runs a graphic user interface (GUI) appears in which the thermal image can be uploaded, and the mean skin temperature of the face can be extracted. During the period the Fanger's PMV and the mean skin temperature of the face were calculated. When the temperature was increased from cold to hot the occupant's neutral sensation was recorded at 20 °C and during the transient temperature change from hot to cold the occupant's neutral sensation was recorded at 26 °C. The clothing insulation level inside the chamber was in a range of 0.4 to 0.9 clo. The participants could change their clothing levels if they wanted. Fig.2 shows the clothing insulation levels of the participants.

The mean facial skin temperature for the participants in the experimental chamber during the transient temperature rise from cold to hot was analysed and is shown in Fig. 3. It can be noted during the cold sensation the skin temperature is less and it increases with the rise

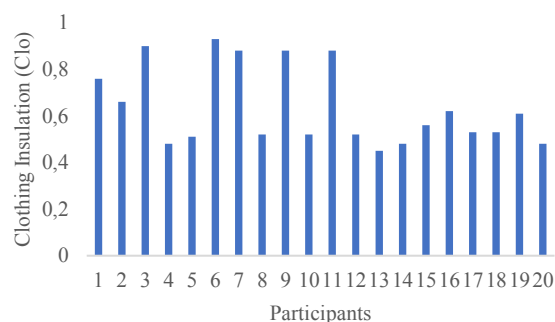


Figure 2. Clothing insulation of participants

in temperature. The temperatures ranges are shown in Table 2. The accuracy is the percentage of votes for the thermal sensation for the corresponding mean skin temperature Likewise, the skin temperature for the transient temperature decreasing from hot to cold was also similar and is shown in Fig. 4. From the Table 3 it can be noted that the PMV scale Hot is not reached. This may be due to the prevailing summer condition that would have affected the PMV from reaching the hot thermal sensation for the participants.

The relation between mean facial skin temperature range and PMV as calculated in the environmental chamber was validated in the open plan building. The facial skin temperature range for a PMV scale of neutral was within the range of 33.9 °C to 35.1 °C and the graph (Fig. 5) shows that 91.15% of the occupants whose PMV was neutral was within the above range. This shows that the range which was calculated from the environmental chamber was applicable to the occupants in the office space (real scenario) irrespective of the clothing insulation. Fig. 6 shows the thermal images for cold sensation, neutral and hot sensation. The difference in the colour map of the image can be easily identified as shown in Fig. 6.

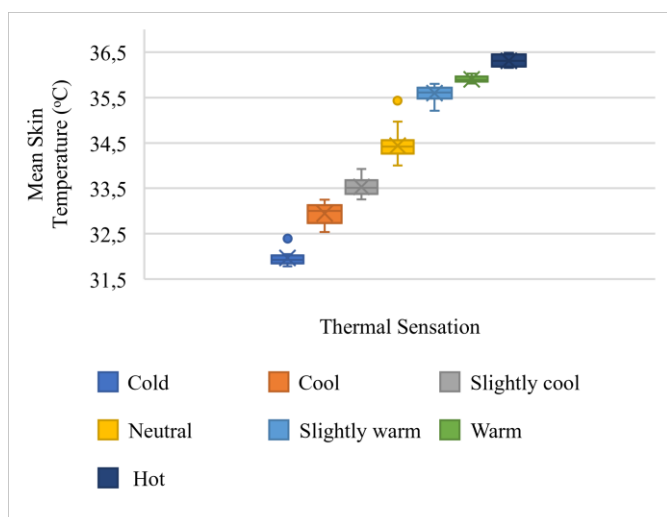


Figure 3. Mean skin temperature and thermal sensation (Cold to hot)

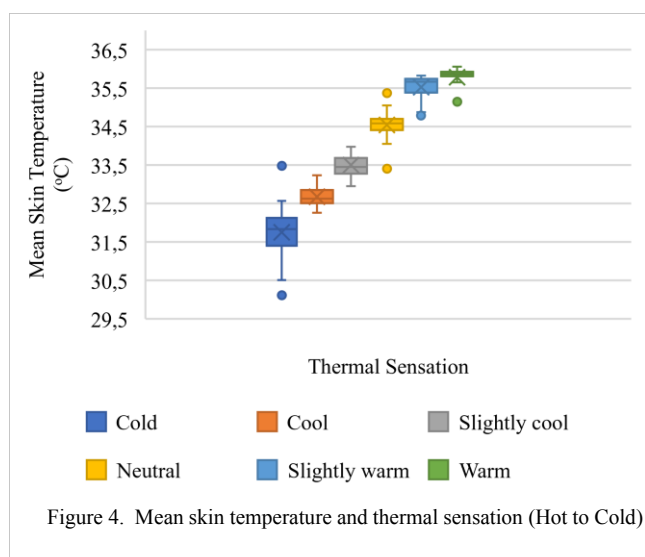


Figure 4. Mean skin temperature and thermal sensation (Hot to Cold)

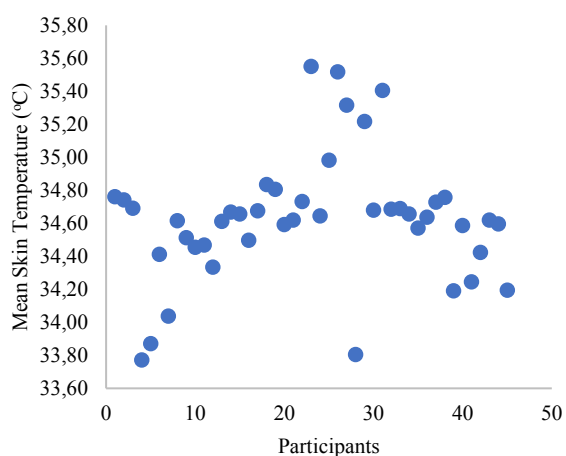


Figure 5. Mean skin temperature of participants in Research hub

TABLE II.
THERMAL SENSATION AND MEAN SKIN TEMPERATURE (COLD TO HOT)

Thermal sensation (PMV)	Mean Skin Temperature range (°C)	Accuracy
Cold	< 32.5	99.1 %
Cool	≥ 32.5 - < 33.2	92.11 %
Slightly cool	≥ 33.2 - < 33.9	95.35 %
Neutral	≥ 33.9 - < 35.1	98.55 %
Slightly warm	≥ 35.1 - < 35.8	97.96 %
Warm	≥ 35.8 - ≤ 36.1	98.55 %
Hot	>36.1	99.15 %

TABLE III.
THERMAL SENSATION AND MEAN SKIN TEMPERATURE (HOT TO COLD)

Thermal sensation (PMV)	Mean Skin Temperature range (°C)	Accuracy
Cold	< 32.5	98.5 %
Cool	≥ 32.5 - < 33.2	78 %
Slightly cool	≥ 33.2 - < 33.9	91.9 %
Neutral	≥ 33.9 - < 35.1	89.37 %
Slightly warm	≥ 35.1 - < 35.8	89.67 %
Warm	≥ 35.8 - ≤ 36.1	80 %

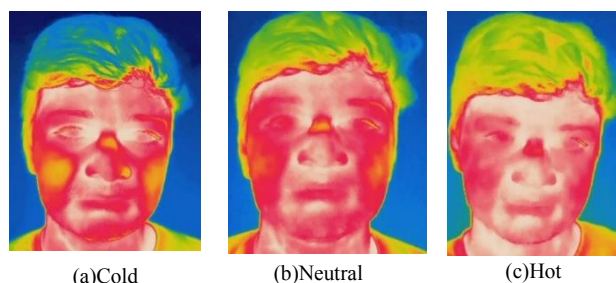


Figure 6. Thermal image and their thermal sensation

V. Discussion

An experimental and field study was carried out in order to use thermal imaging technology to develop a non-intrusive method of predicting thermal comfort. The experiment results from the environmental chamber shows that the mean facial skin temperature represents the thermal sensation of the occupants according to the change in their thermal environment. Due to the increase in temperature of the surroundings the skin temperature increases and the decrease in temperature decreases the skin temperature. Since occupants get adapted to their local air temperature after certain time the extreme thermal sensation such as hot and cold were only recorded a very few times during the experiment. The participants were seated exactly 1 m apart and this may have created a local discomfort for the participant seated in the middle because the participant seated in the middle during the experiments felt slightly warm than the other 2 participants on the either side. Moreover, for a small change in room temperature there was a significant change in the skin temperature. The skin temperature from facial regions reacted in different magnitudes which is due to the different thickness of the subcutaneous fat layer, the amount of skin blood flow and the density of blood vessels [26]. The accuracy as stated in previous section shows that there is a small percentage of skin temperatures which are outside the range. This is due to the adaptivity by the body because some people have body types which tend to heat up or cool down quickly than others. The hot sensation was not noted during the transient temperature change from hot to cold. This may be due to the outdoor temperature during the days of experiments because it was summer season and the heat burden from the outside temperature could have accumulated and this affected the skin temperature during the initial time of the experiment. This effect causes sweating, and this affects the skin temperature and the thermology of the face. The thermal sensation changing from slightly warm to warm and slightly cool to cool was quick and this reflected the sensitivity of the skin and the mean skin temperature for this is in a very little range. The range for mean skin temperatures were chosen because all the nationalities participated in the experimental chamber test and the field survey were mostly within these ranges. A previous study [27] shows similar evaluation model of thermal comfort with maximum thermal comfort associated with mean skin temperature was around 33.5 °C at rest and another study [10] for sedentary subjects showed that at a mean skin temperature of 33.3 °C the occupants felt comfortable and at 31 °C they felt uncomfortably cold. The study by Olesen and Fanger [28] and Sakoi [29] also showed that the occupant at rest had a mean skin temperature of 33.5 °C. All the values recorded during the above experiments for occupants at rest and sedentary were of 33.5 °C and 33.3 °C respectively during which the metabolic rate was 1.0 met. This study shows that the occupants were found to be comfortable from 33.9 °C and this 0.4 °C variation from previous experiments may be due to the metabolic

rate of 1.2 met which should have increased the body temperature.

The aim was mainly to predict the skin temperature for each value of Fanger's PMV scale. The PMV gives the calculated value based on the clothing insulation, indoor temperature, relative humidity and metabolic rate. Generally, PMV is used as an indicator for the thermal comfort survey in the field. The actual mean vote and the PMV had small differences. In some instances where the PMV predicted that the occupant thermal sensation as slightly cool, the actual thermal sensation of the occupant was cool. Some votes by the occupants were in accordance with the PMV. This may be due to the different cultural backgrounds and the occupants may have local draught from the windows during the field study. Previous study [30] states that people tend to choose warm for slightly warm and cool for slightly cool sensation because of their skin sensitivity and they feel that the slight change in the thermal environment as a huge change. Therefore, in this study the skin temperature was mapped to the calculated PMV of the occupants to get clear and global uniformity in the value. The clothing level in the experimental chamber was not controlled and people could change their clothing according to their thermal sensation. The average clothing level during the experiment was 0.69 clo and the clothing level during the field survey was 0.5 clo. As per ASHRAE [5] and CIBSE [31] standards the normal clothing level in summer is 0.5 clo and in winter condition is 0.9 clo. The participants were having a clothing level of 0.9 clo during the cold condition and reduced their clothing level to 0.5 clo and lower during hot condition. The participants were seated in a normal chair therefore an insulation value of 0.1 clo was added. Even though the clothing insulation levels changed it didn't create any significant change to the range of mean skin temperature predicted for the Fanger's PMV scale. This leads to the assumption that the mean facial skin temperature remains the same unaffected by the clothing levels. This helps during the non-intrusive thermal comfort survey because the occupant doesn't have to be disturbed in order to note their clothing level.

VI. CONCLUSION

An exact model to predict thermal comfort using thermal imaging technology has not been developed yet. This study presented a practical approach for real time thermal comfort interpretation using infrared thermography. The main contribution of this study is that a simplified code in MATLAB is developed and it can be used to analyse the thermal images to find the facial mean skin temperature and their thermal sensation in relation to PMV. This helps to collect data, analyse facial skin temperature non intrusively and automatically obtain the thermal sensation. This framework includes interdisciplinary techniques like thermography, computer analysis and heuristic algorithm. The results obtained from the study shows that the facial skin temperature helps in the prediction of thermal comfort of occupants in real time. This involves minimum interruption of the

occupants in a building. The thermal comfort prediction of occupants helps to give a comfortable indoor environment and a simultaneous reduction in energy due to the change in temperature supplied by the HVAC system. This study also confirms that the skin temperature reacts immediately even to a small change in the room air temperature which is useful to predict the thermal comfort sensation easily. Finally, the facial skin temperature is higher when the surrounding air temperature is hot and lower when the air temperature is cold. Therefore, the thermal comfort preference of the occupants can be predicted with a 94% accuracy for neutral or comfort sensation, 92.5% for cold sensation and 90% for hot sensation using the proposed methodology.

REFERENCES

- [1] "Breast Cancer Screening: Thermogram No Substitute for Mammogram," *U.S. Food & Drug*, 2017. .
- [2] Applegate, "FLIR infrared cameras help detect the spreading of swine flu and other viral diseases," *www.applegate.co.uk*, 2009. .
- [3] M. Ö. Korukçu and M. Kılıç, "Tracking hand and facial skin temperatures in an automobile by using IR-thermography during heating period," *Gazi Univ. J. Sci.*, vol. 25, no. 1, pp. 207–217, 2012.
- [4] Z. Y. Wang FL, Chen ZL, Jiang Y, Zhao QC, "Preliminary study on perception-based indoor thermal environment control," 2014.
- [5] ASHRAE, "Standard 55-2013 - Thermal Environmental Conditions for Human Occupancy," *Ashrae*, vol. 8400, p. 58, 2013, doi: ISSN 1041-2336.
- [6] D. Kolokotsa, D. Tsiavos, G. . Stavrakakis, and K. Kalaitzakis, "Advanced fuzzy logic controllers design and evaluation for buildings' occupants thermal-visual comfort and indoor air quality satisfaction," *J. Physcol.*, vol. 41, no. 6, pp. 1258–1267, 2005, doi: 10.1111/j.1529-8817.2005.00141.x.
- [7] M. Frontczak, R. V. Andersen, and P. Wargocki, "Questionnaire survey on factors influencing comfort with indoor environmental quality in Danish housing," *Build. Environ.*, vol. 50, pp. 56–64, 2012, doi: 10.1016/j.buildenv.2011.10.012.
- [8] P. Fanger, "Assessment of thermal comfort practice," pp. 313–324, 1973.
- [9] R. J. De Dear, G. S. Brager, J. Reardon, F. Nicol, and D. Ph, "Developing an Adaptive Model of Thermal Comfort and Preference," *Am. Soc. Heating, Refrig. Air Cond. Eng. Inc., Macquarie Res. Ltd*, vol. 4106, no. March, 1998.
- [10] W. Liu, Z. Lian, and Q. Deng, "Use of mean skin temperature in evaluation of individual thermal comfort for a person in a sleeping posture under steady thermal environment," *Indoor Built Environ.*, vol. 24, no. 4, pp. 489–499, 2015, doi: 10.1177/1420326X14527975.
- [11] Z. Wu, N. Li, H. Cui, J. Peng, H. Chen, and P. Liu, "Using Upper Extremity Skin Temperatures to Assess Thermal Comfort in Office Buildings in," 2017, doi: 10.3390/ijerph14101092.
- [12] W. Liu, Z. Lian, and Y. Liu, "Human heart rate variability at different thermal comfort levels," *Eur. J. Appl. Physiol. Occup. Physiol.*, vol. 103, pp. 361–366, 2008.
- [13] E. ARENS and H. ZHANG, "The skin's role in human thermoregulation and comfort," in *Thermal and Moisture Transport in Fibrous Materials*, Cambridge, UK, 2006, pp. 560–602.
- [14] M. Campero, J. Serra, H. Bostock, and J. L. Ochoa, "Slowly conducting afferents activated by innocuous low temperature in human skin," *J. Physiol.*, vol. 535, no. 3, pp. 855–865, 2001, doi: 10.1111/j.1469-7793.2001.t01-1-00855.x.
- [15] M. Cabanac, "Heat stress and behavior," *Environ. Physiol.*, 2011.
- [16] D. Li, C. C. Menassa, and V. R. Kamat, "Non-intrusive interpretation of human thermal comfort through analysis of facial infrared thermography," *Energy Build.*, 2018.
- [17] H. Liu *et al.*, "The response of human thermal perception and skin temperature to step-change transient thermal environments," *Build. Environ.*, vol. 73, pp. 232–238, 2014, doi: 10.1016/j.buildenv.2013.12.007.
- [18] Z. Wang, Y. He, J. Hou, and L. Jiang, "Human skin temperature and thermal responses in asymmetrical cold radiation environments," *Build. Environ.*, vol. 67, pp. 217–223, 2013, doi: 10.1016/j.buildenv.2013.05.020.
- [19] W. Liu, Z. Lian, Q. Deng, and Y. Liu, "Evaluation of calculation methods of mean skin temperature for use in thermal comfort study," *Build. Environ.*, vol. 46, no. 2, pp. 478–488, 2011, doi: 10.1016/j.buildenv.2010.08.011.
- [20] J. Xiong, X. Zhou, Z. Lian, J. You, and Y. Lin, "Thermal perception and skin temperature in different transient thermal environments in summer," *Energy Build.*, vol. 128, pp. 155–163, 2016, doi: 10.1016/j.enbuild.2016.06.085.
- [21] R. Nielsen and B. Nielsen, "Measurement of mean skin temperature of clothed persons in cool environments," *Eur. J. Appl. Physiol. Occup. Physiol.*, vol. 53, no. 3, pp. 231–236, 1984, doi: 10.1007/BF00776595.
- [22] S. Sunderman and I. Osorio, "Mesial Temporal Lobe Seizures may Activate Thermoregulatory Mechanism in Humans: an Infrared Study of Facial Temperature," *Epilepsy Behav.*, pp. 399–406, 2003.
- [23] T. Söderström; A. Stefanovska; M. Veber and H. Svensson, "Involvement of Sympathetic Nerve Activity in Skin Blood Flow Oscillation in humans," *Am. J. Physiol. Hear. Circ. Physiol.*, vol. 284, pp. 1638–1646, 2003.
- [24] M. Ö. Korukçu and M. Kılıç, "The usage of IR thermography for the temperature measurements inside an automobile cabin," *Int. Commun. Heat Mass Transf.*, vol. 36, no. 8, pp. 872–877, Oct. 2009, doi: 10.1016/j.icheatmasstransfer.2009.04.010.
- [25] Tester, "FLIR T640bx Professional Building Thermal Camera," *www.testers.co.uk*, 2019. .
- [26] P. M. Prendergast, *Anatomy of the Face and Neck*, Cosmetic S. Berlin, Heidelberg: Springer, 2013.
- [27] A. P. Gagge, J. A. J. Stolwijk, and J. D. Hardy, "Comfort and thermal sensations and associated physiological response at various ambient temperatures," *Environ. Res.*, vol. 1, pp. 1–20, 1967.
- [28] B. W. Olesen and P. O. Fanger, "The skin temperature distribution for resting man in comfort," *Archit. Sci. Physiology*, vol. 27, pp. A385–A393, 1973.
- [29] T. Sakoi, K. Tsuzuki, S. Kato, R. Ooka, D. Song, and S. Zhu, "Thermal comfort, skin temperature distribution, and sensible heat loss distribution in the sitting posture in various asymmetric radiant fields," *Build. Environ.*, vol. 42, pp. 3984–3999, 2007.
- [30] R. Yao, B. Li, and J. Liu, "A theoretical adaptive model of thermal comfort - Adaptive Predicted Mean Vote (aPMV)," *Build. Environ.*, vol. 44, no. 10, pp. 2089–2096, 2009.
- [31] Guide A CIBSE, *Environmental design*. 2006.

Passive Design Tool Development using Modified Building Bioclimatic Chart for Indian Composite Climate

Khyati Paghdar¹, Raj Gupta¹, Jyotirmay Mathur², Aneesh Prabhakar²

Centre for Energy and Environment, Malaviya National Institute of Technology, Jaipur 302017, India

Email contacts: khyatirp@gmail.com (Khyati Paghdar), gupta.raj07@gmail.com (Raj Gupta)

Received at Malaviya National Institute of Technology: April, 2021

Abstract— Present research work contributes to proposing a sun-shading polygon for three different air velocity ranges (0-0.5 m/s, 0.5-1 m/s, 1-1.5 m/s) through the simulation of reference building for the Indian composite climate. Effects of Window-to-Wall Ratio (WWR), type of shading device, glass type, and projection factor are studied of which WWR and type of shading device have the most impacts on reducing the solar gain inside the zone. Additionally, a tool is developed to analyze the passive design strategies that have been studied for the Indian composite climate by Indian researchers based on the local climatic condition and thermal adaptation of Indian-specific occupants. The tool takes an EnergyPlus Weather (EPW) file as an input and shows the different curves and plots of weather data. It also plots psychrometric graphs for bioclimatic, ASHRAE 55 (2017) standard, and user-defined thermal comfort to check the comfort hours that passive techniques can achieve for the location. The tool is further extended to design evaporative cooling systems that will assist in the decision-making on evaporative cooling strategies to be used for user-defined operational schedules and evaluate possible comfort hours based on building dimensions and heat load input data.

Index Terms – Building Bioclimatic Chart, Graphical user interface, Passive design techniques, Sun shading polygon

I. INTRODUCTION

Demand for space cooling in buildings is expected to explode and upset the energy budget of India. The total installed capacity of air conditioners in India is already about 80 million tonnes, which will increase to about 250 million tonnes by 2030 [1]. A study projects that within the next decade, India's cooling energy demand will grow 2.2 to 3 times over the current level, under moderate-growth or potential high-growth scenarios respectively [2]. Using passive and low energy design techniques can be effective to replace/reduce the cooling energy required by refrigerants-based vapor compression refrigeration systems in the composite climate zone of India, a region that covers more than 30% of the total geographic area of the country. In this study, common passive design strategies namely, high thermal mass, evaporative cooling, natural ventilation, forced ventilation, and sun shading are focused.

A. Building Bioclimatic Chart (BBCC):

The Building Bio-climatic Design Charts (BBCC) specifies whether ambient conditions descent in the

assigned bounds of a passive design strategy that a building is proposed to implement to keep indoors comfortable. The first comfort zone was made by ASHRAE [3] on a conventional psychrometric chart. It requires comfort boundaries depending on indoor temperature and humidity ratio, for sitting people, inside which the automatic system must uphold the indoor comfort. A few researchers, Olgyay [4], Givoni [5], and Szokolay [6], were the major exponents of the concept of bioclimatic design in Architecture. To make the use of a bioclimatic chart one should study the adaptive nature of the locality first and append some changes to the bioclimatic chart.

B. Sun shading devices as a passive design strategy in naturally ventilated buildings:

The sun shading strategy works to reduce the solar heat gain inside the living area from the windows. Overhangs and fins are the two basic shading devices that are common in India. Cheng [7] in his study for Taiwan provided a methodical procedure to establish a summarized correlation for evaluating shading performance based on projection factor (PF) of shading device, the ratio of the width of the window to height, and azimuth angle. Kirimtat [8] and Kirankumar [9] studied the effect of the shading device material and glass material respectively. Evola [10] found that the implementation of external roller blinds increases the energy savings to 47.7%. Whereas, in the case of the south-facing glazed façade the energy savings sum up to 60.6%. Ghosh [11] revealed through a simulation study that with an increase in WWR the heating and lighting energy decreases.

C. Evaporative cooling as a passive design strategy in Indian composite climate:

Various researchers have been working to evaluate the applicability of evaporative cooling in the composite climate in India. Tewari [12] conducted field measurement and survey, and proposed comfort zones for Evaporative Cooling for three airspeed range (0m/s-0.5 m/s, 0.5m/s-1m/s, 1m/s-1.5m/s) for composite climate of India. Bhamare [13] proposed an analysis tool for the evaluation of the cooling potential of passive strategies for India. The study was carried out in 18 cities of different zones and found an evaporative cooling potential of nearly 13% in the composite climate of India.

II. RESEARCH OBJECTIVE

Based on the literature review, the use of the sun shading passive strategy on BBCC for the Indian composite climate is still not present. Further many tools internationally are developed to study the use of passive design strategies for comfortable indoors. Till now no such tool is present for Indian climatic conditions for comfort analysis and evaporative cooling system designing. To bridge this research gap, the following objectives are identified:

- To evaluate the climatic applicability of sun shading based on local construction practices of building façade/windows in composite climate through simulation.
- Development of a bioclimatic analysis tool considering a region-specific thermal adaptation of people living in the composite climate of India.
- Deduce recommendations for best passive and low energy strategies in buildings using the graphical interface of the proposed bioclimatic analysis tool on Python.
- To integrate evaporative cooling system design and comfort analysis module in the tool.

III. RESEARCH METHODOLOGY

This section discusses the minute details of the defining thermal comfort zone, passive design boundaries on BBCC, design of experiment and dataset, and development of bioclimatic analysis tool.

A. Defining thermal comfort zone on BBCC:

A thermal comfort field study was conducted by Kumar [14] in 32 naturally ventilated buildings in Indian composite climate, collecting a total of 2610 samples spread over a total period of four years, covering all seasons, wide age groups, clothing types, and building types. New extended boundaries different from those suggested by ASHRAE 55 (2017) [20] and ISO-7730 standards of comfort zones are proposed considering various adaptations specific to climate, including the role of thermal preferences and airspeed to offset the temperature for velocity ranges 0-0.5, 0.5-1, and 1-1.5 m/s. The defined adaptive comfort zones are validated using extended thermal comfort data.

B. Defining thermal mass polygons boundaries on BBCC:

Kumar [15] developed mathematical correlations for predicting indoor air temperatures in the monitored high thermal mass buildings for the summer and winter seasons separately. From the results, he suggested bioclimatic boundary of ambient conditions for the use of thermal mass in naturally ventilated buildings for air velocity ranges 0-0.5, 0.5-1, and 1-1.5 m/s. It is demonstrated that a reasonably good agreement ($R^2 > 0.90$) existed between the measured data and the one predicted from correlations during its validation. Further statistical analysis using “F-statistic” and “t-statistic” established the robustness of developed correlations. Correlations are further field-validated to other buildings of similar construction types.

C. evaporative cooling polygons boundaries on BBCC:

Polygon boundaries for direct evaporative cooling are defined by the highest and lowest constant wet bulb temperature lines from the comfort zone [12] [16].

D. Defining sun shading boundary on BBCC:

One of the objectives of the present work is to develop the climatic boundary for the outdoor conditions for which sun shading can produce comfort indoors on the psychrometric chart based on the adaptive comfort approach considering climate-specific adaptations, air-speed variation, and the occupant’s thermal preferences in naturally ventilated buildings.

a) Development of building model:

Low rise building (three floors above ground level) is selected for the simulation study from the reference building model for Indian [17] composite climate. A detailed description of the building including building envelope, construction dimensions, and operational data such as occupancy, ventilation, infiltration, and plug load can be referred from the literature [17]. The building is naturally ventilated with no active heating/cooling devices present and provides adaptive controls such as the use of windows and doors, and operation and speed regulation of fans.

b) Design of experiment:

A total of sixteen building models were developed using the Taguchi method as described in Table 1. Parameters that were taken into account are, window to wall ratio; shading type – Without shading (WS), Overhang (OH), Fins (F), Overhang + fins (OF); projection factor (PF); and window glass type – Clear glass (A), ECBC compatible (B), ECBC non-compatible (C), superior to ECBC (D). Simulation and thermal analysis were performed with ‘Design builder’ software (Version 6.1.4.006).

c) Data analysis:

Data generated from the simulation runs is exported to excel for data segregation. Data points to be considered as comfort points shall confirm a minimum of 100 Lux to a maximum of 2000 Lux of daylight level for the sunshine hours [18] and a minimum allowable visual light transmission (VLT) of 0.27 with a projection factor of more than 0.4 are considered. Vertical fenestration assembly shall comply with the maximum solar heat gain coefficient (SHGC) of 0.27 and U-factor of 3.0 W/m²k.

E. Development of bioclimatic analysis tool:

For the development of a bioclimatic analysis tool, Climate Consultant [19], Mahoney [21] tables, and an Excel tool proposed by N. K. Khambadkone [22] to assess the comfort potential and climate severity were studied. These tools produce weather data graphs and bioclimatic charts.

PyCharm platform with Python language coding is opted to develop the tool. PyQt5 based QtDesigner is used to design a graphical user interface. Weather data graphs are plotted using the ‘Matplotlib’ library of python using weather data.

Evaporative cooling system design module requires additional building data such as building dimensions, heat load, type and saturation efficiency of selected system, and desired indoor air condition. Basic heat load and saturation efficiency equations are used for calculating the evaporative cooling system design parameters such as required airflow rate (1), Room supply air condition (2), air changes (4), and water requirements (5) for evaporative cooling system design module as described below Table 1.

Table 1. Design of experiment

WWR (%)	Direction	Glass Type	Shading device	PF
10	N	A	WS	0.2
10	E	B	OH	0.4
10	W	C	F	0.6
10	S	D	O/F	0.8
20	N	B	F	0.8
20	E	A	O/F	0.6
20	W	D	WS	0.4
20	S	C	OH	0.2
30	N	C	O/F	0.4
30	E	D	F	0.2
30	W	A	OH	0.8
30	S	B	WS	0.6
40	N	D	OH	0.6
40	E	C	WS	0.8
40	W	B	O/F	0.2
40	S	A	F	0.4

$$\text{Required airflow rate (m}^3\text{/s)} = \frac{319.64 \times \text{Sensible heat load (W)}}{(\text{IDB} - \text{LDB})(\text{K}) \times \text{Density ratio}} \quad \dots (1)$$

Where,

$$\text{LDB} = \text{Outdoor DBT} - \{\text{Saturation efficiency} \times (\text{Outdoor DBT} - \text{Outdoor WBT})\} \quad \dots (2)$$

$$\text{Density Ratio} = \exp\left(\frac{-0.0342 \times \text{Altitude (m)}}{\text{LDB (K)}}\right) \quad \dots (3)$$

DBT = Dry Bulb Temperature

WBT = Wet Bulb Temperature

IDB = Desired Indoor Dry Bulb Temperature

LDB = Leaving Dry Bulb Temperature and the word ‘leaving’ indicates cooled air leaving from the evaporative cooler that will be supplied into the rooms or in other words LDB is dry bulb temperature of room supply air

$$\text{Air change per hour (ACPH)} = \frac{\text{Required airflow rate (m}^3\text{/s)} \times 60}{\text{Volume of cooling space (m}^3\text{)}} \quad \dots (4)$$

$$\text{For water requirements, Evaporation rate (m}^3\text{/s)} = \frac{\text{Mass flow rate of air (kg/s)} \times H}{\text{Density of water (kg/m}^3\text{)}} \quad \dots (5)$$

Where,

H = Change in humidity ratio (kg of water vapor/kg of dry air) for direct evaporative cooling systems, and

Ratio of enthalpy (J/kg) change to the latent heat of vaporization (J/kg) for water in the case of indirect evaporative cooling systems.

In the case of indirect evaporative cooling, the following assumptions are made,

1. Mass flow rate of primary and secondary air are equal and
2. Heat transfer between secondary and primary air in *the* heat exchanger is balanced.

IV. RESULTS

A. Simulation analysis results:

The simulation for the whole year shows that shading devices reduce indoor temperature to comfortable conditions for some parts of the year. It was observed that a greater number of hours are comfortable when the orientation of the window is in the East direction and when WWR is 40%.

B. Sun shading polygon on BBCC:

The comfort points from the simulation results after segregation are plotted on the psychrometric chart to

define the sun shading polygon with the comfort zone for naturally ventilated buildings proposed by Kumar [14]. ASHRAE 55 [16] mentions 80% acceptability for the thermal environment and lower than 20% of people dissatisfied (PPD). Here proposed sun shading polygons are defined with 80% acceptability with clothing up to 1.2 clo and metabolic level of 1 met - 1.2 met. Simulation results show that the difference between outdoor dry bulb temperature (blue points) and corresponding indoor operative temperature (red points) is due to the use of shading devices as shown in Fig. 1.

For air velocity up to 0.5 m/s, 0.5-1 m/s, and 1-1.5 m/s, the sun shading polygon extends to 39.58 °C, 39.9 °C, and

40.2 °C respectively, with constant humidity ratio lines. Fig. 2, 3 and 4 shows sun shading polygon (yellow boundary) for air velocity up to 0.5m/s, 0.5-1 m/s and 1-1.5 m/s respectively. Proposed polygon limits relative humidity up to 80%, contrary to 95% suggested by ASHRAE [20] for air velocity greater than 1.2 m/s as very rare polls were found comfortable at RH higher than 80%.

C. Graphical User Interface for the tool:

The tool “Passive Design Consultant” only requires an EnergyPlus Weather (EPW) file of any city as input by the user. The tool consists of different tabs namely, Weather file summary, Temperature Range, Radiation Range, Illuminance Ranges, Ground Temperature, Wind velocity Range, Bioclimatic Design Chart, Design Recommendation, and EvapCal. Menubar of the tool assists users in providing instructions about how to use the tool, terms and conditions, and important definitions of the terms used.

Weather data analysis includes a monthly summary for mean values of weather data and violin plots of different temperatures (refer Fig. 5), radiation, illumination, and wind velocity that show monthly data with maximum value, minimum value, and mean value for the month. In

addition to this value, it represents the frequency of occurrence of values using the curve shape around the vertical line. An hourly heat-map of dry bulb temperature in 2D and 3D form is also included as can be seen in Fig. 6. The tool recommends percentage hours of selected operational time that can be made comfortable with individual strategy as well as the combined approach through the bioclimatic chart as shown in Fig. 7.

The “EvapCal” module of the tool gives results of evaporative cooling system design parameters based on building heat load and dimensions data. Users can also generate heat maps for ambient and room supply air. The psychrometric chart (Fig. 8) shows the number of comfort hours for direct, indirect, and two-stage systems of defined efficiency with energy-saving analysis based on power rating input of the evaporative and alternate active cooling system. The module facilitates users to generate a design report in PDF format for further design assistance.

Psychrometric chart for both passive design techniques and evaporative system design shows results for different comfort zone types namely ASHRAE 55 (2017) standard [20], Bioclimatic comfort zone, and user-defined comfort zone.

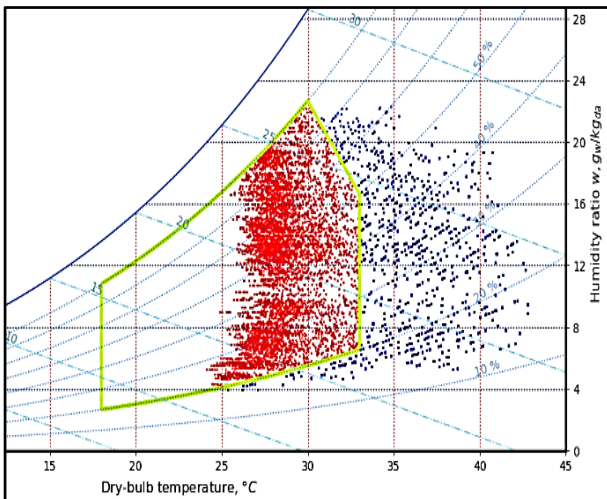


Figure 1. Representation of simulation results on Psychrometric chart

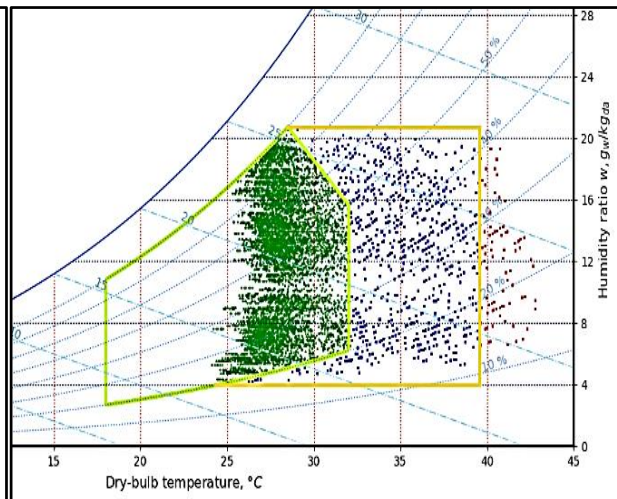


Figure 2. Proposed sun shading polygon for air velocity up to 0.5 m/s

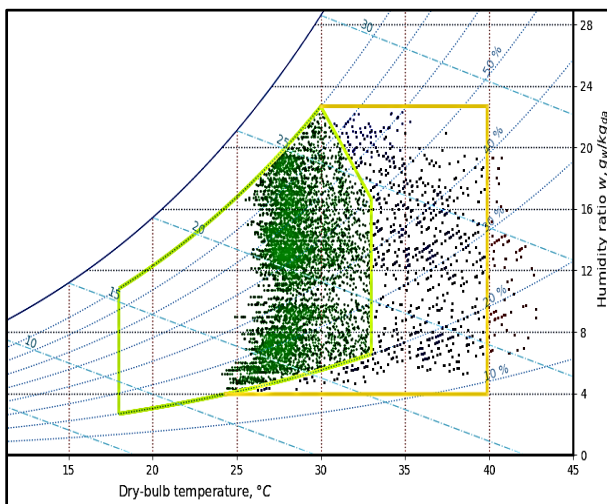


Figure 3. Proposed sun shading polygon for air velocity 0.5-1 m/s

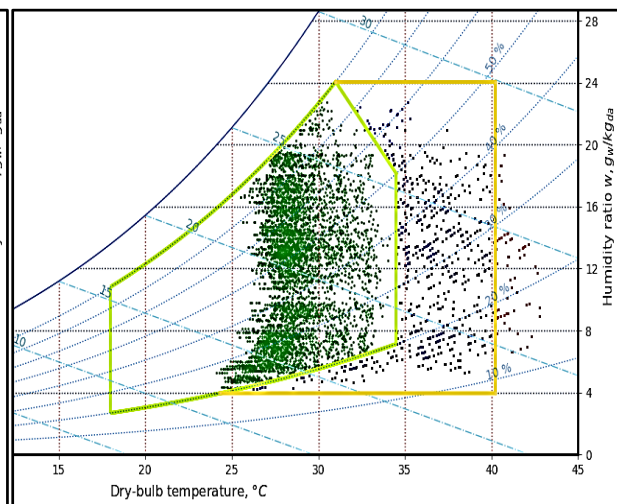


Figure 4. Proposed sun shading polygon for air velocity 1-1.5 m/s

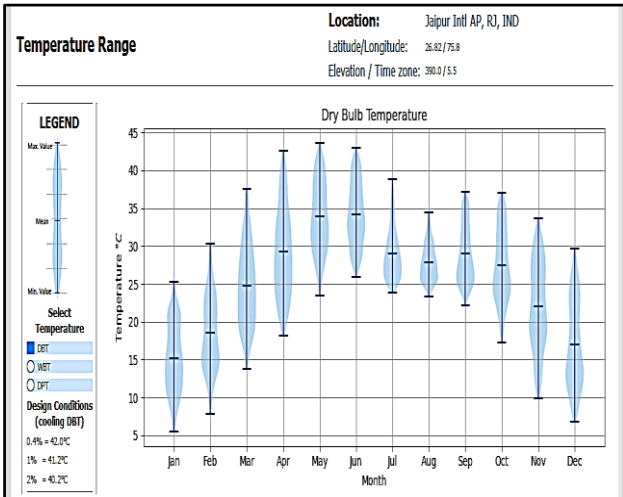


Figure 5. Temperature plot and design conditions

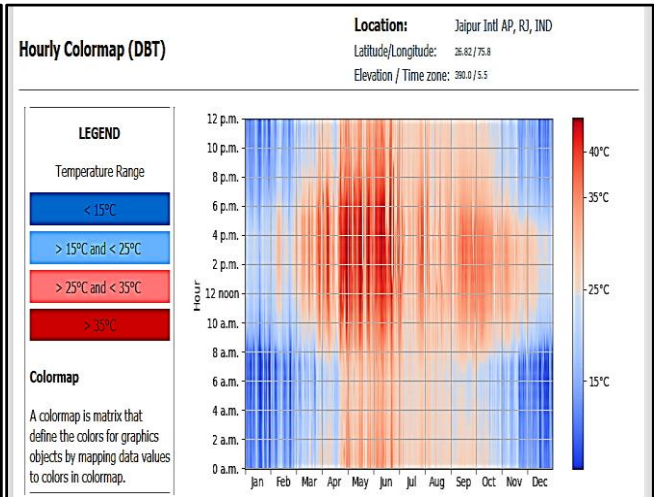


Figure 6. Temperature plot in the color map

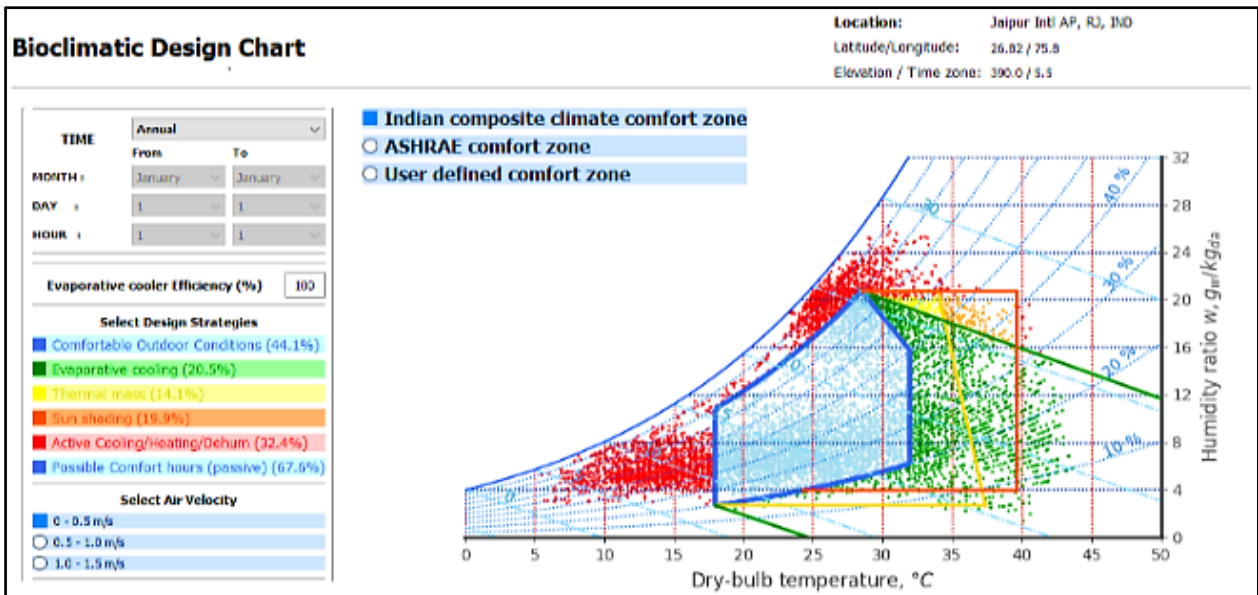


Figure 7. Bioclimatic Design Chart tab: It shows the BBCC for the selected location and provides corresponding comfort values

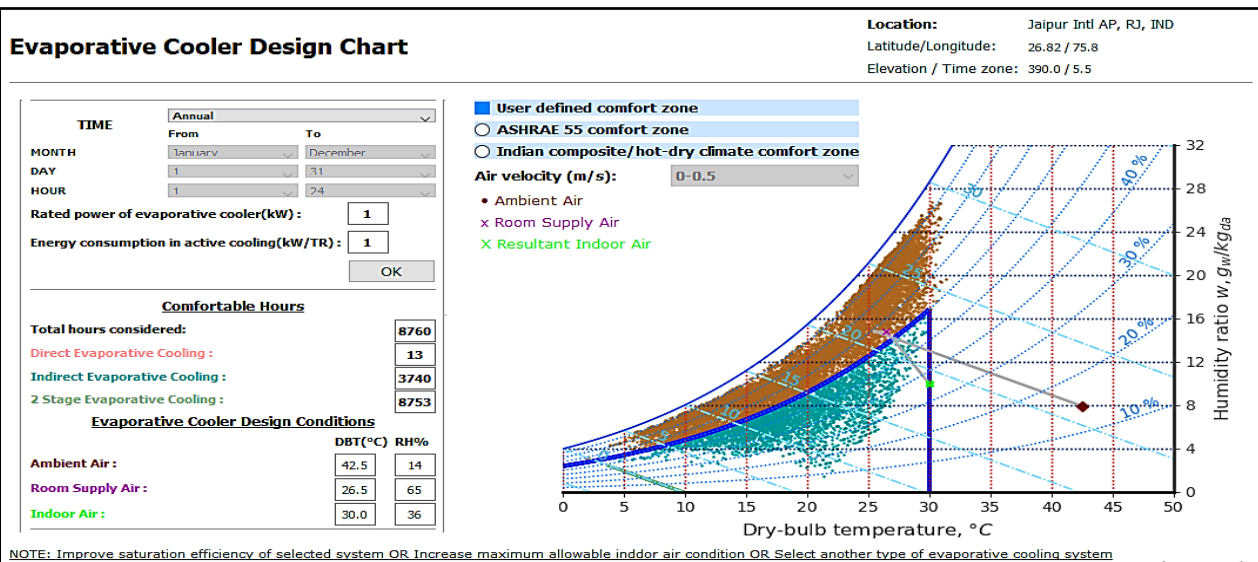


Figure 8. Evaporative Cooler Design Chart tab: It shows the psychrometric chart for the design process and comfort hours for direct, indirect, and two-stage evaporative cooling system

V. CONCLUSION

The research work focuses on the usage of some passive design strategies for the composite climate of India with the help of a psychrometric chart. Findings of the work are listed here:

- The sun shading design polygon is proposed through simulation results of the reference building provided for the composite climate of India on the design-builder software. Considering a percentage of discomfort hours of 20% as per the ASHRAE 55 (2017) standard [20], only 80% of simulation results are taken for proposing sun shading polygons for air velocities up to 0.5, 0.5-1, and 1-1.5 m/s.
- The results of the simulations for sun shading show a decrease in indoor temperature by about 3 °C to 5 °C approximately with on average 15% to 18% of daytime hours shifted to comfort conditions for an entire year.
- Graphical user interface tool assists in selecting the best passive technique from all and sizing evaporative cooling system with comfort analysis.
- The tool also facilitates comparative thermal comfort analysis for the bioclimatic zone, ASHRAE 55 (2017) standard [20], and user-defined comfort zone.

Similar work on the bioclimatic chart for defining thermal comfort zone and passive design polygons can be extended to other climatic zones of India in the future. Also, passive strategy designing modules for thermal mass, sun shading devices, and other techniques can be integrated as done for evaporative cooling in the present work.

ACKNOWLEDGMENT

1. Dr. Priyam Tewari, Associate Fellow, The Energy and Resources Institute, India
2. Mr. Nishant Gupta, Managing Director – Degree Day Pvt. Ltd., Indore (India)

REFERENCES

- [1] Press Information Bureau, Frequently Asked Questions on BEE recommendations on temperature setting of Air Conditioners, Ministry of Power, Govt. of India, (2018) [Release ID:180281]
- [2] S. Kumar, S. Sachar, S. Kachhawa, M. Singh, A. Goenka, S. Kasamsetty, G. George, R. Rawal, Y. Shukla, Projecting National Energy Saving Estimate from the Adoption of Adaptive Thermal Comfort Standards in 2030, Alliance for an Energy Efficient Economy (2018).
- [3] Arens, Thermal Environmental Conditions for Human Occupancy, 1995.
- [4] V. Olgyay, Design with Climate, Bioclimatic Approach to Architectural Regionalism, Princeton University Press, Princeton, New Jersey, 1963.
- [5] B. Givoni, Man, Climate and Architecture, Applied Science Publishers Limited, London, U.K., 1976.
- [6] S.V. Szokolay, Climate analysis based on the psychrometric chart, International Journal of Ambient Energy 74 (1986) 171e182.
- [7] C. L. Cheng, L. M. Liao, and C. P. Chou, A study of summarized correlation with shading performance for horizontal shading devices in Taiwan, Solar Energy. 90 (2013) 1–16, DOI: 10.1016/j.solener.2013.01.007.
- [8] A. Kiritmat, O. Krejcar, B. Ekici, and M. Fatih Tasgetiren, Multi-objective energy and daylight optimization of amorphous shading devices in buildings, Solar Energy. 185 (2019) 100–111, DOI: 10.1016/j.solener.2019.04.048.
- [9] G. Kirankumar, S. Saboor, and T. P. Ashok Babu, Investigation of Various Low Emissivity Glass Materials for Green Energy Building Construction in Indian Climatic Zones, Materials Today Proceedings. 4 (2017) 8052–8058, DOI: 10.1016/j.matpr.2017.07.144.
- [10] G. Evola, F. Gullo, and L. Marletta, The role of shading devices to improve thermal and visual comfort in existing glazed buildings, Energy Procedia. 134 (2017) 346–355, DOI: 10.1016/j.egypro.2017.09.543.
- [11] A. Ghosh and S. Neogi, Effect of fenestration geometrical factors on building energy consumption and performance evaluation of a new external solar shading device in warm and humid climatic condition, Solar Energy. 169 (2018) 94–104, DOI: 10.1016/j.solener.2018.04.025.
- [12] P. Tewari, S. Mathur, J. Mathur, V. Loftness, A. Aziz, Advancing Building Bioclimatic Design Charts for the Use of Evaporative Cooling in The Composite Climate of India. Energy and Buildings. 184 (2019) 177–9, DOI: [10.1016/j.enbuild.2018.12.005](https://doi.org/10.1016/j.enbuild.2018.12.005).
- [13] D. K. Bhamare, M. K. Rathod, J. Banerjee, Evaluation of Cooling Potential of Passive Strategies using Bioclimatic Approach for Different Indian Climatic Zones, Journal of Building Engineering. 31 (2020) 101356, DOI: [10.1016/j.jobe.2020.101356](https://doi.org/10.1016/j.jobe.2020.101356).
- [14] S. Kumar, J. Mathur, S. Mathur, M. K. Singh, V. Loftness, An adaptive approach to define thermal comfort zone on psychrometric chart for naturally ventilated buildings in composite climate of India, Building Environment. 109 (2016) 135–153.
- [15] S. Kumar, P. Tewari, S. Mathur, J. Mathur, Development of mathematical correlations for indoor temperature from field observations of the performance of high thermal mass buildings in India, Building Environment. 122 (2017) 324–342.
- [16] P. Tewari, S. Mathur, J. Mathur, S. Kumar, V. Loftness, Advancing Building Bioclimatic Field study on indoor thermal comfort of office buildings using evaporative cooling in the composite climate of India, Energy and Buildings. 199 (2019) 145–163, DOI: [10.1016/j.enbuild.2019.06.049](https://doi.org/10.1016/j.enbuild.2019.06.049)
- [17] M. Bhatnagar, J. Mathur, and V. Garg, Development of reference building models for India, Journal of Building Engineering. 21 (2018) 267–277, DOI: 10.1016/j.jobe.2018.10.027.
- [18] Energy Conservation Building Code, 2017.
- [19] Climate Consultant 6.0. <http://www.energy-designtools.aud.ucla.edu/climate-consultant>
- [20] ASHRAE (American Society of Heating Refrigeration and Air-conditioning Engineers). Thermal Environmental Conditions for Human Occupancy. ASHRAE Standards 55. Atlanta, G.A., U.S.A., 2017.
- [21] O. H. Koenigsberger, T. G. Ingersoll, M. Alan, and S. V. Szokolay, Manual of tropical housing & buildings, Orient Longman Private Limited, 1975.
- [22] N. K. Khambadkone, R. Jain, A bioclimatic analysis tool for investigation of the potential of passive cooling and heating strategies in a composite Indian climate, Building Environment. 123 (2017) 469–493.

REHVA

Student Competition

Other Participants' Contribution

Paulo Fernandes	Portugal
Mihai Baiceanu	Romania
Damir Kovcic	Serbia
Anastasija Zeiza- Seleznova	Latvia
Tej Zizak	Slovenia
Anna Cazzola	Italy
Helena Kuivjogi	Estonia
Amalie Dokkedal Jensen & Catherine Schermer Riis	Denmark
Basak Dere & Zeynep Hazal Gümüslüol	Turkey
Aurore Wurtz	France
Martina Mudra	Slovakia

Energy Potential in Using a Bypass to the AHU's Heat Recovery System

Paulo Fernandes

The impact of a mechanical bypass to a heat recovery unit in an Air Handling Unit (AHU) raises doubts as to whether it is energetically and economically viable. This analysis was applied to several AHUs with different energy classes (B, A and A+) and three different scenarios were defined: first, an AHU without a heat recovery system (HRS); second, an AHU with a HRS and thermal bypass; and finally, an AHU with an HRS and mechanical bypass. To analyse and compare the energy consumption of each scenario, an Excel calculation tool was developed, which allows annual simulations of the energy consumption of the AHUs according to its location, its operating hours and its characteristics (pressure drop, load, HRS' thermal efficiency, volume flow and the system's ventilation efficiency). It is concluded that the introduction of a bypass to the AHU's HRS is a viable option, mainly in cities in the north of Portugal and with mild climates in the summer. Also, the use of an HRS during the summer months increases the energy consumption of the AHU. The introduction of the bypass enables the use of the HRS during this period, reducing the energy consumption of the AHU when compared to one without a HRS. In any case, the bypass proved to be a solution that allows the reduction of the energy consumption of the AHU, regardless of its operation hours and the climate profile in which it is located. The reduction in energy consumption is enough to amortize, in a few years (maximum 5), the cost of manufacturing and assembling the mechanical bypass system in an AHU.

AHU, consumption, heat recuperator.

Introduction

According to data from Eurostat [1], in 1996, in the European Union (EU), the Residential and Services sectors had a major impact on primary energy consumption, accounting for 38.9% of that year's energy consumption. In an effort to reduce this consumption, the EU has developed a set of initiatives aimed at reducing energy consumption, namely the Directive 2002/91/EC, which obliges Member States to place minimum energy efficiency requirements and to develop and implement a Certificate of Energy Efficiency [2]. Taking into account that the HVAC system (Heating, Ventilation and Air Conditioning) of buildings represents about half of the energy consumed by them [3], it is important that it has a good energy performance, aiming to achieve the lowest possible consumption. Thus, there is an obligation to place a heat recovery system (HRS) in the Air Handling Units (AHU), in order to reduce the energy consumed in ventilation. Despite the clear impact on the reduction of energy consumed in air treatment, it is necessary to assess the energy balance in the AHU, as the presence of the HRS increases the pressure drop inside the AHU, leading to an increase in ventilation energy consumption.

Symbols

F_{pu} - conversion factor of useful energy to primary energy [kWh _{EP} /kWh]	ΔT_{min} - minimum temperature differential for recovery
η_t - thermal efficiency [-]	Δp - pressure differential, Pa
η_{syst} - ventilation group performance [-]	ϵ - efficiency [-]

Given that Portugal's climate is not very severe during the year, unlike other European countries, such as Germany or the Scandinavia region, the impact on the AHU's energy consumption was investigated when introducing a bypass to the heat recovery unit. This work intends to study this impact according to the climate of Portugal, with the objective of evaluating the cost/benefit of the introduction of the mechanical bypass in the AHU.

Methods

A. Characterisation of the AHUs

AHUs were idealized and designed for analysis and their constructive solutions were defined. Square section modules were chosen, for greater ease of construction and lower cost of the bypass insertion. The type of HRS used for the study was the rotary wheel, due to being the most used in the industry. The thermal production equipments that supply the heating and cooling batteries was a boiler and a chiller, respectively. Three scenarios were defined, each with a different constructive solution: scenario 0 - an AHU without a HRS (Fig. 1a); scenario 1 - an AHU with a HRS and thermal bypass (Fig. 1b); and finally, scenario 2 - an AHU with a HRS and a mechanical bypass (Fig. 1c).

For each constructive solution, studies were carried out for AHUs with different energy classes. These energy classes are defined in accordance with the Eurovent certification program and AHUs with energy classes A+ (most efficient class), A and B (least efficient class) were used, resulting in a grand total of 9 AHU's analysis. The



Figure 1. Constructive solution of the AHUs studied.

TABLE I
 VALUES OF THE CHARACTERISTICS OF THE AHU USED FOR THIS STUDY

Energy Class	Air Duct	Δp (Pa)				η_t (%)	η_{syst} (%)	\dot{V} (m ³ /h)
		Scenario 0	Scenario 1	Scenario 2				
				Bypass ON	Bypass OFF			
A+	Return	457	714	714	484	83	64	3650
	Insufflation	635	874	874	644			
A	Return	471	712	712	502	78	62	4150
	Insufflation	672	882	882	672			
B	Return	472	686	686	496	73	60	4700
	Insufflation	681	856	856	666			

paradox of using an HRS is evident in observing the requirements of these classes. For a more efficient energy class, a higher thermal efficiency of the HRS is required, in order to reduce the energy consumption in the air treatment. However, in order to achieve higher efficiencies, the HRS imposes a greater pressure drop in the air flow, increasing the energy consumed in the ventilation system. The AHUs were designed using proprietary software from the company EVAC¹, in order to obtain the main characteristics of the AHUs studied. This software also made it possible to obtain the pressure drop value imposed by the mechanical bypass, assuming a value of 20 Pa. This value is taken as constant for all scenarios, given that the variation in the simulated pressure drop was minimal (± 2 Pa), in all analysed scenarios. Table 1 summarizes the characteristics obtained for each AHU.

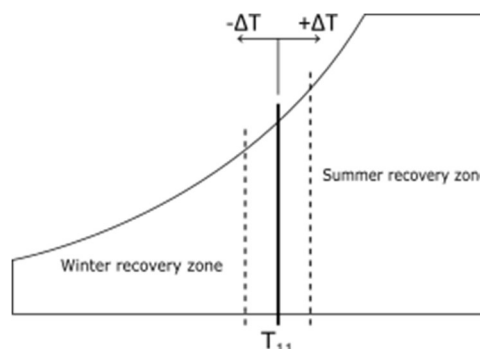
B. Mathematical Model

In order to analyse the energy consumption in the treatment and ventilation of the air, it is necessary to correctly predict the power and energy consumed by the thermal production equipments and by the ventilation group. For this, it is necessary to define the operation of the AHU, that is, when the HRS is in operation, as it will be in the hours when the HRS is inactive that the mechanical bypass will be operating. The operation of the HRS will essentially depend on three parameters: the outside air temperature (T_{21}), the interior design temperature (T_{11}) and the characteristics of the AHU (pressure drop from the HRS, Δp_{HRS} ; thermal efficiency of the HRS, η_t ; and ventilation system performance, η_{syst}). The determination of the HRS operation then depends on an energy balance between the power recovered by the HRS and the ventilation power consumed, $\dot{Q}_{HRS} > P_{vent}$. Since these are different energy vectors, this balance was measured in terms of primary energy, resulting in equation 1, which calculates the minimum temperature difference, ΔT_{min} , between the outdoor and indoor air, so that recovery is feasible.

$$\Delta T_{min} = \frac{\left(\frac{\dot{V} \Delta p_{HRS}}{\eta_{syst}} + P_{aux} \right) \cdot \epsilon}{\dot{m} c_{p,as} \eta_t} \cdot \frac{F_{pu,elet}}{F_{pu,i}} \quad (1)$$

Thus, it is possible to know when the HRS is active, depending on the outside temperature and to plot, in a psychrometric diagram, the recovery zones for the heating and cooling stations – Fig. 2. However, if this temperature

is very low, condensation may occur. This phenomenon is difficult to quantify, due to divergent conclusions in the studies carried out and because there is not much literature that studies the phenomenon. A method was then developed, which among others, was thought to be the most correct. The thermodynamic evolution of air, inside the HRS, during this phenomenon can be consulted graphically in the psychrometric diagram of Fig. 3. This method starts by assuming a sensitive evolution of both air flows inside the thermal wheel. At the extraction rate, while the air temperature decreases, the air reaches the saturation point, when water droplets begin to form in the wheel matrix (evolution 11 to 12'). Since not all the air is in contact with the wheel matrix, some of the air remains at the inlet temperature. At the exit of the recuperator, the air that carried out the heat exchange mixes with the unchanged air, reaching the outlet conditions (mixture of 12' with 11). Thus, the concept of bypass factor was introduced, where a value of 5% was assumed due to the reduced diameter of the wheel tubes. Since the wheel turns on itself, the outside air heats with the heat stored in the wheel matrix (evolution 21 to 22') and the water formed during the passage through the extraction area comes into contact with the air. The droplets, with the effect of air and the heat present in the wheel matrix, evaporate, causing an evaporative cooling at a constant wet bulb temperature (evolution 22' to 22). For the purposes of this study, and from the company's experience, it was considered that all condensed water evaporates into the outside air. Thus, with this method, it is possible to determine the fresh air outlet conditions and quantify the energy recovered.


 Figure 2. Recovery zones according to ΔT_{min} .

¹ EVAC is an AHU design and production company.

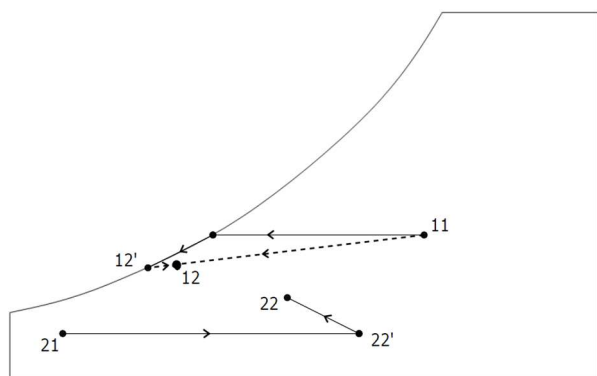


Figure 3. Thermodynamic evolution of air, inside the HRS, during the condensation phenomenon.

Analysis and Discussion of Results

To obtain the energy consumption data of the AHUs, a tool was developed in Microsoft Excel, which allows to define the location where the AHU will operate, its operating hours and characteristics, and the interior conditions. The tool was used to simulate the energy consumption for the 9 AHUs and for 20 different Portuguese cities: the 18 district capitals and the capitals of the Autonomous Regions.

Within the scope of this work, and in order to facilitate the presentation of the results, only the results obtained for the cities of Beja and Porto, which are two cities with a different climate profile, for an AHU with energy class A+, operating 24h /day. Both cities have a good recovery potential for the heating season, with a high frequency of hours below 20°C. However, the climate distinction between these cities is most evident in the cooling season. While Beja has a large number of hours above 25°C, which results in a good recovery potential, the city of Porto has a much lower number, resulting in a weak recovery potential. The climatic profile of each city can be seen in Figs. 4 and 5.

Due to the great recovery potential that both cities present during the heating season, the use of the bypass is not advantageous, as the energy recovered by HRS is much higher than the increase in energy needed to ventilate the air that the HRS implies, as is shown in Table 2.

TABLE II.
ENERGY CONSUMED (MWh_{EP})

City	Scenario 0		Scenario 1	
	Heat	Cool	Heat	Cool
Beja	66,35	25,22	27,41	36,68
Porto	75,01	25,22	28,98	36,68

It is, therefore, in the cooling station, in cities with a profile similar to Porto, that the use of a bypass to the HRS can be advantageous. Figure 6 shows the energy consumption, during the cooling season, for the cities of Beja and Porto.

By analysing Fig. 6, it is possible to notice that, during the cooling season, in Porto, the total energy consumed increases with the introduction of the recuperator, unlike the city of Beja, where the energy decreases due to a sufficient number of hours of recovery that ends up compensating for the increase in ventilation energy. With the introduction of the bypass to the HRS in the AHU, it

was possible to reduce the AHU’s consumption compared to the previous scenario, for both cities. The use of mechanical bypass is therefore particularly advantageous in cities where the potential for recovery is weak. On another positive point, it also allows to reduce energy consumption even in more severe climates.

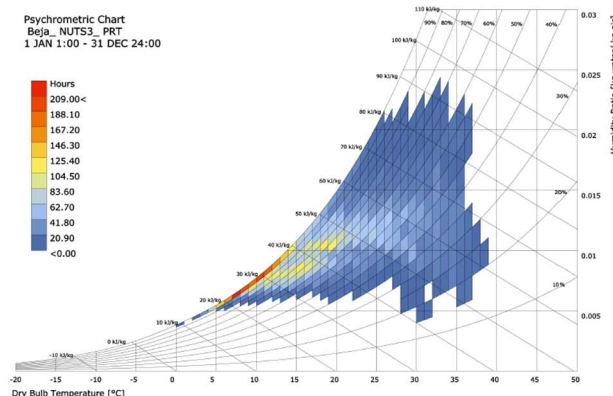


Figure 4. Climate profile of Beja. Data source: CLIMAS-SCE [4].

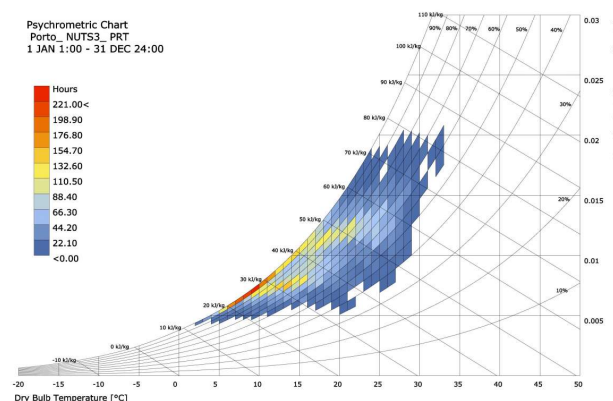


Figure 5. Climate profile of Porto. Data source: CLIMAS-SCE [4].

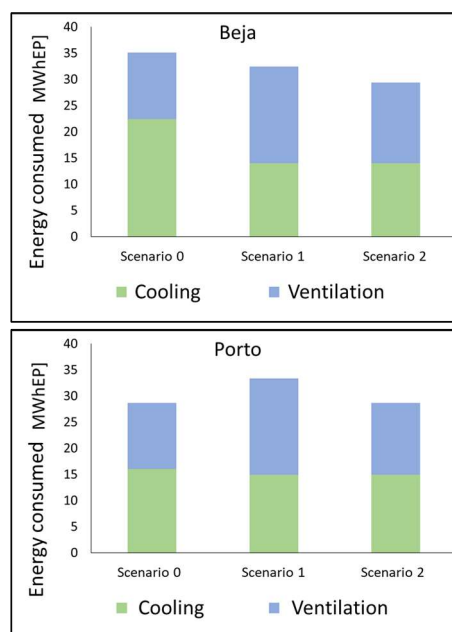


Figure 6. Energy consumed during the cooling season.

Conclusions

This work allows us to affirm that during the cooling season, the presence of the recuperator is disadvantageous for the energy consumption of the AHU in locations with a mild climate during the summer, nullifying the purpose of the component. The use of the mechanical bypass in these places allows to reduce energy consumption to levels below those recorded in the case of an AHU without a recuperator, enabling the use of the recuperator during the cooling season. In addition, the constructive solution with the mechanical bypass proves to be the best, both in terms of energy consumption and in terms of energy cost. The estimated savings in energy cost between the recuperator solutions with and without the mechanical bypass allows for a quick amortization of the additional investment cost in the manufacture of the AHU.

Finally, the introduction of the bypass in the autonomous regions and in the northern coastal locations must be imperative, and in other locations of Portugal, a

better analysis should be made, together with the available budget.

ACKNOWLEDGEMENT

The author wishes to thank Mr. Miguel Jesus and the company EVAC for their collaboration and expertise which made this article possible.

REFERENCES

- [1] Eurostat (online data code: nrg_110a).
- [2] A. Boyano, P. Hernandez, and O. Wolf, "Energy demands and potential savings in European office buildings: Case studies based on EnergyPlus simulations," *Energy and Buildings*, vol. 65, pages 19–28, Oct 2013. Available: doi.org/10.1016/j.enbuild.2013.05.039
- [3] A. Allouhi, Y. El Fouih, T. Kousksou, A. Jamil, Y. Zeraoui, and Y. Mourad, "Energy consumption and efficiency in buildings: Current status and future trends," *Journal of Cleaner Production*, vol. 109, pages 118–130, Dec 2015. Available: doi.org/10.1016/j.jclepro.2015.05.139
- [4] R. L. N. de Energia e Geologia, "CLIMAS-SCE," 2014. [Online]. Available: www.lneg.pt/servicos/328/2263

Experimental and simulation performance investigation of a hybrid PV/T solar panel

Mihai Baiceanu, Tiberiu Catalina

Technical University of Civil Engineering Bucharest, Faculty of Building Services ROMANIA

Abstract— This paper presents a study on hybrid PV/T solar panels performance, using both experimental and simulation methods. The experimental part is intended to measure and compare PV/T and PV electrical and thermal outputs, under measured solar irradiance and ambient temperature, and to assess the potential for further research involving adding phase-change materials inside of the PV/T panel. The simulation part of the study is intended to assess the technical viability of integrating the studied type of PV/T panel into a highly efficient solar house prototype, by comparing a reference system with separate PV and solar thermal collectors with one that uses PV/T panels.

The experimental study concluded the following: the PV was hotter than the PV/T by an average of 5°C on the back of the collector and by an average 16.5°C on the front face. The PV/T panel electrical power yield was greater by 5.2% than the PV and produced 2.1 kWh of thermal energy used for water heating. Also, irregularities in surface temperature and output curve aspect concluded that there is opportunity in studying the integration of phase-change materials in the collector, in future research.

The simulation study showed that the system with integrated PV/T panels results in a solar fraction to the system of 12.2% compared to 8.4% for the separate PV and solar thermal. It produced 5.2% more electrical energy, while the total consumption of the system (fuel and electricity) dropped by a significant 11.1%. Also, the global efficiency of the system increased by an average 10%.

Index terms – hybrid solar panel, photovoltaic, PV/T, simulation, thermography

I. INTRODUCTION

Solar energy is the richest source of renewable energy, it is abundant and inexhaustible. Building using the standard nZEB (nearly zero energy buildings) is now more stringent. To reach such level of energy efficiency the use of renewable sources is therefore a must. Residential buildings energy consumption is mainly related to heating, cooling, domestic hot water (DHW) and electricity. While photovoltaics panels are now more and more popular due to their lower price there is still a need to produce thermal energy for heating/DHW purposes. The use of hybrid solar panels that can produce both electric and thermal energy is a very appealing solution especially when the building roof space is limited. A photovoltaic/thermal (PV/T) hybrid system is an integration of the system composed of photovoltaic cells and solar thermal heat exchanger. The hybrid

system generates electricity and hot water from a combined system that maximizes the energy and/or economic performance of the system [3] [4]. The PV modules can absorb thermal energy and then transported using a copper heat exchanger to a fluid. As a result, the PV module temperature decreases, and its efficiency improves providing more electricity. The application of such hybrid panels can be extended also for other type of buildings. Thin-layer solar drying experiments were conducted in Matsuyama, Japan [1]. Chow TT. [2] proposed a dynamic PV/T collector model for single-plate water heating. A hybrid PV/T solar system was described by Vorobiev et al. [5]. The system consisted of a radiation concentrator, a PV cell and a thermoelectric generator. According to their calculations, the overall efficiency of the hybrid system could be achieved by about 30%. Zhu et al. [6] also proposed the achievement of the hybrid PV / TE system with a high efficiency of about 23% in the outdoor test, which is 25% higher than the PV (photovoltaic) cells. Fine et al. [7] developed a method for predicting hybrid solar panel performances in different operating modes and have experimentally validated it. Similar approach using simulations and experimental measurements was used by Yang et al. [8] and improvement of energy efficiency was realized using functionally graded material (FGM) for better heat transfer to the fluid. Experimental measurements were realized by Zakharchenko et al. [9] for 3 types of PV/T panels (SI, α -Si and CuInSe₂) proving the advantages of using these kinds of systems.

II. EXPERIMENTAL STUDY

A. Objectives of the Experimental Campaign

The scope of the experimental study is to assess the main performance parameters of a hybrid PV/T under typical operative conditions and compare it with a standard PV panel. However, the final objective is to investigate the possibility to further increase the performance of PV/T collectors by integrating phase-changing materials, so the experimental campaign presented in this paper is only a milestone and will provide reference values for the future investigation of PV/T panels with PCM integration.

B. Experimental Stand

The PV/T and PV panels were fixed due south with a 45° tilt angle. Water was circulated through the PV/T with a three-stage circulator pump and the water loop also contains an uninsulated water buffer which would

simulate both heat storage and DHW consumption during the day. Before the experiment, a water flow of 1.5 L/min – the rated flow of the PV/T panel – was set with the use of a regulation valve. Temperatures were measured and logged from key points of the system using thermocouples fed into an ALMEMO data logger. A pyranometer also transferred the measurements into the data logger in order to measure global horizontal solar irradiance. The electrical output parameters of the two collectors were measured with the use of an I-V curve tracer PV analyzer (Fig.1).

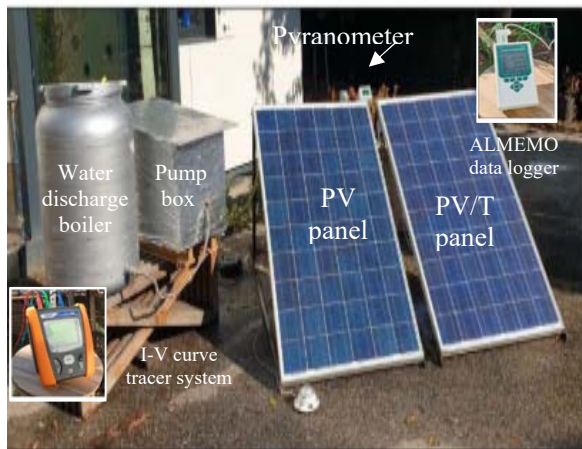


Fig. 1. Experimental stand and measurement systems.

C. Experimental Campaign Methodology

Data acquired with 1 minute sampling time, with the data-logger: ambient temperature, PV/T water inlet temperature, PV/T outlet temperature, PV/T temperature on the back of the cell, PV temperature on the back of the cell, horizontal solar irradiance. Together with the water flow which was constant during the experiment, the water inlet and outlet temperatures of the PV/T water circuit were used to calculate the thermal output of the PV/T collector.

Data acquired once every 30 minutes, with the PV analyzer: I-V and P-V characteristics of the PV/T and PV collectors. After data processing, electrical power outputs are of both collectors are calculated with the above characteristics, together with the solar cells' temperatures and the perpendicular irradiance, also measured by the PV analyzer with an external probe.

D. Results and Discussion

The temperature sensors on the back of the solar cells show a relatively constant temperature difference between the PV/T and the PV, the hybrid collector being an average of 5°C colder (Fig.2), due to the cold water flow which absorbs heat from the solar cells, cooling them.

Fig.(2) and fig.(3) show data from 10th of October, a day with outdoor temperatures and solar irradiance representative of the yearly averages.

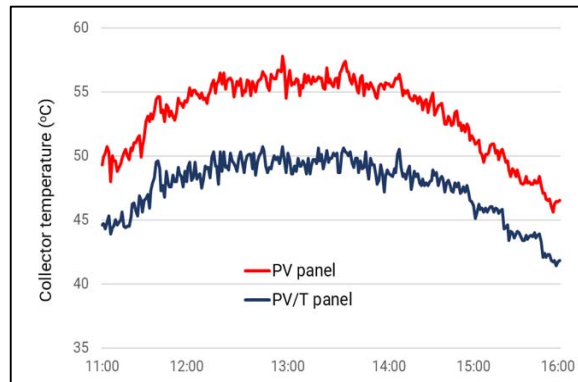


Fig. 2. Collectors temperature over time.

The electrical power output of the PV/T collector was significantly and consistently higher than that of the PV collector during the day. The overall electricity production of the PV/T is 10.1% higher (827 Wh compared to 751 Wh). The largest difference in power output is midday (12:45), when the PV/T outputs 13.75% more power (Fig.3.)

The thermal energy output of the PV/T was calculated using inlet and outlet water temperature and mass flow, which was constant during the experiment.

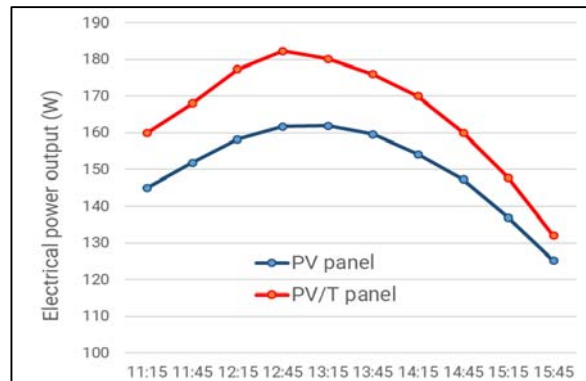


Fig. 3. Electrical power output of the collectors.

The total thermal energy output during the day was 2.1 kWh. The mean temperature difference between the water inlet and outlet was 3.6°C.

E. Thermographic Imaging Study

A thermal imaging camera was used to measure radiant temperature of the surfaces of the panels, simultaneously with the performance parameters measurements. As with the temperatures on the back of the panels, there is a consistent difference in temperature between the two panels' front surfaces. While the mean temperature difference during the day on the back on the panel is 5°C, on the front surface, the mean difference is 16.5°C, the hybrid panel being significantly cooler (Fig.5).

While the temperature distribution on the PV panel is even, on the hybrid PV/T panel we can observe 3 zones that are inconsistent with the rest of the panel (Fig.4). Zone 1 is adjacent to the water inlet, where the water has the lowest temperature and thus the greatest potential to

absorb heat from the panel. Respectively, zone 2 is adjacent to the water outlet, where there is the hottest water with the least heat absorption potential. Zone 3 is an area where the copper coil on the back of the panel bypasses the electrical connections, thus that area is not directly irrigated with water and gets hotter. Average temperatures were calculated for these areas, using the infrared images processing software.

The irregularities in surface temperature distribution as well as the fluctuations in surface temperature, in close accordance to solar irradiance levels show the opportunity to further study methods to reduce these irregularities in order to further improve the efficiency of the PV/T panel. One method to consider for a subsequent phase of this study is to integrate phase-changing materials inside of the PV/T case, in close contact with the photoelectric cells and the water coil.

The phase-changing materials are to be chosen so that the phase change temperature threshold is in accordance with the median collector temperature, as investigated in the present research. According to the temperature readings, both on the back of the collector measured with the temperature but also on the front of the panel measured with the IR camera, the optimal phase change threshold is 55°C, as this is the peak median temperature of the collector.

The assumptions to examine in such a study are whether a more uniform distribution of temperature leads to higher electrical output and whether more time-stable temperature of the PV/T collector would lead to better heat transfer to the receiving media, such as the buffer tank. It is also relevant to study the impact of the PCM-integrated PV/T panel dynamically via simulation, integrated in a heating/DHW productions system, similar to the study presented in the simulation study of the present research, as to be compared to a PV/T panel without phase changing materials integrated.

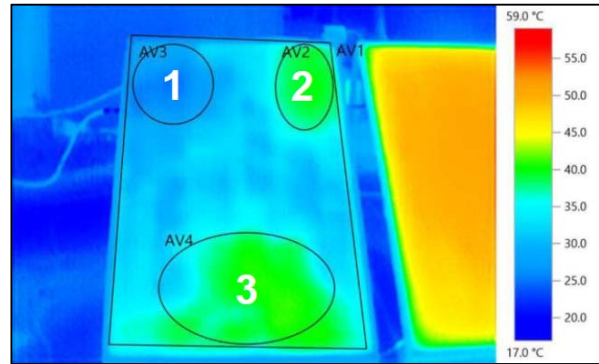


Fig. 4. PV/T panel temperature distribution.

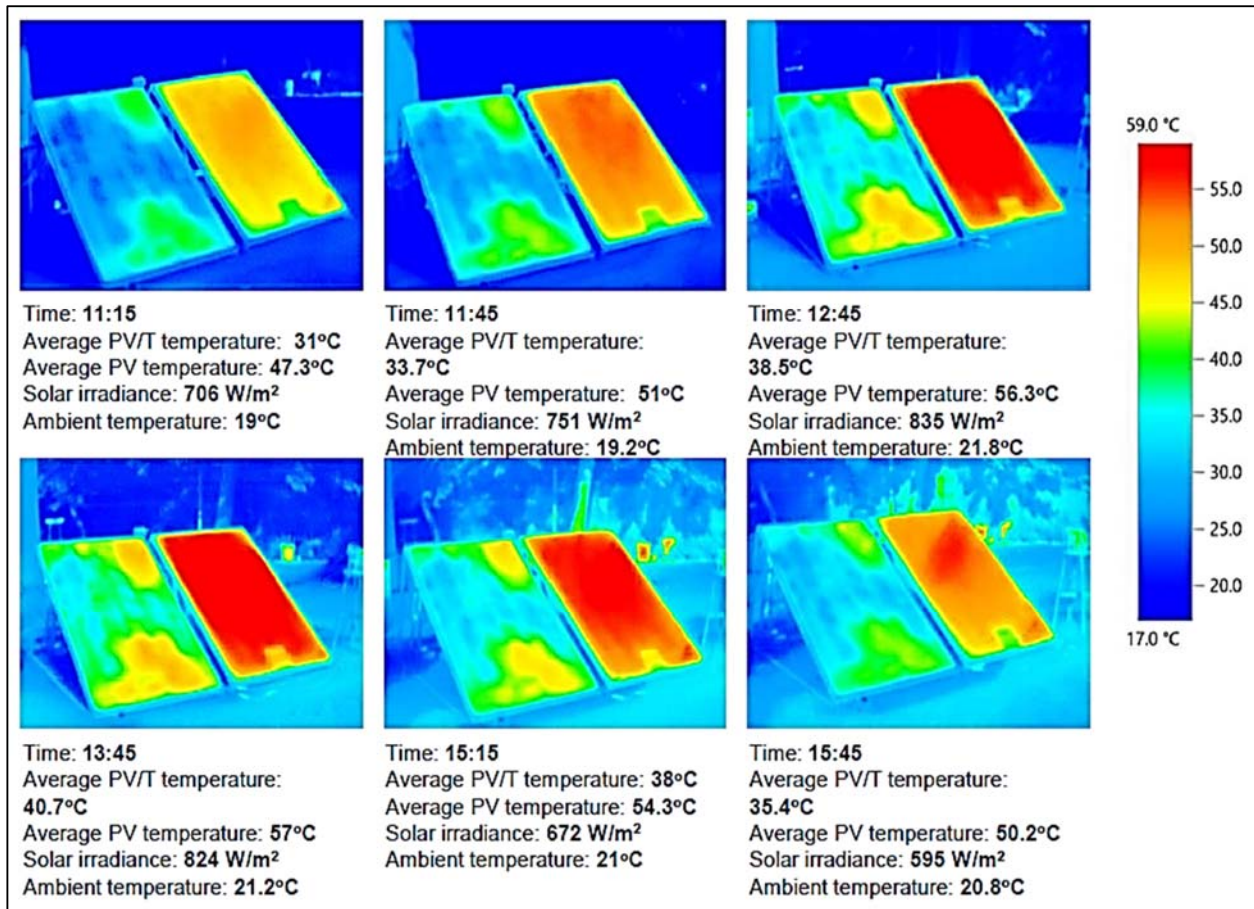


Fig. 5. Thermographic study.

III. SIMULATION STUDY

A. Objectives of the Simulation Study

The scope of the simulation study is to assess whether the implementation of hybrid PV/T panels is viable from a technical standpoint, considering electrical energy production, total electricity and gas consumption and global efficiency, on a highly efficient solar house prototype.

B. Reference building

House EFdeN Signature is the solar house prototype which represented Romania in the Solar Decathlon Middle East competition in 2018, the first to be taking place in an extreme hot and humid climate, Dubai. The main architectural and passive energy efficiency features are two raised volumes above the bedroom and kitchen, inspired by traditional Middle Eastern wind towers and an exterior facade, the “shell”, also inspired by the Middle Eastern “mashrabiya” (Fig.6). With a median U-value of 0.13 W/m²K, walls are structured as follows: aluminum composite facade (4 mm), ventilated air (10 cm), rockwool insulation (20 cm), wooden structural panel (11.5 cm), cork tiles (3 mm). Based on timber frame construction system, the roof and floor slabs have a U-value of 0.19 W/m²K.



Fig. 6. Reference building – Real phot of the House EFdeN Signature

C. Simulation Methodology

For the purpose of the simulation purpose, two technical solutions are compared: one with separate flat plate solar thermal collectors and PV’s, the other with hybrid PV/T panels. The rest of the system is the same for the two situations – tank in tank boiler for combined heating and domestic hot water production, powered by solar thermal source, a gas boiler and an electric coil. All the other simulation assumptions are the same in the two situations.

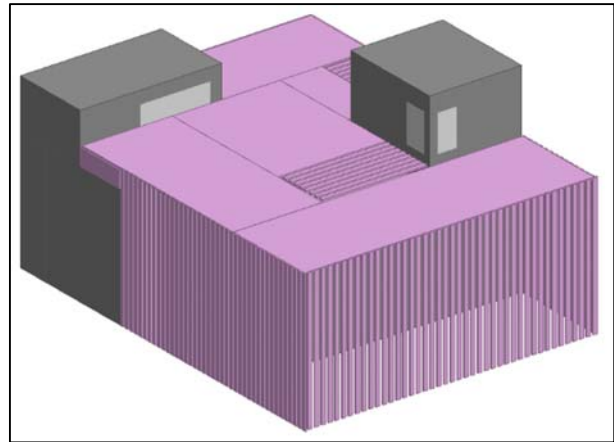


Fig. 7. House EFdeN Signature model in DesignBuilder

The simulation study consists of two parts – house thermal loads calculation in DesignBuilder software and system comparison in Polysun software.

Case scenario 1 (*reference system*) is comprised of Glazed flat plate solar thermal collector and photovoltaic panels, polycrystalline. The PV’s have 250W maximum power output, there are 32 modules (8 kW installed power), placed horizontally. The solar thermal panel has a 2.33 m² absorber area, placed horizontally (Fig.8).

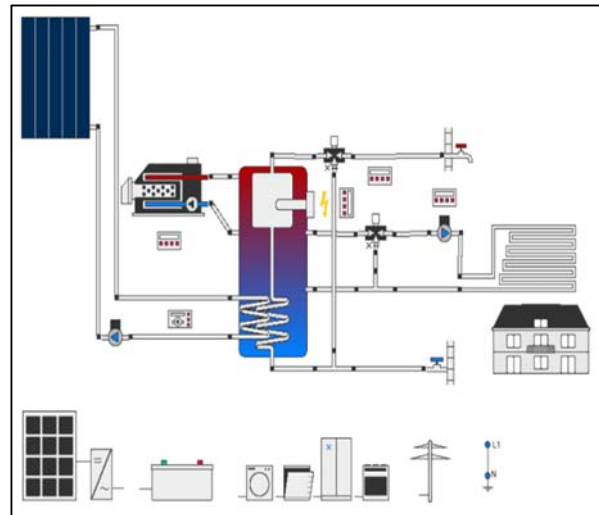


Fig. 8. Polysun model – case scenario 1

Case scenario 2 (*studied system*) is identical to case scenario 1, except for the solar collectors which are replaced with hybrid PV/T panels. The PV/T collectors are also polycrystalline, but with 240W maximum power output. Because of the space provided by removing solar thermal collectors, in case scenario 2 there are 36 PV/T modules, placed horizontally (Fig.9).

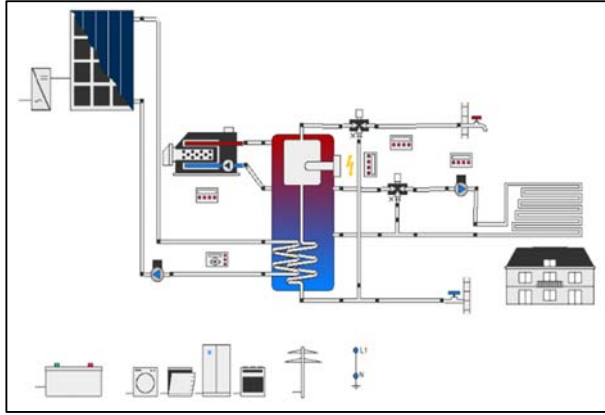


Fig. 9. Polysun model – situation 2

The rest of the system is identical in the two systems and are comprised of the following components. The combined heating and DHW production boiler have a total capacity of 800L and is powered by a lower solar coil, by the gas boiler and by an electric coil. The gas boiler has a heating capacity of 20 kW, in both the situations. The building component is defined by a 7.8 kWh total heating energy demand, excluding DHW preparation loads. The heating element is underfloor heating, with inlet temperature of 40°C. The DHW is to be fed to the consumers at 55°C. The electrical system is equipped with a 13.8 kWh battery bank. The electrical consumers have an annual consumption of 6000 kWh (cooling, appliances, electric vehicle).

D. Results and Discussion

The system in configuration 1, with separate PV's and solar thermal panels, 9152 kWh of electricity are produced, while the PV/T configuration outputs 9652 kWh, a 5.2% increase in electrical PV yield. The solar fraction is the ratio of energy from solar source (both electrical and thermal) over the total energy consumed by the system. The total solar fraction is 8.4% for situation 1 and 12.2% for situation 2 which means a 3.8% increase. The solar fractions for DHW preparation are 17.9% and 37.6% respectively, while the solar fractions for heating are 1.3% and 9.1% respectively. In the first situation, the system total energy consumption (gas and electricity) is 11168 kWh/year, while for the second situation with the PV/T it is 9926 kWh/year, a significant drops of 11.1%.

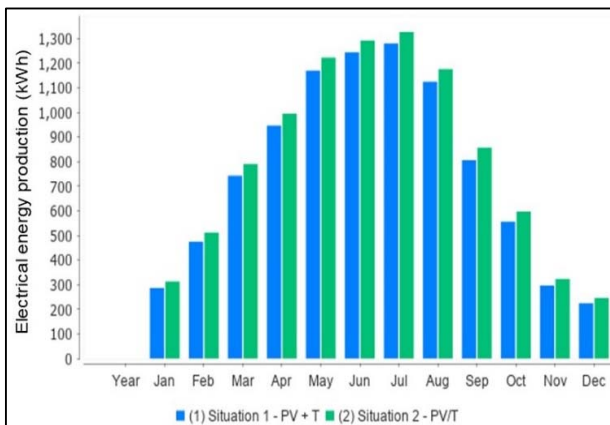


Fig. 10. Electrical energy production

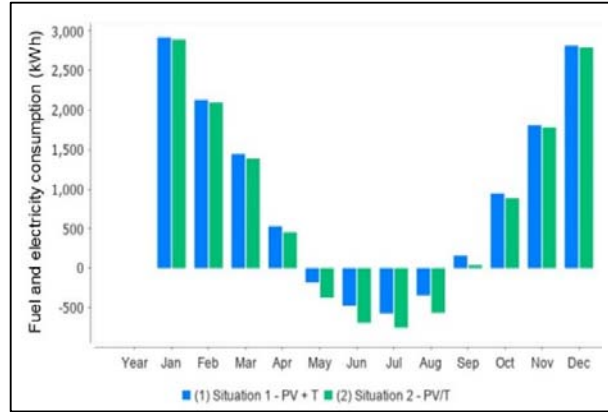


Fig. 11. Total energy (electricity and gas) consumed by the system

For the PV, the maximum efficiency is 12.5%, while for the PVT it is 22% (Fig.12). The simulation day for the global efficiency calculation is 15th of July. We can conclude that PVT are less efficient relative to aperture area compared with solar thermal panels but produce more energy if all PV's are replaced with PVT's.

$$EFF_{PV/T} = \frac{P_E + P_T}{IRR_{array}} \quad (1)$$

$EFF_{PV/T}$ – global efficiency of PV/T panel (%)

P_E – Electrical power output (W)

P_T – Thermal power output (W)

IRR_{array} – Total solar irradiance incident on the array (W)

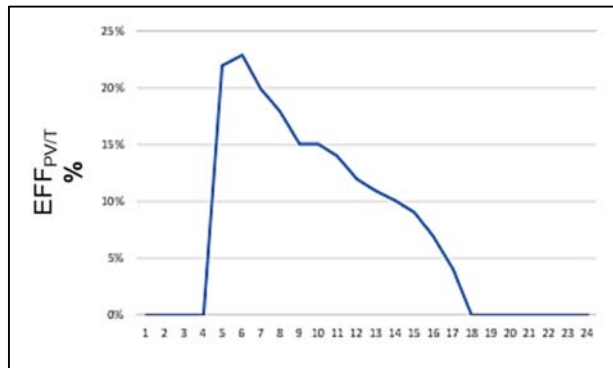


Fig. 12. Global efficiency of the PV/T system.

IV. CONCLUSIONS

From both the experimental and the simulation investigation, the benefits of the hybrid PV/T collector are obvious when compared to standard PV's or systems with separate production of electricity and heat from solar source. The experimental study concluded the following: the PV was hotter than the PV/T by an average of 5°C on the back of the collector and by an average 16.5°C on the front face. The PV/T panel electrical power yield was greater by 5.2% than the PV and produced 2.1 kWh of thermal energy used for water heating. The simulation study concluded that the system with integrated PV/T panels results in a solar fraction to the system of 12.2% compared to 8.4% for the separate PV and solar thermal. It produced 5.2% more

electrical energy, while the total consumption of the system (fuel and electricity) dropped by a significant 11.1%. Also, the global efficiency of the system increased by an average 10%.

The experimental results of the present study also outline the opportunity of further research of this subject by integrating phase-changing materials in the PV/T panel, as suggested by the temperature irregularities on the collector surface. The present study concludes that further research should study the integration of PCM's with 55°C temperature threshold, investigating the change in temperature distribution uniformity effects on electrical output and heat transfer global dynamical effectiveness.

REFERENCES

- [1] Basunia MA, Abe T. "Thin-layer solar drying characteristics of rough rice under natural convection," *Journal of Food Engineering*, 2001; vol. 47, pp/ 295–301.
- [2] Chow TT. "Performance analysis of photovoltaic–thermal collector by explicit dynamic model," *Solar Energy*, 2003, vol. 75, pp.143–52.
- [3] Chow TT. "A review on photovoltaic/thermal hybrid solar technology," *Applied Energy*, 2010, vol.87, pp. 365–379.
- [4] Calise F, Dentice d'Accadia M, Palombo A, Vanoli L. "Dynamic simulation of a novel high–temperature solar trigeneration system based on concentrating photovoltaic/ thermal collectors," *Energy*, 2013, vol.61, pp.72–86.
- [5] Beath AC. "Industrial energy usage in Australia and the potential for implementation of solar thermal heat and power," *Energy*, 2012, vol.43, pp.261–272.
- [6] Vorobiev Y, Gonzalez-Hernandez J, Vorobiev P, Bulat L. "Thermal-photovoltaic solar hybrid system for efficient solar energy conversion," *Solar Energy*, 2006; vol.80, 170–176.
- [7] Fine. P. J. , Dworkin S.B., Friedman J. "A methodology for predicting hybrid solar panel performance in different operating modes," *Renewable Energy*, 2019, vol. 130, pp. 1198-1206
- [8] Yang D.J., Yuan Z.F., Lee P.H., Yin H.M, "Simulation and experimental validation of heat transfer in a novel hybrid solar panel," *International Journal of Heat and Mass Transfer*, 2012, vol. 55, pp. 1076-1082
- [9] Zakharchenko R., Licea-Jiménez L., Pérez-García S.A., Vorobiev P., Dehesa-Carrasco U., Pérez-Robles J.F., González-Hernández J., Vorobiev Yu., "Photovoltaic solar panel for a hybrid PV/thermal system," *Solar Energy Materials and Solar Cells*, 2004, vol. 82, pp. 253-261

OPTIMIZATION OF COOLING PLANT BY APPLYING HEAD PRESSURE CONTROL ON COOLING COMPRESSOR

October 2019.

M. Sc. Damir Kovčić,
 Faculty of Technical Sciences
 Department of Energy and Process Engineering
 University of Novi Sad, Serbia
damirkovcic@yahoo.com

Assoc. Prof. Miroslav Kljajić, Ph.D., Mentor
 Faculty of Tehcnical Sciences,
 Department of Energy and Process Engineering
 Univeristy of Novi Sad, Serbia
kljajicm@uns.ac.rs

Abstract — Cooling plants are huge consumers of electrical energy and their optimization is critical in terms of energy usage. This paper is focused on one approach for cooling plant optimization. Based on calculated cooling requirements and actual energy consumption for one calendar year, optimization of cooling plant is researched and compared, using wet bulb temperature as set point for head pressure. Calculation showed possibility for achieving electricity consumption reduction around 7%, by applying this method.

Index Terms— Brewery, Cooling Plant, Head Pressure Control, Energy Reduction.

I. INTRODUCTION

Breweries could be considered as one type of chemical industry because during beer production many chemical reactions are occurring and as a result beer is produced together with few byproducts such as CO₂. Beside constant raw material import, energy constantly needs to be transformed in order to have stable beer production.

Cooling plants as main consumers of electrical energy within one brewery are very interesting topic. Optimization of those plants in terms of peak consumption shaving or changing the way cooling plants work (like changing evaporation temperature and head pressure) can have mayor influence on total brewery electricity consumption.

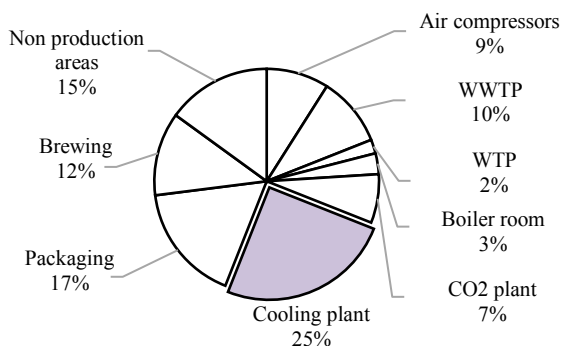


Figure 1. Brewery energy consumption deployment

In recent years in many breweries have done improvements in terms of head pressure control, frequency driven compressor installation or rising evaporation temperatures in order to increase suction pressure. All these improvements are resulting in lower electricity consumption but for this type of optimization teams of technologist and engineers need to collaborate in order to

take care not to damage beer production process. Following chapter is giving quick overview of beer production process and its cooling requirements.

II. BREWING PROCESS

Brewing is process which is done in batches and it is possible to do six to eight batches during one production day (24 hours). Malt is main ingredient for beer production and it is being made in malting plants outside breweries. As a raw material it is transported to brewery where it is being conditioned, grounded in mills and depending on the recipe some adjuncts like barley, maize or wheat are added. During mashing of above mentioned ingredients by controlling the temperature and length of mashing itself long sugar chains are being broken into smaller more simple ones which are needed for good fermentation. Next step in brewing process is mash filtering and as a result of this process clear wort ready for boiling is being made. During boiling hops are added which have influence on future beer bitterness. After boiling wort is at temperature of 100°C and it needs to be cooled to the temperature of +20°C in very short period of time to prevent any microbiological contamination. Whole process is done in the brew house area.

After being cooled yeast is added into wort and it is transported within pipes to the fermentation area where fermenting process starts. During fermentation yeast is using sugar to create alcohol and as a byproduct CO₂ gas and heat are being generated. Generated heat increases fermentation temperature and pressure inside fermenter which as a result speeds up fermentation process. Due to that fact fermentation needs to be kept within certain limits in terms of temperature and pressures, for lager beer temperature needs to be below +16°C during fermentation. Excessive CO₂ is being released through pressure relief valves and it is recuperated, liquefied and kept at -23°C on pressure of 17-20 bar. When needed it is evaporated and sent to consumers.

During main fermentation inactive yeast cells start to settle on the bottom of fermenter and after 4 to 8 days when main fermentation process is done young beer is being cooled to temperature between -1.5°C and 0°C in order to speed up yeast settlement. That phase is called beer maturation. When maturation phase is done beer is sent to filtration unit and before entering filler it is being pasteurized at +74°C and cooled again to prepare it for filling.

From above mentioned it is clear that cooling is one of main factors for stable beer quality parameters. In electricity consumption cooling is taking share of 20-25% of total brewery consumption and for that reason it is important to work on its efficiency increase in order to lower production costs and reduce brewery CO₂ footprint.

III. HEAD PRESSURE CONTROL

Head pressure control is very interesting option in terms of compressor optimization. Idea is based on lowering electricity consumption of cooling compressor and balancing with increased condenser electricity consumption. Because of different nominal powers of compressors and condensers it is possible to achieve better results in terms of lower electricity consumption. By observing Figure 2 it is possible to compare two ammonia cooling cycles with same suction pressure ($T_e = T_e' = -5^\circ\text{C}$, $p = 3.5$ bar) and different condensation pressures ($T_c = 22^\circ\text{C}$, $T_c' = 35^\circ\text{C}$, $p = 13.52$ bar). These two condensing pressures are taken as best and worst case for one cooling compressors. In case of lower condensing pressure heat transfer in evaporator equals $Q_e = 1,152.7$ kJ/kg while in other case heat transfer equals $Q_e' = 1,090.3$ kJ/kg.

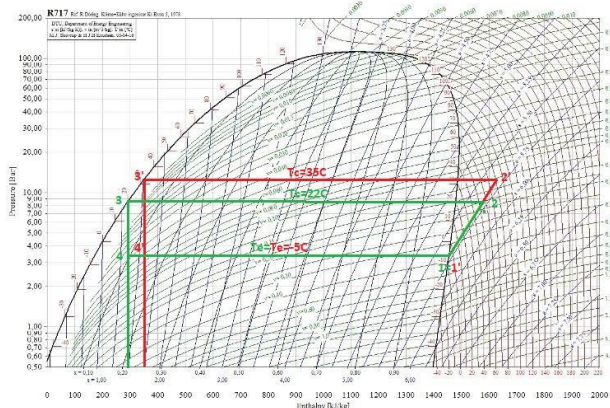


Figure 2. Pressure-enthalpy diagram

Also when compressor works on higher pressures it absorbs more energy on the shaft. From supplier's data sheet absorbed power in case of lower condensing pressure equals 340 kW while in case of 13.52 bar absorbed power equals 412.5 kW. Another parameter which is not negligible is volumetric flow decrease through cooling compressor in case of pressure increase. For compared pressure flow decrease is 1.4%. On Figure 3 values for absorbed power is graphically presented.

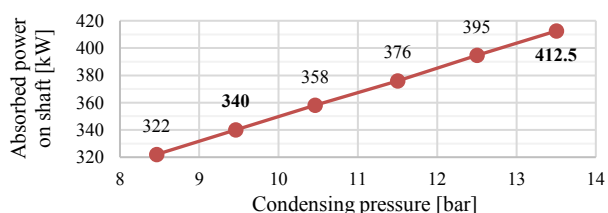


Figure 3. Change of absorbed power on shaft

IV. BREWERY COOLING CAPACITY REQUIREMENTS

In order to calculate monthly cooling energy requirements daily consumptions depending on number of batches have been established. Table 1 gives an overview of daily cooling energy requirements.

TABLE I.
DAILY CONSUMPTIONS DEPENDING OF NUMBER OF BATCHES

Batches per day	#	7	6	5	4
Batch volume	hl	500			
Volume of brewed beer	hl	3500	3000	2500	2000
Ice water heat exchanger	kWh	4171	3575	2979	2383
Fermentation and maturation	kWh	14589	12505	10421	8337
CO2 recuperation plant	kWh	5760	4937	4114	3291
Yeast storage plant	kWh	3600	3086	2572	2058
Building air conditioning	kWh	10800	10800	10800	10800
Consumption in summer mode	kWh	38920	34903	30886	26869
Consumption in winter mode	kWh	28120	24103	20086	16069

Number of working days and number of batches is based on historical data and it was used to determine daily and monthly cooling energy requirements. Figure 4 displays monthly calculated cooling demand consumption in one production year.

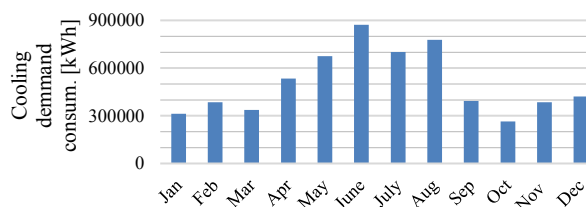


Figure 4. Monthly cooling demand level

From figure above it is evident that this brewery cooling energy demand is affected by production level and season (winter/summer) which is dictating work of air conditioning unit.

Average cooling demand is calculated as relationship between monthly cooling demand and total number of compressor working hours for that month. Average cooling demand and working hours of compressor are presented on figure 5.

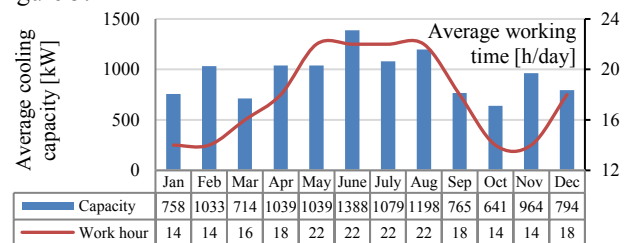


Figure 5. Average cooling demand and working hours of compressor

Compressor and working regimes selection are done based on the cooling demand, suction and discharge pressure. Suction pressure is calculated from equation for heat transfer. Since heat transfer coefficient and area of heat exchanger are known it is possible to calculate mean logarithmic temperature by dividing cooling demand with heat transfer coefficient and area of heat exchanger.

$$Q = k \cdot A \cdot \Delta t_{log} \quad (1)$$

Since ammonia temperature through heat exchanger it is calculated by using equation for mean logarithmic temperature.

$$\Delta t_{log} = \frac{(t_{i(NH3)} - t_{iz(PG)}) - (t_{i(NH3)} + t_{ul(PG)})}{\ln \frac{(t_{i(NH3)} - t_{iz(PG)})}{(t_{i(NH3)} - t_{ul(PG)})}} \quad (2)$$

Values for suction pressure occurring in this system are presented in the table 2.

TABLE II.
AMMONIA EVAPORATION TEMPERATURE

Δt_{log}	$t_{out(NH3)}$	$t_{in(PG)}$	$t_{out(PG)}$
- 3.41	- 5.50	1	- 4
- 2.79	- 5.00	1	- 4
- 2.09	- 4.50	1	- 4
- 1.53	- 4.20	1	- 4
- 1.41	- 4.15	1	- 4
- 1.27	- 4.10	1	- 4
- 1.08	- 4.05	1	- 4

A. Fixed head pressure calculation

In case that head pressure set points are manual setting is done by the operator and it is predetermined for certain month. Overview of parameters is given in table 3 bellow.

TABLE III.
MANUAL SET HEAD PRESSURE PARAMETERS

		Jan	Feb	Mar	Apr	May	Jun	Jul	Aug	Sep	Oct	Nov	Dec
Head pressure set point	bar[g]	9	9	9	10	12	12	12	12	11	11	10	9
Condensing temperature	°C	25	25	25	28.1	33.7	33.7	33.7	33.7	31	31	28.1	25
Mean log. temperature	-	-	-1.43	-1.95	-1.35	-1.96	-2.62	-2.04	-2.26	-1.45	-1.21	-1.82	-1.50
Evaporation temperature	°C	-4.2	-4.5	-4.2	-4.5	-4.5	-5	-4.5	-5	-4.2	-4.1	-4.5	-4.2

By using software delivered from MYCOM values for absorbed power and cooling capacity for each compressor are calculated. Main working compressor is chosen in order to have maximum efficiency depending on cooling demand. Figure 6 represents consumption distribution between compressor and condenser and COP per month for cooling plant respectively.

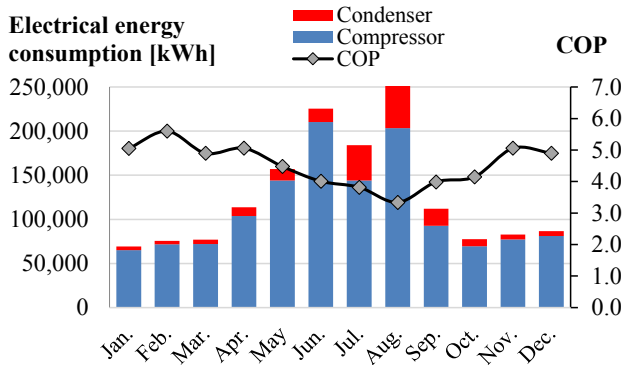


Figure 6. Consumption with fixed head pressure

B. Floating head pressure calculation

Head pressure regulation is done in accordance with atmospheric condition. Ideal condensation temperature is

being calculated by using software. Set point for ideal condensation temperature is 8°C above measured wet bulb temperature. For this type of compressor set up there is requirement for minimum head pressure in order to have good separation of oil in oil separator. For MYCOM compressors VLD250-N and VLD200-N minimal allowed head pressure is 8.1 bar[g] which in temperature terms equals 22°C.

Main principal is to lower compressor electricity consumption on the cost of condensers electricity consumption increase. As a result trade of is positive and COP of engine room is increasing.

Figure 7 represents difference between previously set condensation parameters and calculated condensation parameters based on mean dew point temperature values. Values below 22°C have limits in order to protect equipment from potential damage.

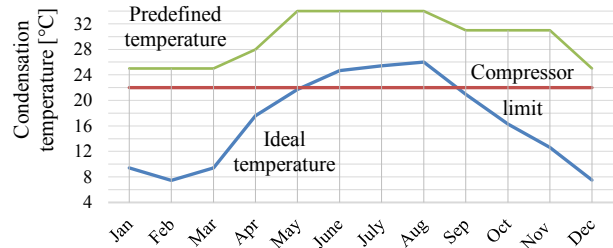


Figure 7. Manual set points vs calculated set points

Figure 7 represents difference between previously set condensation parameters and calculated condensation parameters based on mean dew point temperature values. Values below 22°C have limits in order to protect equipment from potential damage.

Leading compressor is selected with same criteria as in case with fixed head pressure, difference in absorbed power is result of less work due to lower head pressures.

Evaporative condensers capacity is chosen to be doubled comparing to compressor cooling capacity in winter season, while in summer season capacity is tripled in order to keep condensation parameters within measured limits. Regulation of condensers start up is in cascade order, first all compressors start one by one with low fan speed in combination with water pump then high speed fans start in case of need.

On figure 8 it is clear that electricity consumption has risen on condensers while consumption of compressors has lowered comparing to figure 6. Also, it can be noted that COP of engine room has risen on monthly and yearly level.

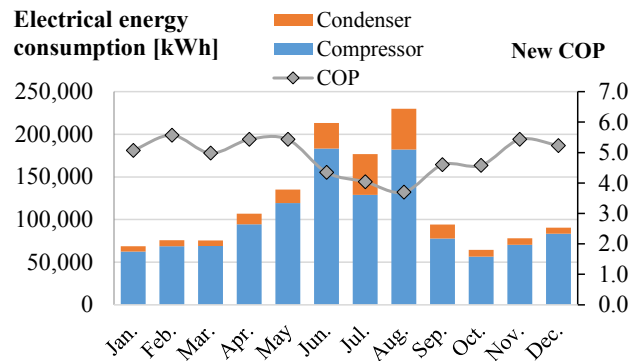


Figure 8. Consumption with floating head pressure

V. CONCLUSION

Subject of this paper was cooling plant within brewery where calculation for potential optimization savings is done. Point of calculation was comparison between fixed head pressure and floating head pressure set point based on wet bulb temperature.

Calculation of required cooling capacities is done based on historical data of beer production for 2018, also for calculation purposes data regarding compressors and condensers were used. Based on that data COP of engine room is calculated for fixed head pressure mode.

For same conditions model was created where head pressure set point was changing in time based on wet bulb measurements. For purpose of calculation mean values of atmospheric conditions per month were taken. Based on variation during day it is possible to have even greater savings of electricity.

Calculation displays that it is possible to achieve electricity consumption reduction by applying this method and that are around 7% which for brewery this size equals to 100,000 kWh on yearly level. For this type of regulation some investments are needed in order to improve cooling capacity of condensers to achieve required pressure set points. In case of this brewery capacity already exists.

In comparison to current fixed head pressure best savings are in spring and autumn where there are biggest deviations between conditions during the day and night.

Figure 9 displays improvement of engine room COP during one year depending on which type of parameters are applied.

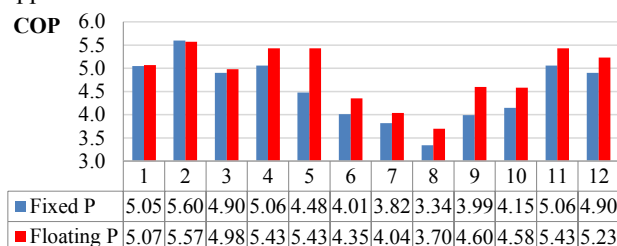


Figure 9. COP of engine room

REFERENCES

- [1] I. Vanjur, V. Sovilj, Mogućnosti smanjenja potrošnje električne energije amonijačnih rashladnih instalacija u velikim pivarama, Međunarodni kongres i izložba o KGH
- [2] K. A. Manske, D. T. Reindl, S. A. Klein, “Evaporative Condenser Control in Industrial Refrigeration Systems”, International Journal of Refrigeration, Vol. 24, No. 7, pp 676-691, 2001
- [3] R. J. Love, D. J. Cleland, I. Merts, B Eaton, “What is the optimum compressor discharge pressure set point for condensers”, IRHACE technical conference, 2005
- [4] T. W. Davies, “A universal floating head system”, international Congress of Refrigeration, ICR0079, Washington D.C, 2003
- [5] D. Demma, “Understanding the fundamentals of head pressure control”, 2004
- [6] MYCOM SCREW COMPRESSOR design software

Impact of flue gas recirculation on the efficiency of hot-water boilers

Anastasija Zeiza-Seļezņova,

Riga Technical University, Address: 1 Kalku Street, Riga, e-mail: rtu@rtu.lv, 2020.

Abstract—The topicality of the work is related to the fact that the combustion processes of various fuels, such as heat production, produce emissions that are harmful to the environment. The combustion of fossil fuels produces nitrogen oxides, which are about 10 times more dangerous than carbon monoxides. There are different methods to reduce nitrogen oxides emissions and one of effective methods is flue gas recirculation. Despite efficiency, flue gas recirculation has an impact on the efficiency of the boiler.

The efficiency coefficient for the hot-water boiler was calculated with and without flue gas recirculation. The calculation with flue gas recirculation leads to a slight reduction in the efficiency factor, herewith flue gas recirculation reduced emissions of nitrogen oxides by 44,5%.

Index Terms—flue-gas recirculation, boiler, nitric oxide.

Introduction

The point of the work is to study the impact of flue gas recirculation on the efficiency of a hot water boiler to reduce nitrogen oxide emissions.

The combustion processes of various fuels, such as heat production, produce emissions which are harmful to the environment. The main harmful elements of flue gases are nitrogen oxides (NO_x), carbon dioxide (CO₂), carbon monoxide (CO), sulfur dioxide (SO₂), particulate matter and others.

A. Nitrogen oxides (NO_x)

Nitrogen oxides (NO_x) are the main toxic components of natural gas and fuel oil combustion [1][2]. Nitrogen oxides are considered to be major pollutants for the reason that in addition to environmental problems, they cause health-threatening problems such as photochemical smog, acid rains and ozone layer depletion. Nitrogen oxides have a negative effect on human health, mainly on the respiratory system [3].

The abbreviation NO_x stands for nitrogen monoxide (NO) and nitrogen dioxide (NO₂), which are produced in flue gas as the result of reactions of nitrogen and oxygen. Nitric oxide is a colourless poisonous gas and nitrogen dioxide is a very poisonous gas with a brownish tinge. NO_x, emitted during combustion, consists of 95% NO and 5% NO₂[4].

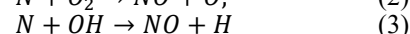
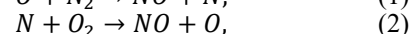
B. NO_x formation mechanisms

Currently, three mechanisms of nitrogen oxide formation are known: fuel NO_x mechanism, thermal NO_x mechanism and prompt NO_x mechanism.

Fuel NO_x is formed on reactions after the release of fuel bound nitrogen when fuel is heated during devolatilization. Important primary nitrogen-containing components are ammonia (NH₃) and hydrogen cyanide (HCN). If sufficient O₂ is available, these components will mainly

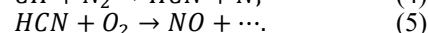
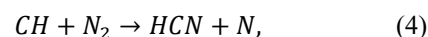
convert to NO through different reaction routes. In fuel-rich conditions NO will react with NH₃ and HCN forming N₂. Formation of fuel NO_x depends mostly on chemically bound fuel nitrogen content in the fuel. Thus, fuel NO_x is produced at low temperature [3].

The reactions of thermal formation of nitric oxide are characterized by a high activation energy; therefore, nitrogen oxides are formed at high temperatures above 1800°K. The reactions can be expressed by extended *Zeldovich* mechanism[1]:



The concentration of thermal nitrogen oxides rapidly increases in the combustion zone, and its maximum values are in the zone of the maximum combustion temperature.

However, Fenimore's studies on the combustion of hydrocarbon fuels showed that, in a very short period of time, nitrogen oxides are formed in front of the flame by a mechanism different from *Zeldovich* mechanism. The detected nitric oxide is called prompt [1]. Formation of NO_x by prompt NO_x mechanism takes place in reactions of atmospheric nitrogen with hydrocarbon radicals in fuel-rich regions by reactions [3]:



The formation of prompt nitric oxide occurs at temperatures of 1200–1600°K, when the thermal formation of nitrogen oxide does not occur [1].

The correlation between combustion temperature and NO_x formation is shown in Figure 1.

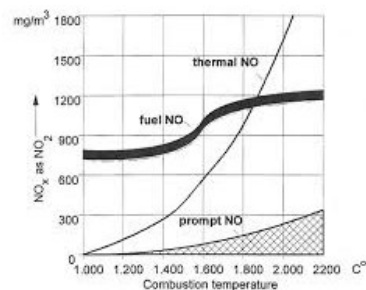


Figure 1. The correlation between combustion temperature and NO_x formation mechanisms [5].

Although the positive correlation between fuel, prompt NO_x and temperature are approximately linear, the amount of thermal NO_x increases disproportionately with increasing combustion temperature.

C. NOx reduction methods

In recent years, environmental protection requirements have become more stringent, that is why the fight against toxic emissions into the atmosphere has become especially important.

Currently, a large number of methods for reducing the concentration of nitrogen oxides in flue gases are known, and they can be divided into two large groups: cleaning flue gases by chemical or physicochemical methods, as well as technological methods.

The chemical or physicochemical method is based on the reducing of nitrogen oxide amount in the flue gases formed during combustion, while the technological method is based on preventing the formation of nitrogen oxide during combustion [4][6][7]. New methods of reducing oxides are also emerging. An overall picture of reducing nitrogen oxides methods is shown in Figure 2.

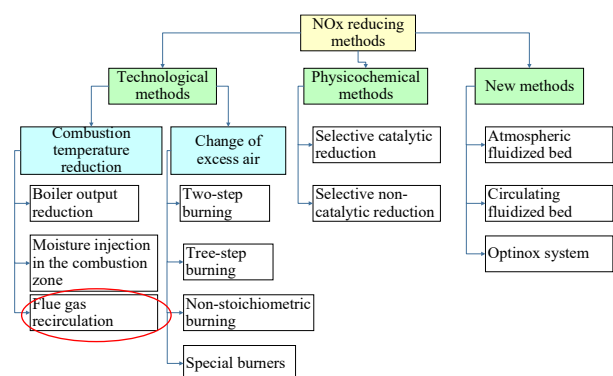


Figure 2. Nitrogen oxides reducing methods.

Flue gas recirculation (FGR) belongs to technological method, as a way to reduce combustion temperature. The flue gas recirculation method became widespread in the late 1970s and since has been widely used in boiler technology. This method involves taking part of the flue gas from the flue pipe and pump it into the active combustion zone (furnace).

A standard forced draft burner has an excess of oxygen to ensure complete combustion. The recirculation of flue gases, in turn, reduces the excess oxygen and partially replaced by inert flue gases, which mix and absorb some of the flame energy, thereby reducing the temperature. NO_x production increases exponentially with increasing temperature, so a maximum combustion temperature reduction can easily reduce NO_x emissions up to 7–80%. The flue gas temperature is usually around 250–350°C [8][9][10].

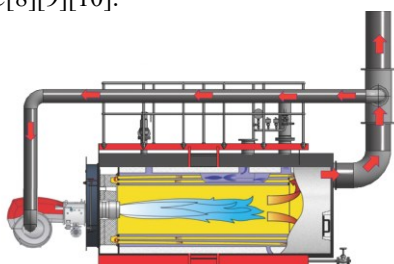


Figure 3. A boiler with flue gas recirculation [16].

Practically, the flue gas recirculation ducting (shown in Figure 3) connects between a special port on the burner air intake and a branch in the flue close to the boiler outlet – and, potentially, a fan – with the flow of flue gas being modulated by a damper. The duct is insulated to reduce condensate formation, and includes condensate drainage points in the duct adjacent to the burner inlet.

The effectiveness of the flue gas recirculation method depends on way the flue gases are supplied to the boiler (Figure 4).

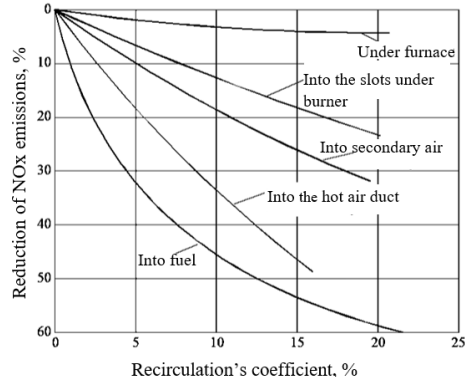


Figure 4. Reduction of NOx formation depending on therecirculation gases input method [12].

It is important how flue gases are supplied, because with the recirculation of 1% of flue gases, the boiler efficiency decreases by 0.03–0.06% [11]. The most efficient way, how to supply flue gas to the boiler is with fuel [17].

Main data of the analyzing object

As the object of research is hot-water boiler “BOSCH UT – M 64”. The boiler is installed in one of the heating plants in Riga (Figure 5).



Figure 5. Hot-water boiler “BOSCH UT M-64”.

Boiler’s output is 18 MW, fuel – natural gas, reserve fuel – diesel. The boiler is equipped with a flue gas recirculation to reduce the nitrogen oxide content to 50 mg/Nm³ (permissible value). The recirculated flue gas is supplied together with the secondary air directly to the burner.

Boiler design is three-pass single-flame tube/smoke tube technology. The inserted flame tube ends in an inner, fully wetback smoke gas reversing chamber, which leads into the first smoke tube pass. The first smoke tube pass and second smoke tube pass are free of flow components. The functional round design ensures optimal pressure resistance [16].

Also, hot-water boiler is equipped with LOWNOx burner – ELCO RPD 70. Burner is shown in Figure 6.

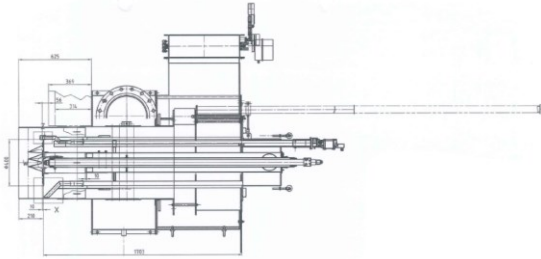


Figure 6. Burner ELCO RPD 70.

Dependence of the boiler “BOSCH UT M-64” efficiency and NOx emissions on the boiler output is shown in Figure 7. Boiler efficiency slightly decreases with increasing boiler output, however, nitrogen oxide emissions increase.

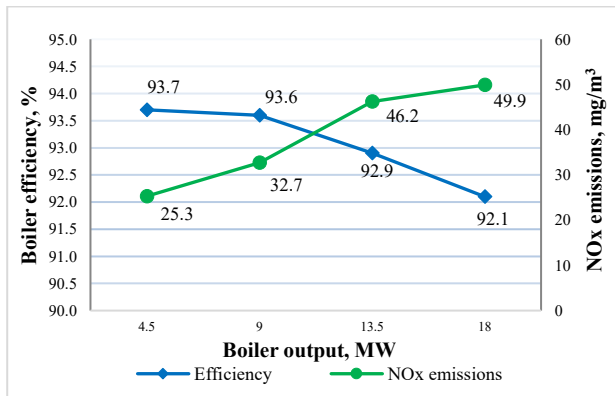


Figure 7. Dependence of the boiler efficiency and NOx emissions on the output.

All the data necessary for calculations are collected in Table 1. For calculations were taken two boiler operating regimes (o.r.) – at maximum output and at reduced output.

TABLE I
DATA FOR CALCULATIONS

Nr.	Parameter name	Symbol	Measurement	Values	
				1.o.r.	2.o.r.
Gas parameters					
1.	Low heat value	Q_i^d	$\frac{\text{kJ}}{\text{nm}^3, \text{g}}$	36485	
2.	Specific heat capacity	C_g	$\frac{\text{kJ}}{\text{nm}^3, \text{g} \cdot ^\circ\text{C}}$	1,557	
3.	Temperature	t_n	$^\circ\text{C}$	5,59	
4.	Enthalpy	$h_g = C_g \cdot t_n$	$\frac{\text{kJ}}{\text{nm}^3, \text{g}}$	$1,557 \cdot 5,59 = 8,7$	
5.	Combustion energy	$Q_c = Q_i^d + h_g$	$\frac{\text{kJ}}{\text{nm}^3, \text{g}}$	$36485 + 8,7 = 36494$	
Hot-water boiler parameters					
6.	Boiler output	Q_1	MW	18,11	5,58
7.	Air temperature	t_a	$^\circ\text{C}$	25,1	14
8.	Excess air coefficient	α_b^{out}	-	1,11	1,15
9.	Flue gas temperature	v_{fg}^{out}	$^\circ\text{C}$	174,72	98,5
10.	RGR fan frequency	-	Hz	50,81	

11.	Heat losses due to chemical underburning	q_3	%	0	
12.	Heat losses from external cooling	q_5	%	0,09	1,48
13.	Recirculation coefficient	r	%	0,126	0,403
Another data					
14.	Electricity costs		€/kWh	0,18	
15.	Natural gas costs		€/m³	0,21	

Methods

The coefficient of efficiency of a hot-water boiler is the ratio of the useful heat (consumed to generate steam/hot water) to the available heat of the heating boiler.

The boiler efficiency η [%] can be calculated using the forward balance (6) or reverse balance (7) equation [13]:

$$\eta = \frac{Q}{Q_c} \cdot 100, \quad (6)$$

$$\eta = 100 - (q_2 + q_3 + q_4 + q_5 + q_6). \quad (7)$$

In equation (6) Q [kJ/kg] is the amount of useful heat used and Q_c [kJ/kg] is available heat.

In equation (7) boiler efficiency directly depends on heat losses q_x : q_2 – with flue gas, q_3 – due to chemical underburning, q_4 – with mechanical underburning, q_5 – from external cooling, q_6 – with the physical heat of the ash.

The main difference in efficiency calculation is the calculation of losses with flue gases with (8) and without (9) FGR. More precisely, in calculating the enthalpy of flue gases [14] [15]:

$$q_2 = \frac{(H_{fg} - \alpha \cdot H_a^0) \cdot (100 - q_4)}{Q_c}, \quad (8)$$

$$q_2^r = \frac{(H_{fg} \cdot (1+r) - \alpha \cdot H_a^0) \cdot (100 - q_4)}{Q_c}. \quad (9)$$

Equation (8) is for heat losses without FGR and enthalpy is taken simply for flue gases H_{fg} [kJ/m³], but in equation (9) for calculations with FGR there is also recirculation coefficient r .

$$r = \frac{v_{fg}^r}{v_{fg}^{\text{out}}}, \quad (10)$$

Recirculation coefficient r is equal to the ratio of the flow rate of recirculating gases to flue gas mass flow rate.

Calculating the enthalpy of flue gases, their temperature must be taken into account, as well as the composition of natural gas. H_a^0 [kJ/m³] is air enthalpy.

Fuel – consumption rate is calculated using the equation (11) and flue gas mass flow – equation (12):

$$B_p = \frac{Q_1 \cdot 10^3}{Q_c \cdot \eta} \cdot (100 - q_4), \quad (11)$$

$$V_{fg}^{\text{out}} = V_{fg} \cdot B_p \cdot \frac{273 + \vartheta_{fg}}{273}. \quad (12)$$

Data Presentation and Discussion

Using the inverse balance equation (7), the boiler efficiency was calculated for two operating regimes. All data is shown in Table 2.

TABLE II
RESULTS

Nr.	Parameter name	Symbol	Measurement	Values	
				1.o.r.	2.o.r.
Without FGR					
1.	Heat losses with flue gas	q_2	%	6,96	4,09
2.	Efficiency	η	%	92,95	94,43
3.	Fuel – consumption rate	B_p	$\frac{\text{nm}^3, \text{g}}{\text{h}}$	1922	583
4.	Flue gas mass flow	V_{fg}^{out}	$\frac{\text{m}^3, \text{dg}}{\text{h}}$	37793	9814
With FRG					
5.	Heat losses with flue gas	q_2^r	%	7,96	5,94
6.	Efficiency	η^r	%	91,95	92,58
7.	Fuel – consumption rate	B_p^r	$\frac{\text{nm}^3, \text{g}}{\text{h}}$	1944	594

The results show that when flue gas recirculation is taken into account, the boiler efficiency decreases. If the boiler is operating at maximum output, decrease is 1%, but if output is reduced, then decrease is 1,85%.

Although, at boiler maximum output, if recirculation coefficient is 13%, nitric oxides emissions decreases by 44,5%. It happens because of LOWNOx burner, which reduces NOx emissions to 90 mg/m³. There are no data about NOx emissions, when boiler is operating without flue gas recirculation.

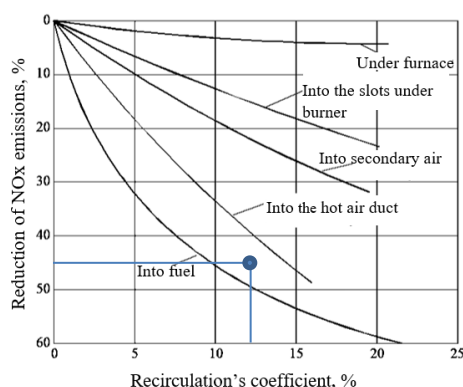


Figure 8. Comparison of the obtained value with theoretical values.

Fig. 8 shows, that obtained values conform with theoretical data. Since the flue gas recirculation for the boiler is supplied with secondary air directly to the burner, the result is better than recirculation with just secondary air, but worse than with fuel.

From viewpoint of economic, at maximum boiler output, the total costs of flue gas recirculation are 13,24 €/h. Only electricity and gas costs are taken into account, and installation, working costs and service life are not included.

Conclusions

- Boiler-houses are one of the largest pollutants. Combustion of fossil fuels releases repugnant substances into the atmosphere together with flue

gases, such as nitrogen oxides, carbon dioxide and monoxides, sulfur dioxide, particulate matter etc. The most harmful of these is nitric oxide.

- There are several methods for reducing nitrogen oxides in flue gases, which can be divided into three groups: physicochemical methods, technological methods and new methods. To maximize the reduction, combine physicochemical and technological methods.
- One of the technological methods is flue gas recirculation, which is one of the most effective methods. Despite the efficiency of the method, theoretically, the recirculation of 1% of flue gases, can decrease the boiler efficiency by 0.03 – 0.06%.
- Boiler efficiency directly depends on heat losses. The important value for the heat loss calculation with flue gases is enthalpy.
- The boiler “BOSCH UT M– 64” efficiency at maximum output with the FGR is less than 1% than in the case when flue gas recirculation was not taken into account.
- Flue gas recirculation reduces NO_x emissions by 44.5% at the boiler “BOSCH UT M–64” maximum output. The recirculation ratio in this case should be 13%. Consequently, NO_x emissions will be lower at lower outputs.

REFERENCES

- Batrakov, P., “The nitrogen oxide formation studying at natural gas combustion in non-circular profile furnaces of fire tube-boilers,” *Procedia Engineering*, vol. 7, pp. 144–150, 2015.
- Shalaj, V., Mikhajlov, A., Novikova, E., Terebilov, S., Novikova, T. “Gas recirculation impact on the nitrogen oxides formation in the boiler furnace,” *Procedia Engineering*, vol. 5, pp. 434–438, 2016.
- Korpela, T., Kumpulainen, P., Majanne, Y., Hayrinen, A. “Model based NOx emission monitoring in natural gas fired hot water boilers,” *Elsevier*, vol. 6, pp. 385–390, 2015.
- Šteļgovskis, R., 2007. “Siltuma ieguves tehnoloģijas,” LLU, Jelgava. Vol. 96.
- “Reduction of NOx emissions,” *TFTEI*, 2018.
- Blumberga, D., Veidenbergs, I., “Slāpekļa oksīdu izmešu samazināšana,” LU Ekoloģiskais centrs, Rīga. Vol. 20, 1992.
- Zhujkov, A., “Reduction of nitrogen oxides in boiler furnaces (in Russian),” *Journal of Siberian Federal University. Engineering & Technologies*, vol. 9, pp. 620–628, 2011.
- Dwyer, T., “Natural gas boiler flue gas recirculation to reduce NOx emissions,” *Cibse Journal*, 2016.
- Belikov, S., Kotler, V., “Boilers for thermal power plants and protection of the atmosphere (in Russian),” *Аква-Терм*, Vol. 360, 2008.
- Chelnokov, A., Mironchik, A., Zhmihov, I., “Engineering methods for the protection of atmospheric air (in Russian),” *Вышэйшая школа*, Minsk. Vol. 397, 2016.
- Bogatova, T., Osipov, P., “General energy: development of combustion technologies, 2.Part (in Russian),” Publisher Ural University, Moscow. Vol. 209, 2018.
- Vereshchetin, A., “Improvement of low-emission gas burner devices for boilers at TPPs (in Russian),” All-Russian twice Orders of the Red Banner of Labor Thermal Engineering Research Institute, vol. 131, 2018.
- Shumilin, J., Psarov, S., “Thermal calculation of the boiler (in Russian),” edition *ТОГУ*, Khabarovsk. Vol. 79, 2013.
- Кузнецов, Н., Митор, В., “Thermal calculation of boilers (Standard method), Third ed. (in Russian),” PAO “ЕЭС РОССИИ,” St. Petersburg. Vol. 259, 1998.

- [15] SIA TORI, "Brutto lietderības koeficienta patieso vērtību noteikšanas metode dabasgāzes katliem ar dūmgāzu recirkulāciju katla deglī," *unpublished*.
- [16] Bosch Thermotechnology, 2020.
- [17] Byenghun, Y., Seungro, L., Chang-Eon, L., "Study of NOx emission characteristics in CH₄/air non-premixed flames with exhaust gas recirculation," *Energy*, vol. 9, pp. 119–127, 2015.

Guidelines for Single-side Airing of Primary School Classrooms during Breaks

Tej Žižak (author); Prof. Sašo Medved (supervisor)

University of Ljubljana, Faculty of Mechanical Engineering, Laboratory for Sustainable Technologies in Buildings,
Aškerčeva 6, 1000 Ljubljana, Slovenia; Master seminar in academic year 2019/2020

zizak.tej@gmail.com, saso.medved@fs.uni-lj.si

Abstract—This paper focuses on indoor air quality in single-sided intermittent natural ventilation of classrooms in primary schools which is the most common technique of ventilation in the majority of older schools in Slovenia, despite intensive energy renovation in last decades. Study focuses on thermal response and air exchange rates established in single-site airing with single and double row windows. Results from transient CFD simulations were used to develop multi-parameter linear regression empirical models for prediction of airing time duration. The application of developed models as guidelines for teachers is presented as smart phone application based on the use of cost-effective IT devices.

Index Terms- Primary school's classroom airing, indoor air quality (IAQ), transient 3-D CFD modeling of heat and air flows, guidelines for airing of classrooms, information technologies for smart homes.

Introduction

Extensive energy renovation of primary school buildings was done in Slovenia in the last decade supported by EU and national funds, nevertheless improved building envelope was the most common measure, while measures on improved room temperature control, and especially on indoor air quality did not follow. As consequence, airtightness of the classrooms n_{50} are typically below $1,5 \text{ h}^{-1}$. An extended survey made by Galičič et al. [1] found that almost 85% of 434 primary schools in Slovenia are naturally ventilated. In the same study it was reported that the teachers were initiating “the action of improving indoor air quality” in 45% of cases, which means that they pointed out that the classroom needs to be ventilated by opening the windows. The same study also points out that teachers surge for some kind of guidelines about efficient airing of the classrooms to improve indoor air quality (IAQ) while maintain thermal comfort. This is an important task, because studies have shown that low ventilation rates can be associated with reduced cognitive performance and increased health risks [2].

Pupils in the classrooms are exposed to multiple physical (e.g. PM_{xx}), biological (e.g. bacteria and fungal groups) and chemical pollutants (e.g. CO , CO_2 , VOC) [3]. Despite that, CO_2 concentrations are commonly used as IAQ quality level indicator, both because IAQ required is most often related to CO_2 concentrations and because wide

range of suitable meters are available [4]. For that reason, CO_2 concentrations will be used in presented study for dynamic evaluation of IAQ in the reference classrooms.

A. Indoor Air Quality and thermal comfort in buoyancy and wind driven natural ventilated classrooms

Many experimental studies have been made on indoor air quality in schools [5-7], showing generally poor indoor air quality with an average concentration levels at around 2000 ppm and maximum exceeding 4000 ppm. Natural ventilation in classrooms is often limited to intermittent airing during breaks due thermal comforts requirements and possible noise pollution. Limitation could be poor quality of outdoor air, especially in the urban environment near roads, nevertheless this cannot be treated as general problem. Stabile et al. [8] report on IAQ in schools ventilated during the breaks of different length while in the reference [9] it is stated that continuous ventilation is only possible at outdoor air temperature above 8°C because of impact of cold air on thermal comfort. Since pupils commonly exit the classroom during breaks, it is of great importance that during a break, the IAQ improves (concentration of CO_2 should be decreased in our case) to such extend that requirements regarding to the IAQ will be fulfilled up to the end of next class. In Fig. 1. the results of indoor air concentrations in the 3rd grade classroom is shown, clearly illustrate that duration of breaks significantly influence on the IAQ during the next lecture. As airing efficiency depends on the initial concentration of CO_2 (before the break), indoor and outdoor air temperature and wind velocity in the vicinity of the building, there is a need for simple guidelines to instruct the teachers and pupils how intensive and how long airing must be. This task was the main goal of our research.

B. Single-sided natural ventilation of rooms

Pressure difference for single-sided natural ventilation is generated from temperature difference (buoyancy driven) and/or wind on the façade. Warren and Perkins have done extensive experiments and derived separate expressions for buoyancy or wind driven single sided natural ventilation [10]. The combined effect was derived by De Gids and H. Phaff [11] and is usually used in standards to determine air flows. Because of the complexity of the problem, CFD numerical simulations are often used for evaluating natural ventilation and its effectiveness on air pollutants removal.

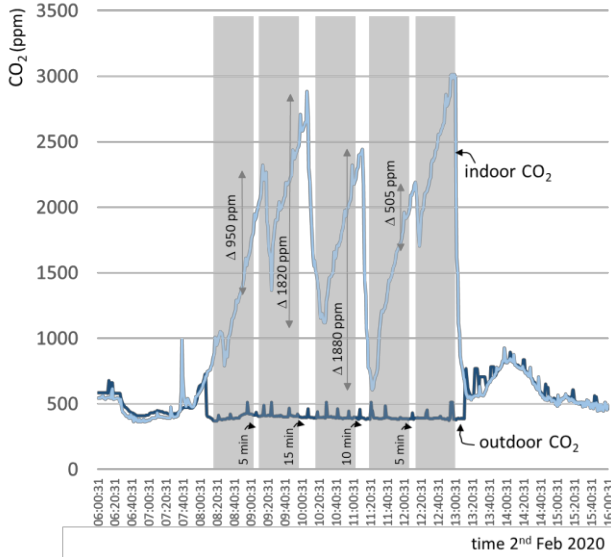


Figure 1: Concentration of CO₂ in single-side natural ventilated primary school classroom during the winter day in Ljubljana [1].

C. Planing of the research

The research was designed taking into account two phases of educational process that repeat throughout the school day – lesson and break. In the first phase, IAQ conditions in classroom during a 45 min long lesson are modeled; during this phase windows are closed, and classroom is only ventilated by infiltration. The research objective in this phase is to determine the local and average concentrations of CO₂ at the end of lesson at constant indoor air temperature. In such a way initial condition for second phase of research are defined. In addition to this, the CFD results are validated by first order concentration model (1), assuming constant rate of infiltration:

$$C_{CO_2}(t) = \frac{\dot{q}}{n \cdot V} \left(1 - \frac{1}{e^{n \cdot t}} \right) + (C_{CO_2, t=0} - C_{CO_2, out}) \cdot \left(\frac{1}{e^{n \cdot t}} \right) + C_{CO_2, out} \quad (1)$$

Second stage of the research lasts as long as a break. The (theoretical) duration of the break was adapted to initial conditions and the range of meteorological parameters. During the break, the classroom is aired through completely opened windows. Single-sided airing is modeled numerically as transient phenomena. The main goal of this phase was to determine the required airing duration needed to decrease the CO₂ concentration to an acceptable value.

Based on the results from 2nd phase, the prediction multi-parametric models, which give the required duration of airing t_{airing} , were developed for the case of single and for double row windows. The indoor and outdoor air temperatures, wind speed and indoor CO₂ concentration were assumed as influence parameters (x_i).

$$t_{airing} = a_0 + \sum_{i=1}^3 a_i \cdot x_i + b_i \cdot x_i^2 \quad (\text{sec}) \quad (2)$$

where a_0 , a_i and b_i are approximation coefficients.

II. RESEARCH METHOD

A. CFD simulation tool

Natural ventilation efficiency depends on several architectural and meteorological impact factors. Because of that, the IAQ can be best predicted with empirical models based on experimental study or by means of Computational Fluid Dynamics (CFD) simulations. Phoenics CFD software [12] was used in this study for transient numerical modelling of temperature and concentration fields in a naturally ventilated classroom. 5 seconds time step was used with global convergence criterion 0.1% for each step. LVEL turbulence model developed by Phoenics software team was used.

B. Geometry and boundary conditions

Fig. 2 shows the geometry of the classroom studied in this research. Two different windows geometries are studied: single row openings and double row openings. In both cases the ratio of opening area to floor are 5.1%.

In the 1st phase of modeling, infiltration in the classroom with different airtightness levels is assumed and constant infiltration rates from 0.1 h⁻¹ to 1 h⁻¹ were taken into account during the lesson.

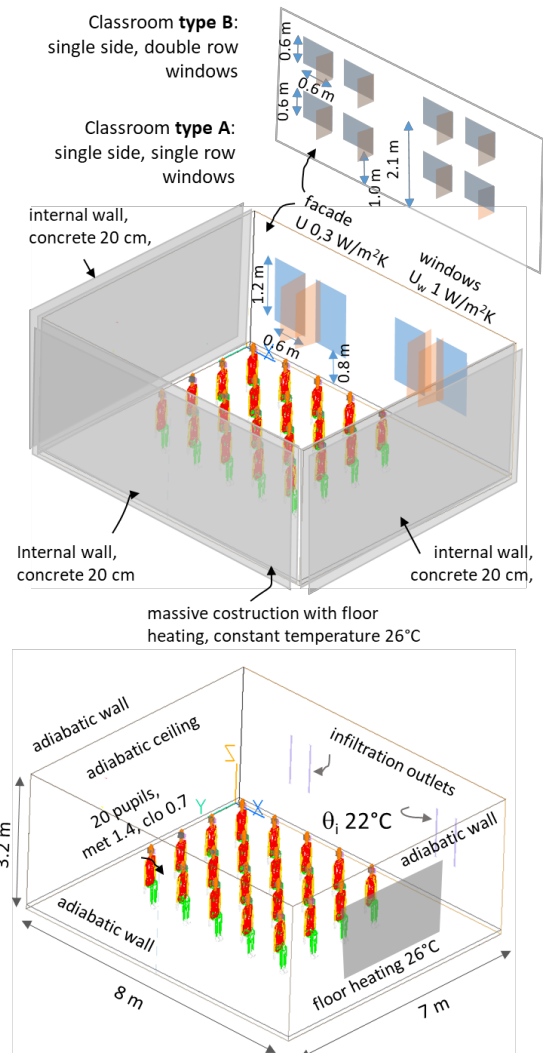


Figure 2: Model of classroom and boundary conditions assumed in 3-D CFD transient simulations.

20 pupils are in the classroom during the lesson. It was assumed that each of them emits 448 mg of CO₂ per minute [13] and 58 W per 1 m² of body area [14]. Initial indoor air temperature was set to 22°C and maintained by the heat flux emitted from floor heating system with constant surface temperature 26°C, pupils and infiltration heat sink. CO₂ mass flux was modelled as constant fluid flow at the height of mouth for each pupil individually.

In 2nd phase of modeling, all windows are fully opened and students are not present. Natural ventilation is modelled as transient phenomena with thermal buoyancy and wind on façade driving the air exchange through the open windows. Outdoor air temperatures from -5°C to 15°C and outside local wind velocities from 0 m/s to 2 m/s are considered. Following initial conditions of CO₂ indoor concentrations were considered – 1000, 1727, 2500 and 3000 ppm. Wind is modelled as a constant value perpendicular to the wall with reference value 2 meters away from the façade.

III. RESULTS AND DISCUSSION

A. An example of CFD simulation results

Fig. 3 shows an example of CO₂ conditions during school day in a classroom study case with type A geometry. Starting concentration of outdoor 500 ppm is assumed in the simulation case. During a school hour (45min), 1727 ppm is reached after 45 min with 0.1 ACH airtightness assumed. The simulation results with forced ventilation during phase 1 are in good agreement with theoretical concentration balance model. The same end conditions can be met with 800 ppm starting concentration and 0.5 ACH airtightness assumed. In 2nd phase, single sided natural ventilation with single openings and no wind (buoyancy driven only) is assumed, with -5°C being the outdoor temperature. At these conditions, the CO₂ concentration drops to 800 ppm in 365 seconds from the start of ventilation. 800 ppm is then initial condition for the next school hour. The results show that any infiltration rate higher than 0.34 h⁻¹ will result in end concentration after 45 min below 1850 ppm (cat. III). In Figure 3 infiltration rate of 0.5 h⁻¹ is shown, which results in 1750 ppm after 45 min from initial 800 ppm.

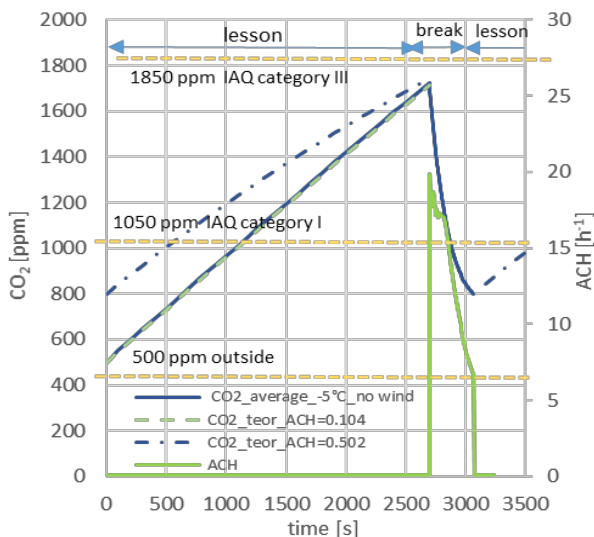


Figure 3: An example case: CO₂ concentration levels in classroom during school day.

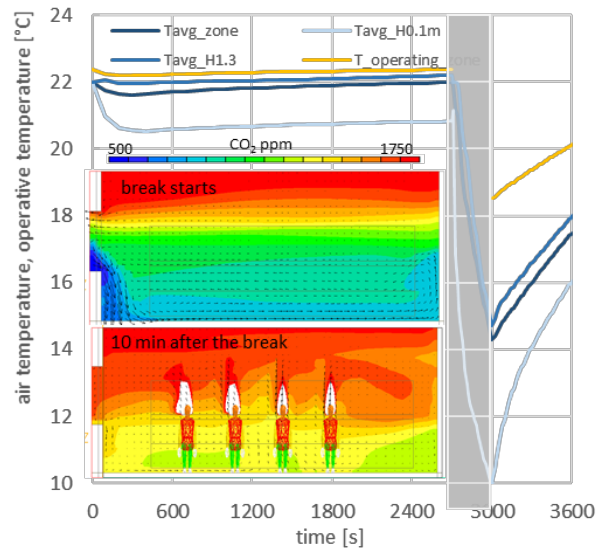


Figure 4: Model of classroom and boundary conditions assumed in CFD transient simulations.

Air changes per hour and temperature in the classroom show the benefits of transient modeling with CFD, as the cooling of air inside the room slows down the temperature driven ventilation, consequently lowering the starting 17 air changes per hour to 7 air changes per hour after 365 seconds.

Figure 4 shows the temperatures on different heights and operative temperature of the living zone for the example case. The living zone is considered to be 0.1 m from the ground, 1 m from the external wall and 0.5 m from the internal walls, with height of 1.9 m. As it is assumed there is no students occupying the classroom during the natural ventilation time, the thermal comfort indicators during that time are not relevant. However, they are important at the time when students return to the classroom after the brake. Concrete walls with good thermal accumulation properties are assumed, so combining the radiation and air temperatures (weighted 0.5 each), the operative temperature drops is considerably higher than air temperature. The results show that thermal comfort after the airing time needs to be evaluated and further studies are needed for additional time for operating temperatures to rise back to acceptable levels.

B. Decrease of CO₂ concentration due to airing during the break

Figures 5-8 show the results of simulation for 2nd phase - single sided airing during the break. The CFD simulations were performed for two types of classrooms – Type A and B are shown in Fig. 2. Classroom Type A has single row windows, while classroom Type B is aired through double row windows. Both have the same opening areas. Double row windows are in theory more effective, enabling higher air exchange rates due to the larger height difference between inlet and outlet openings. Another reason is that double row windows have the pressure neutral plane in-between the windows causing unidirectional air flow through both openings. For single row windows the pressure neutral plane is in the opening itself, which cause bidirectional flow and complex flow interactions.

Figures 5 and 6 show the average CO₂ concentration in classroom at different outdoor conditions. The initial air exchange rates at the start of airing are the highest due to the highest temperature difference, which is shown in Fig. 5 as a steeper slope on CO₂(t) curve. In the first 200 seconds for conditions with outside air temperatures below 5°C and wind velocity above 1 m/s concentration drops below 1000 ppm for single row windows and below 800 ppm for double row windows.

Figure 7 shows the airing time needed for CO₂ concentrations to reach 800 ppm depending on boundary conditions. For double row windows, the ventilation time is below 300 seconds for all conditions except 15°C outdoor temperature and 0 m/s wind conditions. Single row windows however need more than 700 seconds for some less effective boundary conditions with wind velocities below 1 m/s and outdoor temperatures above 5°C.

The effect of combined temperature and wind conditions is also dependent on window geometry. Generally lower outside temperatures and higher wind speeds result in more air exchanged through the openings, which is the case with

double row windows results (Figs. 6 and 7). It can be seen that temperature difference is a dominant factor at lower velocities and vice-versa. For single row openings, temperature is a dominant factor with wind speeds up to 1 m/s. With velocities higher than 1 m/s temperature becomes practically irrelevant, furthermore as we can see in figure 7, higher outside temperatures with velocities above 1 m/s result in more air exchange than lower temperatures. The reason for that behavior could be in the numerical model with uniform perpendicular wind velocity, which amplifies the effect of lower air density at higher temperatures, which allows for “easier” airflow through the opening in the wind dominated case.

Figure 8 shows operative temperatures at airing time, when CO₂ concentration drop to 800 ppm from different initial concentrations. The results for 1727 ppm initial concentrations show that the operating temperature is independent of wind velocity and window geometry. It is however dependent on outside temperature and initial concentration. At 3000 ppm initial concentration the operative temperature drops to 12°C at outdoor temperature -5°C.

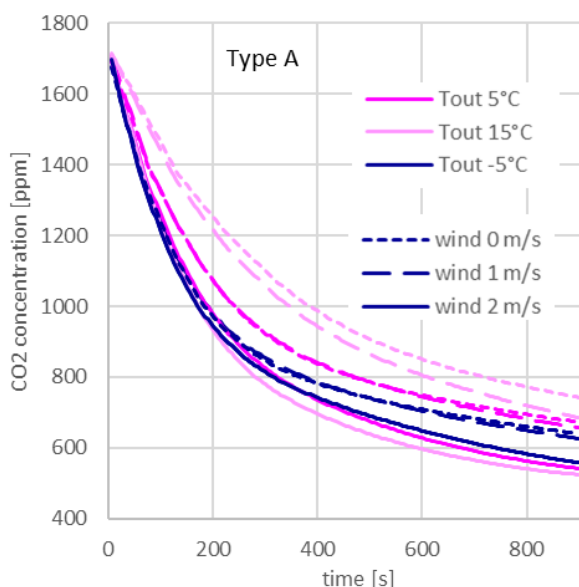


Figure 5: Average C_{CO2} in classroom during airing, Type A.

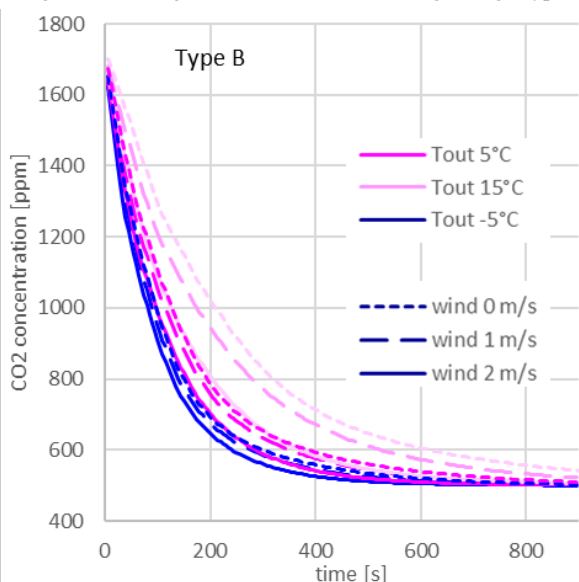


Figure 6: Average C_{CO2} in classroom during airing, Type B.

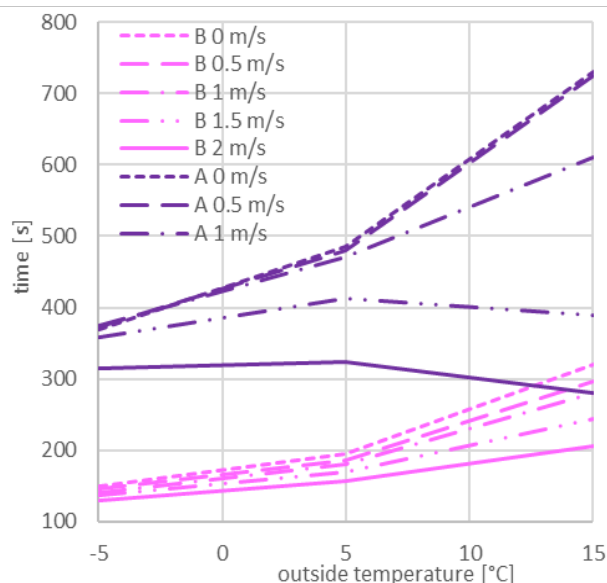


Figure 7: Airing time (1727 to 800 ppm) at different conditions.

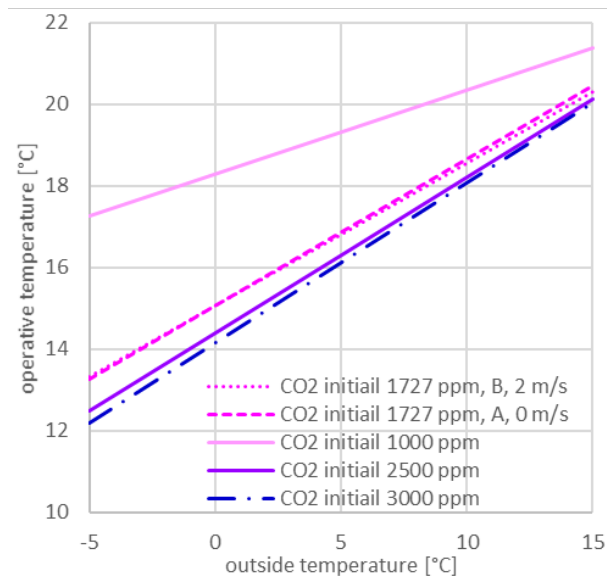


Figure 8: Operative temp. at end of airing (C_{CO2} 800 ppm).

C. Prediction models for airing duration

Linear regression model was developed for the prediction of airing duration required for the CO₂ concentration to decrease to 800 ppm from initial concentration at the beginning of airing. The duration depends on outdoor air temperature and wind velocity in front of the façade. The prediction model for Type A classroom is defined by Eq. 3, while prediction model for Type B classroom, having double row windows, is defined by Eq. 4:

$$t_{\text{airing,A}} = -4020 - 37.38 \cdot v - 62.65 \cdot v^2 - 117.15 \cdot \ln(22 - T_{\text{out}}) + 663.6 \cdot \ln(C_{\text{CO}_2}) \quad (3)$$

$$t_{\text{airing,B}} = -1113 - 18.56 \cdot v - 7.05 \cdot v^2 - 100.92 \cdot \ln(22 - T_{\text{out}}) + 215 \cdot \ln(C_{\text{CO}_2}) \quad (4)$$

Where v (m/s) is wind velocity in front of façade at the height of the openings, T_{out} outdoor air temperature (°C) and C_{CO_2} (ppm) is CO₂ concentration in indoor air at start of the airing. Figure 9 shows the correlation between the numerical and predicted values of t_{airing} . Double row windows (Type B) has a slightly better statistical correlation with R^2 being 0.91, versus 0.88 for model of single row windows (Type A), nevertheless both models can be classified as adequate.

D. Application of prediction models

One of the prediction model applications could help teachers to maintain the adequate indoor environment conditions in schools. We can assume that classrooms could be equipped with low cost and nowadays widely used devices for smart homes. Smart phone application based on the developed prediction models can help teachers to decide which measure will be the most effective at particular indoor/outdoor conditions. Proposed design of such application is shown in Figure 10.

Such smart-phone application that gathers data from the indoor measuring device and the meteorological station nearby and uses the developed prediction model to suggest a proper airing time together with proposed actions.

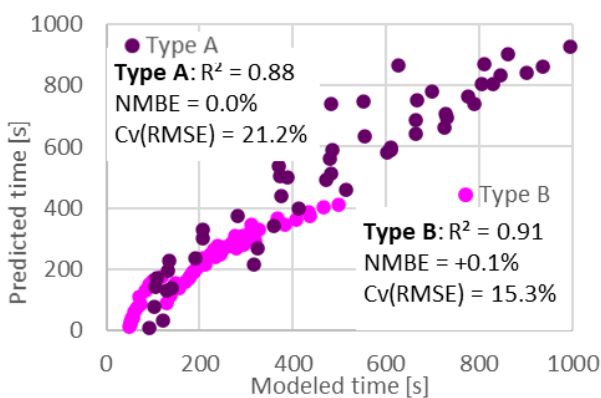


Figure 9: Correlation between modeled and predicted airing time with multi parametric linear regression models (Eqs. 3, 4).

IV. CONCLUSION

Conditions in a school classroom during a school lesson (1st phase) and during a naturally ventilated break - airing (2nd phase) were shown, with the focus on indoor air quality through CO₂ concentration monitoring. Thermal conditions were also addressed through operative temperatures. The temperature and concentration fields were numerically modelled with CFD simulation program.

The results show that during a school hour with 20 students (moderate activity) the CO₂ concentration levels rise from the ambient 500 ppm to 1727 ppm with 0.1 h⁻¹ air changes per hour infiltration rate assumed. The goal was to keep the concentration levels below 1850 ppm at any time during the day, which is the upper limit of cat. III. The aim concentration levels for natural ventilation time during the break was 800 ppm. The minimum air exchange rate for initial 800 ppm concentration in the next school hour to 1850 ppm at the end is 0.34 h⁻¹, which corresponds to moderate infiltration in older buildings.

Airing results during break were shown for two geometries: single row windows and double row windows, both with the same total opening area. As expected, double row windows we proven to be much more efficient (higher air changes per hour rates). Lower outside temperature

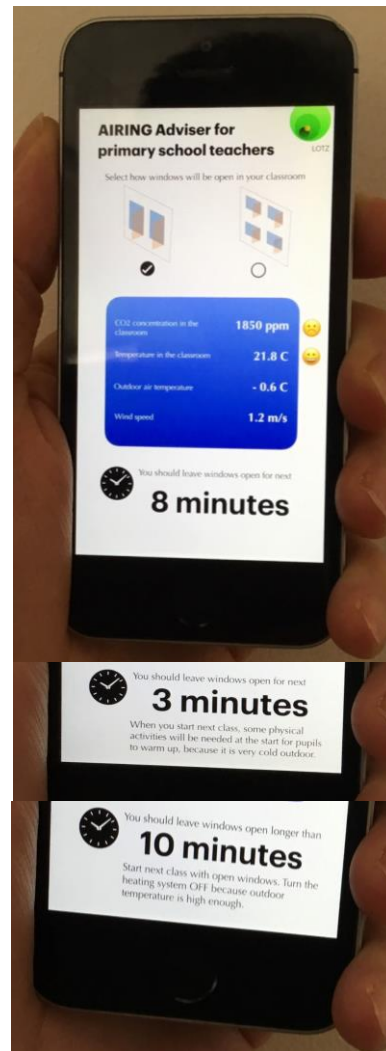


Figure 10: Virtual application with guidelines examples.

(more temperature difference) and higher wind velocities result in more air exchanged. For single row windows, results show a dominant driving force being the temperature difference to velocities up to 1 m/s and a velocity a dominant driving force after that. For double row windows, the temperature effect does lower with higher velocities, but is still important to maximum velocities considered - up to 2 m/s.

The importance of transient modeling of intermittent natural ventilation are shown though the rapid change in air exchanges per hour, as the temperature conditions change in the room during ventilation.

Airing time for concentration levels to drop from 1727 ppm to 800 ppm during natural ventilation are below 300 seconds for almost all conditions with double row windows and under 500 seconds for outdoor temperatures below 5°C with single row windows. Operative temperatures at the end of ventilation drop to 13.3°C at -5°C outdoor temperatures. A high rise in operative temperature is predicted because of concrete walls with high thermal storage.

A prediction model using linear regression is developed for airing time needed for concentration levels to drop to 800 ppm based on the outside temperature, wind velocity on and initial CO₂ concentration in the room at the start of airing. The prediction model can be used as guidelines for teachers and a possible use through a smart-phone application is presented.

A. Limitations and further work

For the purpose of this study the wind profile was modelled with perpendicular uniform profile in vicinity of the façade, the effect of complex wind behavior such as pulsation and turbulent eddies could be evaluated in further work.

Only two most often window geometries were presented in this work, further analysis of different window geometries is needed. With more data of different window geometries, an upgrade to the prediction model is possible with the height difference and window area as an additional parameter in the model. The resulting prediction model would be a general prediction model for variety of classroom’s geometries.

Further analysis needs to be made on thermal comfort at the end of airing time. Operative temperature at the end of airing time are shown, which is often out of thermal comfort range. Thermal conditions after the airing time need to be studied, with possibility of adding extra time after airing ends, with windows closed, before the students re-enter the classroom.

ACKNOWLEDGEMENT

Author and supervisor acknowledge the financial support from the Slovenian Research Agency (CRP research funding No. V3-1904).

Author would like to thank to Assoc. Prof. Ciril Arkar for his valuable support.

Table 1: Nomenclature

a, b	regression coefficients
C	concentration (ppm)
n	air changes per hour (h ⁻¹)
q̇	pollutant source (m ³ /h)
t	time (s)
T	temperature (°C)
v	velocity (m/s)
V	volume (m ³)
x	independent variable

Table 2: Index

airing	airing
A	Type A geometry
B	Type B geometry
CO ₂	carbon dioxide
i	number of independent variables
out	outdoor

REFERENCES

- [1] A. Galičič, I. Eržen, S. Domjan, S. Medved, “Razvoj modela za napovedovanj eizpostavljenosti onesnaževalom v notranjem zraku v šolah in priprava z dokazili podprtih ukrepov za načrtovanje učinkovitega naravnega prezračevanja učilnic”, Nacionalni inštitut za javno zdravje, 2020.
- [2] W.J. Fisk, “The ventilation problem in schools”, *Indoor Air*, 2017, 27, pp. 1039-1051.
- [3] S. Banerjee, L. Annesi-Maesano, “Spatial variability of indoor air pollutants in schools. A multilevel approach”, *Atmospheric Environment* 61, 2012, pp. 558-561.
- [4] D.F. Acosta-Acosta, K. El-Rayes, “Optimal design of classroom spaces in naturally-ventilated buildings to maximize occupant satisfaction with human bioeffluents/body odor levels”, *Building and Environment* 169, 2020, 106543.
- [5] L. Stabile, M. Dell’Isola, A. Frattolillo, A. Massimo, A. Russi, “Effect of natural ventilation and manual airing on indoor air quality in naturally ventilated Italian classrooms”, *Building and environment*, 98, pp. 180-189, 2016.
- [6] C. David, A. Beisteiner, “Carbon dioxide levels and ventilation rates in schools”, *International journal of ventilation* vol 1., 2002.
- [7] V. Kukadia, P. Ajiboye, M. White, "Ventilation and indoor air quality in schools", BRE Information Paper IP 6/05, BRE Publications, Watford, 2005.
- [8] L. Stabile, M. Dell’Isola, A. Russi, A. Massimo, G. Buonanno, “The effect of natural ventilation strategy on indoor air quality in schools”, *Science of the total environment*, 595, pp. 894-902, 2017.
- [9] C. Angelopoulos, M. Cook, “Natural ventilation in schools: window design and performance”, conference paper, People and buildings, London, 2016.
- [10] P.R. Warren, L.M. Parkins (1985) “Single-sided ventilation through open windows”. In conf. Proceedings, Thermal performance of the exterior envelopes of buildings, Florida, ASHRAE SP 49, pp. 209-228.
- [11] W. De Gids, H. Phaff (1982) “Ventilation rates and energy consumption due to open windows: A brief overview of research in the Netherlands”, *Air infiltration review*, 4(1), pp. 4-5.
- [12] PHOENICS 2019, Concentration, Heat and Momentum Limited (CHAM), 2019.
- [13] P. N. Smith, “Determination of ventilation rates in occupied buildings from metabolic CO₂ concentrations and production rates. *Build. Environ.*, 23: 95–102.
- [14] G. Havenith, “Metabolic rate and clothing insulation data of children and adolescents during various school activities”, *Ergonomics* 50, 1689-1701; 2007.

Photovoltaic cogeneration to activate a double source heat pump

Student: Anna Cazzola (anna.cazzola94@gmail.com)

Supervisors: Renato Lazzarin (renato@gest.unipd.it), Marco Noro (marco.noro@unipd.it)

Department of Management and Engineering, University of Padova, stradella San Nicola, 3 – 36100 Vicenza (Italy),
email: urp@unipd.it, 2018

Abstract - This paper presents the study of a photovoltaic cogeneration system composed by photovoltaic-thermal (PVT) collectors coupled with a double source heat pump to provide heating and cooling as well as domestic hot water (DHW) in the complex of a gym and laboratories of a secondary school located in Vellai di Feltre (BL), Italy. The modelling of the building in TRNBuild (TRNSYS® extension) was first used to identify heating and cooling loads to be satisfied. Successively, the dynamic simulation TRNSYS® software was used to implement the system and analyse it from the energy fluxes point of view. Five different cases were studied varying the size of the PVT field and the length of ground borehole heat exchangers to identify the solution with the greatest performance results. Finally, a comparison with a traditional heating-cooling system was conducted to investigate the viability of the innovative system proposed from both primary energy consumption and economical point of view. The results showed that the cogeneration system studied is able to totally satisfy the heating, cooling and DHW demand using only electrical energy produced by the plant itself for most of the year; therefore, in an overall annual energy balance, the building turns out to be independent from no-renewable energy sources.

Index Terms – Design optimization, ground source heat pump, photovoltaic cogeneration

Introduction

More than one third of the EU energy consumption is due to the heating and cooling of building processes with the result of high CO₂ emissions. Looking at the decline of the climate changes, it is more and more important to come up with solutions that lead to the independence from no-renewable sources to produce energy. This study was set up with the aim to implement a cogeneration system composed by PVT collectors integrated with an electrically driven ground source heat pump (GSHP) to satisfy the heating, cooling and DHW demands of a building. The PVT collector is an innovative technology that can supply heat and electricity with one component and achieve a very high area specific energetic yield and higher photovoltaic performance [1]. The retrofitting of a school building located near Feltre in Northern Italy allows the utilization of several modern technologies with the purpose of realizing something more of a Nearly Zero Energy Buildings (NZEB, i.e. a building that can be realized with a minimum requirement of traditional fuels and electricity), that is a Plus Energy Building. This is a building which is not only energy self-sufficient on a yearly basis, but it can provide energy to nearby buildings, or to the grid.

The study has been developed in three main phases: the modelling of the building in the TRNBuild extension to

study the distribution of the heating, cooling and DHW loads; the conceptualization of the system and its implementation in TRNSYS to analyse the energy fluxes; the optimization of the design from the energetic and economical point of view.

I. METHODS

A. Modelling of the building

The building is a three floors complex of a secondary school built in 1960, composed by a gym, a bar, a library, offices and laboratories. It has been object of a retrofitting project that reduced the heating and cooling annual thermal energy requirements from 329 kWh/m² to 41 kWh/m². The plant will satisfy heating and cooling loads by a floor heating system, fan-coils and radiators in the toilet, and DHW demand too till late in the evening due to the fact that the gym will be used also for the work out by external users. The building is divided into 20 different thermal zones, each of which is defined by means of TRNBuild software in terms of volume; walls and windows structural components; gains related to the presence of people, light and electronic devices; heating, cooling and ventilation mode (defined by suitable scheduling, supply temperature and radiative component percentage) (Table 1). The modelling of the building is used to both obtain the heating and cooling loads and to study their contemporaneity during the day and the year. The results are shown in Fig. 1: the peak of heating load (44 kW) is reached in January (part a) of the figure, this information is necessary to size the system; the contemporaneity of heating, cooling and DHW demands during the day and in the different periods of the year (summer, winter and middle seasons) (part b)) is a useful piece of information to correctly set up the control and three-way valves operation strategy.

B. System conceptual design

In the second part, the conceptual design of the cogeneration system was developed to be implemented by TRNSYS software. The complexity of the system relies on the control strategies used to drive the plant equipment to satisfy the energy demands determined previously. Furthermore, heat storages management is strongly necessary to optimise the operation of the main heat sources, the PVT collectors and the electric driven heat pump (HP)/chiller.

Finally, the control logic of three-way valves and pumps is also important for the energy performance of the plant. Table 2 summarizes the variables and related conditions used to set up the control system in order to vary the system function basing on the external conditions.

Table 1.
Brief description of the building and project data.

Location	Vellai di Feltre, Italy		Altitude	325 m asl
A _{build}	33.08 x 25.10 m ²		3097 degree days	
Heating mode	Gym - radiant heating 99% → T _{setpoint} =18 °C Changing room, bar, library, offices, atrium - radiant heating (25%) + fan-coils → T _{setpoint} =20 °C/21 °C		Cooling mode	Gym – fan coils → T _{setpoint} =24 °C Offices, laboratories, atrium – fan-coils → T _{setpoint} =26 °C Changing room, bar – radiators → T _{setpoint} =26 °C
Ventilation mode	Primary air system	Winter season: T _{supply} =19 °C - 18 °C (gym) Summer season: T _{supply} =24 °C - 21 °C (gym) Middle season: T _{supply} =21 °C - 20 °C (gym)	Thermal Storage	DHW storage volume → 2000 L

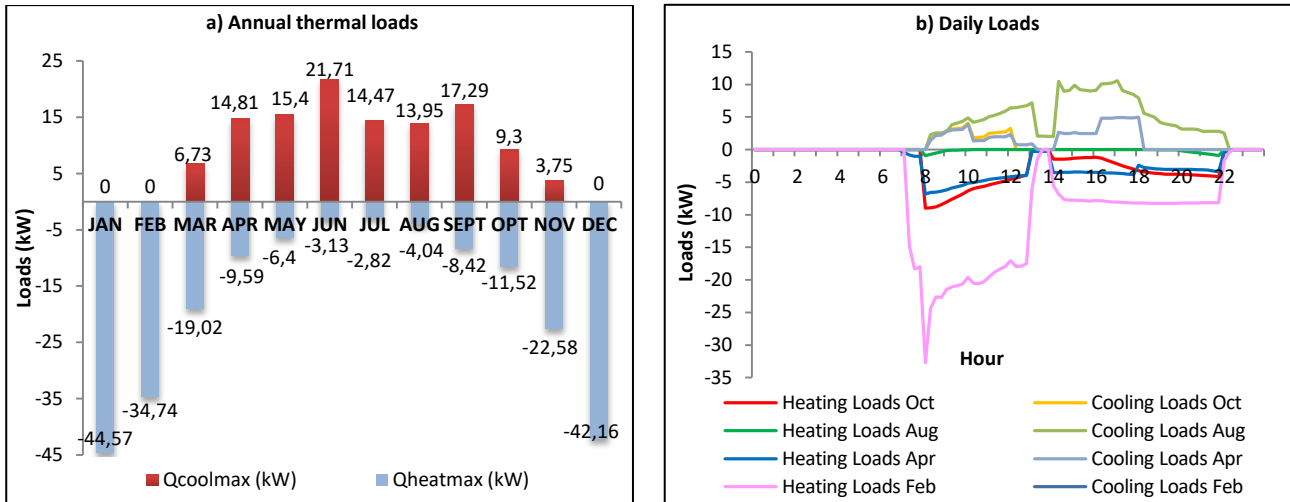


Figure 1. a) Daily heating and cooling maximum load of the building for each month (Qheatmax and Qcoolmax respectively); b) Daily distribution of heating and cooling loads in a summer day (August), winter day (February) and middle-season day (April and October).

The system is composed by four loops, each divided by three heat storages (Fig. 2):

- 1) Ground – Source Tank – PVT loop;
- 2) DHW loop;
- 3) Heat pump – Chiller loop;
- 4) Heating – DHW loop.

The first loop includes PVT collectors and borehole heat exchangers that, through a plate heat exchanger, provide heat to the Source Tank. The first function of this loop is to exchange heat between PVT water and the Source Tank to permit both the cooling of the PVT, in order to improve the PVT collectors performance, and an increase of the Source Tank temperature, used as heat source for the HP. Moreover, PVT thermal energy is useful to recharge the ground. The latter is used as heat source when the HP operates in heating mode, whereas it is a heat sink when the thermal machine is in chiller operating mode. In this case, it uses the Source Tank to reject the condenser heat, re-directing it to the ground by the plate heat exchanger when the Source Tank temperature rises.

The DHW loop is directly linked to the first one because the solar thermal energy provides heat also to pre-heat the DHW. In fact, two different storages are required in order to maximize the heat exchanged between the PVT water and the water from the grid, thus cooling the PVT as much as possible. Glazed PVT collectors have been considered rather than unglazed ones (normally used for this kind of application). This is due to the fact that thermal energy produced by the collectors is used mainly for DHW heating, and to rise the Source Tank temperature to a suitable level for heat source in HP operation mode, taking into account the severe winter climate [2].

Five different operating modes are defined for the first and second loop (numbers refer to the conditions in Table 2).

1) *Ground as heat source of the HP / heat sink of the chiller*: in winter season, the heat pump uses the ground as source to satisfy both heating and DHW loads, when PVT collectors cannot provide sufficient thermal energy due to low value of solar radiation (1). This happens only if the temperature of the ground is higher than the Source Tank one (3). In summer season, the ground is used as sink of the Source Tank when the temperature of this one exceeds 25 °C (2) and it is necessary to dissipate heat to the ground to not penalize the chiller performance.

2) *PVT and ground are used in parallel configuration to produce DHW*: if the global solar radiation on the plane of the collectors (G) is greater than 50 W/m² and the temperature of the PVT water is higher than the Source Tank one (4.1), PVT heat will be useful to: a) pre-heat DHW or b) increase the temperature of the source of the HP. Both the temperature of the pre-heat DHW Tank and that of the DHW Tank drive the choice between a) and b). If PVT thermal energy is useful to be exchanged with the pre-heating DHW Tank (5) and the DHW temperature is below 45 °C (6), solar energy will provide heat to pre-heat DHW and, at the same time, ground will be used as explained in the functioning 1).

3) *PVT as heat source of the HP*: the solar radiation could provide useful thermal energy at low temperatures, not sufficient to be directly used to pre-heat DHW. In this case, PVT thermal energy is used to increase the temperature level of the Source Tank (4.1) only if the PVT temperature is below 20 °C (4.2) in

order to avoid the grow of the Source Tank temperature over 25 °C and improve HP efficiency.

4) *Ground regeneration by the PVT and cooling of the condenser*: if the PVT temperature rises above 20 °C but the DHW Tank doesn't need to be heated, it is necessary to cool PVT water before exchanging heat with the Source Tank, so the PVT water is made to circulate into the borehole heat exchangers, in order to recharge the ground. The cooled PVT water could either finish its function (see functioning mode 5) or subtract heat from the Source Tank. Especially in middle-season months (from April to June and from September to November), switching from HP to chiller operating mode (and vice-versa) happens more times in a day to satisfy both heating and cooling loads, as well as DHW demand. This event can cause the rises of the Hot Tank temperature above 50 °C (7.1) with the necessity to reject the condenser heat to the Source Tank instead of the Hot Tank. As a result, T_{source} could increase too much and it would be necessary to remove heat by PVT water previously cooled by recharging the ground.

5) *Ground regeneration from PVT*: if there is no need to cool the condenser by the PVT, only the ground regeneration by PVT is done.

The third loop is related to the thermal machine. It includes two storages, the Hot Tank and the Cold Tank, that provide heat and cold to satisfy the heating, DHW and cooling loads; the Source Tank, directly connected to both the evaporator and the condenser of the thermal machine and, finally, the thermal machine itself.

There are two requirements that have to be taken into account in this loop: a) the contemporaneity of the cooling, heating and DHW demands; b) the necessity to maintain the supply water temperature of the Hot Tank at 50 °C and the supply water temperature of the Cold Tank below 12 °C. Whenever $T_{outhott}$ isn't at the defined supply temperature (8), the thermal machine switches on and the condenser transfers the heat absorbed by the Cold Tank or the Source Tank to the Hot Tank. The heat is collected by the Cold Tank every time there are cooling loads to be satisfied (9) in order to maintain the outlet temperature of the Cold Tank below 12 °C. If the Hot Tank is saturated, but the Cold Tank still needs to be cooled (9), the heat absorbed by the Cold Tank will be transferred to the Source Tank. As it can be seen, the Source Tank plays an important role because it is used both as source and sink of the thermal machine.

Finally, the last loop is related to the connection of the Hot Tank to the DHW Tank and building to provide heat to satisfy both the heating and DHW loads. As the DHW demand is required at higher temperature (set at 45 °C) than the one used for heating loads (35 °C) and there is a contemporaneity of the DHW demand (10) and heating loads (11) especially during evening hours (in which no or very low contribution is given by PVT collectors), DHW demand and heating loads are satisfied in series: first, heat at 50 °C is transferred by the Hot Tank to the DHW Tank through the internal DHW Tank heat exchanger, then, the same Hot Tank cooled water is made to circulate into the building circuit. If only DHW demand is required (10) or heating loads (11), the M three-way valve drives the heat transfer.

Table 2.
Variables used to define the system and related conditions that define the valves and pumps control strategy.

Variable	Variable Description	Conditions	Pumps value	Explanation
Ground-Source Tank-PVT and DHW Loop				
G	Solar Radiation	$G < 50 \text{ W/m}^2$ (1)	SP=0	The value of the radiation is too low to provide useful heat both to the pre-heating DHW Tank and the Source Tank → No PVT water is circulating in the loop
T_{source}	Outlet temperature from the Source Tank	$T_{source} > 25 \text{ °C}$ (2)	P6=1	The temperature of the Source Tank is too high and it could penalize the thermal machine performance → dissipation of the Source Tank heat to the ground or by the PVT water
T_{ground}	Outlet temperature from the borehole heat exchangers	$T_{ground} > T_{source}$ (3)	P5=1 P6=1	Ground is used as heat source of the heat pump and exchanges heat with the Source Tank in order to increase the Source Tank temperature
T_{pvt}	Outlet temperature of water from the PVT collectors	$T_{pvt} > T_{source}$ (4.1)	SP, P6=1	The PVT thermal energy is useful to increase the Source Tank temperature as much as needed in order to maintain $T_{source} < 25 \text{ °C}$ → PVT used as heat source of the heat pump
		$T_{pvt} < 20 \text{ °C}$ (4.2)	A, C=0	
		$T_{pvt} > T_{predhw}$ (5)	SP=1 A=1	
T_{DHW}	DHW supply temperature to users	$T_{DHW} < 45 \text{ °C}$ (6)	A=1	It is necessary to provide heat to the DHW Tank through the PVT thermal energy in order to maintain the DHW supply temperature at 45 °C
$T_{outhott}$	Hot Tank supply water temperature	$T_{outhott} > 50 \text{ °C}$ (7.1) HP/Chiller= ON (7.2)	P6=1	The thermal machine is switched on and the condenser can't exchange heat with the Hot Tank because it is saturated → Source Tank is used as sink instead of the Hot Tank
Heat Pump/Chiller Loop				
$T_{outhott}$	Hot Tank supply water temperature	$T_{outhott} < 50 \text{ °C}$ (8)	P4=1 P3=1	The HP is powered on and the Hot Tank is used as sink (condenser side)
COOLING LOADS		COOLING LOADS > 0 (9)	P3_A=1	Cold Tank as source of the heat pump (evaporator side) in order to maintain its supply temperature (T_{toload}) below 12 °C and satisfy the cooling loads
Heating - DHW Loop				
T_{DHW}	DHW supply temperature to users	$T_{DHW} < 45 \text{ °C}$ (10)	P4_A=1 M=1	It is necessary to transfer heat from the Hot Tank to the DHW Tank in order to maintain the DHW supply temperature at 45 °C
HEATING LOADS		HEATING LOADS > 0 (11)	P4_A=1 M=0	It is necessary to provide heat from the Hot Tank directly to the building circuit in order to satisfy heating loads.

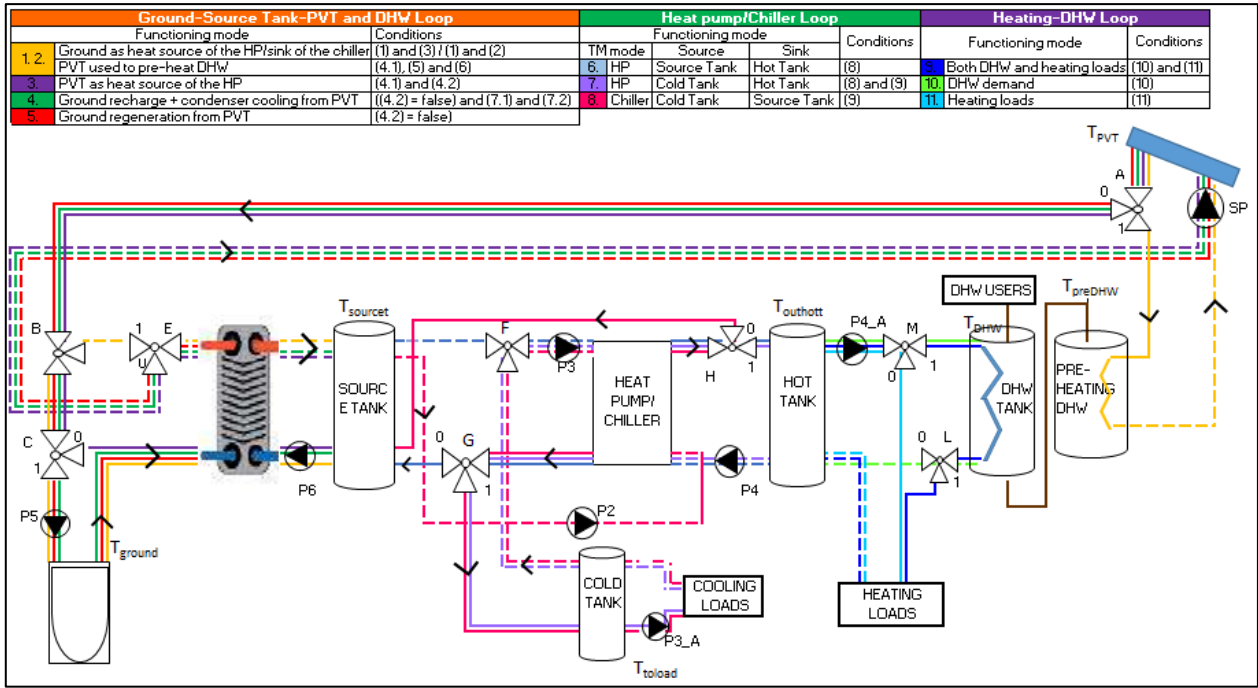


Figure 2. System conceptual development with evidence of the different operation modes for each of the loops.

Finally, an additional 60 m² of traditional PV is considered to be installed in order to provide more electrical energy to satisfy the plant consumption.

C. System implementation in Trnsys

The virtual dynamic simulation of the cogeneration system developed in TRNSYS allows to compare the performance of the system under different values of the design parameters. Most of the component models used to develop the simulation were the standard ones available in the TRNSYS library: water-to-water heat pump model (*Type 927*); vertical U-tube GHE model (*Type 557 a*); stratified storage Tank with fixed inlets and uniform losses (*Type 4a*); stratified storage Tank with multiple heat exchangers (*Type 60d*); PV-thermal flat plate collectors (*Type 50c*).

Table 3. Values of the main parameters required for the definition of the *Types* used in TRNSYS simulation.

Type 927: single stage water-water heat pump		
	Heating	Cooling
Rated capacity per HP	35 kW	31 kW
Rated power per HP	9.12 kW	9.12 kW
Rated Source Flowrate per HP	5364 l/h	
Rated Load flowrate per HP	6947 l/h	
Type 4a: Stratified fluid storage Tank		
Type 60d: Stratified Fluid storage Tank + internal heat exchangers		
Tank loss coefficient	0.3 W/(m ² K)	
Energy input by the heater (Hot Tank and DHW Tank)	3 kW	
Surface area of heat exchanger (pre-heating DHW Tank)	5.4 m ²	
Surface area of heat exchanger (DHW Tank)	3.8 m ²	
Type 557a: Vertical Ground Heat Exchanger		
Reference borehole flow rate	1200 kg/h	
Storage thermal conductivity	2.87 W/(m K)	
Storage heat capacity	2016 kJ/(m ³ K)	
Type 50c: PV-Thermal collectors – flat plate collectors		
Nominal Power	260 W _p	
Module Efficiency	16.01%	
Thermal Efficiency	59%	

Table 3 reports the values of parameters of the main system components, chosen according to data sheets of products in the market.

Regarding the Hot Tank, the Cold Tank and the Source Tank, *Type 4a* is chosen because it allows to better define the stratification [3]. The total height of these tanks is 2 m, 2 m and 2.5 m respectively. In the Hot Tank also an auxiliary heater is considered to reach the supply temperature (50 °C). The presence of internal heat exchangers to exchange heat with PVT water and the Hot Tank is required; it is simulated with *Type 60*. DHW Tank is also provided with an auxiliary heater to maintain the supply temperature (45 °C).

The heat exchanger used to deliver heat from PVT/ground to the Source Tank is a plate cross flow one with effectiveness of 0.8. The control strategy is implemented through 9 *Type 2b* (Differential controller) that give a digital signal to drive the three-way valves and switch on/off the pumps and the thermal machine.

II. DATA PRESENTATION AND DISCUSSION

Energy flows are measured by TRNSYS and each of them is used to calculate PVT thermal and electrical performance and the overall system efficiency. In order to determine the optimal design, 5 different plant configurations are simulated, varying the length of the borehole heat exchangers and the PVT collectors area (Table 4).

The comparison of the 5 cases with regards to the solar energy is summarized in Table 5. Under the same borehole length, with the increase in the PVT collectors area, the solar thermal fraction, defined in (13), indicates that a higher percentage of thermal needs (both heating and DHW, $EM_{\text{heating}} + EM_{\text{DHW}}$) is satisfied by thermal energy provided by the PVT collectors ($EM_{\text{th,PVT}}$). Moreover, from 40 m² of PVT collectors area the system is able to totally satisfy the DHW demand (EM_{DHW}), as suggested by the solar thermal DHW fraction (determined by (14)).

Table 4.
Size of the PVT and GSHP system for the parametric analysis.

Plant components	a)	b)	c)	d)	e)
PVT collectors area A_{PVT} (m ²)	20	40	40	60	60
Total boreholes length (m)	500	300	400	300	500

Table 5.
Solar electrical, thermal (heating and DHW) and only thermal (DHW) fractions comparison.

	a)	b)	c)	d)	e)
$F_{sol,el,PVT}$	22.3%	47.5%	46.9%	71.4%	71.1%
$F_{sol,th,PVT}$	32.3%	56.0%	56.2%	72.4%	71.9%
$F_{sol,th,DHW,PVT}$	66.2%	114.4%	114.4%	147.1%	147.1%

The electrical energy ($EM_{el,PVT}$) provided by 60 m² of PVT collectors area covers most of the total electrical energy required by the plant to activate the thermal machine, pumps and auxiliary heaters ($EM_{HP,i, res}$), as suggested by the PVT solar electric fraction defined in (12). The further electrical energy necessary to make the plant independent from the grid is provided by the PV field.

$$F_{sol,el,PVT} = EM_{el,PVT} / (EM_{HP,i, res}) \quad (12)$$

$$F_{sol,th,PVT} = EM_{th,PVT} / (EM_{heating} + EM_{DHW}) \quad (13)$$

$$F_{sol,th,DHW,PVT} = EM_{th,PVT} / EM_{DHW} \quad (14)$$

Fig. 3 shows that the PVT electrical efficiency, determined by (15), is very little influenced by the plant size, while the PVT thermal efficiency and the overall PVT efficiency (defined in (16) and (17) respectively) have a negative trend from case a) to case e): this is caused by the increment of PVT losses in percentage related also to the nature of the PVT chosen (glazed one).

$$Eff_{el,PVT} = EM_{el,PVT} / (S * A_{PVT}) \quad (15)$$

$$Eff_{th,PVT} = EM_{th,PVT} / (S * A_{PVT}) \quad (16)$$

$$Eff_{tot,PVT} = (EM_{el,PVT} + EM_{th,PVT}) / (S * A_{PVT}) \quad (17)$$

The indexes of the specific primary no-renewable energy consumption ($EP_{gl,nren}$) and the specific primary renewable energy consumption ($EP_{gl,ren}$) express respectively the ratio of the electrical energy provided by the grid ($E_{el,from,grid}$) and of the electrical energy produced by the PV and PVT (EM_{PV} and $EM_{el,PVT}$) - used to satisfy the plant electrical requirements -, and the building area A_{build} (18), (19).

$$EP_{gl,nren} = E_{el,from,grid} / (\eta_{el} * A_{build}) \quad (18)$$

$$EP_{gl,ren} = (EM_{el,PVT} + EM_{PV}) / (\eta_{el} * A_{build}) \quad (19)$$

As matter of fact, the best solution, i.e. the one that minimizes the consumption of no-renewable energy and maximizes the electrical and thermal PVT contribution, is the case d).

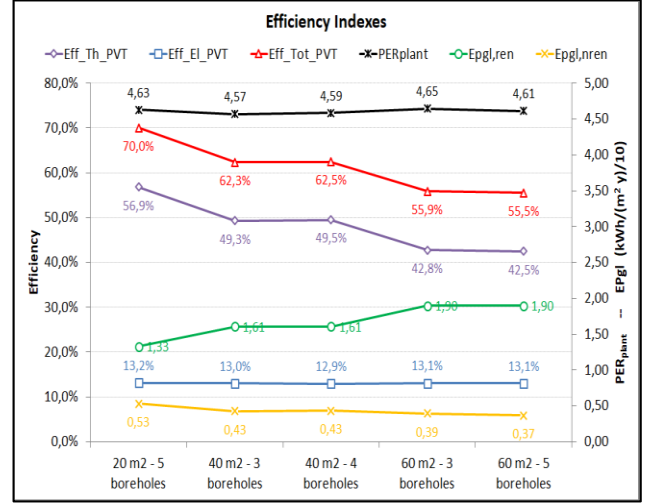


Figure 3. PVT thermal, electrical and overall efficiency, primary energy ratio (PER_{plant}), specific primary renewable and no-renewable energy consumption ($EP_{gl,ren}$, $EP_{gl,nren}$) comparison for the five cases.

For this solution, the main performance indexes are reported in Fig. 4.

The graph 4a) shows that the electrical efficiency varies from the 15.5 % (December and January) to the 12.5 % (July) due to the fact that in the summer season the PVT watertemperature is too high to reduce the PVT cell temperature as much as needed to improve the electrical. In fact, comparing the $Eff_{el,PVT}$ (orange curve) with the Eff_{PV} (purple curve), it can be seen that the PV performance is greater in hotter months.

The thermal efficiency decreases in summer because of the lower heat removed by the PVT water, due to higher average temperature. COP and EER referred to the thermal machine - (20) and (21) where the terms at numerators indicate the thermal energy provided by the condenser to the Hot Tank and the thermal energy absorbed from the Cold Tank by the evaporator respectively, and the denominator EM_{HP} is the electrical energy consumed by the heat pump) have a general upward trend from winter to summer season due to the decrease in the temperature difference between the fluids at the evaporator and at the condenser sides. The average values are high, around 4.5 (COP) and close to 6 (EER) (Fig. 4b)). As a consequence, the total energy ratio index (TER) (calculated as the sum of COP and EER) trend is similar, and reaches the value of 11.5 in the hotter months.

The primary energy ratio of the plant (PER_{plant} , calculated as defined in (22)) is above 4 for most of the year; this means that the useful energy obtained by the system is nearly four times higher than the primary input one.

$$COP = E_{hottank-cond} / EM_{HP} \quad (20)$$

$$EER = E_{coldtank-evap} / EM_{HP} \quad (21)$$

$$PER_{plant} = \frac{EM_{cooling} + EM_{heating} + EM_{DHW}}{\frac{EM_{HP,i, res}}{\eta_{el}}} \quad (22)$$

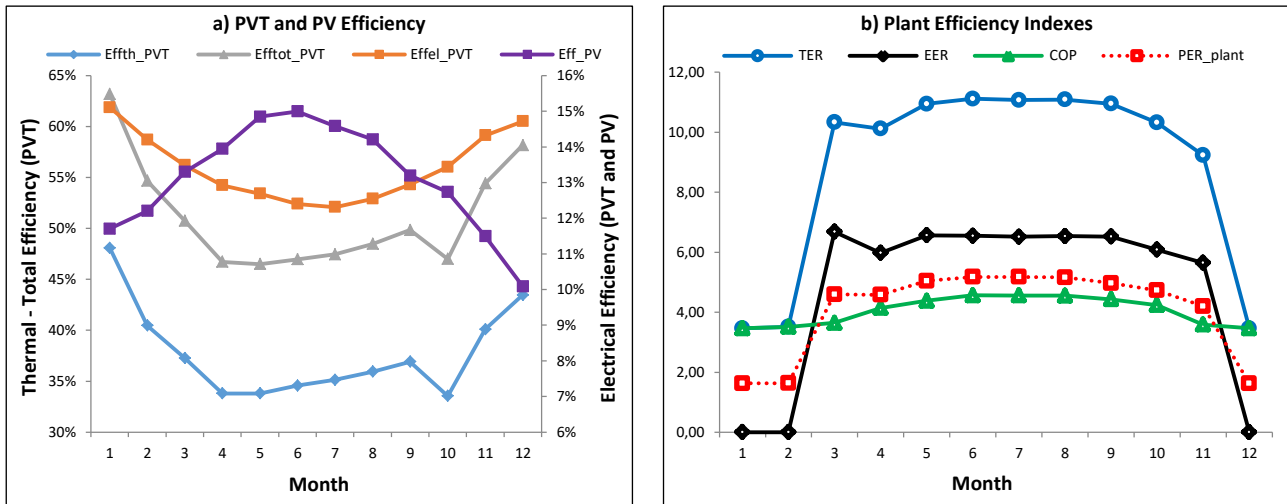


Figure 4. In graph a): the PVT and PV electrical efficiency (Eff_{el_PVT} and Eff_{PV}) (right axes), PVT thermal and PVT overall efficiency (Eff_{th_PVT} and Eff_{tot_PVT}) (left axes). In graph b): the thermal machine performance indexes (TER, EER and COP) and the plant primary energy ratio (PER_{plant}).

Finally, Fig. 5 shows an economical overview and a comparison with a traditional system.

The system self-produces more electrical energy than the required for most of the year, except from November to February when about 4917 kWh (983 € considering a unitary cost of the electrical energy of the grid of 0.2 €/kWh) are taken from the grid.

The system produces 13645 kWh in excess that corresponds to 2729 € of saving or gain (depending if this electricity is available for other uses in the building or it is sold to the grid). In comparison with a traditional system (electric driven air water chiller + natural gas boiler), the system implemented allows to save 5186 € and reset the annual cost of the electric energy from the grid.

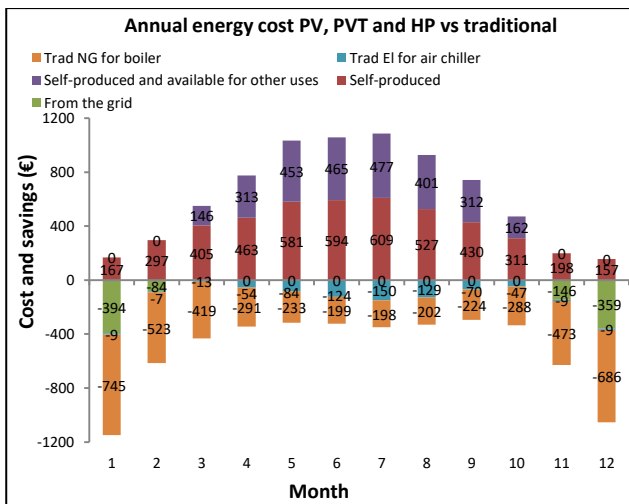


Figure 5. Energy costs of a traditional system (Trad El for air chiller and Trad NG for boiler) compared to the energy cost of the electrical energy bought from the grid (PV/PVT El from the grid) and the electrical energy self-produced by the system and used in the plant (PV/PVT self-produced and used in the plant) and available for other uses (PV/PVT self-produced and available for other).

III. CONCLUSIONS

The current study aimed at implementing a dual source heat pump system coupled to ground and glazed PVT technology. Electric and thermal energy produced by the plant are used to provide heat, cool and DHW for a part of the renovated buildings of a secondary school located in the North East Italy.

The conceptualization and control logic of the plant have been described. Five different sizings of the system were examined and simulated using TRNSYS software. In the best solution, the PVT collectors are able to totally satisfy the DHW demand and cover most of the electrical energy required by the system. In comparison with a traditional PV with the same nominal efficiency, the glazed PVT electrical performance is better only in the cooler months due to its cooling during the ground recharge, using as source of the heat pump and pre-heating of the DHW.

The increase of the source temperature in HP operation and of the heat removal from the sink in chiller mode determines a better performance of the thermal machine and of the entire plant. The total energy required to satisfy heating, cooling and DHW demands is provided entirely by the electric energy self-produced by the plant except for the months from November to February, when it is necessary to buy energy from the grid. In an overall annual balance, due to the exceeded electrical energy self-produced by the system, the building can be categorized as a NZEB.

REFERENCES

- [1] M.Noro, G. Bagarella, R. Lazzarin, "Advancements in hybrid photovoltaic-thermal systems: performance evaluations and applications" 71st Conference of the Italian Thermal Machines Engineering Association, ATI2016, 14-16, 2016.
- [2] F. Leonforte, N. Aste, C. Del Pero, "Water PVT collectors performance comparison". *Energy Procedia*, 2017.
- [3] M. Y. Haller, E. Bertram, R. Dott, T. Afjei, D. Carbonell, F. Ochs et al. "Components and thermodynamic aspects". in *Solar and Heat Pump Systems for Residential Buildings*, 2015, pp. 50-52.

Patients and surgical staff thermal comfort in operating rooms at St. Olavs Hospital in Norway

Helena Kuivjõgi¹, Guangyu Cao², Martin Thalfeldt³, Anna Bogdan⁴

¹Tallinn University of Technology, Department of Civil Engineering and Architecture, helena.kuivjogi@taltech.ee

²Norwegian University of Science and Technology, Department of Energy and Process Engineering, guangyu.cao@ntnu.no

³Tallinn University of Technology, Department of Civil Engineering and Architecture, martin.thalfeldt@taltech.ee

⁴Warsaw University of Technology, Faculty of Environmental Engineering, Prof. PW, anna.bogdan@pw.edu.pl

Abstract— In healthcare facilities and hospital environment, it is essential to enable thermal comfort for occupants. Unstable thermal conditions in operating room (OR) will influence the performance of surgical staff and infection possibility of patient. In this study, thermal comfort of patients and surgical staff was measured with two ventilation solutions at St. Olavs hospital ORs. Research methods includes the thermal environment measurements during mock (imitation) surgery, a survey among surgical staff and observations during real operation. The results show, that the mean air velocity near occupants in mixing ventilation (MV) OR was low (max 0,08 m/s) and in laminar air flow (LAF) ventilation OR considerably higher, 0,36 m/s. In conclusion, there was good general thermal comfort of surgical staff in LAF OR, but the surgical staff felt mainly uncomfortable in MV OR.

Index Terms— thermal comfort, observation, surgery, survey, ventilation.

Introduction

A. Background and the motivation of the work

Thermal comfort is condition of mind that expresses satisfaction with the thermal environment and is assessed by subjective evaluation. [1] In common HVAC systems principal purpose, the thermal comfort is the first aspect to provide for human [2], but in hospital ORs, the main aim is to prevent the infection of the surgical wound by airborne infectious microorganisms. [3] As a supplement, the technical HVAC standards state that to prevent surgical site infection (SSI), the thermal comfort must be achieved for the patient and all members of the surgical staff in the operating room. [4] One general reason is that the thermal satisfaction influences productivity and health of surgical staff. [5] Furthermore, the American Society of PeriAnesthesia Nursing standard recommends controlling patient thermal comfort level, because it will influence the wellbeing of patient – hazard of hypothermia. [6]

R. Van Gaever et al. brings out in their study, that „it is not possible to achieve thermal comfort for each member of the surgical staff by only revising the HVAC standard.“ The reason is that, in OR, different people will have very extreme demands on thermal satisfaction.

In spite of several studies about thermal comfort in operating rooms, there is still lack of information. Therefore, the idea of this study to collect more information

for making the better overview about thermal comfort in operating rooms.

B. The objective and framework of this study

The overall objective of this thesis is to analyze thermal comfort of surgical staff and patient in various operating rooms with two different ventilation solutions at St. Olavs hospital. To achieve the objective and estimate the thermal comfort levels of occupants in operating rooms, the following tasks were conducted:

1. field measurements of indoor thermal environment during mock surgery,
2. the survey about surgical staff sensation, and
3. observation during real operation.

II. METHOD

A. Two operating rooms at St. Olavs hospital

The investigation puts the focus on three following methods in two operating room at St. Olavs hospital (Fig. 1). There are four occupant group under investigation: surgeon, patient, anesthetist and assistant nurse. The ventilation system of this building is mainly controlled by service center and can be adjusted by surgical staff in room via three scenarios with different condition settings (controlled by sensors in the exhaust ducts): operation is ongoing, infection risk/cleaning, operating room prepared. The humidity of airflow is not controlled due to hazard of bacterial distribution. During the measurements, the scenario was operation is ongoing and the temperature was set to 23°C. The supply air temperature was about 22 °C.

One operating room was with LAF ventilation and another with mixing ventilation solution. Mixing ventilation ORs area is 59.1 m² and there are four wall mounted exhaust outlets and four supply diffusers on the ceiling. LAF ventilation OR area is 56.1 m² and it has 4x4m LAF zone on the ceiling (surrounded with 110 cm long walls), two wall mounted exhaust outlets near floor and six exhaust outlets on the ceiling around LAF area. General boundary conditions in ORs during measurements and observations are in Table I.

B. Field measurements

This study includes measurements of thermal comfort variables in real OR at St. Olavs hospital during March 2019 (Table I).

TABLE I. BOUNDARY CONDITIONS IN LAF AND MV OR AT ST. OLAVS HOSPITAL DURING FIELD INVESTIGATION IN MARCH 2019

Variables	Date	MIXING VENTILATED OR				LAF VENTILATED OR			
		Field experiment			Observation and survey		Field experiment		Observation and survey
		4 th	8 th	15 th	27 th	2 th of April	23 th	29 th	21 th
outdoor air temp, °C (1)		-1,8	0,6	2,7	5,3	4,7	0,6	1,6	6
outdoor air RH, % (1)		78	54	49	82	44	92	93	54
room air Temp, °C (2)		23,5	23,7	24,2	NM		23,7	22,3	NM
room air RH, % (2)		15	12,8	12,1	NM		20,9	24,3	NM
Surface temp. of surroundings (average), °C (5)		20,7	20,8	22,4	22,5	22,4	21,1	21,7	NM
vapor partial pressure. kPa (3)		0,43	0,38	0,37	0,74	0,37	0,61	0,65	0,49
RH, %		15,0	12,8	12,1	26,4	13,3	20,9	24,3	17,3
pas, kPa		2,90	2,93	3,03	2,81	2,81	2,93	2,70	2,81
ta, °C		23,5	23,7	24,2	23,0	23,0	23,7	22,3	23,0
Room area, m ²		59,1			56,1			56,1	
Room volume, m ³		170,68			168,3			168,3	
Supply airflow, m ³ /h		3700			12850 (ca 60% recirculated)			12850 (ca 60% recirculated)	
Air change rate, ACH		21,68			22,5			22,5	

(1) Forecast data from YR.no; (2) Measured with Pegasor AQ Indoor device near wound area, at the center of room; (3) Calculated with (2) or (4); (4) data from service center of St.Olavs hospital for comparison; (5) Measured with Bosch PTD1 contact free device; NM – not measured



FIGURE 1. MIXING (LEFT) AND LAMINAR AIR FLOW (RIGHT) VENTILATION SOLUTION OR IN ST. OLAVS HOSPITAL

Before the measurement, 15 min intensive mock surgery with 5 people have been presented. Experiments in MV OR has been done during three weekdays and in LAF OR, two weekdays. Surgical lamps were turned on and OR doors were closed. The height of operating bed was 84.5 cm, the height of surgical lights from floor was in MV room 2.1 m and in LAF ventilated room 2.15 m.

The measurements have been done according to [7]. In this study the environment is heterogeneous, due to air movement and radiation from equipment. Regarding that and, the physical quantities have been measured in the vicinity of four subjects from head, abdomen and ankle level (Table II) with TSI uni-directional instrument VelociCalc Plus. Specifically, the air temperature measurement for 2 minutes and air relative velocity for 1 minute.

Besides, velocity measurements in MV OR has been taken as probe tip measuring the airflow vertically from ceiling to floor, because the airflow direction is unknown. In LAF OR, the measuring description is in Table III.

The VelociCalc Plus temperature sensor has been calibrated with the Reference Temperature Calibrator Model RTC-157 (accuracy ±0.04 °C) and the anemometer has been calibrated with TSI Flow Calibrator.

TABLE II. MEASURING HEIGHTS FROM FLOOR FOR THE PHYSICAL QUANTITIES OF AN ENVIRONMENT (ISO 7726)

Location level of the sensors	Sitting person (m)	Standing person (m)	Patient (m)
Head	1,1	1,7	0,9
Abdomen	0,6	1,1	0,9
Ankle	0,1	0,1	0,9

TABLE III. PROBE TIP MEASURING DIRECTION IN LAF OR

Measuring point	Probe tip measuring direction
1 – Surgeon	Under the LAF area: airflow vertically from ceiling to floor
2 – Anesthetist	Outside of LAF area: airflow horizontal from LAF area to person
3 - Assistant nurse	Outside of LAF area: airflow horizontal from LAF area to person
4 – Patient	Under the LAF area: airflow vertically from ceiling to floor

There has been measured the dimensions of room and the surface temperature of surfaces as walls, ceiling, floor, doors and windows. Last measurements have been done with Bosch PTD 1 contact free device and the results are used to calculate the mean radiant temperature (T_{mrt}). Regarding to the standard ISO 7726:1998 [7], that due to building materials high emissivity, there has been

disregarded the reflection to assume that all the surfaces are black, so the emissivity has been taken 0.95.

Also, using previous data, there have been calculated the operative temperature for every occupant. Finally, there have been measured overall conditions during measurements with Pegasor AQ Indoor device at the center of standing human (1,1 m) and it is used for the calculation of vapor partial pressure.

C. Observations

There have been used several observation methods described in Table V, but in this paper, only these results are considered, what are directly related with PMV-PPD calculation.

The tabulated values for observations taken from ISO 8996:2004 [8] are generalized and concern an „average“ individual: A man 30 years old weighing 70kg and 1.75 m tall (body surface area 1,8 m²); A woman 30 years old weighing 60 kg and 1.70 m tall (body surface area 1.6 m²).

D. Survey

The survey among surgical staff in both above mentioned OR have been conducted to get knowledge about occupants’ real sensation in ORs thermal climate. The questions in survey, corresponded to [9] and [10], are asked to answer as based on last operation occupants had. Occupants have been answered to seven subjective questions about thermal sensation, comfort and acceptance. In addition, they have been asked to evaluate their work level (according to [8] Table A.2) and clothing.

The final mean thermal sensation level has been correlated with Fanger scale and the standard deviation (SD) has been calculated by IBM SPSS software. The survey has been conducted in two parts, one during the

observation days in MV OR (at 27 of March and 2 of April) and in LAF OR (at 21 of March). The second part took place in between 29.04-5.05.

There were 30 participants in MV OR and 13 in LAF ventilated OR survey (also clean zone nurse is included to extend the investigation). Altogether, 44 filled questionnaires.

III. DATA PRESENTATION

The boundary conditions during experiments have been brought out in Table I and during survey, in Table IV.

TABLE IV. ORS CONDITIONS DURING SURVEY LOGGED WITH TINITAG PLUS 2 AT ST. OLAVS HOSPITAL

		ta, °C	RH%
Dilution ventilated OR	Measure point near anesthetist		
	MAX	24,12	39,24
	MIN	22,80	13,93
	Measure point near surgeon		
	MAX	24,91	38,88
	MIN	23,13	14,34
Laminar air flow OR	Measure point near assistant nurse		
	MAX	22,68	44,65
	MIN	20,72	17,05
	Measure point near surgeon		
	MAX	24,11	44,22
	MIN	20,97	17,06
Outdoor	MAX	12,8	53
	MIN	1,2	81

A. Field measurements in ORs

Let’s take the operative temperature (T_{op}) as indicative value.

In MV solution OR, during the experiments, the average room air temperature was around 23.6 °C.

TABLE V. OBSERVATIONS DESCRIPTION

Task	Object	OR	Source/tool	Method/input
Activity level	Surgical staff	MV LAF	recorded video according to ISO 8996:2004 [8]	Duration aprox. 2h; after every movement end, the body segment work together with mean value of metabolic rate and time has been stated.
	Patient	MV, LAF	Malcolm A. Holliday et al. Study	averaged person, who have weight of 65 kg and body surface area 1,7 m ² , due to this, the metabolic rate is 2400 kcal/day, what is 68,4 W/m ² .
Thermal comfort of real patient	Real patient	MV	Body temperature: hospital surgery team	Measured as bladder temperature. Three surgeries. First measuring point: after the patient enters the room. The measuring period: after every 0.5 hour. Duration: 1.5-4.5h.
			Air temperature and RH: TinyTag near surgical area	Logged after every 5 minutes near surgical area.
Clothing	Surgical staff and patient	MV, LAF	Material info from hospital and manufacturer	Surgical staff: surgical underwear, cap, hat, mask, socks, shoes and gloves (in MV OR lead apron for x-ray). For surgeons also sterilized surgical gown. Patient: naked; covered with warm blanket, surgical drape and polyethylene film (in MV OR-s forced-air warming blanket system).
			From literature	Thermal resistance of clothing is taken from the study of Anna Bogdan et al. (20) ¹ Brought out in Table VIII.
Surface temperature	surgeon forehead	MV, LAF	infrared thermograph camera FLIR E60 ²	Duration: the first 40 minutes of real surgery. The skin temperature of surgeon forehead has been marked down after every 1 minute.
	surgical lights			Analysis of the thermal camera picture of surgical lights

¹clothing also manufactured by barrier according to the requirements of EN ISO 9001 and EN 13795

² The emissivity to walls, human skin and equipment has been taken 0,95.

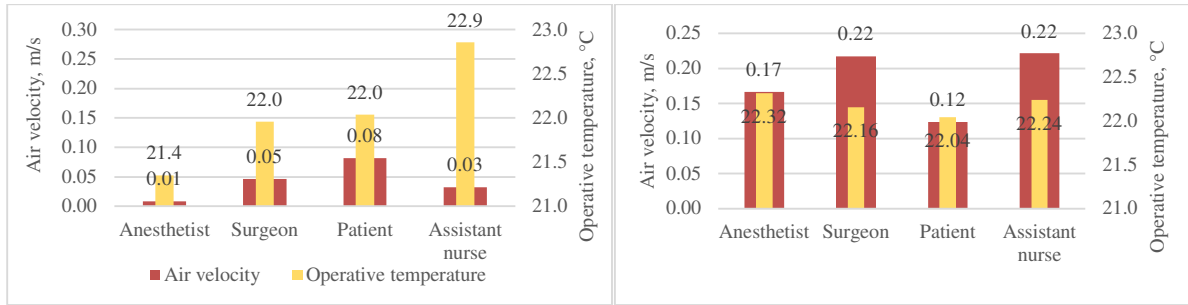


FIGURE 2. AVERAGE OPERATIVE TEMPERATURE AND AIR VELOCITY IN THE VICINITY OF OCCUPANTS IN MV(LEFT) AND LAF (RIGHT) OR

However, the thermal comfort conditions of occupants will vary in wide range. For patient, the T_{op} was 22.0° C (Fig. 2), and the air velocity at range 0.06-0.11 m/s (respectively head level and ankle level). For surgeon, the T_{op} was slightly below 22.0 °C, and the air velocity 0.0-0.09 m/s (last on head level). For the anesthetist, T_{op} was 21.4 °C (Fig. 2), and the air velocity is near zero.

For assistant nurse, the experiment was in one additional day, where the average room air temperature was around 24.2 °C (air temperature in the vicinity of assistant nurse is lower – 23.4°C). Operative temperature is higher (22.9°C) and not comparable with other occupant conditions, because also the mean radiant temperature was higher at this day. The air velocity is at range of 0.07- 0.09 m/s.

In LAF solution OR, during the two main experiment the room air temperature was 22.3°C and 23.7°C. Results in Fig. 2 shows, that the thermal comfort conditions will not vary that much as in MV OR. For patient, the T_{op} was 22.04° C, and the air velocity at range 0.03-0.3m/s (respectively abdomen and head level). For surgeon, the T_{op} was 22.16 °C, and the air velocity 0.32 m/s in abdomen level. For the anesthetist, the T_{op} was 22.3 °C, and the air velocity 0.17 m/s. For the assistant nurse, the T_{op} was 22.2°C, and the air velocity 0.22 m/s.

B. Observation in operating rooms

In this paper, we will focus on main results from observations. The principal was the estimation of activity level and clothing insulation of surgical staff and patient. The results for 101 and 135 minutes (respectively in MV and LAF OR) lasting surgery and estimated clothing insulation are in Table VIII. The highest activity level and also clothing insulation is for surgeon and the lowest is for patient. Therefore, they are the two extremes and thermal comfort will be discordant.

C. Results from survey

Following results presents the answers received from surgical staff in mixing and LAF ventilation solution OR.

In mixing ventilation OR, only 17% of repliers says, that the environment is comfortable, other 83% says, that it is slightly uncomfortable (53%), uncomfortable (20%) and very uncomfortable (10%). The thermal sensation, SD of answers and dissatisfaction in MV OR has been brought in Table VI and comparison with PMV is in Figure 3.

In LAF ventilation OR, about 46% of repliers says, that the environment is comfortable, other 54% says, that it is slightly uncomfortable (38%), uncomfortable (7%) and 7% did not give the answer. The thermal sensation, SD of answers and dissatisfaction in LAF OR has been brought in Table VII, and comparison with PMV is in Figure 4.

From the questionnaire came out, that in MV OR, two anesthetist felt draught or breeze near chest or head, and 5 occupants from staff gently breeze near chest or head. But still, the thermal sensation was slightly warm. In LAF OR, one assistant nurse and one anesthetist often felt slightly draught near chest or head from ventilation.

TABLE VI. OCCUPANTS GENERAL THERMAL SENSATION DURING OPERATIONS IN MV OR (SURVEY)

Occupant	Thermal sensation (Fanger scale)	SD	Dissatisfied, %
Anesthetist	neutral or slightly warm (0.14)	1.07	0
Assistant nurse	slightly warm or warm (1.6)	0.55	60
Surgeon	slightly warm or warm (1.7)	0.68	10

TABLE VII. OCCUPANTS GENERAL THERMAL SENSATION DURING OPERATIONS IN LAF OR (SURVEY)

Occupant	Thermal sensation (Fanger scale)	SD	Dissatisfied, %
Anesthetist	neutral (0.0)	-	0
Assistant nurse	slightly cool to slightly warm (0.0)	1.16	0
Surgeon	slightly warm (1.0)	0.0	0

TABLE VIII. THE CLOTHING AND ACTIVITY LEVEL OF OCCUPANTS IN OR

Occupant group	Clothing insulation, m ² K/W (clo)		Activity level, W/m ² (met)	
	LAF solution OR	MV solution OR	LAF solution OR	MV solution OR
Surgeon	0.202 (1.3)	0.234 (1.5)	138.3 (2.38)	103.0 (1.78)
Assistant nurse	0.154 (0.99)	0.193 (1.25)	74.8 (1.29)	92.2 (1.59)
Patient	0.165 (1.06)	0.165 (1.06)	68.4 (1.18)	68.4 (1.18)
Anesthetist	0.154 (0.99)	0.193 (1.25)	90.1 (1.55)	85.0 (1.47)

D. The estimation of PMV level of occupants in ORs

The PMV level for estimation of thermal comfort has been calculated by using the well-known Fanger equation from [8]. There have been taken into account the measurement results from experiments, T_{mrt} , the clothing and activity level.

The calculation has been done first to local body parts and then, the final mean PMV level has been correlated and the SD has been calculated by IBM SPSS.

The results of MV OR have been brought out in Figure 3 (occupant_PMV) and data is in Table IX and the results of LAF OR have been brought out in Figure 4 and data is in Table X. There should be careful with conclusion of patient comfort, because the PMV level varies in big interval among local body parts due to difference in air velocity.

IV. DISCUSSION

The objective of this study was to clarify the thermal comfort of four occupant groups in two different ventilation solution operating rooms at St. Olavs hospital. There has been concentrated on predicted and real thermal comfort of surgical staff and patient using three main methods: field experiment, observation and survey.

Wyon et al. [11] has been investigated, that 20.5°C is the comfortable operative temperature for average staff member in the OR. However, Mora et al. [3] found from surveys, that the air temperature 19°C is good for surgeon thermal comfort.

Generally, all surgical staff in MV OR at St. Olavs hospital will experience higher operative temperature than suggested. As can see from PMV calculation and answers from survey, for the anesthetist and patient, the thermal environment is comfortable, but for surgeon and assistant nurse, there will be too warm.

However, in LAF OR, the operative temperature is at least 1.6 degrees higher than suggested, and the PMV calculation shows also, that surgeon will have more warm feeling. But rest of all will feel comfortable. Furthermore, the answers from survey will confirm it.

On the basis of this study, can be suggest that one option to improve the thermal comfort level in OR at St. Olavs, is to reduce the mean radiant temperature. Mixing ventilation OR have many equipment, mostly surgical lights, what will influence occupants by radiant heating. There have been investigated also in thermal camera observation results, that the lamps surface temperature is around 32.7-34°C in MV OR and around 31-32.9°C in LAF OR. This is very high, if to compare with other surfaces around, and even due to that, they are closer to surgeon, the radiant heat to surgeon will be very high.

Another possibility is, to investigate, how much it is possible to raise the air change rate in mixing ventilated OR (as suggested by [12] - to take out the heat gain produced by equipment) to be in comfort zone and without enlarging the SSI.

Anesthetist, who have low activity level and at the same time, feel slightly draught from the ventilation, should wear warmer clothing. The problem is mainly in LAF OR, because the air velocity is larger.

As can see from Figure 3 and Figure 4, that even, if the PMV calculation could be similar to real sensation, then percentage of dissatisfaction is totally different, perhaps due to local discomfort. Therefore, there is not right to do fundamental conclusions and the further investigations should be on local thermal comfort, instead of calculating the PMV level. About survey, the best is to investigate the environment, conducting the field survey with asking questions about thermal comfort at the precise moment and on particular body part.

TABLE IX. PMV LEVEL OF EVERY OCCUPANT IN MV OR (EXPERIMENT)

Occupant	PMV	SD
Anesthetist	0.25	0.27
Assistant nurse	0.69	0.04
Patient	-0.14	0.13
Surgeon	0.91	0.03

TABLE X. PMV LEVEL OF EVERY OCCUPANT IN LAF OR (EXPERIMENT)

Occupant	PMV	SD
Anesthetist	0.39	0.19
Assistant nurse	0.07	0.31
Patient	-0.49	0.51
Surgeon	1.29	0.17

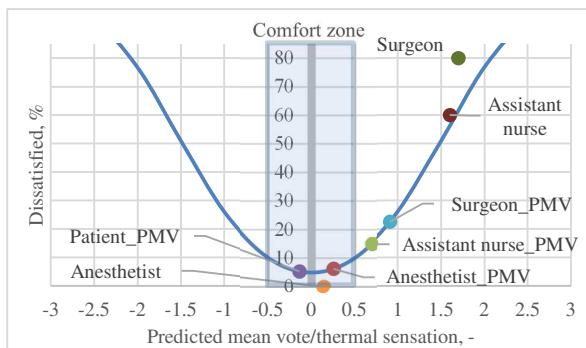


FIGURE 3. THE COMPARISON BETWEEN OF PREDICTED AND REAL THERMAL COMFORT IN MV OR

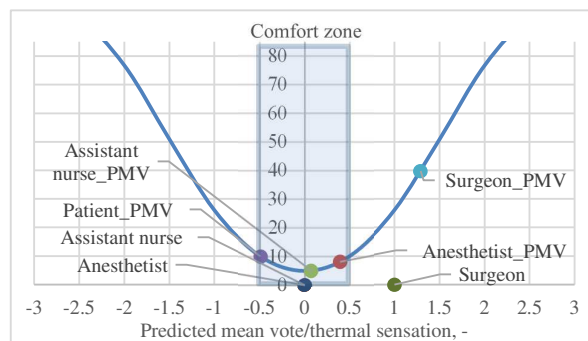


FIGURE 4. THE COMPARISON BETWEEN OF PREDICTED AND REAL THERMAL COMFORT IN LAF OR

V. CONCLUSION

The challenging around thermal comfort in operating room is in its beginning, but to reach somewhere, there is need to collect the information constantly. This study has been focusing on the thermal comfort of the surgical staff and patient in OR. The two research questions were, what is the predicted and what will be the real thermal sensation in OR. However, the investigation is conducted in real OR environment and there has been used three methods: experimental measurements to measure the variables influencing the thermal comfort; observation to estimate the metabolic rate and clothing thermal resistance; and the real sensation of surgical staff has been discovered through survey in two ORs. The study will be therefore good overview of actual conditions in OR.

The conclusion over calculations and survey shows, that thermal comfort conditions in OR will vary in wide range:

1. In mixing ventilation OR, the surgeon and assistant nurse will experience the environment as slightly warm or warm, anesthetist as neutral. From survey came out, that assistant nurse and surgeon will have substantial dissatisfaction about thermal environment in MV OR. The conditions for patient seem to be comfortable, but need more investigation, because of the patient actual wellbeing – we do not know about actual local comfort.

2. In LAF OR, the operative temperature is similar to all occupants, and the air velocity has bigger impact as it is higher and may cause slight draught. For anesthetist and assistant nurse, the environment is comfortable, for surgeon, it is slightly warm. The patient will experience slightly cool climate in LAF OR.

The gap of thermal sensation is significantly caused by different clothing and activity level of occupants. Surgeon, who is wearing several layers of clothing (1.3/1.5 clo), is doing hard and active movements (ca 2 met) during surgery. At the same time anesthetist, who is wearing just one layer of clothing (0.99/1.25 clo), is mainly sitting/standing (ca 1.5 met). The patient has little higher clothing level, but smaller activity, so one could be the most critical case. In this study has been investigated the thermal comfort of patient through observation of body and air temperature, but this is not enough to investigate patient total thermal comfort in OR.

To investigate more the thermal comfort aspect as mean radiant temperature, it will be interesting to examine the equipment effect in OR. As found out, that the surgical lights will affect surgeons' thermal comfort, but there is also many other equipment what will produce the heat.

Overall, this is challenging to adjust the temperature in operating room, but it is not impossible. For future work,

author suggests investigating, how low the air temperature could be and how can improve the clothing thermal insulation of the patient and anesthetist, that they still meet thermal comfort and will be in the normothermia condition.

ACKNOWLEDGEMENT

This present study is written during the exchange studies in Norwegian University of Science and Technology at Department of Energy and Process Engineering. My thank goes to Erasmus+ and NTNU; Liv-Inger Stenstad, Gabriel Kiss, Jan Gunnar Skogås and staff from St. Olavs hospital for providing OR facilities, supporting experimental measurement, assisting survey and field observation; my supervisors Guangyu Cao, Martin Thalfeldt, Anna Bogdan; Jarek Kurnitski and not least, to our research team: Christoffer Pedersen, Minchao Fan, Yixian Zhang, Jakub Wladyslaw Dzedzicand and Masab Khalid Annaqeeb.

REFERENCES

- [1] *ANSI/ASHRAE standard 55-2017: Thermal environmental conditions for human occupancy*, 2017.
- [2] *ASHRAE Handbook - Fundamentals*, 2017.
- [3] R. Mora, M. J. English and A. K. Athienitis, "Assessment of Thermal Comfort During Surgical Operations," *ASHRAE Transactions*, p. pg. 52, 2001.
- [4] R. V. Gaever, V. Jacobs, M. Diltoer, L. Peeters and S. Vanlanduit, "Thermal comfort of the surgical staff in the operating room," *Building and Environment*, vol. 81, pp. 37-41, Nov. 2014.
- [5] S. Sadrizadeh and M. G. Loomans, "Thermal comfort in Hospital and Healthcare Facilities - a Literature Review," in *IAQVEC, Korea*, 2016.
- [6] V. D. Hooper et al., "ASPAN's Evidence-Based Clinical Practice Guideline for the," *Journal of PeriAnesthesia Nursing*, vol. 24, pp. 346-365, 2010.
- [7] *ISO7726. Ergonomics of the thermal environment - Instrument for measuring physical quantities.*, 1998.
- [8] *ISO 8996. Ergonomics of the thermal environment — Determination of metabolic rate*, 2004.
- [9] *ISO 28802. Ergonomics of the physical environment — Assessment of environments by means of an environmental survey involving physical measurements of the environment and subjective responses of people*, 2012.
- [10] *ISO 10551. Ergonomics of the physical environment — Subjective judgement scales for assessing physical environments*, 2019.
- [11] D. P. Wyon, O. M. Lidwell and R. E. Williams, "Thermal comfort during Surgical Operations," *The Journal of Hygiene*, vol. 66, no. 2, pp. 229-248, Jun 1968.
- [12] *ANSI/ASHRAE/ASHE Standard 170-2017 - Ventilation of Health Care Facilities*, 2017.

Modification of the Comfort Equation by P.O. Fanger for Elderly People

Amalie Dokkedal Jensen, Cathrine Schermer Riis, Anne Sørensen (Supervisor)

Aarhus University School of Engineering, Inge Lehmanns Gade 10, 8000 Aarhus C, Denmark.

Email: asv@ase.au.dk

Year of Thesis (B.Sc.) acceptance 2020 (January)

Abstract – Aging involves changes to the physiology, for instance reduced metabolism, reduced skin permeability etc., which might influence the criteria for thermal comfort. The present study seeks to modify the comfort equation by P.O. Fanger to account for these physiological changes, through a combination of field study and literature review. 13 elderly test subjects in Danish nursing homes participated in heart rate measurements, and it was recorded when they were in the activity level “relaxed, seated”. These measurements were used to modify the comfort equation.

P.O. Fanger thought that the comfort equation was valid for elderly, but this study indicates that it cannot account for all the physiological changes, and should therefore be used with caution to determine a comfort temperature for elderly people.

Index Terms - Comfort Equation, physiological age-dependent changes, thermal comfort

INTRODUCTION

Research on thermal indoor climate is ambiguous when it comes to determining how and if elderly citizens’ thermal comfort and perception differ from that of younger adults. It is, however, widely accepted that several vital functions in how the human body responds to ambient temperatures change when the body ages.

Elderly people have a lower metabolic rate and thereby a lower heat production. Shivering and sweating are some of the tools that the body uses to react to a change in ambient temperature, and it has been shown that sweating and shivering starts at higher and lower temperatures, respectively, for elderly people. [1].

Changes also happen to the skin itself and thereby the heat loss through the skin [2-4]. The result is that the interval of feeling thermally neutral is narrower for elderly [5], than for younger persons. The changes in the thermoregulation shown by previous research are visualised in Fig. 1.

Despite these changes, a statistical difference between comfort temperatures of elderly and younger adults has not been shown. The present study investigated the topic in a context of Danish nursing homes, where the residents are older than the test subjects in previous research. Many of the elderly citizens also suffer from illnesses, e.g. different types of dementia. This means that they might find it difficult to express dissatisfaction with the thermal environment. It all emphasises that knowledge on the

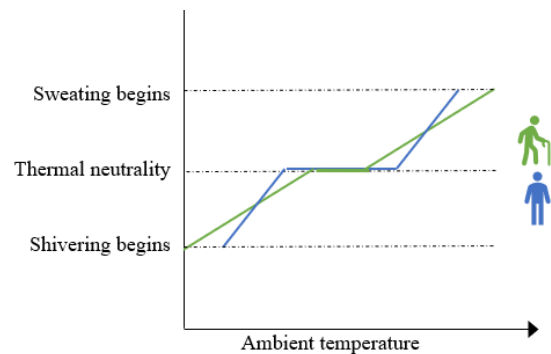


Figure 1. Visualisation of how the human body thermoregulation changes with age

thermal comfort and perception of elderly living in nursing homes is important.

ISO 7730 [6] and the comfort equation by Danish researcher P.O. Fanger is fundamental in how thermal indoor climate is understood and adapted in the building industry. The comfort equation is based on a double heat balance for the human body, and Fanger, being aware of metabolism changing with age, thought that the lower dissipation would counterbalance the lower heat production, and that his comfort equation is therefore valid for elderly people. [7].

The present study investigates the validity of the comfort equation for elderly people by developing a modified version of the comfort equation and comparing it with the original equation. This investigation was made as a part of Ref. [8] that is furthermore a part of an extensive project on indoor climate in nursing homes in “InnoBYG”, a Danish innovation network in the building environment.

The double heat balance: The comfort equation is based on the double heat balance, where a set of regressions is used to describe a correlation between comfort temperature, activity level, clothing level, air speed and relative humidity. The double heat balance states that:

$$H - E_{dif} - E_{sw} - E_{res} - C_{res} = K = R + C \left[\frac{W}{m^2} \right] \quad (1)$$

H = Internal heat production

E_{dif} = Heat loss through evaporation and diffusion of water vapour through the skin

- E_{sw} = Heat loss through evaporation of sweat from the skin surface
- E_{res} = Heat loss by respiratory evaporation
- C_{res} = Dry heat loss through respiration
- K = Heat conduction through clothing
- R = Radiative heat flow from the surface of the dressed human
- C = Convective heat flow from the surface of the dressed human

METHOD

To investigate the validity of the comfort equation for elderly people, a field study and a literature review were made. The comfort equation was derived from the double heat balance, (1), in order to detect which parameters are physiological and could thereby change with age. A literature review was made to assess if and how the parameters should be changed in a modified comfort equation. To investigate metabolism, a field study was furthermore conducted using heart rate measurements.

The field study on metabolism was at two Danish nursing homes and lasted for a week. 13 residents (8 males, 5 females) participated in heart rate measurements that were conducted using Garmin Vivosmart 4 heart rate monitors, see Fig. 2.

One of the reasons for measuring heart rates in stead of adapting a more classical climate chamber study is that, as the measurements were a part of Ref. [8], it was important to interfere as little as possible in the everyday life on the nursing homes. The test subjects wore the heart rate monitors during daytime for 5 days, and it was therefore possible to track their activities with a very little amount of interfering.

Another reason for measuring heart rates in the field is that some of the test subjects suffer from dementia, meaning that it is difficult to interview them and have them answer questionnaires. Heart rate measurements are therefore considered more valid.



Figure 2. Equipment used for heart rate measurements

The method described in “ISO 8996 Ergonomics of the thermal environment - Determination of metabolic heat production” was used to calculate the metabolism from the heart rate data.

As the metabolism for the activity level “relaxed, seated” is an important constant in the comfort equation, it was recorded when the test subjects were in fact seated and relaxed. The heart rate data from these time periods then formed the basis for the modification of the comfort equation in the project.

RESULTS

Data on the test subjects and results of the heart rate measurements are presented in Table I.

TABLE I.
RESULTS OF THE HEART RATE MEASUREMENTS

n=13	Age	Mean heart rate
Average	82 years	72 BPM
Interval	67-93 years	56-92 BPM

The data was sorted to only include heart rate measurements for when the residents were in the activity level “relaxed, seated”. The metabolism for each of the subjects in these situations were calculated as described in [9], and the average results for the 13 test subjects are presented in Fig. 3 along with the constant 58 W/m that is used by P.O. Fanger as the metabolism when relaxed and seated.

The average metabolic rate when the test subjects were “relaxed, seated” was 44 W/m². The metabolism for the elderly test subjects is lower than that used by Fanger, but he was aware of this difference. The question now is whether the metabolism of 44 W/m² is so low that the other parameters in the comfort equation are not able to counterbalance, thereby indicating that the comfort equation is not valid for elderly people. This was investigated by reviewing literature.

Derivation of the comfort equation from the double heat balance: Each parameter in the comfort equation has been investigated to determine possible alteration of the equation to accommodate the physiological age-related changes in metabolism, skin temperature and sweating.

H - Internal heat production: It describes the heat produced by a human as a function of the metabolism M [W/m²] and mechanical work W [W/m²] conducted by the person. This relation is age-independent.

$$H = M - W \left[\frac{W}{m^2} \right] \tag{2}$$

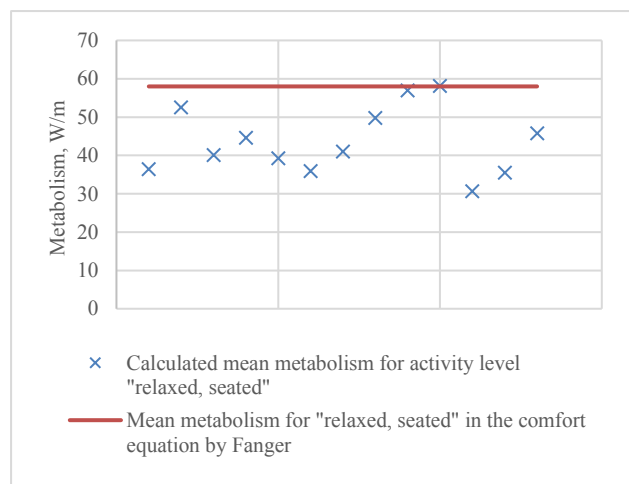


Figure 3. Average metabolic rate when the test subjects were “relaxed, seated” compared to the corresponding metabolic rate used by P.O. Fanger.

E_{dif} - Heat loss from evaporation and diffusion of water vapor through the skin: This parameter is dependent on the specific evaporation heat at average skin temperature, λ [kJ/kg], the permeability coefficient of the skin, m [kg/h·m·Pa], and the water vapor pressure at skin and air temperature, respectively p_s og p_{da} [Pa].

$$E_{dif} = \lambda \cdot m \cdot (p_s - p_{da}) \left[\frac{W}{m^2} \right]$$

In the interval 27-36 °C, which can be defined as a normal skin temperature t_s , λ varies with less than 1% and is therefore defined to a non-age dependant constant at λ (35°C) = 2418 kJ/kg [10, p. 27-28], and p_s can in the same interval according to [7] be described by a linear regression to

$$p_s = 256 \cdot t_s - 3373 \text{ [Pa]},$$

$$\text{Where } t_s = 35.7 - 0.0275 \cdot (M - W).$$

It has, however, in [11] been documented that the skin temperature of older people is generally lower than for young people. An estimation of the results in [11] gives an indication for a possible age related adjustment of the skin temperature to $t_{s,old} = 34.8 - 0.0275 \cdot (M - W)$.

The permeability coefficient of the skin is in [7] defined as a constant, $m = 4.575 \cdot 10^{-6}$ [kg/h·m·Pa] whether this value has been corrected in relation to age variation is unknown. Newer research generally found that m decreases with age by 15-40% acc. [2], [3] and [4], therefore it has been chosen to use a reduction of the skin permeability of 28%, giving $m_{old} = 3.294 \cdot 10^{-6}$ $\left[\frac{kg}{h \cdot m^2 \cdot Pa} \right]$

E_{sw} - Heat loss trough evaporation of sweat from the skin surface: For a person in thermal comfort, the relationship between activity and preferred sweating was defined by an experiment on college students in 1967 by P.O. Fanger [6]

$$E_{sw} = 0.42 \cdot ((M - W) - 58.15) \left[\frac{W}{m^2} \right] \quad (3)$$

In (3), the constant 58.15 describes the metabolism at the activity level "Seated, relaxed". The regression is only valid for this activity level or higher.

In the present study, the average metabolism of the test subjects was found to be 44 W/m² at the activity level "Seated, relaxed", and the regression is therefore modified to

$$E_{sw,old} = 0.42 \cdot ((M - W) - 44) \left[\frac{W}{m^2} \right]$$

It has in this study not been possible to validate whether 0.42 is applicable for all ages and it is therefore left untouched.

E_{res} - Heat loss by respiratory evaporation: This parameter describes the wet heat loss related to respiration, or more specific the latent heat loss in the saturated exhalation air, depending on the exhaled air volume V , the specific evaporation heat λ , and the difference in saturation between exhaled and inhaled air acc. W_{ex} og W_a .

$$E_{res} = V \cdot \lambda \cdot (W_{ex} - W_a)$$

The exhaled air volume depends on the activity level described by the metabolism as $V = 0.0052 \cdot M$ [kg/h], which is expected to be age independent. The saturation in exhaled and inhaled air is also age independent. Combined with the value for specific evaporation heat λ at 35 °C (see the reasoning under E_{dif}), the equation is valid for both young and old, and can be reduced to:

$$E_{res} = 17 \cdot 10^{-6} \cdot M \cdot (5867 - p_a) \left[\frac{W}{m^2} \right]$$

C_{res} - Dry Heat loss trough respiration: This describes the energy needed to heat the inhaled air volume V from surrounding air temperature, t_a , to body temperature, t_{ex} .

$$C_{res} = V \cdot c_p \cdot (t_{ex} - t_a) \left[\frac{W}{m^2} \right]$$

As for E_{res} , the air volume is defined by the metabolism $V = 0.0052 \cdot M$ kg/h. c_p is the specific heat capacity of dry air, set at 20 °C to $c_p = 1007$ J/(kg · K).

In general, the dry heat loss from respiration is relatively small, the exhalation temperature can be set a constant of 34 °C [7, s. 30]. This gives an expression of C_{res} valid for both young and old:

$$C_{res} = 0.0014 \cdot M \cdot (34 - t_a) \left[\frac{W}{m^2} \right]$$

R - Radiative heat flow from the surface of the dressed human: The heat loss from radiation is described by Stefan-Boltzmanns law, based on the surface temperature of the clothing (t_{cl}) and the mean radiative temperature of the body to the surrounding room (\bar{t}_r).

$$R = f_{eff} \cdot f_{cl} \cdot \epsilon \cdot \sigma \cdot ((t_{cl} + 273)^4 - (\bar{t}_r + 273)^4)$$

f_{eff} is the effective radiation factor, set at 0.7 for the human body. f_{cl} is the clothing area factor depending on the clothing insulation (I_{cl}) $\left[\frac{m^2 \cdot K}{W} \right]$

$$f_{cl} = \begin{cases} 1.00 + 1.290 \cdot I_{cl} & \text{for } I_{cl} \leq 0.078 \\ 1.05 + 0.645 \cdot I_{cl} & \text{for } I_{cl} > 0.078 \end{cases}$$

The value of I_{cl} is estimated from table found in ex. ISO 7730. ϵ , the emissivity for skin and clothing, is normally set to 0.97, and σ , the Stefan-Boltzmann's constant which is $5.667 \cdot 10^{-8}$.

This means that the parameters R , from an isolated point of view, is age independent, written as

$$R = 39.8 \cdot 10^{-9} \cdot f_{cl} \cdot ((t_{cl} + 273)^4 - (\bar{t}_r + 273)^4) \left[\frac{W}{m^2} \right]$$

Meanwhile the temperature of the clothing (t_{cl}) is age-dependant based on the following definition

$$t_{cl} = t_s - I_{cl} \cdot (H - E_{dif} - E_{sw} - E_{res} - C_{res})$$

C - Convective heat flow from the surface of the dressed human: This is, just like the radiative heat loss, from an isolated point of view, independent of age because it is defined by the area factor of the clothing, f_{cl} , the temperature difference between the clothing t_{cl} , and the surrounding air, t_a , and the heat transfer coefficient at the surface of the clothing, α_k .

$$C = f_{cl} \cdot \alpha_k \cdot (t_{cl} - t_a)$$

But besides the clothing temperature, the heat transfer coefficient also has an age-related variation because it is defined as

$$\alpha_k = \text{Largest value of } \begin{cases} 2.38 \cdot (t_{cl} - t_a)^{0.25} \\ 12.1 \cdot v_{ar}^{0.5} \end{cases}$$

where v_{ar} is defined by the air velocity in the room v_a to $v_{ar} = v_a + 0.005 \cdot (M - 58)$

To sum up, three parameters were modified in the comfort equation to account for physiological changes, namely the metabolic rate when “relaxed, seated”, the skin temperature, and the skin permeability. The modified and the original comfort equation were compared by calculating the comfort temperature with identical assumptions regarding clothing level (1 clo), relative humidity (50%RH) and air speed (0.15 m/s). The activity level “relaxed, seated” is used in the comparison, meaning 58 W/m² in the original comfort equation and 44 W/m² in the modified comfort equation.

The comfort temperature was found as the combined air temperature and surface temperature, meaning that the comfort temperature equals the operative temperature. The results are presented in Table II.

TABLE II.
COMFORT TEMPERATURES USING TWO VERSIONS OF THE COMFORT EQUATION

Comfort equation	Metabolic rate, “relaxed, seated”	Comfort temperature
Original	58 W/m	23.7°C
Modified	44 W/m	25.4°C
Original	44 W/m	26.2°C

DISCUSSION

These findings indicate that the comfort equation is not valid for elderly people, meaning that the low metabolic rate for elderly people is not counterbalanced by low heat loss. If this was the case, the result in Table II for the modified comfort equation should have been equal to the comfort temperature calculated from the original comfort equation and a metabolic rate of 58 W/m², but there is a difference of 1.7°C between the two comfort temperatures.

However, it is important to note that the present study did not complete the modification of the comfort equation. That the comfort equation is not valid for elderly is therefore only one way to analyse the result, another being that the differences between the original and the modified comfort equation are due to the use of wrong regressions in E_{sw} or t_s . In climate chambers, these regressions should be

investigated, but in the present study, only the intercept was changed.

A third option is that 44 W/m² is not accurate for the metabolic rate when the elderly citizens are “relaxed, seated”. This points to the small sample size in the field study consisting of 13 test subjects. But the calculation of metabolic rate from heart rate measurements using ISO 8996 is also problematic, since it should only be used for hearts rates over 120 BPM, which was not the case. Since the present study was part of a larger field study, it was chosen to use real life measurements of heart rates and not direct measurements of metabolic rates, but the metabolic rate could be measured more directly in another study.

CONCLUSION

Even if the comfort equation is valid for elderly people, it is still problematic to use it in field studies: According to P.O. Fanger, the comfort equation is valid for elderly people because a decrease in metabolic rate is followed by a decrease in heat loss, so the equation manages to balance itself out. But that means that in the case of elderly people, one should only use the comfort equation if the metabolic rate is based on metabolic rate charts defining the metabolic rate for different activities. In this case, it means that the last result in Table II should not be used, since only the heat production, metabolism, is changed, and not the heat loss. By only inserting a measured metabolic rate, the effect of heat production balancing heat loss out is ignored. Measurements of heart rate or metabolic rate cannot be used in the comfort equation for elderly people, and that is a scientific problem, because it complicates field studies in nursing homes or other facilities for the elderly.

The present study was a part of Ref. [8], where the goal was to compare residents and nursing staff in terms of comfort and thermal indoor climate in general, and thereby improve our understanding of how future nursing homes should be built. By measuring heart rates, it was possible to gain a much deeper understanding of the everyday life in nursing homes than by just assuming an activity level. At least for scientific purposes, it is strongly recommended that further research is done on the topic of physiological changes and how they affect the comfort temperature. A modified comfort equation that applies for elderly people is needed.

ACKNOWLEDGEMENT

Special thanks are extended to InnoBYG and to the staff members and residents at the Danish nursing homes Aarhus Frøplejehjem and Meta Mariehjemmet.

REFERENCES

- [1] G.S. Anderson, G.S. Meneilly, I.B. Mekjavic, Passive temperature lability in the elderly, Eur. J. Appl. Physiol. Occup. Physiol. Vol. 73 (1996) 278–286.
- [2] Wepierre, J. and J.P. Marty, Percutaneous absorption and lipids in elderly skin. Journal of Applied Cosmetology, 1988. 6: p. 79-92.
- [3] Wilhelm, K.-P., A.B. Cua, and H.I. Maibach, Skin Aging - Effect on transepidermal Water Loss, Stratum Corneum Hydration, Skin Surface pH, and Casual Sebum Content. Arch Dermatol, 1991. 127: p. 1806-1809.

- [4] Boireau-Adamezyk, E., A. Baillet-Guffroy, and G.N. Stamatias, Age-dependent changes in stratum corneum barrier function. *Skin Research and Technology*, 2014: p. 409-415.
- [5] Wang, Z., de Dear, R., Luo, M., Lin, B., He, Y., Ghahramani, A., Zhu, Y., Individual difference in thermal comfort: A literature review. *Building and Environment*, 2018. 138: p. 181-193.
- [6] Danish Standards Association, DS/EN ISO 7730:2006, "Ergonomics of the thermal environment - Analytical determination and interpretation of thermal comfort using calculation of the PMV and PPD indices and local thermal comfort criteria"
- [7] Fanger, P.O., *Thermal comfort : Analysis and applications in environmental engineering*. 1970, Copenhagen: Danish Technical Press. 244.
- [8] Jensen, A.D. and Riis C.S, "Dimensioneringsgrundlaget for termisk indeklima på plejehjem", Bachelor Thesis, Aarhus University 2020, unpublished
- [9] Danish Standards Association, DS/EN ISO 8996:2004, "Ergonomics of the thermal environment - Determination of metabolic heat production"
- [10] Arens, E. and H. Zhang, *Thermal and Moisture Transport in Fibrous Materials*, Chapter 16: The skins role in human thermoregulation and comfort, ed. N. Pan and P. Gibson. 2006: Woodhead Publishing Limited. 50.
- [11] Taylor, N.A., N.K. Allsopp, and D.G. Parkes, Preferred room temperature of young vs aged males: the influence of thermal sensation, thermal comfort, and affect. *The journals of gerontology. Series A, Biological sciences and medical sciences*, 1995. 50(4): p. M216-M22

NUMERICAL AND EXPERIMENTAL ANALYSIS OF INNOVATIVE GREENHOUSE AIR CONDITIONING SYSTEM

Dere B.*, Gumusluol Z.H. and Colak L.

*Author for correspondence

Department of Mechanical Engineering,

Baskent University

Ankara

Turkey

E-mail: basakddere@gmail.com

Abstract— The aim of the project is to design an energy efficient and innovative air distribution channel and air conditioning system designed for use in greenhouse air conditioning. It is easier and more economical for the consumers to reach the product by providing the producers of greenhouse agriculture to present the product on the market for 12 months. The air distribution channels will distribute the air more efficiently in the greenhouse and minimize the fan power required for ventilation. The microclimatic layers obtained by CFD analysis is ensured that only the volume of air in which the plants live is effective and reduce unnecessary energy input.

The air duct and air conditioning system that is designed in this way will be more environmentally friendly and more economical by providing efficient use of energy input. The innovative aspect and technological value of the project is; It is found that the systems currently used in greenhouse air conditioning are weak in terms of energy efficiency. In order to ensure energy efficiency in the greenhouse, only the volume of plants will be air conditioned with effective air distribution channels. In order to achieve this aim, it will be possible to form microclimatic layers with CFD (Computational Fluid Dynamics) In addition, the boundary conditions to be used in the first run of CFD analysis is determined by pre-tests instead of theoretical values.

The first step of the project is included literature research and creation of mathematical models. Secondly, CFD analysis is run with the boundary conditions used in the verification tests to be performed on the designed prototype. Verification of the final numerical model is done with the results from the verification tests. After verification of the numerical model, different air conditioning

scenarios is run and the most efficient scenario is determined. Thermo-economic optimization is performed on specified scenario and final technical information package is created.

Index Terms— Air Conditioning System, Computational Fluid Dynamics, Energy Efficient, Microclimatic Layer.

INTRODUCTION

Many commercial applications are aimed to supply products during a whole year period. To achieve this goal producers are wasting great effort to generate suitable climatic conditions for plants. Accordingly, the effectiveness of greenhouse air conditioning system is one of the most critical considerations in the system design because of the impact on the price of the products.

The mass of hot air charged into the greenhouse is expected to reach the target volume, that is the place where the plants are located, change the ambient temperature, but the temperature of the air charged into the greenhouse is higher than the local temperature. This upward movement of air causes the charged air to reach or partially reach the target volume. To solve the heating problem of the plants, extra hot air is charged into the target volume of the plants. To create an extra mass of hot air, the heating system must draw more power and consume more fuel. Fuel spent unnecessarily damages the environment by increasing carbon emissions. Also, while only the volume of plants should be heated, this process, which is carried out to bring the entire greenhouse environment to the desired temperature, causes a serious energy loss and causes a decrease about efficiency.

Since the temperature of the charged air is lower than the ambient temperature during the blowing of cold air into the greenhouse, the cold air settles on the greenhouse floor and cooling can be done easily. In this

way, the limits of the target volume are easily achieved. However, modelling cold airflow, defining flow barriers and evaluating numerical analysis results is an analysis problem in itself. Also, the instantaneous temperature of the greenhouse environment should be considered to keep the desired temperature within the greenhouse within a certain range, because the amount of cold air that needs to be charged will be determined accordingly. Sending too much cold air to the location can create excessive cooling energy and cause plants to be damaged by cold as the cold air reaches the target volume effectively.

To prevent the explained reasons of the efficiency decreases, zone air conditioning techniques are used as microclimatic layers are created into the greenhouse by CFD analyses, heating and cooling processes are evaluated separately with particularly designed components. The creation aim of the microclimatic layers is to block the extra air conditioning cost with conditioned just the target volume.

There is also a scientific background about greenhouse air conditioning systems, mechanical ventilation and specific turbulence models are examined. The first experiments studying the air circulation in a greenhouse were conducted by Businger, Morris and Neale [1]. At the same time, some theoretical models are described to explain the air exchange in the greenhouses that are depending on external wind speed and temperature difference [2]. Also, some experimental studies are done to explain the air circulation in the greenhouse that is made with wind tunnels by Sase et al. [3]. The first CFD application about greenhouse air conditioning system was conducted by Okushima [4]. The validation of the numerical model is supplied by Sase's wind tunnel experiment.

There are studies on active and passive heating methods to meet the heating need of the greenhouse in winter. Active heating was applied using geothermal energy, using soil-air heat exchangers and phase-changing storage materials [7-8]. Passive heating is; water tanks, rock beds, north-facing wall applications, mulching, movable insulation elements, thermal curtain applications. When these applications are evaluated in terms of energy efficiency to be provided in the greenhouse; thermal curtain application is the most practical and convenient way [7-9].

The most appropriate thermal behaviour of a greenhouse for cooling is due to the high performance of the cooling system it contains in extreme conditions. Natural ventilation prevents solar radiation input, which can be used in combination with forced ventilation (exhaust fans) or with reflective materials placed locally, causing extremely high-temperature values for plants. Such cooling systems can only be effective in regions where the summer season is not very hard and the average temperature does not exceed 33 degrees. In regions where extreme temperature

conditions are experienced and the average temperature exceeds 40 degrees, evaporative cooling is the most efficient form of cooling. Roof type cooling systems are used as an alternative to evaporative cooling, which creates a fog image and is provided with the help of a fan when used in the greenhouse. The daily temperature difference between the capillary heat exchanger and soil and the blowing temperature has been reduced. Apart from this, some studies suggested using excessive heat that is harmful to plants during the daytime in a water tank to reduce the negative effect of low temperatures during the night hours. When these studies are examined, it was seen that heating, cooling and ventilation units should be used together. In experimental studies on the control of greenhouse microclimate, according to the temperature conditions of the region where the greenhouse is located, simultaneously; solar energy for heating, greenhouse soil for heat storage, greenhouse soil and cold water were used for cooling. Experimental studies on greenhouses have shown that the improvements to be made in the temperature factor are directly related to the manufacturability of the product in the greenhouse [10].

In this study numerical and experimental analysis are evaluated together, a prototype greenhouse is modelled concerning the dimensions that are calculated from similitude analysis. Required heating installation is constructed as pipes that are filled with thermal oil which involves an electrical heater inside. For the cooling side, air distribution channels are modelled with a calculated geometric similitude scale. The setup will be constructed and combined at the further time of the project.

This project aims to design an efficient, innovative air-conditioning system and an integrated heating/cooling components that can be produced in high quality and quantity throughout the year, and the efficient use of energy, which has become an important design condition all over the world, and that the air conditioning system to be used in greenhouses is environmentally friendly.

EXTERNAL BOUNDARY CONDITIONS

Thermal Load Calculations

To evaluate the best efficient air conditioning scenario, environmental conditions of the greenhouse must be considered. We assumed the discussed greenhouse is located in the Mediterranean region. The heat flux values that are given as a heat gain or heat loss from the sidewalls of the greenhouse is calculated with HAP (Hourly Analysis Program). For the best report results from HAP, given information must be as real-like as possible because HAP uses algorithms that are working with ASHRAE standards for specified regions, building materials and air conditioning devices.

Model of the considered greenhouse as given at Figure 1, the structural components of the greenhouse is defined as follows:

Walls. One common wall construction is used for all exterior walls. The construction, whose data are; thermal conductivity of nylon 6.6 is 0.25 W/m-K consist of 3m*1.5m*6m. The overall weight of the nylon 6.6 is 0.001539 kg. The exterior surface absorption is in the “reflective” category.

Roofs. One uniform horizontal roof construction is used for the greenhouse. The construction material of the roof is same with wall construction material Nylon 6.6. The exterior surface absorption is in the “reflective” category.

Windows & External Shading. There is no window in the greenhouse but gate gap exists in the dimensions of 1m*1m. No internal shading materials are used.

Lighting. Recessed fluorescent lighting fixtures are use in the space. A lighting density of 1.00 W/m² is used.

For greenhouses, %100 day lighting levels are used. The lighting profile applies for the days the greenhouse in session. For unused months lighting levels of %0 is used.

Occupants. The maximum number of occupants discussed in this section. During harvest time, design day occupancy 10 to 20 is very frequent. This occupancy profile applies for only harvest time at the greenhouse.

Air System Data. One air conditioning system will used for cooling process. Therefore, air conditioning equipment must be represented into HAP. Data for this air conditioning system must be taken from the supplier.

Equipment Type. Ventilation. Outdoor ventilation airflow will be calculated using the ASHRAE Standard 62.1-2007 method. “Constant” control for ventilation will be used so the system uses the design flow of outdoor air at all times. Ventilation dampers are closed during the unoccupied period of the damper leak rate is %5.

Supply Fan. The supply fan in the air conditioning unit will be forward curved with variable frequency drive.

Return Air Plenum. The system uses a return air plenum. It is estimated that %70 of the roof load, %20 of the wall load and %30 of the lighting load is removed by plenum air.

Sizing Criteria. Required zone airflow rates will be based on the peak sensible load in each zone. Required space airflow rates will be based on peak space loads for the individual spaces.

The results obtained when the thermal load calculations of the greenhouse are made with the HAP program with the inputs described above:

Loads calculated to dimension the unit to be used for cooling operation; sensible coil load is 1.4 kW and the volumetric airflow required for the unit area of the space is 10.16 L/s.

Loads calculated to dimension the unit to be used for heating operation; Sensible coil load of 3.4 kW and required volume flow of 17 L/s.

When the sensible load calculation was made for the whole space, it was calculated as 2.7 kW for cooling and 1.4 kW for heating. In the sensible heat load calculation, the heat loss from the greenhouse roof is higher than the heat losses from the walls and most of the heat loss is from the roof. The covered thermal load is 13 W and the factor that constitutes this value is the people who enter and exit the place periodically.

Air conditioning loads are calculated as cooling load dry-bulb temperature 30.6°C and wet bulb temperature 3375 W below 16.7, heating load at 1428 W under dry thermometer temperature -16.7°C and wet bulb temperature 17.7°C.

Input values commonly used for greenhouse cultivation

The charging rate of conditioned air in a greenhouse has limits according to the properties of greenhouse plants. To avoid harmful effects on the plants that are caused by the mass flow rate of the air conditioning system, the limits must be considered as boundary conditions as velocity inlet 5 m/h. The heating installation also has limits about the temperature of the hot water it carries maximum 50°C. At last, plants are added heat to the greenhouse ambient by their photosynthesis processes. At last, plants are added heat to the greenhouse ambient by their photosynthesis processes but the heat gain is added into latent heat gain but HAP calculations show that it is not significant because of that the heat gain of the plants does not include to the analyses.

Inputs given for components used for air conditioning

For air conditioning of the greenhouse specific heating, cooling and channel systems are used. The heating installation is located on the sidewalls of the greenhouse. The heat gain from the side walls to the greenhouse ambient is given as 600 W. On the other hand, the cooling is done by two systems by passive cooling from the ground that takes -300 W and the air distribution channels that are charged conditioned air to the greenhouse ambient. The charged rate from the entrance of channels is given as 1000 m³/h

The boundary conditions to be used during the run of the final numerical model will be determined by the inputs given to the verification test unit. In the design of conditioned air distribution channels, the geometries of the duct and the air blowing openings on the duct will be optimized by evaluating different geometries.

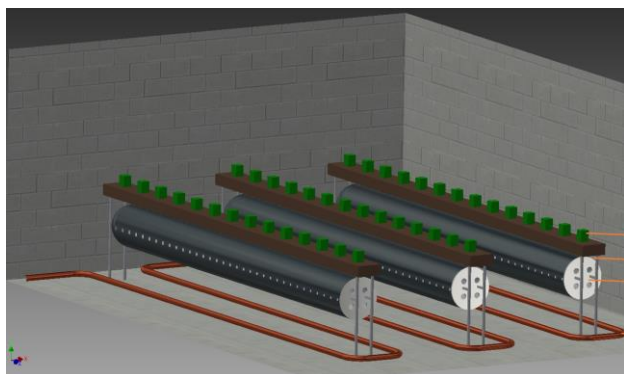


Figure 1 Considered Greenhouse

NUMERICAL METHOD

The CFD analysis to be made will consist of three parts. The first is the analysis to be run in the control volume specified in the greenhouse to create microclimatic layers in the greenhouse. The second one is to analyse the friction losses that will occur within the air distribution channels to be designed. The third part is to analyse the geometry of the heating installation.

For cooling, the main problem is using unnecessary energy to cool a restricted layer that is the region where the plants live. The decrease in the amount of excess energy of the air conditioning system by increasing the efficiency of the system reduced the consumption. The numerical analysis is done by using SimScale and Fluent CFD analysis programs. For the analyses that are run on the greenhouse ambient, flow domain is generated as shown in Figure 2.

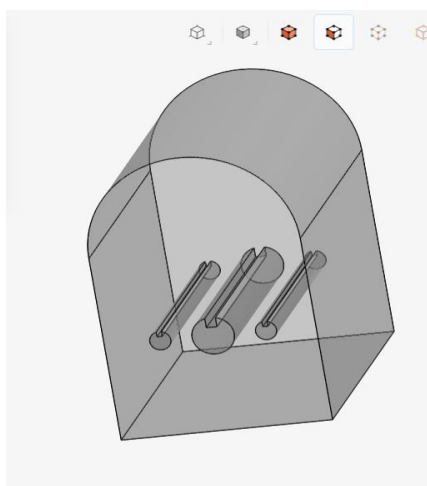


Figure 2 Flow Domain

The charging channels are half of the suction channel that is located in the middle of the greenhouse. When the cooling case is run on the SimScale platform, for given values the main purpose of the cooling case has been reached as shown in Figure 3.

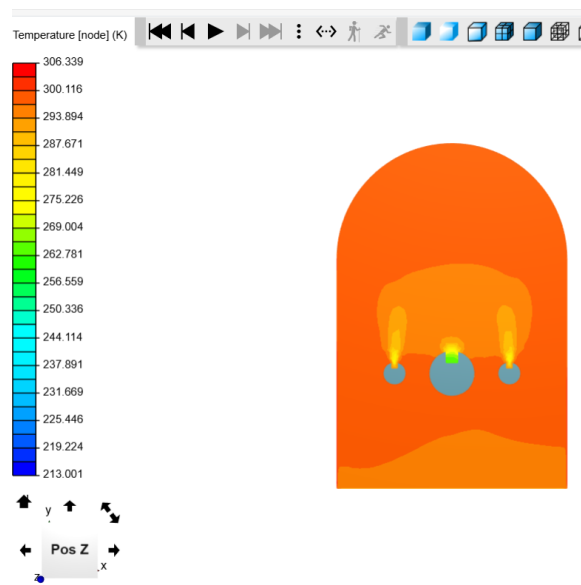


Figure 3 Cooling case, Temperature Contour

On the other hand, analyses to obtain the best efficient channel design about to stabilize the mass flow rate through the inlet of the channel to the end of the channel. The first analysis is run on the case that includes the constant diameter spaces then the conical and changed diameter spaces are examined. The following figures show the contours of the channels about the mass flow rate.

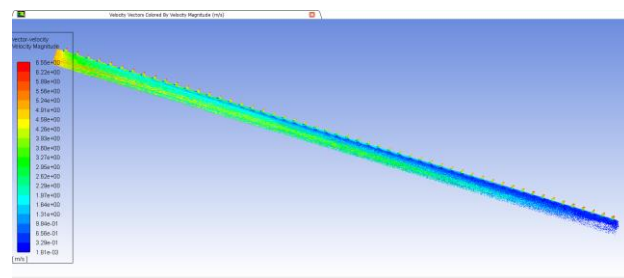


Figure 4 Constant Diameter Spaces

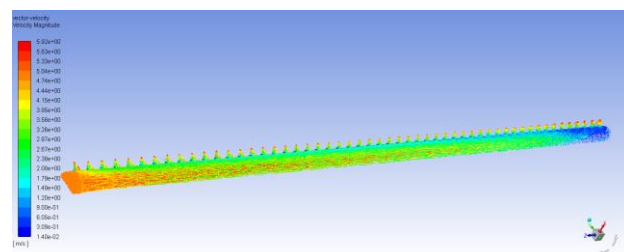


Figure 5 Changed Diameter Spaces

Validation of Numerical Models

Verification tests to be carried out within the project can be summarized as follows; by integrating a pre-prototype, which has been reduced by similitude analysis, into the test unit, results will be obtained such as the speed of air exit from the duct, pressure drops to occur along the duct and the temperature distribution within the greenhouse. During

the tests, the data to be taken from thermocouples and flowmeters can be observed momentarily from the display screens integrated into the test units and intervened when an unexpected situation is encountered.

In verification tests, studies will be carried out to verify the numerical model that has been run and whose mesh structure has been checked. It is aimed that the deviation between the airflow rate, speed, pressure drop values and the values obtained from the verification tests when the conditioned air is blown into the greenhouse and the air duct on the test mechanism formed by combining the produced prototype and the test unit. Also, the microclimatic layers intended to be formed are intended to meet the 5% temperature change requirement between these layers in addition to the numerical analysis and validation test results.

Verification tests will be performed on the model that is shown in Figure 6.

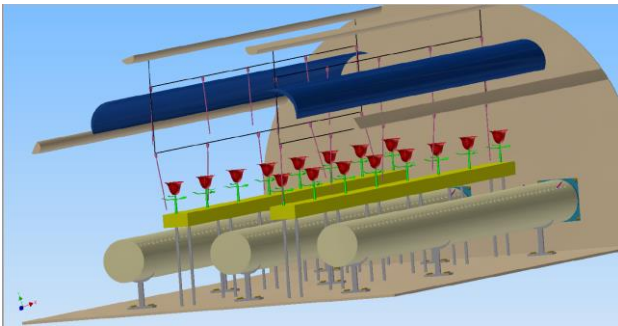


Figure 6 Test Set-up

To create the heating installation effect, electrical heating units will be used with the given heat flux value in numerical analysis. The cooling function of the test unit will be provided by a fan-coil unit to the air distribution channels. Plants and their benches are acting as a flow barrier, therefore plastic plants and stands will be used instead of plants and benches. To calculate the mass flow rate inside the channels pitot tubes are used as a couple by the distances that are shown in Figure 7.

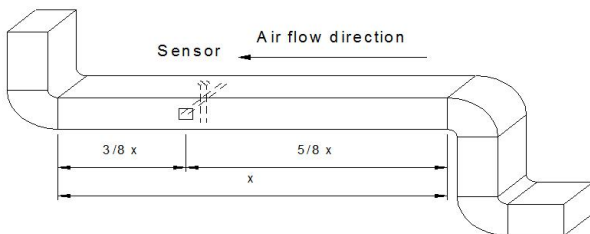


Figure 7 Placement of pitot tubes

To verify the temperature values, 4 rows at 5 each thermocouple will be used. The number of thermocouples may be increased according to the accuracy of the measurements.

RESULTS

This work aimed first to improve the efficiency level of the greenhouse air conditioning system by that producers are increase their profit and the prices of the products will be decreased, the accessibility of the products will increase for the consumers.

The increase in efficiency, prevents the excessive wasting energy that is used to heat or cool greenhouse. By microclimatic layer creation, only the volume where the plants are living is air-conditioned this prompt to lower energy requirements for the whole air conditioning system. Accordingly, the restricted energy sources of our country are used sparingly.

At the end of the cooling case analyses, the following results have been reached, firstly passive cooling that is commonly used by greenhouse cooling is not efficient when compared with the channel system. Secondly, when the ambient temperature of the greenhouse is increased, instead of cooling the entire ambient, a system that only cools the layer where the plants live has been reached. In Mediterranean regions the temperature of the summer months is changed between 30-35°C, the cooling system may be decreased the excessive temperature to 20°C and below easily.

Designed air conditioning system components that are air distribution channel and heating installation results in a more efficient air conditioning system for greenhouse. Air distribution channels are examined as constant cross-section area with the gaps constant and increasing diameter through the channels, conical shape with the gaps constant and increasing diameter. Then, the model that has a conical shape with constant diameter is more effective than the other channel alternatives.

At the end of the thermo-economic evaluation, the innovative greenhouse has more investment cost than the conventional greenhouse. The investment cost of the innovative greenhouse is %4.24 higher, it means, for a unit area of the greenhouse cultivation there is a 10,5 Euros more. Commonly used greenhouses used with an operational area as 10000-meter-square. There is a significant difference for agricultural producers. Most of the annual cost difference sourced from the investment and air conditioning costs. Air conditioning costs differ related to the operational time and operation type as cooling or heating. The innovative greenhouse 3-4 harvest may occur however in conventional one, the maximum harvest number maybe only 2. The difference sourced from the operation type of air conditioning. At the conventional greenhouse, there is no cooling process, because of that, in summer months, production cannot be possible. An innovative greenhouse, cooling and heating processes occurred at the same time; the phenomenon brings an advantage as longer annually operational time. That is the main reason for the profit increase.

These are the air conditioning costs comparison of the innovative and conventional greenhouse. The cooling cost of the conventional greenhouse air conditioning system is

“0” since there is no cooling process in this type of greenhouse. Because of that, the annual total energy cost of the conventional one is greater than the innovative one.

Table 1 Heating, Cooling and Energy Cost

Heating Cost (Euro/kWh)	Cooling Cost (Euro/kWh)	Energy Cost (Euro/kWh)	Operating Time (Hour)	Air Conditioning System Type
217	0	217	4320	Conventional
74	91	165	7200	Innovative

In that point, due to the long operational time, the compulsory costs like water, seeding, planting, labor cost etc. increased too. It may affect the annual total cost between innovative and conventional greenhouse air conditioning systems.

Table 2 Investment, Compulsory and Annual Total Cost

Investment Cost (Euro/kWh)	Compulsory Cost (Euro/kWh)	Annual Total Cost (Euro/kWh)	Operating Time (Hour)	Air Conditioning System Type
9,8	3,96	231,5	4320	Conventional
20,57	5,28	241,7	7200	Innovative

However, because of the improvements in the innovative greenhouse air conditioning system, the production for a unit area is increased, annually profit became higher too. Due to the profit difference, in 4 year the innovative greenhouse pays back itself and brings 25000 Euros annually profit for a 10000-meter-square greenhouse.

When the whole system is evaluated by CFD analysis with best efficient components, microclimatic layers are created and to validate the numerical model a test setup is designed. For the validation of the numerical model, results that are taken from CFD analyses and tests are compared, %5 of error is enough for the validation of the numerical model.

The specified air conditioning scenario will be evaluated with thermo-economic analysis, thermo-economic analysis will run with constituted excel macros.

DISCUSSION

It is important to mention some limitations of this study:

- In this study a room with heating installation and three air distribution channels was considered. Earlier studies have shown the importance of physical parameters on the performance of air conditioning systems such as charged air velocity and temperature, room geometry and the number of heat sources. Further researches needed to evaluate the performance of different physical characteristics.

- This study was performed for a single isolated greenhouse and the radiation heat transfer are calculated from Carrier HAP program. Further research is needed to validate these heat flux values.

- The study only considered a geometrically reduced test set up, to validate the numerical model the data that are taken from the geometrically scaled test unit is used. Further research is necessary on exploring the impact of the test set up with real dimensions.

- This paper includes only the analyses about air distribution channels and cooling system. The heating case has still worked on and improved day by day.

ACKNOWLEDGEMENT

- This research was supported by TUBITAK 2209-B program. We thank our colleagues from UNTES Air Conditioning Systems Inc. who provided insight and expertise that greatly assisted the research.

REFERENCES

- Businger, J.A.,1954. De invloed van raamstanden op de ventilatie van kassen.(The influence of window openings on the ventilation of greenhouses.)Meded. Dir.Tuinbouw(Neth.), 17:897 (in Dutch)
- Okada M. and Takakura T.,1973. Guide and data for greenhouse air conditioning 3. Heat loss due to air infiltration of heated greenhouse. J.Agric Meteorology., 28:223
- Sase S., Takakura T., and Nara M., 1984, wind tunnel testing on airflow and temperature distribution of a naturally ventilated greenhouse, Acta Horti.,148:329
- Okushima L., Sase S., and Nara M.,1989.,A support system for natural ventilation design of greenhouses based on computational aerodynamics. Acta Horti. 248:129
- Jain D., Tiwari GN., Modelling and optimal desing of ground air collector for heating in controlled environment greenhouse, Energy Convers Manage 2003;8:1357-72
- Kurklu A., Energy storage applications in greenhouses by means of phase change materials(PCMs):a review.Renew Energy 1998;1:89-103
- Naili N.,Attar I.,Hazami M.,Farhat A., First in situation operation of a low energy consumption passive solar agricultural greenhouse : a transient analysis. Energy Convers Manage 2002;43:95-101
- Ghosal MK, Tiwari GN.,Mathematical modelling for greenhouse heating by using thermal curtain and. Build and environment 2006;7;843-50
- Shukla A., Tiwari GN.,Sodha MS., Thermal modelling for greenhouse heating by using thermal curtain and an air-earth heat exchanger. Build and environment 2006;7:843-5
- I.attar, N.Naili, N.Khalifa, M.Hazami, M.Lazaar, A. Farhat,Experimental Study of an air conditioning system to control a greenhouse microclimate, Energy Conversion and Management 79 (2014), 543-553.

Application of life cycle assessment to a building sample in order to help in projects evaluation

Aurore Wurtz^{1*}, Bruno Peuportier¹

*1: Mines ParisTech, PSL Research University
CES – Centre for Energy efficiency of Systems
5 rue Léon Blum 91120 PALAISEAU, France*

web: <http://www.mines-paristech.eu/Research-valorization/Fields-of-Research/Energy-and-processes/>

**e-mail: aurore.wurtz@mines-paristech.fr,*

Abstract— Life cycle assessment (LCA) is particularly adapted to evaluate the environmental performance of buildings thanks to its multi-criteria approach on the entire life cycle. This method constitutes a basis for the eco-design of buildings and will play a key role in meeting current environmental challenges; it is therefore necessary to have reliable LCA tools which allow an easy interpretation of the results.

This communication presents an aid in the evaluation of projects by developing performance benchmarks for several environmental indicators. On the principle of the European energy label, different levels of environmental impacts are evaluated and classified on a scale from A to G. The study is carried out over the entire life cycle, based on samples of buildings (housing and offices) with various construction dates from 1880 to 2016.

Extreme values of environmental indicators are first calculated for each sample, corresponding to the best and the worst environmental performance of these building types. Then intermediate environmental performances are obtained by varying some parameters in a large number of simulations, particularly: the structure of the building (concrete or timber), the heating energy (gas, electricity or wood), the thickness of the walls and the type of windows. These simulations are carried out using a python program associated to dynamic energy simulation and LCA models of the software Pléiades, with the ecoinvent 3.4 database. Results present environmental labels corresponding to twelve environmental indicators: primary energy, CO₂, health, biodiversity... The large number of simulations provides distribution functions for the samples, from A to G levels.

Index Terms—Life cycle assessment (LCA), Building Energy Simulation (BES), environmental label

Introduction

The building sector represents the biggest part of the final energy consumption in France. In the current context of energy transition, countries have to reduce their energy consumption and improve buildings environmental performance.

Today's decisions are determining environmental impacts for the next decades, due to the long building life span. This paper proposes LCA benchmarks for three samples of buildings: single family houses, apartment and office buildings to provide an order of magnitude of impact indicators and help designers to evaluate the environmental performance of their projects.

For each sample of buildings extreme values of environmental indicators are calculated, corresponding to

best and worst environmental performance. Then, a parametric variation is carried out using a python program and the Pléiades software (Peuportier, 2015) to create an environmental label, using the ecoinvent 3.4 database.

Results present environmental classes from A to G for each environmental indicator studied, over the whole life span of the buildings.

I. SCOPE OF THE STUDY

A. Objectives of the life cycle assessment

The methodology of life cycle assessment allows evaluating environmental impacts of materials, systems and processes over their entire life cycle. Building LCA takes into consideration all existing flows, from raw materials extraction to the end of life of a building, including the transport of materials, construction, use and renovation stages. The goal is to avoid pollution displacement in time (e.g. reducing fabrication impacts by avoiding a photovoltaic system but increasing operation impacts), in location (avoiding local impacts by electric vehicles but increasing impacts at the electricity plant) or between impact categories (for example reducing CO₂ emissions but increasing radioactive waste).

One aim of LCA is to identify the stage and contributors of the life cycle which generate the biggest part of impacts, in order to help designers to define priorities. But once the designer has improved a project, is it sufficient or should further efforts be performed? This study contributes to answer this question by establishing benchmarks, which can also be used to evaluate existing buildings.

This requires to compare harmonized functional units, for instance defining benchmark indicators per m² net area and per year, related to an occupancy scenario and comfort level according to the use (residential, office, etc.).

Environmental indicators are evaluated contextualizing the ecoinvent 3.4 database, and include: cumulative energy demand, greenhouse effect, water used, waste, radioactive waste, damage to health, damage to biodiversity, abiotic resources depletion, land use, acidification, eutrophication and photochemical ozone production.

B. Digital tools

Pléiades software was used in this study, including Building energy simulation (BES) and LCA tools intended for eco-design and optimisation of projects. The optimisation module, called Amapola, allows varying

some design parameters like the type and thickness of insulation which was adapted for this study.

II. METHODOLOGY

This project is part of the Annex 72 of the International Energy Agency's Energy in Buildings and Communities Programme. The objectives are the establishment of a common methodology for LCA and the creation of benchmarks for different types of buildings in order to help building designers. LCA methodology needs common assumptions; this paper doesn't consider occupant transport, household waste or furniture impacts because they are not related to the performance of the building itself, which is studied here. However, impacts of foundations, plumbing and electric equipment, are added using a ratio per area. The life span of each material is also defined, as well as systems efficiency, water consumption and end of life processes.

This section presents the methodology applied; first extremes levels (A and G) were calculated and parametric variation was performed in a second step.

A. Calculation of levels A and G

Three samples of buildings were used in this study, individual and collective housing, and office buildings. Existing buildings were selected to evaluate the worst and the best environmental performance of each sample. Then, buildings used to calculate level A have a high insulation, double or triple glazed windows, photovoltaic panels and are located in Nice, South of France; whereas buildings for level G are not insulated, with simple glazed windows and are located in Trappes (coldest zone considered in the regulation). The samples are presented in table 1.

First, a set of LCA calculations is performed on each cell of Table 1 with the following variations: building structure (concrete, wood or limestone), heating energy (electricity, gas or wood), presence of photovoltaic panels or not for level A. Levels A and G are then established for each environmental indicator; the value of level A corresponds to the lowest of all simulations, and the one with the biggest impact defines level G.

TABLE I. PRESENTATION OF BUILDINGS CHOSEN TO ESTABLISH BENCHMARKS

	Single family houses	Apartments buildings	Office buildings
Level A	Energy positive house, 2018	Residential building, 2016	High energy performance offices, 2015
Level G	Uninsulated house, 1950	Hausmann building without renovation, 1880 Social housing without renovation, 1960	Variant without insulation nor PV system

B. Parametric variation

Parametric variations are performed using BES coupled with LCA. Parameters are modified to expand samples of buildings to different heating loads and materials, and simulations provide a range of environmental impacts for each indicator.

A Python program is used to generate the parametric variation, coupled with the Amapola module and the software Pléiades calling Building Energy Simulation (BES) and LCA. Impacts of the use stage are calculated for each new building performance and integrated in the LCA results. This way allows carrying out many simulations automatically, starting from a few typical archetype models.

III. RESULTS AND DISCUSSION

A. Establishment of levels A and G

Values corresponding to level G for the apartment buildings sample were established comparing nine simulations; heating energy of both representative buildings was changed, as well as the structure of one building. Regarding level A, twelve simulations were run, varying the structure, heating energy and the presence of photovoltaic panels. These variations were also performed for the two others samples and the following results were obtained.

TABLE II. ENVIRONMENTAL CLASSES A AND G ESTABLISHED FOR THE THREE SAMPLES OF BUILDINGS

Environmental impact /m ² /year	Collective housing		Individual housing		Office buildings	
	Label A	Label G	Label A	Label G	Label A	Label G
Greenhouse effect (100 years) (kgCO ₂ eq.)	1,46E+01	1,60E+02	1,48E+01	3,64E+02	6,54E+00	1,18E+02
Acidification (kg SO ₂ eq.)	1,88E-01	1,46E+00	1,99E-01	3,25E+00	1,55E-01	1,09E+00
Cumulative energy demand (kWh)	2,20E+02	1,33E+03	2,83E+01	2,77E+03	-1,94E+02	8,29E+02
Water used (m ³)	3,10E+00	3,70E+00	2,96E+00	5,11E+00	9,47E-02	8,43E-01
Wastes (t)	1,54E-02	5,63E-02	1,51E-02	1,11E-01	1,24E-02	3,95E-02
Eutrophication (kg PO ₄ eq.)	4,94E-02	9,45E-02	5,19E-02	1,58E-01	2,54E-02	6,85E-02
Photochemical ozone production (kg d'éthylène eq.)	5,18E-02	7,10E-01	5,76E-02	1,82E+00	3,36E-02	5,51E-01
Radioactive wastes (cm ³)	2,47E+00	1,36E+01	-1,03E+00	2,65E+01	-3,81E+00	7,52E+00
Land use (m ² .year)	7,52E-01	4,26E+01	1,03E+00	1,13E+02	9,64E-01	3,38E+01
Abiotic resource depletion (kg d'antimoine eq.)	8,64E-03	1,55E-02	9,10E-03	9,12E-03	1,79E-02	1,89E-02
Damage to biodiversity (PDF.m ² .year)	1,10E+01	6,23E+01	1,23E+01	1,35E+02	7,27E+00	4,46E+01
Damage to health (DALYs)	1,36E-04	4,32E-04	1,43E-04	9,57E-04	8,40E-05	3,09E-04

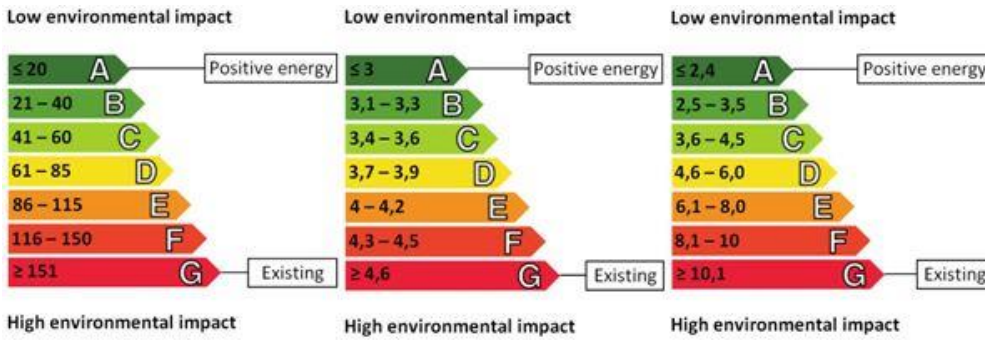


Figure 1. Environmental labels of single family houses, for CO₂ emissions (on the left) in kgCO₂/m²/year, water used (in the middle) in m³/m²/year and radioactive wastes (on the right) in cm³/m²/year

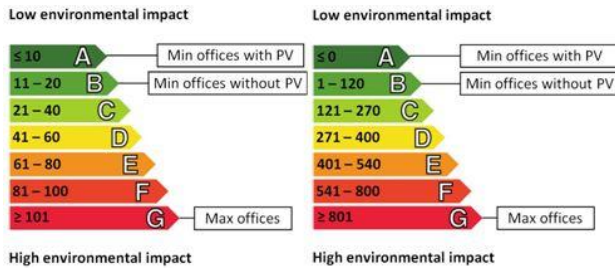


Figure 2. Environmental labels of apartments buildings, for CO₂ emissions (on the left) in kgCO₂/m²/year and damage to biodiversity (on the right) in PDF.m².year/m²/year

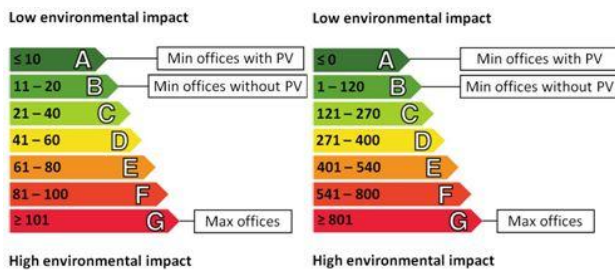


Figure 3. Environmental labels of office buildings, for CO₂ emissions (on the left) in kgCO₂/m²/year and primary energy demand (on the right) in kWh/m²/year

B. Presentation of environmental labels

Level G of the single family houses sample corresponds to a house located in Ile-de-France, which has a low energy performance. A parametric variation is performed, progressively increasing the performance; variations carried out represent more than 700 variants. Environmental labels of greenhouse gas emissions, water used and radioactive wastes are presented in Fig. 1.

Three archetype buildings are considered in the apartment buildings sample. The type of windows and insulation thickness are then varied. CO₂ emissions vary between 13 and 110 kgCO₂ eq./m²/year in this sample. Fig. 2 presents benchmarks for CO₂ emissions and damage to biodiversity generated by collective housing.

A parametric variation was also carried out for office buildings, based upon an existing high-performance building. CO₂ emissions vary between 10 and 100 kg of CO₂ eq./m²/year. Environmental labels of CO₂ and primary energy demand are presented in Fig. 3.

As an example, an office building was studied in the Annex 72; CO₂ emissions were evaluated to 15 kg CO₂ eq./m²/year, which corresponds to the environmental class B.

Conclusion

In this study, environmental labels of three samples of buildings were established for twelve environmental indicators through many simulations carried out using a Python program, based on typical archetypes. Environmental levels A and G were first established and then parametric variations (around 2000 simulations) allowed representing a part of the existing building stock. The project is currently pursued to improve the results including more parameters, and expand the labels to other samples of buildings. Finally, approaches in different countries are compared in the Annex 72 project.

ACKNOWLEDGEMENTS

This work was supported by ADEME and the lab research environment VINCI ParisTech.

REFERENCES

ADEME, Climat, air et énergie, Chiffres-clés, 2018
 Frischknecht R. et al, Assessing life cycle related environmental impacts caused by buildings, IEA EBC draft Annex 72, Copenhagen, May 2017.
 Peuportier B., Eco-design for buildings and neighbourhoods, Taylor Francis Group, London, 286p, 2015
 Pannier, M.-L.. 2017. « Etude de la quantification des incertitudes en analyse de cycle de vie des bâtiments ». Doctoral thesis, Paris Sciences et Lettres.
 Peuportier B., Thiers S., Beinstener P., «ENSLIC Case studies – Case study 2: Social housing in Montreuil», internal report ARMINES, Août 2009
 Ecoinvent: Swiss Centre for life Cycle inventories, <http://www.ecoinvent.org/>

Application of Alternative

Energy Sources in a District Heating System

Ing. Martina Mudrá (martina.mudra@stuba.sk)

Supervisor: prof. Ing. Ján Takács, PhD. (jan.takacs@stuba.sk)

Department of Building Services, Faculty of Civil Engineering, Slovak University of Technology in Bratislava, Slovakia, 2019

Abstract— The content of the paper is a proposal for streamlining the existing operation of a heat source for the district heating system of the West housing estate in the town of Brezno. The existing heat source consists of three hot water boilers burning natural gas. A cogeneration unit and water-to-water heat pumps will be added to the existing heat source operation. The operation of the cogeneration unit and heat pumps is designed without an external connection to the electricity grid. Aligning the output of the cogeneration unit with the consumption of heat pumps and their peripherals is the main goal of the design. The cogeneration unit and heat pumps will be used to prepare hot water in an accumulative manner. The flow of the heating heat transfer medium passes first through the heat pump and then through the cogeneration unit, if the temperature of the working medium is not sufficient, the flow of the heat transfer medium for heating the hot water also passes through the boiler. The real operational data on which I based my proposal were provided to me by the heat source operator for the period 2016 - 2018. I assessed the proposal from the point of view of energy and economy.

Index Terms—cogeneration unit, district heating system, heat pump, hot water

Introduction

According to Act No. 657/2004 Coll. on thermal energy, as amended, the term district heating system (DHS) means the supply of heat through public heat distribution from one or more heat production facilities [1]. It is a network, where heat sources (heating plants) are located at a sufficient distance from the supplied areas. The plants supply heat to secondary heat sources (heat exchange stations), which are connected to the heating systems of individual buildings [2]. District heating systems allow for a flexible response to the needs of heat consumers, thereby preventing construction of additional local sources of air pollution [3].

Simultaneously, the depletability of fossil fuels, climate change, and the consequences of human activity that result in rising levels of atmospheric CO₂ concentration force society to consider using alternative or renewable energy sources. In buildings, more than 80% of energy is used in the form of heat, cold or electricity to ensure the comfort of their users through energy systems such as heating, ventilation and air conditioning, domestic hot water, and electrical installations [4]. Therefore, the European Union (EU) is issuing decrees, directives, and strategy papers aimed at increasing the use of renewable energy sources and reducing the energy intensity of heating, ventilation and air conditioning systems [4].

Directive 2010/31 / EU of the European Parliament and of the Council of 19 May 2010 on the energy performance

of buildings states, inter alia, that EU Member States shall encourage and consider high-efficiency alternative systems such as:

- a. decentralized energy supply systems using energy from renewable energy sources,
- b. combined heat and power generation - cogeneration,
- c. block heating or district heating or cooling, especially if it uses energy from renewable energy sources in full or in part,
- d. use of environmental energy by means of heat pumps, as far as it is technically, functionally and economically feasible [5].

Point 35 of Directive 2012/27/EU of the European Parliament and of the Council of 25 October 2012 on energy efficiency states that high-efficiency cogeneration and district heating offer significant potential for primary energy savings [6].

I. OPERATION OF THE EXISTING HEAT SOURCE

A. Description of the Site

Combined heat and power through a cogeneration unit and heat pumps will be designed for the West housing estate located in the town of Brezno, Slovakia. The existing hot water boiler plant is situated near the Hron River in the residential area of the Ladislav Novomeský District. The proximity of a watercourse creates preconditions for an excess of groundwater in the surrounding subsoil – a source of low-temperature energy. This energy will be transformed to a higher temperature level by water-to-water heat pumps [4,7]. Fig. 1 shows an external view of the boiler plant.



Figure 1. External view of the boiler plant [7]

The district boiler plant is a source of heating water and domestic hot water for 782 flats, ice arena, restaurant and a retirement home. The total length of hot water networks is 1 458 meters [8].

B. Condition of the Boiler Plant

During heating season, there is uninterrupted 24-hour operation. In summer, the boiler plant is in operation from 4:00 am to 11:00 pm, i.e. 19 hours. The heat transfer medium is hot water with the original design temperature gradient of 90/70°C. The heat source is represented by three hot water boilers with a total output of 6.76 MW. A flue gas heat exchanger is installed after each of these boilers. Hot water preparation is realized through plate heat exchangers connected in series as pre-heating and water heating with the circulation of these exchangers leading to better cooling of the return water to the boilers. The cold water is preheated in condensing economizers connected to a 6 300 litre preheating water storage tank to store heat at a time when there is little or no hot water withdrawal [7]. Fig. 2 shows the interior view of the existing boiler plant.



Figure 2. Interior view of the existing boiler plant [7]

C. Energy Balance of the Heat Source

Hourly consumption of natural gas in m³ was provided by the heat source operator for the period of 2016 - 2018. Fig. 3 logically shows that the largest consumption of natural gas was in the heating season and the lowest in the summer season. The natural gas consumption also depends on the climatic conditions in a given period [7].

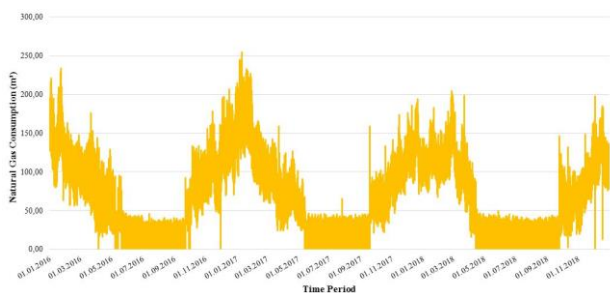


Figure 3. Natural gas consumption in m³ over 2016 - 2018 [7]

By multiplying the values of natural gas consumption by the calorific value of the fuel, the total amount of heat contained in the natural gas was obtained. By comparing the annual consumption of natural gas and the total heat contained in natural gas, it was found that in 2017 was the largest consumption of natural gas and thus the value of total heat in natural gas [7]. On the contrary, in 2018, the consumption of natural gas was 11.6 % lower than in 2017, as evidenced by the graph in Fig. 4.

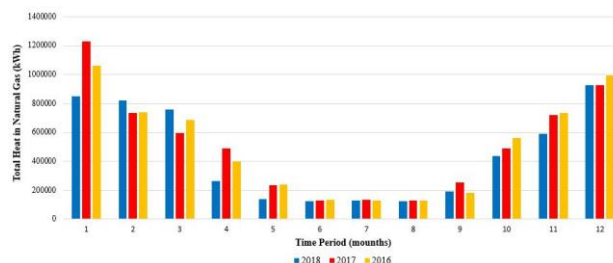


Figure 4. Monthly values of total heat in kWh of natural gas during 2016 - 2018 [7]

II. DESIGN MODEL FOR THE APPLICATION OF NEW DEVICES

A. Operation of the New Heat Source

A cogeneration unit and heat pumps shall be installed instead of the existing heat source - hot water boilers. The energy source for driving the cogeneration unit will be natural gas. The energy source for driving the heat pumps will be the electricity produced by the cogeneration unit. The cogeneration unit and heat pumps will be used to prepare hot water in an accumulative way. The storage tank will be located behind the cogeneration unit and heat pumps and, at a time when the demand for hot water consumption is reduced, the heated hot water will accumulate in it. The accumulated heat will be supplied to the grid at the time of increased demand. The essence of the design is ensuring a continuous operation of the equipment so that it works as long as possible and with a minimum of starts [7].

B. Power of the Cogeneration Unit and Heat Pumps

To determine the optimal heat output of the device, we need to know the domestic hot water consumption over 24 hours. The heat output of the device can be determined based on the average hourly heat demand for domestic hot water preparation in June. Working days - Monday, Wednesday will be compared with a free day - Saturday. Fig. 5 shows that the domestic hot water is supplied between 4:00 am and 11:00 pm, i.e. 19 hours. On weekdays, the hot water consumption is highest in the morning and evening. On weekends, the hot water consumption is increased compared to working days and it is on average the same throughout the day [7].

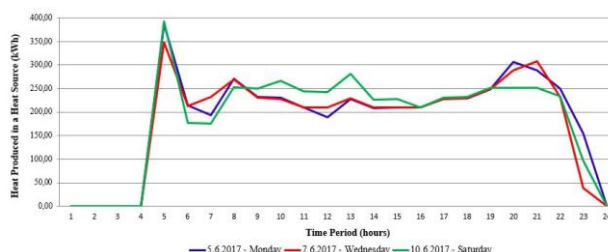


Figure 5. Hourly heat demand for domestic hot water preparation over 24 hours on 3 June 2017 [7]

The average hourly heat demand for domestic hot water preparation in 2016 was 275 kW, in 2017 it was 280 kW, and in 2018 it was 267 kW. By comparing the data for the period 2016 - 2018, the heat output of the cogeneration unit and two heat pumps was set to 270 kW [7].

The cogeneration unit and heat pumps will be located in front of the boilers in the direction of the return heating water flow. The heat transfer medium - heating water has a temperature of 45 °C. The aim is to produce a heat-transfer working substance - heating water with a temperature of 60 °C. The temperature drop in the hot water system is therefore 60/45 °C, which means that the temperature difference ($\Delta\theta$) is 15 K. A very important parameter in the design of thermal outputs of the equipment is also the volume flow that will flow through the system. The volume flow that enters the system must be equal to the volume flow that leaves it. The volume flow at a heat output of 270 kW and a temperature difference of 15 K is 15.48 m³/h. The heat pumps operate with a primary gradient of 5/1 °C - this means that a low-temperature heat source enters the heat pumps (groundwater from wells) and is transformed in the heat pumps to a higher temperature, transferred to the secondary heating system circuit. Return heating water with a temperature of 45 °C enters the heat pump and is heated up by 10 K, which means that the water temperature at the outlet of the heat pump will be 55 °C. This time the temperature difference ($\Delta\theta$) is known to be 10 K and the volume flow (M) through both heat pumps is 15.48 m³/h. The output of both heat pumps was calculated to be 180 kW. It follows from the above that the heat output of the cogeneration unit will be 90 kW. The cogeneration unit works with a temperature gradient ($\Delta\theta$) of 20 K as standard. This means that if water with a temperature of 55 °C enters the cogeneration unit, the cogeneration unit will heat the water to 75 °C at the outlet of the cogeneration unit. I know determine the volume flow rate that the cogeneration unit must take to reach 60 °C at the outlet of the unit and before entering the hot water storage tank. The volume flow through the cogeneration unit to reach 60 °C at the outlet of the unit and before entering the hot water storage tank is 3.87 m³/h. For better controllability of the system, two identical two-stage water-water heat pumps are proposed. The

advantage of a two-stage heat pump is that it has two output stages and can therefore be operated on a single compressor with half the output. Because the heat transfer medium cools the primary heat transfer medium - the pumped water, it could freeze and form icing on the heat pump evaporator, which would be destroyed after a certain time. Therefore, a separation heat exchanger was used in the primary circuit to ensure an intermediate circuit with antifreeze between the pumped groundwater and the heat pump. Through a detailed recalculation, the design of two identical heat pumps was determined, while the heat output of one was 89.6 kW. For the cogeneration unit together with the heat pumps to create a set, it is necessary to harmonize their thermal outputs and also electrical inputs, as the cogeneration unit will supply electricity to the heat pumps. The interaction between the heat pumps and the cogeneration unit was simulated using calculation programs in cooperation with the supplier of these devices. From the three simulations performed, the most solution was selected, which set the heat output of the cogeneration unit at 90 kW [7]. Fig. 6 shows a circuit diagram of the cogeneration unit and heat pumps.

C. Hot Water Storage Tank

During the operation of the cogeneration unit and heat pumps during the heating season, all the heat energy produced by these devices is used to prepare domestic hot water and to heat the heating water. In summer, when the produced thermal energy is consumed only for the preparation of heat, there may be an excess of heat produced. These surpluses must be stored in a hot water storage tank, from which they are tapped during peak periods in the event of greater heat demand. If this excess energy does not accumulate but flows into the system, the temperature of the return heating water entering the heat pumps can gradually increase, leading to overheating of the heat pumps that may reach complete shutdown [7].

The volume of the storage tank was determined to be 10,000 litres by detailed calculations [7].

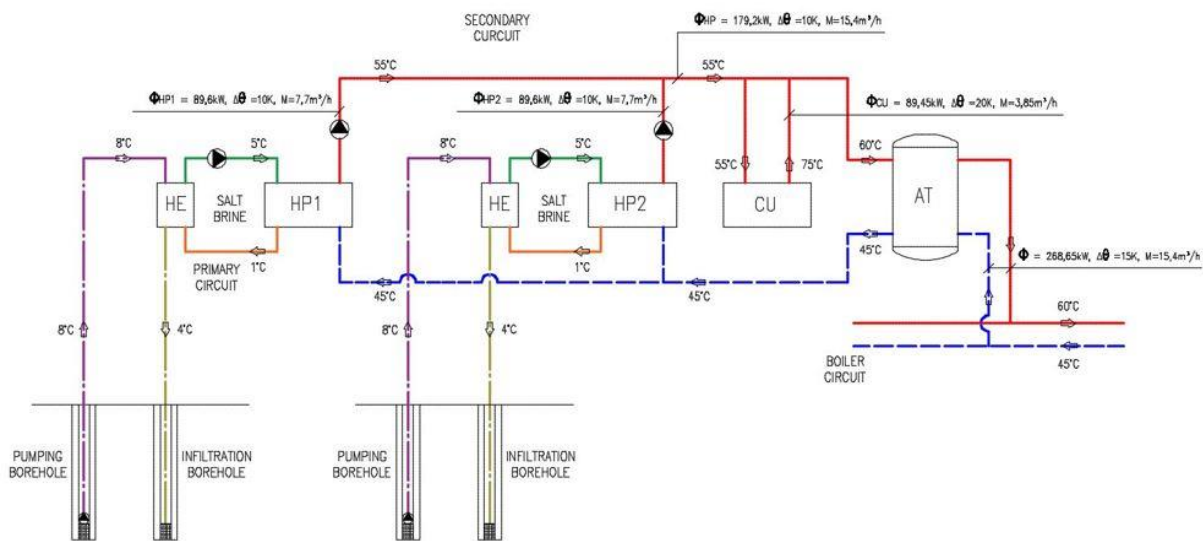


Figure 6. Circuit diagram of the cogeneration unit and heat pumps [7]
 HE – heat exchanger, HP – heat pump, CU – cogeneration unit, AT – storage tank

III. RESULTS – ENERGY ASPECTS

A. Natural Gas Consumption

To be able to assess the proposed design from an economic point of view, it is important to determine how much natural gas is saved by installing new technological equipment, a cogeneration unit and heat pumps, as compared to the original condition. The equipment was designed based on the operation and average energy consumption in 2016 - 2018. The average natural gas consumption was 598,740 m³/year and the average heat produced by the heat source was 6,066,354 kWh/year for the period 2016 – 2018 [7].

To estimate the future consumption of natural gas, we have to determine the number of operating hours of the individual devices and their output in winter, transition, and summer season [7].

The number of days in individual periods, the number of operating hours during the day, and the expected hourly outputs of the set are given in Tab. I. Using these data, the amount of thermal energy produced per year can be determined. In real operation, however, there may be moments when the equipment breaks down or there is a planned shut down due to its maintenance, which is taken into account by reducing the produced thermal energy by 5% [7]. For clarity, the data are shown in Tab. I.

The total thermal energy produced by the cogeneration unit and heat pumps throughout the year is 2,249,049 kWh = 2,249.05 MWh [7].

The thermal energy produced by boilers is 3,817,305 MWh. A very important data is the consumption of natural gas by the cogeneration unit. The producer of the cogeneration unit declares that the maximum hourly consumption of natural gas is approximately 24 nm³/h at a calorific value of natural gas of 35.5 MJ/m³ [9].

The consumption of natural gas for the cogeneration unit in individual periods and throughout the year is shown in Tab.II.

The total natural gas consumption by the cogeneration unit throughout the year is 189,240 m³ [7].

The value of the total heat in natural gas is obtained as the product of the total consumption of natural gas by the cogeneration unit and the average calorific value of the fuel (9.701 kWh / m³), which is 1,835,817 kWh. These findings show that 1,835,817 kWh of energy consumed in natural gas is needed to produce 2,249,049 kWh of heat energy per year by the cogeneration unit and heat pumps. To determine the total consumption of natural gas at a heat source, we need to know the consumption of natural gas by gas boilers. The consumption of natural gas by boilers was calculated to 401,527 m³. It follows from the above that the estimated total consumption of natural gas at the heat source is 590,767 m³. If we look at the average natural gas consumption before the installation of the unit, which is 598,740 m³/year and the expected natural gas consumption after the installation of the unit, which is 590,767 m³/year, it is seen that applying a cogeneration unit and heat pumps should save 7,973 m³ of natural gas as compared to the existing operation of gas boilers. At the time when the application was being addressed, the purchase price of natural gas per 1 kWh was 0.04234 euros [8]. By multiplying the saved amount of natural gas by the average value of combustion heat (10.754 kWh/m³) and the purchase price of natural gas, an annual saving of 3,631 euros is determined [7].

B. Electricity Consumed

A cogeneration unit is a device for the combined production of heat and electricity [10]. A part of the generated electricity is used for its consumption, the predominant part is used to drive the heat pumps. It will also power submersible pumps in pumping wells and circulating pumps on the primary and secondary side.

Given that we produce electricity by high-efficiency cogeneration, we can claim a supplement following the Decree of the Office for Regulation of Network Industries no. 18/2017 Coll. laying down price regulation in the electricity sector [11].

TABLE I.
USE OF COGENERATION UNIT AND HEAT PUMPS THROUGHOUT THE YEAR [7]

Season	Months	Days	Operating hours	Operating hours in the season (h)	Hourly power of equipment (kW)	Produced thermal energy reduced by 5% (kWh)
Winter	7	212	24	5,088	300	1,450,080
Transition	2	61	24	1,464	270	375,516
Summer	3	92	19	1,748	255	423,453
Σ CU +HP	12	365	-	8,300	-	2,249,049

TABLE II.
NATURAL GAS CONSUMED BY THE COGENERATION UNIT [7]

Season	Hourly natural gas consumption by cogeneration unit (nm ³ /h)	Operating hours in the season (h)	Final consumption of natural gas by the cogeneration unit reduced by 5% (m ³)
Winter	24	5,088	116,006
Transition	24	1,464	33,379
Summer	24	1,748	39,854
Σ	-	8,300	189,240

Section 10, point 1, letter c of this Decree states that the price of electricity produced by high-efficiency cogeneration in the electricity producer's facility put into operation from 1 January 2017 in a combustion engine with natural gas fuel is 75.04 euros/MWh [11]. However, this price is reduced by the price of electricity at a loss - it is the arithmetic average of electricity prices to cover the losses of all regional distribution system operators without deviation costs [12]. The price of electricity for losses is 40.49 euros/MWh [12]. This value can be used to calculate the amount of the own surcharge. The surcharge on electricity is found from the difference between the price of electricity produced by high-efficiency cogeneration and the price of losses. The surcharge for electricity is 34.55 euros/MWh [7].

To find the prices of revenues for high-efficiency cogeneration, we have to determine how much electricity is produced by the cogeneration unit each month and throughout the year. The data and information provided by the manufacturer of the cogeneration unit indicate that the electrical power at full load of the unit will reach 86 kW_e and when alternating full and three-quarters of power in the summer, we approach the average value of hourly electrical power of 81 kW_e [9]. To obtain the final values of the electricity supplied to the equipment, for which we can charge a surcharge, the own electricity consumption needs to be deducted from the electric power of the unit, as it is not covered by the surcharge. The manufacturer states that the actual electricity consumption of the cogeneration unit is 13 kW_e [9]. The obtained data are shown in Tab. III.

The electricity produced during the annual operation of the facility will be 567,302 kWh per year, which represents 567.302 MWh per year. This value is again reduced by 5% due to a fault or maintenance on the equipment [7].

As we know the surcharge for electricity and the amount of electricity produced, we can use the product of these items to find out what the revenues for high-efficiency cogeneration will be [7].

Annual revenues for high-efficiency cogeneration amount to 19,600 euros [7].

IV. RESULTS – ECONOMIC ASPECTS

A. Investment Costs

If we want to find out the return on streamlining the operation of the heat source through the cogeneration unit and heat pump, we must first know what the investment costs. As the manufacturer of the cogeneration unit also deals with the installation and implementation of these devices, he provided an indicative price offer [7].

The total investment costs for the implementation of the work amount to 502,820 euros [9].

B. Cogeneration Unit Maintenance Costs

For the cogeneration unit, I consider the costs of maintenance service of the cogeneration unit, including work and transport within Slovakia, spare parts following the expected engine wear, consumables, lubricating oil, and coolant. The average cost per operating hour of a cogeneration unit, including all the costs mentioned above, is 1.54 euros/Mth [9].

The number of year-round operating hours of the cogeneration unit was estimated to 8,300. Due to possible failures or repairs on the equipment, we will reduce the operating hours by 5 %. The resulting number of operating hours is 7,885. If this figure is multiplied by the average cost per 1 operating hour, the resulting annual maintenance costs of the cogeneration unit amounts to 12,143 euros [7].

C. Heat Pump Maintenance Costs

The maintenance is considered to take place once a year. Maintenance costs include routine maintenance, refrigerant inspection, transport from Bratislava to Brezno and back [7].

The annual maintenance costs for both heat pumps are 1,206 euros. The work of a service technician is already included in this final price [7].

D. Profitability Based on Cash Flow

Since the streamlining of the operation of the heat source is solved in the boiler plant, which is managed by the energy company, I can claim a legitimate claim from depreciation in the price of heat. We have to divide the individual equipment and works into depreciation groups and write off the relevant amount each year. This written-off amount represents cash income through the price of heat (quasi-profit item without the need for taxation). Subsequently, in the individual years, we apply the saved finances on natural gas and revenues for high-efficiency cogeneration. During these years, we also have to think about the maintenance of the cogeneration unit equipment and heat pumps, which represent negative items. With the sum of profit and loss items in individual years, we work towards the overall benefit from the operation of the facility. Since the investment in the work is also a negative item, its sum with the total benefit in the operation of the equipment, I will work on the return of the equipment, if the items will not be negative but positive [7]. The results are visualized in the form of accumulated cash flow as shown in Fig. 7.

Fig. 7 shows that the revenue from depreciation, financial savings on natural gas and revenues for high-efficiency cogeneration will return the investment in 6 years from the installation of the equipment [7].

TABLE III.
AMOUNT OF ELECTRICITY PRODUCED BY THE COGENERATION UNIT [7]

Season	Months	Days	Operating hours	Operating hours in the season (h)	Hourly electricity production (kWe)	Electricity produced reduced by 5% (kWh)
Winter	7	212	24	5,088	73	352,853
Transition	2	61	24	1,464	73	101,528
Summer	3	92	19	1,748	68	112,921
Σ CU +HP	12	365	-	8,300	-	567,302

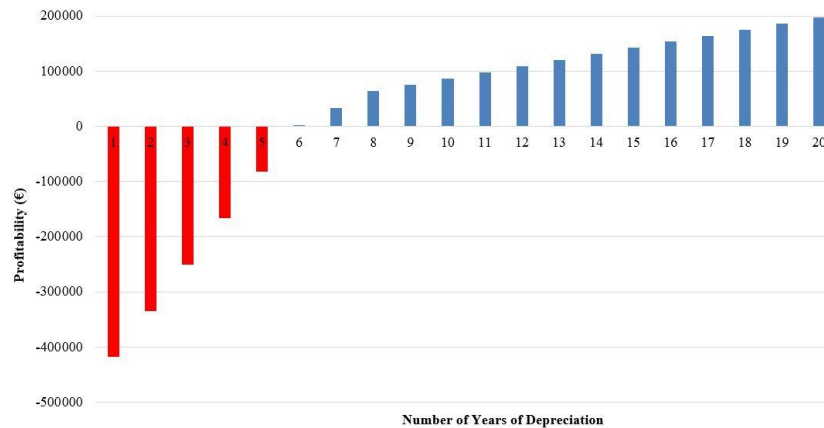


Figure 7. Cumulated cash flow [7]

V. DISCUSSION

The reason to apply the cogeneration unit and heat pumps in the given operation was the fact that district heating systems have the potential for high-efficiency combined heat and power generation and efficient use of environmental energy through heat pumps. These devices can be installed separately, but as mentioned in the article, there is also a presumption of the interaction of both devices.

The cogeneration unit could also supply electricity to the public electricity network, but at the time of this optimization study, there was a ban on connecting new larger sources of electricity to the public electricity network.

The application of a cogeneration unit and heat pumps to the existing operation of hot water gas boilers saves fossil fuel - natural gas, the reserves of which are gradually running out. The energy of the environment - groundwater - is used instead. From an energy point of view, the same or more heat energy is produced but less fuel is consumed. As far as the economy is concerned, saving fuel also saves money that would otherwise be spent on buying it. Electricity is produced through a cogeneration unit and there is no need to supply electricity to the installations from the public grid, except in cases where there is a failure or maintenance of the cogeneration unit. They also evaluate the annual sales for combined heat and power generation positively.

VI. CONCLUSION

To ensure energy efficiency, the original technologies are gradually being replaced by modern equipment. First of all, it is important to determine the area of operation of these facilities, which is also affected by the determination of performance. A cogeneration unit and heat pumps were used to produce the heat needed to prepare hot water in an accumulative way, especially in the summer. During the heating season, the additional heat produced will not accumulate but will be supplied to the heating network.

Only through the application of renewable energy sources and combined production of electricity and heat in district heating systems will Slovakia manage to meet its targets by 2030. These include reduction of greenhouse gas emissions by 20 % and increasing the share of energy from renewable energy sources in gross final energy consumption by 19.2 %. [13]

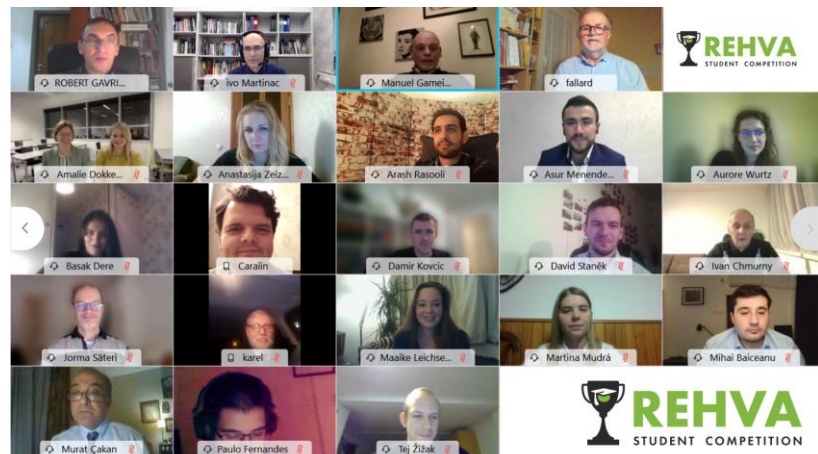
ACKNOWLEDGEMENT

This work was supported by the Ministry of Education, Science, Research and Sport of the Slovak Republic through the grant VEGA 1/0847/18.

REFERENCES

- [1] Act No. 657/2004 Coll. on thermal energy. From: <https://www.slov-lex.sk/pravne-predpisy/SK/ZZ/2004/657/20151229.html> (on line)
 - [2] SAYEGH, M. A. – DANIELEWICZ, J. – NANNOU, T. – MINIEWICZ, M. – JADWISZCZAK, P. – PIEKARSKA, K. – JOUHARA, H. Trends of European research and development in district heating technologies. From: <https://www.sciencedirect.com/science/article/pii/S1364032116002318> (on line)
 - [3] <https://www.veolia.sk/pre-zakaznikov/mesta-obce/centralne-zasobovanie-teplom> (online)
 - [4] PETRÁŠ, D. - LULKVIČOVÁ, O. - TAKÁCS, J. - FÜRI, B. Renewable energy sources for low temperature systems. Bratislava: Jaga Group, 2009. 223 p. ISBN 978-80- 8076-075-5.
 - [5] Directive 2010/31/EU of the European Parliament and of the Council of 19 May 2010 on the energy performance of buildings. From: <https://eur-lex.europa.eu/legal-content/EN/TXT/HTML/?uri=CELEX:32010L0031&from=SK> (on line)
 - [6] Directive 2012/27/EU of the European Parliament and of the Council of 25 October 2012 on energy efficiency. From: <https://eur-lex.europa.eu/legal-content/EN/TXT/HTML/?uri=CELEX:32012L0027&from=SK> (online)
 - [7] MUDRÁ, M. Streamlining the operation of heat source TP5 for the housing estate Západ in Brezno [diploma thesis]. Bratislava: Slovak University of Technology in Bratislava, Faculty of Civil Engineering, Department of Building Services, 2019. 106 p.
 - [8] Veolia Energia Brezno a.s. From: <https://vesr.sk/sk/veolia-energia-brezno> (on line)
 - [9] Engul, s.r.o. From: <https://www.engul.sk/kontakt/> (on line)
 - [10] PASTOR, P. – HORÁK, M. - HORNÍK, Š. Efficient use of energy in the operation of equipment and buildings. Bratislava: Jaga group, 2000. 159 p. ISBN 80-88905-33-8.
 - [11] Decree of the Office for Regulation of Network Industries no. 18/2017 Coll. establishing price regulation in the electricity sector. From: <https://www.slov-lex.sk/pravne-predpisy/SK/ZZ/2017/18/20180720.html> (on line)
 - [12] Regulatory Office for Network Industries. 2018. Decision No. 0019/2019/E of 8 November 2018. From: [http://www.urso.gov.sk:8088/CISRES/Agenda.nsf/0/ABC9F4E48DF45E36C125833F002892A2/\\$FILE/0019_2019_E.pdf](http://www.urso.gov.sk:8088/CISRES/Agenda.nsf/0/ABC9F4E48DF45E36C125833F002892A2/$FILE/0019_2019_E.pdf) (on line)
- Integrated National Energy and Climate Plan 2021 – 2030. Ministry of Economy of the Slovak Republic. Bratislava. October 2019. From: <https://www.mhsr.sk/uploads/files/zsrwr58V.pdf> (online)

Event Pictures



The REHVA Community of Young Professionals brings together participants from past editions of the student competitions to share knowledge and best practices.

This Book of Papers aims at concentrating the knowledge of each edition of the competition and serves to commemorate the occasion.

REHVA warmly thanks all the people involved in the organization of, and participation to, the events.

Join the discussion on the
@RCYP LinkedIn group!

